Karlsruher Institut für Technologie

Monotonicity Methods for Inverse Scattering Problems

Zur Erlangung des akademischen Grades eines

Doktors der Naturwissenschaften

von der KIT-Fakultät für Mathematik
des Karlsruher Instituts für Technologie (KIT)
genehmigte

Dissertation

von

Annalena Albicker (M. Sc.)

Referent:	Prof. Dr. Roland Griesmaier
Koreferent:	PD Dr. Tilo Arens
Tag der mündlichen Prüfung:	24. Mai 2023

Danksagung

Das Leben ist wie ein Fahrrad. Man muss sich vorwärts bewegen, um das Gleichgewicht zu halten.
Albert Einstein

Es gibt eine Reihe von Personen, die mir in den vergangenen Jahren dabei geholfen haben, mich vorwärts zu bewegen. An erster Stelle möchte ich meinen Betreuer Prof. Dr. Roland Griesmaier nennen, dessen Unterstützung wesentlich zum erfolgreichen Fertigstellen dieser Arbeit beigetragen hat. Weiterhin gilt mein Dank PD Dr. Tilo Arens für die Übernahme des zweiten Gutachtens. Nicht zu vergessen ist PD Dr. Frank Hettlich als dritter „Chef“ der Arbeitsgruppe. Natürlich gehören auch weitere Doktoranden und Doktorandinnen zu unserer Gruppe, bei denen ich mich ebenfalls bedanken möchte – sei es für Rückendeckung in der Lehre, fachliche Gespräche, Korrekturlesen oder Unterhaltungen, die nichts mit der Uni zu tun hatten. Ein besonderer Dank gebührt Marvin, der zeitgleich mit mir angefangen hat und mir insbesondere bei dem ein oder anderen Programmierproblem kompetent weiterhelfen konnte.

Daneben stehen diejenigen Menschen aus meinem privaten Umfeld, die dazu beigetragen haben, dass ich in stressigen Phasen nicht das Gleichgewicht verloren habe, oder die mir (sowohl im metaphorischen als auch im wörtlichen Sinne) aufgeholfen haben, wenn ich vom Rad gefallen bin. Namentlich nennen möchte ich meine Eltern Martina und Andreas, meine Schwester Johanna und meinen Verlobten Dominik.

This work was funded by the Deutsche Forschungsgemeinschaft (DFG, German Research Foundation) – Project-ID 258734477 – SFB 1173.

Abstract

We consider two inverse scattering problems in unbounded free space. On the one hand, we investigate an inverse acoustic obstacle scattering problem governed by the time-harmonic Helmholtz equation. On the other hand, we examine an inverse electromagnetic medium scattering problem modeled by the time-harmonic Maxwell equations. In both cases, our goal is to recover the position and the shape of compactly supported scatterers D from far field observations of scattered waves. For the acoustic scattering problem, we assume that the scatterers are impenetrable obstacles that carry mixed Dirichlet and Neumann boundary conditions. For the electromagnetic scattering problem, the media are supposed to be penetrable, non-magnetic and non-absorbing but the electric permittivity may be inhomogeneous inside the scattering objects.

We approach both shape identification problems utilizing a monotonicity-based reconstruction ansatz. First, we establish monotonicity relations for the eigenvalues of the far field operators which map superpositions of plane wave incident fields to the far field patterns of the corresponding scattered fields. In addition, we discuss the existence of localized wave functions that have arbitrarily large energy in some prescribed region while at the same time having arbitrarily small energy in some other prescribed region. Combining the monotonicity relations and the localized wave functions leads to rigorous characterizations of the support of the scattering objects. More precisely, we develop criteria that allow us to evaluate whether certain probing domains B are contained inside the unknown scatterer D or not and vice versa. Therefore, we introduce probing operators corresponding to the probing domains B and show that the number of positive or negative eigenvalues of suitable linear combinations of the far field operator corresponding to D and these probing operators is finite if and only if B is contained within D or if and only if B contains D. Finally, we complement our theoretical findings with numerical reconstruction algorithms and give some examples to illustrate the reconstruction procedure.

Contents

CHAPTER 1

Introduction

1.1. Approaching the Shape Identification Problem

Generally speaking, scattering theory consists of studying the effects of an inhomogeneity on some moving particles or waves. In this work, we restrict ourselves to acoustic or electromagnetic waves that are periodic in time. When an incoming or incident wave hits an inhomogeneity it gets deviated and gives rise to a scattered wave. In practice, it is impossible to identify the scattered wave alone but we observe the total field which is the superposition of the incident and the scattered wave. We suppose that the background against which the waves travel is homogeneous and call the support of the inhomogeneities the scattering object or simply scatterer. Given an incident wave together with some relevant properties of the scatterer, the problem of finding the corresponding scattered wave and especially its behavior at great distances from the scatterer – also known as its far field behavior – is called the *direct scattering problem*. This problem is approached by solving the partial differential equation modeling the wave propagation, and it is well investigated. More interesting from a mathematical point of view is the *inverse scattering problem*. Here, one tries to recover some information about the unknown scatterer given the far field behavior of scattered waves. Possible applications are, for example, medical imaging, material science, remote sensing and nondestructive testing. For a first insight into the framework of direct and inverse scattering of acoustic and electromagnetic waves, we exemplary refer to the monographs by Colton and Kress [CK19], Kirsch and Hettlich [KH15] and Monk [Mon03].

Throughout, we focus on reconstructing the position and the shape of unknown scatterers and thus examine a *shape identification problem*. This problem is typically nonlinear and ill-posed, i.e., the position and the shape of the scatterers do not depend continuously on the far field observations of the scattered waves. One strategy approaching its solution are *iterative methods*. Thereby, the inverse scattering problem is transformed into a nonlinear optimization problem, and iterative schemes are applied to solve the latter. The first contribution goes back to Roger [Rog81] who utilized a regularized Newton-type iteration. Afterward, further procedures involving, e.g., different iteration schemes and various regularization strategies have been proposed by a multitude of researchers. Just to name a few, we mention Kirsch [Kir93], Hettlich [Het98] and Kress [Kre03]. Up to now, iterative methods are still popular and widely used. Nevertheless, difficulties like high

computational costs evolving from the necessity of solving a direct scattering problem in every step led to the development of *non-iterative methods*. These include for instance *decomposition methods* that build on the idea of separating the two major challenges concerning the inverse scattering problem, which are its ill-posedness and its nonlinearity, from each other. In a first step, one addresses the ill-posedness by using analytic continuation to reconstruct the scattered waves from their far field behavior. Afterward, the boundary of the unknown scatterer is found as the location where the total field fulfills the boundary condition. This represents a nonlinear step. We exemplary mention the methods by Colton and Monk [CM85, CM86] and by Kirsch and Kress [KK87]. The approach that we investigate in this work belongs to another class of non-iterative methods called *sampling methods*. Whereas the two classes of methods that we only just presented both require some a priori information about, e.g., the number of components the scatterer consists of, its approximate position or its boundary conditions, the sampling methods mainly overcome this disadvantage. However, these require in general more data. While iterative and decomposition methods work with far field data generated from one incident wave, sampling methods need data for many incident waves. Besides, when considering penetrable media only the support of the scatterer, not its material parameters are reconstructed. This is why sampling methods are sometimes also referred to as *qualitative methods* since they only recover limited information about the scatterers. The key ingredient that underpins the shape reconstruction consists in developing criteria that allow deciding whether a given probing object lies inside or outside the scatterer. The methods differ in the definition of the probing objects which could, e.g., be points, sets or curves and in the specification of the criteria. Placing a grid over the region of interest and sampling over the probing objects then gives an idea of the characteristic function of the scatterer. Two very famous sampling methods are the *Linear Sampling Method* [CK96] by Colton and Kirsch and the *Factorization Method* [Kir98, KG08] by Kirsch. Both use points as probing objects and are based on evaluating a special series in every probing point. Whereas the Linear Sampling Method only provides a sufficient criterion, the Factorization Method yields a criterion that is sufficient and necessary. Furthermore, it is worth mentioning the *Probe Method* [Ike98a] by Ikehata, the *Method of Singular Sources* [Pot00] by Potthast and a method using the *Convex Scattering Support* [KS03] by Kusiak and Sylvester. Moreover, we recommend the survey [Pot06] by Potthast which gives an overview of different sampling methods as well as the monograph [CC14] on qualitative methods.

As the title of this thesis suggests, we apply a *monotonicity-based* qualitative shape reconstruction technique. Thereby, the sampling criterion is formulated in terms of the so-called far field operator that maps superpositions of incident plane waves to the far field patterns of the corresponding scattered waves and can be considered as the "measurement operator". More precisely, we examine monotonicity properties of the eigenvalues of appropriate linear combinations of these far field operators with suitable probing operators. Early contributions regarding monotonicity properties for the Laplace equation were published in [KSS97, Ike98b] when studying the inverse conductivity problem. A first monotonicity-based reconstruction scheme was proposed in [TR02] for electrical impedance tomography. A detailed mathematical analysis can be found in [HU13]. For further developments, we refer to [HU15, HM16, BHHM17, HM18]. In [GS17a, Gar18, GS19] the authors present a regularization strategy and work toward the numerical implementation of the reconstruction scheme. The monotonicity-based shape recon-

struction ansatz was transferred to an inverse coefficient problem for the Helmholtz equation on unbounded domains in [HPS19a, HPS19b]. This has been extended to an inverse scattering problem with penetrable scatterers in unbounded free space in [GH18, GH21]. For the sake of completeness, we also mention some recent progress concerning monotonicity methods. An application to an inverse crack detection problem has been studied in [Fur20]. In [HL19, HL20] the concept was extended to fractional order Schrödinger equations. Finally, eddy current problems and magnetic induction tomography have been discussed in [SVUT17, TPZ21], and in [BHKS18, CEFP$^+$21, GKM22, HL23] the research focuses on nonlinear materials.

Throughout, we examine two different scattering problems in unbounded free space. The first one is an **inverse acoustic scattering problem** which is modeled by the time-harmonic Helmholtz equation. We suppose that the scatterers D are impenetrable and carry Dirichlet or Neumann boundary conditions. More precisely, we assume that $D = D_1 \cup D_2$ with $\overline{D_1} \cap \overline{D_2} = \emptyset$, where we impose a Dirichlet boundary condition on ∂D_1 and a Neumann boundary condition on ∂D_2. Furthermore, the scatterer may consist of finitely many connected components, and we do not assume any a priori information neither about the number of components nor the type of boundary condition on the single components. As already mentioned we aim to recover the position and the shape of the scatterers from far field observations of scattered waves. In the past, for instance, the Linear Sampling Method found use (see, e.g., [CCM01, CC14]) when considering this inverse mixed obstacle scattering problem. Besides, the Factorization Method has been successfully applied (see, e.g., [Gri02, GK04, KG08]). Thereby, the major drawback is that this method is only justified in the case when the Dirichlet and the Neumann components can be separated a priori. Broadly speaking, one needs to have a rough idea about where the Dirichlet and the Neumann components are located. With the monotonicity-based ansatz, we overcome this restriction and apart from that we succeed in classifying the different components with regard to their boundary conditions. The main idea for the shape characterization consists of comparing the real part of the given far field operator corresponding to the unknown scatterer D to probing operators corresponding to certain probing domains B. These probing operators could be simulated far field operators or appropriate linearizations of such operators. We show that suitable combinations of the given far field operator and the probing operators are positive or negative definite up to some finite-dimensional subspace if and only if the scatterer D contains the probing domain B or if and only if the scatterer D is contained inside the probing domain B. Sampling over the region of interest choosing sufficiently many test domains provides a foundation for numerical reconstruction algorithms. The theoretical justification of the shape characterization builds on the one hand on the factorization of the far field operator (see, e.g., [KG08]) and on the other one on the existence of *localized wave functions*. These are certain pairs of functions with one component having arbitrarily large norm on some prescribed part of a boundary whereas the other component has arbitrarily small norm on another prescribed part of a boundary. Analogous concepts have been introduced in [Geb08] for the Laplace equation, as well as in [HPS19b] and [GH18] for the Helmholtz equation on bounded and unbounded domains, respectively. We transfer these approaches to the problem we are concerned with and show the existence of the required localized wave functions.

Proceeding similarly, we advance toward the second problem. Here, we examine an **inverse electromagnetic scattering problem** where the wave propagation is governed by the time-

harmonic Maxwell equations. We assume that the scatterers are penetrable and non-absorbing. Moreover, we restrict ourselves to non-magnetic scatterers, i.e., the magnetic permeability is constant throughout the whole space. The real-valued electric permittivity is supposed to be constant outside the scatterer but may be inhomogeneous in its inside. As in the first situation we are interested in the reconstruction of the position and the shape of the scatterer which we again denote by D. The Linear Sampling Method (see, e.g., [HM02, CCM11]) as well as the Factorization Method (see, e.g., [Kir04, KG08]) have been utilized also against the background of Maxwell's equations. However, these only work under a definiteness assumption on the relative electric permittivity saying that it has either to be larger or smaller than one on the whole scatterer. The method proposed by us overcomes this assumption and thus applies to indefinite scatterers where the relative electric permittivity is allowed to take values smaller and larger than one inside the scatterer. To this end, we stick to a monotonicity-based ansatz and again develop criteria in terms of the far field operator corresponding to the scatterer D and certain probing operators corresponding to probing domains B that tell us whether B is contained within D or not and vice versa. Our results build on one side on a novel monotonicity relation for the magnetic far field operator. We prove a monotonicity property for the eigenvalues of the difference between two far field operators corresponding to two scatterers with different relative electric permittivities. On the other side, we need to show the existence of localized vector wave functions. These can be seen as the analog of the localized wave functions that we employ when studying the inverse acoustic obstacle scattering problem. More precisely, these are special solutions to the direct scattering problem that have arbitrarily large energy in some prescribed domain while at the same time having arbitrarily small energy in another prescribed domain. Recently, similar functions have been proposed in [HLL18] for Maxwell's equations on bounded domains.

The main contribution of this work is the development of a novel shape characterization in two different settings by exploiting monotonicity properties for the eigenvalues of suitable modifications of the underlying far field operators. Thereby, we primarily focus on a rigorous theoretical justification but nevertheless present some first numerical examples to underpin our findings.

1.2. On the Structure of this Thesis

This thesis is mainly divided into two parts. On the one hand, we investigate an inverse acoustic obstacle scattering problem governed by the Helmholtz equation in Chapter 2, and on the other hand, an inverse electromagnetic medium scattering problem governed by the Maxwell equations in Chapter 3. Both chapters begin with a section on some preliminary remarks where we introduce notation and some basic definitions of, for example, function spaces and operators. Having completed this preparatory work we are in the position to give a short overview of acoustic obstacle scattering in Section 2.2 and of electromagnetic medium scattering in Section 3.2, respectively. Thereby, we classify the scattering objects according to specific characteristics. When handling the inverse acoustic obstacle problem, these are Dirichlet, Neumann and mixed obstacles corresponding to the boundary conditions. When investigating the inverse electromagnetic medium scattering problem, we distinguish sign-definite and indefinite scatterers corresponding to the definiteness of the contrast function. In all cases, we aim to establish shape characterizations

of unknown scattering objects in terms of far field operators and certain probing operators. We always approach this goal employing a monotonicity-based reconstruction ansatz. However, the way of proceeding differs. In Chapter 2, we utilize factorizations of the considered far field operators that we present in Subsections 2.3.1 and 2.4.1. Combining these with (simultaneously) localized wave functions, established in Subsections 2.3.2 and 2.4.2, leads to the desired shape characterizations in Subsections 2.3.3 and 2.4.3. In Chapter 3, we begin with developing a monotonicity relation for the magnetic far field operator in Section 3.3 by using several integral identities. Afterward, we continue similarly as before by introducing (simultaneously) localized vector wave functions in Subsections 3.4.1 and 3.5.1. Again, the connection of these concepts provides the foundation for the shape characterizations in Subsections 3.4.2 and 3.5.2. Chapter 2, as well as Chapter 3, conclude with some numerical examples. Both times we examine radially symmetric scattering objects before developing sampling strategies for the simpler cases, i.e., Dirichlet or Neumann obstacles and sign-definite scatterers, respectively. In the end, we turn to the more involving mixed or indefinite scattering configurations and propose strategies that at least allow separating Dirichlet or Neumann obstacles in the acoustic as well as sign-definite components in the electromagnetic scenario. This work is completed in three appendices – in Appendix A, we investigate a special space of functions, in Appendix B, we collect some basic rules from vector and differential calculus, and in Appendix C, we summarize useful properties of spherical harmonics.

1.3. Prior Publications

The results of Chapter 2 and Chapter 3 have already been published in [AG20] and [AG23], respectively.

CHAPTER 2

Monotonicity in Inverse Obstacle Scattering for the Helmholtz Equation

2.1. Preliminaries

We begin by introducing some notation and various function spaces that we use throughout this work. Generic points in $\mathbb{R}^d$, $d = 2, 3$, are denoted by the Latin letters $\boldsymbol{x}, \boldsymbol{y}$ in bold. We write $\boldsymbol{x} \cdot \boldsymbol{y}$ for the Euclidean inner product of $\boldsymbol{x}$ and $\boldsymbol{y}$, and $|\boldsymbol{x}|$ is the corresponding norm of $\boldsymbol{x}$. By $B_R(\boldsymbol{x}) := \{\boldsymbol{y} \in \mathbb{R}^d \mid |\boldsymbol{x} - \boldsymbol{y}| < R\} \subseteq \mathbb{R}^d$ we denote the ball of radius $R > 0$ centered at $\boldsymbol{x} \in \mathbb{R}^d$, and $S^{d-1} := \{\boldsymbol{x} \in \mathbb{R}^d \mid |\boldsymbol{x}| = 1\}$ is the unit sphere in $\mathbb{R}^d$.

Let $\Omega \subseteq \mathbb{R}^d$ be an open, not necessarily bounded set. If Ω is also connected, we call it a *domain*, and we write $\widetilde{\Omega} \subset\subset \Omega$ if $\widetilde{\Omega}$ is compactly contained in Ω. As usual, we use the notation $C^j(\Omega)$, $j = 1, 2, \ldots$, for the space containing all complex-valued functions for which all partial derivatives up to order j exist in Ω and are continuous. For $j = 0$, $C^0(\Omega)$ is the set of continuous functions in Ω. We write $C_0^j(\Omega)$ for the space of functions in $C^j(\Omega)$ that have compact support in Ω, where the support of a function $u : \Omega \to \mathbb{C}$ is given by $\operatorname{supp} u := \overline{\{\boldsymbol{x} \in \Omega \mid u(\boldsymbol{x}) \neq 0\}}$. Then, the space $C^j(\overline{\Omega})$ contains all functions in $C^j(\mathbb{R}^d)$ restricted to Ω. Finally, we set $C^\infty(\Omega) := \cap_{j \in \mathbb{N}} C^j(\Omega)$. A function u on Ω is *uniformly Hölder continuous* with exponent $0 < \alpha \leq 1$ if there exists a constant $C > 0$ such that

$$|u(\boldsymbol{x}) - u(\boldsymbol{y})| \leq C|\boldsymbol{x} - \boldsymbol{y}|^\alpha \qquad \text{for all } \boldsymbol{x}, \boldsymbol{y} \in \Omega\,.$$

For $\alpha = 1$, we call u *Lipschitz continuous*. The *Hölder space* of all bounded and uniformly Hölder-continuous functions with exponent α on Ω is denoted by $C^{0,\alpha}(\Omega)$. Analogously, we define the Hölder space $C^{j,\alpha}(\Omega)$, $j = 1, 2, \ldots$, as the space of differentiable functions for which the gradient belongs to $C^{j-1,\alpha}(\Omega)$.

Further, the standard Lebesgue spaces are given by

$$L^p(\Omega) := \{u : \Omega \to \mathbb{C} \mid u \text{ is Lebesgue measurable and } \|u\|_{L^p(\Omega)} < \infty\}\,,$$

where

$$\|u\|_{L^p(\Omega)} := \begin{cases} \left(\int_\Omega |u(\boldsymbol{x})|^p \, \mathrm{d}\boldsymbol{x}\right)^{\frac{1}{p}}, & 1 \le p < \infty, \\ \operatorname{ess\,sup}_{\boldsymbol{x}\in\Omega} |u(\boldsymbol{x})|, & p = \infty. \end{cases}$$

The space $L^2(\Omega)$ is a Hilbert space equipped with the inner product

$$\langle u, v\rangle_{L^2(\Omega)} := \int_\Omega u(\boldsymbol{x})\overline{v(\boldsymbol{x})} \, \mathrm{d}\boldsymbol{x}, \qquad u, v \in L^2(\Omega). \tag{2.1}$$

For the sake of simplicity, we often omit the index and write $\langle \cdot, \cdot \rangle$ instead of $\langle \cdot, \cdot \rangle_{L^2(\Omega)}$. The local spaces $L^p_{\mathrm{loc}}(\Omega)$ contain all functions u such that $u|_{\widetilde{\Omega}} \in L^p(\widetilde{\Omega})$ for all compact subsets $\widetilde{\Omega}$ of Ω. Sometimes, we write $u = v$ for $u, v \in L^p(\Omega)$ which is always to be understood in the L^p sense meaning that $\|u - v\|_{L^p(\Omega)} = 0$.

Let $\boldsymbol{\alpha} := (\alpha_1, \ldots, \alpha_d)$, $\alpha_i \in \mathbb{N}$, be a multi-index of order $|\boldsymbol{\alpha}| := \alpha_1 + \ldots + \alpha_d$. We define the differential operator

$$\partial^{\boldsymbol{\alpha}} u := \frac{\partial^{|\boldsymbol{\alpha}|}}{\partial x_1^{\alpha_1} \cdots \partial x_d^{\alpha_d}} u.$$

As usual, $\partial^{\boldsymbol{\alpha}} u$ denotes the weak derivative of $u \in L^2(\Omega)$, i.e., we write $\partial^{\boldsymbol{\alpha}} u = v$ if $v \in L^2(\Omega)$ and

$$\langle \varphi, v\rangle = (-1)^{|\boldsymbol{\alpha}|} \langle \partial^{\boldsymbol{\alpha}} \varphi, u\rangle \qquad \text{for all } \varphi \in C_0^\infty(\Omega).$$

Then, the Sobolev space $H^j(\Omega)$, $j \in \mathbb{N}$, contains all functions $u \in L^2(\Omega)$ that possess weak derivatives $\partial^{\boldsymbol{\alpha}} u$ for all $|\boldsymbol{\alpha}| \le j$. Together with the inner product

$$\langle u, v\rangle_{H^j(\Omega)} := \sum_{|\boldsymbol{\alpha}|\le j} \langle \partial^{\boldsymbol{\alpha}} u, \partial^{\boldsymbol{\alpha}} v\rangle,$$

the space $H^j(\Omega)$ becomes a Hilbert space. For instance, we will use $H^1(\Omega)$ to set up boundary value problems on a bounded domain Ω. The local spaces $H^j_{\mathrm{loc}}(\Omega)$ are defined analogously to the local Lebesgue spaces. We utilize them when studying boundary value problems in the unbounded exterior of a domain. Finally, the Sobolev space $H^s(\Omega)$ of fractional order $s \in \mathbb{R}$, $s \ge 0$, is defined as the space containing all functions $u \in H^m(\Omega)$, where $s = m + \sigma$, $0 < \sigma < 1$, such that

$$\int_\Omega \int_\Omega \frac{|\partial^\alpha u(\boldsymbol{x}) - \partial^\alpha u(\boldsymbol{y})|^2}{|\boldsymbol{x} - \boldsymbol{y}|^{d+2\sigma}} \, \mathrm{d}\boldsymbol{x} \, \mathrm{d}\boldsymbol{y} < \infty.$$

In order to formulate boundary conditions in an appropriate way we require some regularity on the boundary. We call the boundary $\partial\Omega$ of a domain Ω C^j *smooth* if there exists a local parameterization of the boundary by C^j functions. More precisely, we assume that there exists a finite number of open cylinders

$$U_n := \{R_n \boldsymbol{x} + \boldsymbol{z}^{(n)} \mid \boldsymbol{x} \in B'_{r_n}(0) \times (-2s_n, 2s_n)\}, \qquad n = 1, \ldots, N, \tag{2.2}$$

where $B'_{r_n}(0) := \{\boldsymbol{x}' = (x_1, \ldots, x_{d-1}) \in \mathbb{R}^{d-1} \mid |\boldsymbol{x}'| \le r_n\} \subseteq \mathbb{R}^{d-1}$ is the $d-1$-dimensional ball of radius r_n centered at the origin, $\boldsymbol{z}^{(n)} \in \mathbb{R}^d$ is a translation vector and $R_n \in \mathbb{R}^{d\times d}$ a rotation. Furthermore, we assume that there are real-valued functions $\zeta_n \in C^j(\overline{B'_{r_n}(0)})$ with $|\zeta_n(\boldsymbol{x}')| \le s_n$

for all $\boldsymbol{x}' \in B'_{r_n}(0)$ such that

$$\begin{aligned}
\partial\Omega &\subseteq \cup_{n=1}^{N} U_n\,,\\
\partial\Omega \cap U_n &= \{R_n\boldsymbol{x} + \boldsymbol{z}^{(n)} \mid \boldsymbol{x}' \in B'_{r_n}(0)\,,\ x_d = \zeta_n(\boldsymbol{x}')\}\,,\\
\Omega \cap U_n &= \{R_n\boldsymbol{x} + \boldsymbol{z}^{(n)} \mid \boldsymbol{x}' \in B'_{r_n}(0)\,,\ x_d < \zeta_n(\boldsymbol{x}')\}\,,\\
U_n \setminus \overline{\Omega} &= \{R_n\boldsymbol{x} + \boldsymbol{z}^{(n)} \mid \boldsymbol{x}' \in B'_{r_n}(0)\,,\ x_d > \zeta_n(\boldsymbol{x}')\}\,.
\end{aligned}$$

Analogously, we say that $\partial\Omega$ is $C^{j,\alpha}$ *smooth* if the functions ζ_n are in $C^{j,\alpha}(\overline{B'_{r_n}(0)})$. In the special case when $j = 0$ and $\alpha = 1$, i.e., when the functions ζ_n are Lipschitz continuous, we call Ω *Lipschitz bounded*. Using the local coordinate system $\{(U_n, \zeta_n) \mid n = 1, \dots, N\}$ one can define the spaces $L^p(\partial\Omega)$, $C^j(\partial\Omega)$ and $C^{j,\alpha}(\partial\Omega)$ on the boundary $\partial\Omega$ (for more details, see, e.g., [KH15, Def. A.14]). For $p = 2$, we use the notation $\langle\,\cdot\,,\,\cdot\,\rangle_{L^2(\partial\Omega)}$ for the inner product in $L^2(\partial\Omega)$.

Rademacher's theorem (see, e.g., [EG92, p. 81]) guarantees that every Lipschitz-continuous function ζ_n is differentiable almost everywhere with $\|\nabla\zeta_n\|_{L^\infty(\mathbb{R}^{d-1})} \le L$, where L is the Lipschitz constant. Thus, if Ω has a Lipschitz boundary the *exterior unit normal* $\nu(\boldsymbol{x})$ exists in almost every $\boldsymbol{x} \in \partial\Omega$. In the following, we shall therefore always assume Ω to be Lipschitz bounded.

Next, we clarify how boundary values of Sobolev functions are to be understood. For $u \in C^\infty(\overline{\Omega})$, the restriction $u|_{\partial\Omega}$ of u to the boundary $\partial\Omega$ is called the *trace* of u, and it is well defined. We introduce the *trace operator*

$$\gamma : C^\infty(\overline{\Omega}) \to L^2(\partial\Omega)\,, \quad \gamma u := u|_{\partial\Omega}\,.$$

Then, γ has a bounded extension that maps from $H^1(\Omega)$ to $H^{1/2}(\partial\Omega)$ (see, e.g., [Mon03, Thm. 3.9]). Moreover, this operator has a bounded right inverse $\eta : H^{1/2}(\partial\Omega) \to H^1(\Omega)$, i.e., $\gamma(\eta f) = f$ for all $f \in H^{1/2}(\partial\Omega)$ (see, e.g., [KH15, Thm. 5.10]). The norm on the range space

$$H^{1/2}(\partial\Omega) = \{f \in L^2(\partial\Omega) \mid \text{there exists } u \in H^1(\Omega) \text{ such that } f = u|_{\partial\Omega}\}$$

is given by

$$\|f\|_{H^{1/2}(\partial\Omega)} := \inf\{\|u\|_{H^1(\Omega)} \mid u \in H^1(\Omega) \text{ with } \gamma u = f\}\,.$$

We denote the dual space of $H^{1/2}(\partial\Omega)$ by $H^{-1/2}(\partial\Omega)$. Besides, we define the duality pairing $\langle\,\cdot\,,\,\cdot\,\rangle_{H^{-1/2}(\partial\Omega)\times H^{1/2}(\partial\Omega)}$ between $H^{-1/2}(\partial\Omega)$ and $H^{1/2}(\partial\Omega)$. For better readability, we usually use the shorter notation $\langle\,\cdot\,,\,\cdot\,\rangle_{\partial\Omega}$. The duality pairing extends the inner product (2.1) on $L^2(\partial\Omega)$, i.e.,

$$\langle g, f\rangle_{\partial\Omega} = \int_{\partial\Omega} g(\boldsymbol{x})\overline{f(\boldsymbol{x})}\,\mathrm{d}\boldsymbol{x} \qquad \text{for all } f \in H^{1/2}(\partial\Omega)\,,\ g \in H^{-1/2}(\partial\Omega) \cap L^2(\partial\Omega)\,.$$

Furthermore, we require trace spaces $H^s(\partial\Omega)$ for $s > 1$. These can be defined via

$$H^s(\partial\Omega) := \{f \in L^2(\partial\Omega) \mid \text{there exists } u \in H^{s+1/2}(\Omega) \text{ such that } f = u|_{\partial\Omega}\}\,.$$

Now, we introduce the trace $\partial u/\partial\boldsymbol{\nu}$, where $\boldsymbol{\nu}$ is again the exterior unit normal. If $u \in C^2(\overline{\Omega})$ and

$v \in H^1(\Omega)$, Green's first theorem (see, e.g., [KH15, Thm. A.12]) yields

$$\int_{\partial\Omega} \frac{\partial u}{\partial \boldsymbol{\nu}} v \, \mathrm{d}s \;=\; \int_{\Omega} (v\Delta u + \nabla u \cdot \nabla v) \, \mathrm{d}\boldsymbol{x}\,,$$

where $\partial u(\boldsymbol{x})/\partial\boldsymbol{\nu} := \boldsymbol{\nu}(\boldsymbol{x}) \cdot \nabla u(\boldsymbol{x})$ denotes the *normal derivative* of u in $\boldsymbol{x} \in \partial\Omega$. This motivates the definition of the *normal derivative trace operator* γ_n via the duality pairing

$$\langle \gamma_n u, \varphi \rangle_{\partial\Omega} \;:=\; \int_{\Omega} (v\Delta u + \nabla u \cdot \nabla v) \, \mathrm{d}\boldsymbol{x}\,, \qquad \varphi \in H^{1/2}(\partial\Omega)\,,$$

with $v \in H^1(\Omega)$, $\varphi \in H^{1/2}(\partial\Omega)$ such that $\gamma v = \varphi$. Let $H^1_\Delta(\Omega) := \{u \in H^1(\Omega) \mid \Delta u \in L^2(\Omega)\}$ and $\|u\|_{H^1_\Delta(\Omega)} := \|u\|_{H_1(\Omega)} + \|\Delta u\|_{L^2(D)}$. Then, γ_n can be extended to a bounded linear operator from $H^1_\Delta(\Omega)$ to $H^{-1/2}(\partial\Omega)$ (see, e.g., [KH15, Thm. 5.17]).

Throughout, we make use of several embedding results. If $-\infty \le t < s < \infty$, then the space $H^s(\Omega)$ is compactly embedded in $H^t(\Omega)$ (see, e.g., [McL00, Thm. 3.27]), and we use the notation $J : H^s(\Omega) \hookrightarrow H^t(\Omega)$ for the compact embedding operator. This means that J is the identity map from $H^s(\Omega)$ to $H^t(\Omega)$, and it is compact. The compact embedding property carries over to the trace spaces $H^s(\partial\Omega)$, $H^t(\partial\Omega)$ (see, e.g., [KH15, Thm. 5.6]), and we again denote the compact embedding operator by J. In addition, the space $H^{1/2}(\partial\Omega)$ is compactly embedded in $L^2(\partial\Omega)$ (see, e.g., [KH15, Cor. 5.9]).

Finally, we require Sobolev spaces over only a part of the boundary $\partial\Omega$. Let $\Gamma \subseteq \partial\Omega$ be relatively open. That is, $\Gamma = \partial\Omega \cap O$ for some open set $O \subseteq \mathbb{R}^d$. Then, we define the Sobolev spaces

$$H^{1/2}(\Gamma) \;:=\; \{\varphi|_\Gamma \mid \varphi \in H^{1/2}(\partial\Omega)\}\,, \tag{2.3a}$$

$$\widetilde{H}^{1/2}(\Gamma) \;:=\; \{\varphi \in H^{1/2}(\partial\Omega) \mid \operatorname{supp}\varphi \subseteq \overline{\Gamma}\}\,. \tag{2.3b}$$

Further, we denote the dual spaces of $H^{1/2}(\Gamma)$ and $\widetilde{H}^{1/2}(\Gamma)$ by $\widetilde{H}^{-1/2}(\Gamma)$ and $H^{-1/2}(\Gamma)$, respectively.

Without loss of generality, we assume that

$$\Gamma \;=\; \{\boldsymbol{x} \in \mathbb{R}^d \mid x_d = \zeta(\boldsymbol{x}') \text{ for all } \boldsymbol{x}' = (x_1, \ldots, x_{d-1}) \in B'_r(0) \subseteq \mathbb{R}^{d-1}\} \tag{2.4}$$

for some function $\zeta : \mathbb{R}^{d-1} \to \mathbb{R}$. Otherwise, we rotate and translate our coordinate system appropriately and repeat this procedure for all of the cylinders U_n, $n = 1, \ldots, N$, from (2.2). If Γ is C^j smooth, ζ is a C^j function. Furthermore, we call a function u *piecewise linear* on Γ, if the function u_ζ given by

$$u_\zeta(\boldsymbol{x}') \;:=\; u(\boldsymbol{x}', \zeta(\boldsymbol{x}'))\,, \qquad \boldsymbol{x}' \in B'_r(0)\,, \tag{2.5}$$

is piecewise linear on $B'_r(0) \subseteq \mathbb{R}^{d-1}$. In Appendix A, we show some properties of a special subspace of continuous piecewise linear functions.

Let $A : X \to Y$ be a linear operator. We denote by $\mathcal{R}(A) \subseteq Y$ and $\mathcal{N}(A) \subseteq X$ the range and the null space of A, respectively. Besides, we use the notation A^* for the adjoint operator of A. For better readability, we write $\|A\| := \|A\|_{X\to Y}$ for the operator norm of A. The real part of a linear operator $A : X \to X$ on a Hilbert space X is the self-adjoint operator defined by

$\mathrm{Re}(A) := \frac{1}{2}(A + A^*)$. We use the notation

$$\begin{bmatrix} A_1 \\ A_2 \end{bmatrix} \phi := \begin{bmatrix} A_1\phi \\ A_2\phi \end{bmatrix} \qquad \text{for all } \phi \in X\,, \tag{2.6}$$

if both operators $A_1 : X \to Y$ and $A_2 : X \to Z$ have the same domain of definition.

Remark 2.1. If $A : X \to X$ is a compact and self-adjoint linear operator on a Hilbert space X with inner product $\langle \cdot, \cdot \rangle_X$, then there holds the *spectral theorem for compact self-adjoint operators* (see, e.g., [McL00, Thm. 2.36]). It states that there exist sequences of real eigenvalues $\lambda_1, \lambda_2, \ldots$ with $|\lambda_1| \geq |\lambda_2| \geq \cdots > 0$ and corresponding orthonormal eigenvectors $\phi_1, \phi_2, \ldots$ in X, i.e., $A\phi_i = \lambda_i \phi_i$ and $\phi_i \neq 0$, $i = 1, 2, \ldots$. The sequences are either finite or infinite but converging to zero. It is

$$A\phi \;=\; \sum_{i \geq 1} \lambda_i \langle \phi, \phi_i \rangle_X \phi_i \qquad \text{for all } \phi \in X\,,$$

which converges in X if the sequences are infinite. Moreover, we have

$$X \;=\; \overline{\mathrm{span}\{\phi_1, \phi_2, \ldots\}} \oplus \mathcal{N}(A)\,,$$

where $\oplus$ stands for the direct sum. If we complement $\{\phi_1, \phi_2, \ldots\}$ by an orthonormal basis of $\mathcal{N}(A)$, which means that we add eigenvectors corresponding to the eigenvalue zero, we obtain a complete orthonormal system of X. ◊

Now, let $A_1, A_2 : X \to X$ be compact self-adjoint linear operators on a Hilbert space X, and let $r \in \mathbb{N}$. We follow [HPS19b] and say

$$A_1 \;\leq_r\; A_2\,, \tag{2.7}$$

if $A_2 - A_1$ has at most r negative eigenvalues. For $r = 0$, we get the standard Loewner order which is a partial order for compact self-adjoint operators according to the operator definiteness. Similarly, we write $A_1 \leq_{\mathrm{fin}} A_2$ if $A_1 \leq_r A_2$ holds for some $r \in \mathbb{N}$, and the notations $A_1 \geq_r A_2$ and $A_1 \geq_{\mathrm{fin}} A_2$ are defined in the same way.

In [HPS19b, Cor. 3.3], using the spectral theorem and the min-max theorem the authors establish a useful characterization of (2.7) that we cite in the next lemma.

Lemma 2.2. *Let $A_1, A_2 : X \to X$ be two compact self-adjoint linear operators on a Hilbert space X with inner product $\langle \cdot, \cdot \rangle_X$, and let $r \in \mathbb{N}$. Then, the following statements are equivalent:*

(a) $A_1 \leq_r A_2$.

(b) There exists a finite-dimensional subspace $V \subseteq X$ with $\dim(V) \leq r$ *such that*

$$\langle (A_2 - A_1)v, v \rangle_X \;\geq\; 0 \qquad \textit{for all } v \in V^\perp\,.$$

Remark 2.3. The proof of Lemma 2.2 carries over to complex Hilbert spaces. ◊

From Lemma 2.2, it follows that $\leq_{\mathrm{fin}}$ and $\geq_{\mathrm{fin}}$ are transitive relations (see, e.g., [HPS19b, Lem. 3.4]). Since $\leq_{\mathrm{fin}}$ and $\geq_{\mathrm{fin}}$ are reflexive, these are preorders.

2.2. Acoustic Scattering by Impenetrable Obstacles

After having established the function spaces and some further notation that we require, we give an introduction to the scattering of time-harmonic acoustic waves. Thereby, we focus on relevant results for the theory we build below. First, we give a short derivation of the Helmholtz equation summarizing the physical motivations from the textbooks [CK19, KG08].

Sound waves are modeled as small perturbations in a medium like gas or fluid, and their propagation in a homogeneous medium is governed by the *wave equation*

$$\frac{1}{c_0^2}\frac{\partial^2 p(\boldsymbol{x},t)}{\partial t^2} \;=\; \Delta_{\boldsymbol{x}} p(\boldsymbol{x},t)\,, \qquad \boldsymbol{x}\in\mathbb{R}^3\,,\, t>0\,, \tag{2.8}$$

where p is the *pressure* and c_0 the *speed of sound*. The velocity of the gas or fluid is proportional to the gradient of the pressure. Time-harmonic solutions to the wave equation are of the form

$$p(\boldsymbol{x},t) \;=\; \mathrm{Re}\left(u(\boldsymbol{x})e^{-\mathrm{i}\omega t}\right)$$

with complex-valued *amplitude* u and *frequency* $\omega>0$. Substituting this into (2.8) we conclude that the space-dependent function u is a solution to the *Helmholtz equation*

$$\Delta u + k^2 u \;=\; 0 \qquad \text{in } \mathbb{R}^3\,.$$

The positive constant $k := \omega/c_0$ is called *wave number*.

Furthermore, we examine the Helmholtz equation in two dimensions, i.e., for $d=2$. The underlying physical concept is the scattering from infinite cylinders in $\mathbb{R}^3$ which results in exterior boundary value problems for the two-dimensional Helmholtz equation. Besides, we stick to two dimensions when presenting our numerical examples in Section 2.5.

We concentrate on the scattering of time-harmonic scalar waves in an unbounded homogeneous background by a collection $D\subseteq\mathbb{R}^d$ of obstacles. The wave motion is caused by an *incident field* u^i that satisfies the Helmholtz equation

$$\Delta u^i + k^2 u^i \;=\; 0 \qquad \text{in } \mathbb{R}^d$$

and is scattered by the obstacle D. This gives rise to the *scattered field* u^s. Then, the superposition $u=u^i+u^s$, which is called the *total field*, is a solution to

$$\Delta u + k^2 u \;=\; 0 \qquad \text{in } \mathbb{R}^d\setminus\overline{D}\,.$$

We assume that the incident field cannot penetrate into the scatterers and therefore call these scatterers *impenetrable*. We consider a collection D of obstacles that can be divided into a *sound-soft* part D_1 and a *sound-hard* part D_2 that both may consist of finitely many connected components. Scattering from sound-soft obstacles leads to a Dirichlet boundary condition $u=0$ on the boundary ∂D_1, because in this case, the total pressure vanishes on the boundary. For sound-hard obstacles, the normal component of the total velocity vanishes on the boundary ∂D_2. This gives a Neumann boundary condition $\partial u/\partial\boldsymbol{\nu}=0$ on ∂D_2. According to the boundary conditions, we refer to D_1 as *Dirichlet obstacles* and to D_2 as *Neumann obstacles*. In addition,

one could also consider *impedance boundary conditions*, where $\partial u/\partial \boldsymbol{\nu} + \mathrm{i}\lambda u = 0$ with a positive constant λ on the boundary. However, we focus on sound-soft and sound-hard obstacles. In the following, D is always supposed to be open and Lipschitz bounded. We assume that the Dirichlet and the Neumann parts of the scatterer have disjoint closures, i.e., $\overline{D_1} \cap \overline{D_2} = \emptyset$, and that the complement $\mathbb{R}^d \setminus \overline{D}$ is connected. Moreover, we assume that the scattered field satisfies the *Sommerfeld radiation condition*

$$\lim_{r\to\infty} r^{\frac{d-1}{2}} \Big(\frac{\partial u^s}{\partial r}(\boldsymbol{x}) - \mathrm{i}k u^s(\boldsymbol{x}) \Big) \;=\; 0\,, \qquad r = |\boldsymbol{x}|\,, \tag{2.9}$$

uniformly with respect to all directions $\widehat{\boldsymbol{x}} := \boldsymbol{x}/|\boldsymbol{x}| \in S^{d-1}$. This condition guarantees that the scattered waves are outgoing. For example, there exist two spherically symmetric solutions $e^{\pm \mathrm{i}k|\boldsymbol{x}|}/|\boldsymbol{x}|$ to the Helmholtz equation but only the one with the positive sign fulfills the radiation condition. We refer to solutions to the Helmholtz equation in the connected complement $\mathbb{R}^d \setminus \overline{D}$ that satisfy the Sommerfeld radiation condition uniformly with respect to all directions as *radiating solutions*.

The function

$$\Phi_k(\boldsymbol{x},\boldsymbol{y}) \;:=\; \begin{cases} \dfrac{\mathrm{i}}{4} H_0^{(1)}(k|\boldsymbol{x}-\boldsymbol{y}|)\,, & \boldsymbol{x} \neq \boldsymbol{y}\,, \quad d = 2\,, \\[2ex] \dfrac{1}{4\pi} \dfrac{e^{\mathrm{i}k|\boldsymbol{x}-\boldsymbol{y}|}}{|\boldsymbol{x}-\boldsymbol{y}|}\,, & \boldsymbol{x} \neq \boldsymbol{y}\,, \quad d = 3\,, \end{cases}$$

is called the *fundamental solution* to the Helmholtz equation. Here, $H_0^{(1)}$ denotes the Hankel function of the first kind of order zero. For fixed $\boldsymbol{y} \in \mathbb{R}^d$, the fundamental solution solves the Helmholtz equation in $\mathbb{R}^d \setminus \{\boldsymbol{y}\}$, and it is radiating.

Solutions to the Helmholtz equation that are defined in all of $\mathbb{R}^d$ are known as *entire solutions*. Applying Green's representation theorem (see, e.g., [KH15, Thm. 3.3]) together with Green's second identity (see, e.g., [KH15, Thm. A.12]) shows the next lemma.

Lemma 2.4. *Every entire solution to the Helmholtz equation that satisfies the Sommerfeld radiation condition* (2.9) *must vanish identically.*

One class of entire solutions to the Helmholtz equation is given by

$$u^i(\boldsymbol{x},\boldsymbol{\theta}) \;:=\; e^{\mathrm{i}k\boldsymbol{x}\cdot\boldsymbol{\theta}}\,, \qquad \boldsymbol{x} \in \mathbb{R}^d\,,\, \boldsymbol{\theta} \in S^{d-1}\,.$$

These are called *plane waves* with *incident direction* $\boldsymbol{\theta}$ because the corresponding time-dependent waves $\mathrm{Re}\,(e^{\mathrm{i}k\boldsymbol{x}\cdot\boldsymbol{\theta} - \mathrm{i}\omega t})$ are constant on the lines ($d = 2$) or planes ($d = 3$), respectively, which are given by $\{k\boldsymbol{x}\cdot\boldsymbol{\theta} - \omega t = C \mid \boldsymbol{x} \in \mathbb{R}^d,\, t > 0,\, C \in \mathbb{R}\}$, and the wavefronts propagate in direction $\boldsymbol{\theta}$. The superposition

$$u^i_\phi(\boldsymbol{x}) \;:=\; \int_{S^{d-1}} u^i(\boldsymbol{x},\boldsymbol{\theta})\phi(\boldsymbol{\theta})\,\mathrm{d}s(\boldsymbol{\theta}) \;=\; \int_{S^{d-1}} e^{\mathrm{i}k\boldsymbol{x}\cdot\boldsymbol{\theta}}\phi(\boldsymbol{\theta})\,\mathrm{d}s(\boldsymbol{\theta})\,, \qquad \boldsymbol{x} \in \mathbb{R}^d\,, \tag{2.10}$$

is referred to as *Herglotz wave function* with density $\phi \in L^2(S^{d-1})$.

For a given incident field u^i, the problem of finding a scattered field u^s that satisfies the Helmholtz equation in the exterior of a given domain D together with the Sommerfeld radiation

condition such that the total field fulfills the boundary conditions on $\partial D = \partial D_1 \cup \partial D_2$ is known as the *direct scattering problem*. Choosing $f = -u^i|_{\partial D_1}$ and $g = -\partial u^i/\partial \boldsymbol{\nu}|_{\partial D_2}$ we find that u^s solves the following exterior mixed boundary value problem:

$$\begin{aligned} \Delta w + k^2 w &= 0 && \text{in } \mathbb{R}^d \setminus (\overline{D_1 \cup D_2})\,, && \text{(2.11a)} \\ w &= f && \text{on } \partial D_1\,, && \text{(2.11b)} \\ \frac{\partial w}{\partial \boldsymbol{\nu}} &= g && \text{on } \partial D_2\,, && \text{(2.11c)} \\ \lim_{r\to\infty} r^{\frac{d-1}{2}} \Big(\frac{\partial w}{\partial r}(\boldsymbol{x}) - \mathrm{i}kw(\boldsymbol{x})\Big) &= 0\,, && r = |\boldsymbol{x}|\,, && \text{(2.11d)} \end{aligned}$$

uniformly with respect to $\widehat{\boldsymbol{x}} \in S^{d-1}$. The solution to this boundary value problem is to be understood in the variational sense. To be more precise, $w \in H^1_{\mathrm{loc}}(\mathbb{R}^d)$ is called *variational solution* to (2.11a)–(2.11c) if $w|_{\partial D_1} = f$ in the sense of traces, and it holds

$$\int_{\mathbb{R}^d \setminus \overline{D}} (\nabla w \cdot \nabla \overline{\varphi} - k^2 w \overline{\varphi})\, \mathrm{d}\boldsymbol{x} = -\langle g, \varphi \rangle_{\partial D_2} \tag{2.12}$$

for all $\varphi \in H^1(\mathbb{R}^d \setminus \overline{D})$ with compact support and $\varphi|_{\partial D_1} = 0$ in the sense of traces.

Remark 2.5. In the special case when $D_2 = \emptyset$, i.e., when only Dirichlet obstacles are present, (2.11) reduces to the *exterior Dirichlet boundary value problem*. Analogously, if $D_1 = \emptyset$, i.e., when only Neumann obstacles are present, then (2.11) reduces to the *exterior Neumann boundary value problem*. ◊

The next theorem states existence and uniqueness of solutions to the exterior mixed boundary value problem.

Theorem 2.6. *For every $f \in H^{1/2}(\partial D_1)$ and $g \in H^{-1/2}(\partial D_2)$, the exterior mixed boundary value problem* (2.11) *has a unique solution $w \in H^1_{\mathrm{loc}}(\mathbb{R}^d)$ in the sense of* (2.12).

Proof. Uniqueness is shown in [McL00, Thm. 9.10]. Moreover, in [McL00, Thm. 7.15 (iii)], the author proves the equivalence of the exterior mixed boundary value problem to a system of boundary integral equations, for which the Fredholm alternative is valid (see, e.g., [McL00, Thm. 7.10]). Therewith, one can proceed as in [McL00, Thm. 9.11], where the exterior Dirichlet boundary value problem is treated, to get existence. □

Remark 2.7. Interior regularity results (see, e.g., [GT01, Thm. 8.10]) yield that every solution to the boundary value problem (2.11a)–(2.11c) is in $C^\infty(\mathbb{R}^d \setminus \overline{D})$. Therefore, the Sommerfeld radiation condition is well defined. It can be shown that the solutions are even analytic in the exterior of D (see, e.g., [KH15, Thm. 3.4]). ◊

Now, we have a closer look at the behavior of radiating solutions to the Helmholtz equation at great distances from the scatterer. The following lemma shows that, far away from the scatterer, the scattered field is asymptotically an outgoing spherical wave.

Lemma 2.8. *Let D be open and Lipschitz bounded such that $\mathbb{R}^d\setminus\overline{D}$ is connected. If $u^s \in C^2(\mathbb{R}^d\setminus\overline{D})$ is a radiating solution to the Helmholtz equation in $\mathbb{R}^d \setminus \overline{D}$, then it has the asymptotic behavior*

$$u^s(\boldsymbol{x}) \;=\; C_d \frac{e^{\mathrm{i}k|\boldsymbol{x}|}}{|\boldsymbol{x}|^{\frac{d-1}{2}}} u^\infty(\widehat{\boldsymbol{x}}) + \mathcal{O}(|\boldsymbol{x}|^{-\frac{d+1}{2}})\,, \qquad |\boldsymbol{x}| \to \infty\,,$$

uniformly in all directions $\widehat{\boldsymbol{x}} \in S^{d-1}$, where

$$C_d \;=\; e^{\mathrm{i}\pi/4}/\sqrt{8\pi k}\,, \quad \text{if } d=2 \qquad \text{and} \qquad C_d \;=\; 1/(4\pi)\,, \quad \text{if } d=3\,, \tag{2.13}$$

and $u^\infty \in L^2(S^{d-1})$ is called the acoustic far field pattern *of u.*

Proof. For $d = 3$, a proof can be found in [CK19, Thm. 2.6]. For $d = 2$, we refer to [CK19, Sec. 3.5]. □

The following lemma is known as Rellich's lemma. It indicates that the correspondence between radiating waves and the corresponding far field patterns is one-to-one.

Lemma 2.9 (Rellich)**.** *Let D be open and Lipschitz bounded such that $\mathbb{R}^d \setminus \overline{D}$ is connected. If $u^s \in C^2(\mathbb{R}^d \setminus \overline{D})$ is a radiating solution to the Helmholtz equation in $\mathbb{R}^d \setminus \overline{D}$, and the corresponding far field pattern fulfills $u^\infty \equiv 0$, then u vanishes identically in $\mathbb{R}^d \setminus \overline{D}$.*

Proof. This is shown in [CK19, Thm. 2.14]. □

If the incoming field is a plane wave, we indicate the dependence of the far field pattern on the incident direction $\boldsymbol{\theta} \in S^{d-1}$ of this incoming plane wave $u^i(\,\cdot\,;\boldsymbol{\theta})$ by a second argument, and accordingly, we write $u^\infty(\,\cdot\,;\boldsymbol{\theta})$. The problem of identifying the obstacle D from the knowledge of the far field patterns $u^\infty(\widehat{\boldsymbol{x}};\boldsymbol{\theta})$ for all $\widehat{\boldsymbol{x}},\boldsymbol{\theta} \in S^{d-1}$ is called the *inverse scattering problem.*

The far field patterns define the *acoustic far field operator* via

$$F_D^{\mathrm{mix}} :\, L^2(S^{d-1}) \to L^2(S^{d-1})\,, \quad (F_D^{\mathrm{mix}}\,\phi)(\widehat{\boldsymbol{x}}) \;:=\; \int_{S^{d-1}} u^\infty(\widehat{\boldsymbol{x}};\boldsymbol{\theta})\phi(\boldsymbol{\theta})\,\mathrm{d}s(\boldsymbol{\theta})\,. \tag{2.14}$$

We see that this integral operator maps superpositions of incident plane waves to the far field patterns of the corresponding scattered waves. The operator F_D^{mix} is compact from $L^2(S^{d-1})$ to $L^2(S^{d-1})$ since its kernel is analytic in both variables (see, e.g., [Kre14, Thm. 2.28]). Furthermore, F_D^{mix} is normal (see, e.g., [KG08, Thm. 3.3]). Moreover, we define the *acoustic scattering operator* by

$$\mathcal{S}_D^{\mathrm{mix}} \;:=\; I + 2\mathrm{i}k|C_d|^2 F_D^{\mathrm{mix}} :\, L^2(S^{d-1}) \to L^2(S^{d-1})\,,$$

where C_d is again the constant from (2.13). The operator $\mathcal{S}_D^{\mathrm{mix}}$ is unitary implying that the eigenvalues of $\mathcal{S}_D^{\mathrm{mix}}$ lie on the unit circle (see, e.g., [KG08, Thm. 3.3]). Consequently, the eigenvalues of F_D^{mix} lie on the circle of radius $1/(2k|C_d|^2)$ centered at $\mathrm{i}/(2k|C_d|^2)$ in the complex plane.

Remark 2.10. In the special case when only Dirichlet obstacles are present, i.e., when $D_2 = \emptyset$, we denote the corresponding far field operator by $F_{D_1}^{\mathrm{dir}}$. Similarly, when only Neumann obstacles are present, i.e., when $D_1 = \emptyset$, we use the notation $F_{D_2}^{\mathrm{neu}}$ for the corresponding far field operator. ♢

Throughout this work, it is our goal to derive characterizations of the shape and position of unknown obstacles in terms of far field operators. We approach this *shape identification problem* utilizing a monotonicity-based reconstruction ansatz. Initially, we examine scatterers that consist solely of a Dirichlet or a Neumann part, before moving on to mixed scatterers.

2.3. Dirichlet or Neumann Obstacles

In this section, we consider the case when either only Dirichlet or Neumann obstacles are present. We work toward a monotonicity-based shape characterization that we present in Subsection 2.3.3. Beforehand, we derive factorizations for the far field operators $F_{D_1}^{\mathrm{dir}}$ and $F_{D_2}^{\mathrm{neu}}$ in Subsection 2.3.1 and establish the concept of localized wave functions in Subsection 2.3.2.

2.3.1. Factorizations of the Far Field Operators

We aim to better understand the correspondence between the far field operators and the obstacles. Therefore, we recall two factorizations of the far field operators $F_{D_1}^{\mathrm{dir}}$ and $F_{D_2}^{\mathrm{neu}}$ that are of the form

$$F = GTG^*$$

with some compact operator G and an isomorphism T. These factorizations have been used in the traditional Factorization Method (compare, e.g., [Kir98, KG08]), and we apply it to develop the shape characterization results in Subsection 2.3.3 below.

We define *data-to-pattern operators* that map boundary data to the corresponding far field patterns. They are given by

$$G_{D_1}^{\mathrm{dir}} : H^{1/2}(\partial D_1) \to L^2(S^{d-1}), \quad G_{D_1}^{\mathrm{dir}} f := w^{\mathrm{dir},\infty}, \tag{2.15a}$$

$$G_{D_2}^{\mathrm{neu}} : H^{-1/2}(\partial D_2) \to L^2(S^{d-1}), \quad G_{D_2}^{\mathrm{neu}} g := w^{\mathrm{neu},\infty}, \tag{2.15b}$$

where $w^{\mathrm{dir},\infty}$ is the far field pattern of the unique radiating solution to the exterior Dirichlet boundary value problem (2.11a) and (2.11b), and $w^{\mathrm{neu},\infty}$ the far field pattern of the unique radiating solution to the exterior Neumann boundary value problem (2.11a) and (2.11c).

Theorem 2.11. *The operators $G_{D_1}^{\mathrm{dir}}$ and $G_{D_2}^{\mathrm{neu}}$ are compact and one-to-one with dense ranges in $L^2(S^{d-1})$.*

Proof. For a proof, we refer to [KG08, Lem. 1.13 and Thm. 1.26 (b)]. □

We introduce the surface potentials

$$(\mathrm{SL}_{D_1}\varphi)(\boldsymbol{x}) := \int_{\partial D_1} \Phi_k(\boldsymbol{x},\boldsymbol{y})\varphi(\boldsymbol{y})\, \mathrm{d}s(\boldsymbol{y}), \qquad \boldsymbol{x} \in \mathbb{R}^d \setminus \partial D_1, \tag{2.16}$$

$$(\mathrm{DL}_{D_2}\psi)(\boldsymbol{x}) := \int_{\partial D_2} \frac{\partial \Phi_k}{\partial \boldsymbol{\nu}(\boldsymbol{y})}(\boldsymbol{x},\boldsymbol{y})\psi(\boldsymbol{y})\, \mathrm{d}s(\boldsymbol{y}), \qquad \boldsymbol{x} \in \mathbb{R}^d \setminus \partial D_2, \tag{2.17}$$

for $\varphi \in H^{-1/2}(\partial D_1)$ and $\psi \in H^{1/2}(\partial D_2)$. As usual, we call SL_{D_1} *single layer potential* and DL_{D_2} *double layer potential* with densities φ and ψ, respectively. Please note that the integral (2.16)

is to be understood in the dual system $\langle H^{-1/2}(\partial D_1), H^{1/2}(\partial D_1)\rangle$. Taking the traces of these potentials gives rise to bounded linear operators (see, e.g., [McL00, Thm. 6.11]). The *single layer operator* is defined by

$$S_{D_1} : H^{-1/2}(\partial D_1) \to H^{1/2}(\partial D_1), \quad (S_{D_1}\varphi)(\boldsymbol{x}) := \int_{\partial D_1} \Phi_k(\boldsymbol{x},\boldsymbol{y})\varphi(\boldsymbol{y})\, \mathrm{d}s(\boldsymbol{y}) \tag{2.18}$$

for $\boldsymbol{x} \in \partial D_1$, and the *hypersingular operator* is defined by

$$N_{D_2} : H^{1/2}(\partial D_2) \to H^{-1/2}(\partial D_2), \quad (N_{D_2}\psi)(\boldsymbol{x}) := \frac{\partial}{\partial \boldsymbol{\nu}} \int_{\partial D_2} \frac{\partial \Phi_k}{\partial \boldsymbol{\nu}(\boldsymbol{y})}(\boldsymbol{x},\boldsymbol{y})\psi(\boldsymbol{y})\, \mathrm{d}s(\boldsymbol{y}) \tag{2.19}$$

for $\boldsymbol{x} \in \partial D_2$. This classical notation in the definition of N_{D_2} makes only sense for densities in $C^{1,\alpha}(\partial D_2)$, $0 < \alpha \leq 1$, and N_{D_2} should be interpreted as the bounded extension operator.

Later, we will observe that the operator T appearing in the middle of the factorization is strongly related to the boundary integral operators (2.18) and (2.19). Before establishing the factorizations we summarize some useful properties of the single layer operator S_{D_1}. By $S_{D_1,\mathrm{i}}$ we denote the single layer operator corresponding to the wave number $k = \mathrm{i}$.

Theorem 2.12.

(a) If k^2 is not a Dirichlet eigenvalue of $-\Delta$ in D_1, i.e., there does not exist a non-trivial solution u to the Helmholtz equation $\Delta u + k^2 u = 0$ in D_1 such that u vanishes on the boundary ∂D_1, then S_{D_1} is an isomorphism from $H^{-1/2}(\partial D_1)$ to $H^{1/2}(\partial D_1)$.

(b) The operator $S_{D_1,\mathrm{i}}$ is self-adjoint and coercive, i.e., there exists a constant $c_1 > 0$ such that

$$\langle \varphi, S_{D_1,\mathrm{i}}\varphi\rangle_{\partial D_1} \geq c_1 \|\varphi\|^2_{H^{-1/2}(\partial D_1)} \qquad \text{for all } \varphi \in H^{-1/2}(\partial D_1).$$

(c) The difference $S_{D_1} - S_{D_1,\mathrm{i}}$ is compact from $H^{-1/2}(\partial D_1)$ to $H^{1/2}(\partial D_1)$.

Proof. This is shown in [KG08, Lem. 1.14]. □

The hypersingular operator has similar properties as the single layer operator. As before, $N_{D_2,\mathrm{i}}$ denotes the hypersingular operator corresponding to the wave number $k = \mathrm{i}$.

Theorem 2.13.

(a) If k^2 is not a Neumann eigenvalue of $-\Delta$ in D_2, i.e., there does not exist a non-trivial solution u to the Helmholtz equation $\Delta u + k^2 u = 0$ in D_2 such that $\partial u/\partial \boldsymbol{\nu}$ vanishes on the boundary ∂D_2, then N_{D_2} is an isomorphism from $H^{1/2}(\partial D_2)$ to $H^{-1/2}(\partial D_2)$.

(b) The operator $-N_{D_2,\mathrm{i}}$ is self-adjoint and coercive, i.e., there exists a constant $c_2 > 0$ such that

$$-\langle N_{D_2,\mathrm{i}}\psi, \psi\rangle_{\partial D_2} \geq c_2 \|\psi\|^2_{H^{1/2}(\partial D_2)} \qquad \text{for all } \psi \in H^{1/2}(\partial D_2).$$

(c) The difference $N_{D_2} - N_{D_2,\mathrm{i}}$ is compact from $H^{1/2}(\partial D_2)$ to $H^{-1/2}(\partial D_2)$.

Proof. A proof can be found in [KG08, Thm. 1.26]. □

Recalling that $H^{-1/2}(\partial D_1) \subseteq L^2(\partial D_1) \subseteq H^{1/2}(\partial D_1)$ and the embeddings are compact, we find that $S_{D_1,\mathrm{i}}$ is compact as an operator from $L^2(\partial D_1)$ to $L^2(\partial D_1)$. The following lemma shows that the operator $S_{D_1,\mathrm{i}}$ possesses a square root, i.e., there exists an operator $S_{D_1,\mathrm{i}}^{1/2}$ such that $S_{D_1,\mathrm{i}}^{1/2} S_{D_1,\mathrm{i}}^{1/2} = S_{D_1,\mathrm{i}}$.

Lemma 2.14. *There exists a self-adjoint square root $S_{D_1,\mathrm{i}}^{1/2} : L^2(\partial D_1) \to L^2(\partial D_1)$ of the operator $S_{D_1,\mathrm{i}} : L^2(\partial D_1) \to L^2(\partial D_1)$ which can be extended to an isomorphism from $H^{-1/2}(\partial D_1)$ to $L^2(\partial D_1)$.*

Proof. For a proof, we refer to [KR00, Lem. 3.3]. □

We denote the inverse operator of $S_{D_1,\mathrm{i}}^{1/2} : H^{-1/2}(\partial D_1) \to L^2(\partial D_1)$ by

$$S_{D_1,\mathrm{i}}^{-1/2} := \left(S_{D_1,\mathrm{i}}^{1/2}\right)^{-1} : L^2(\partial D_1) \to H^{-1/2}(\partial D_1)\,. \tag{2.20}$$

Furthermore, we write

$$S_{D_1,\mathrm{i}}^{*/2} := \left(S_{D_1,\mathrm{i}}^{1/2}\right)^* : L^2(\partial D_1) \to H^{1/2}(\partial D_1)\,, \tag{2.21a}$$

$$S_{D_1,\mathrm{i}}^{-*/2} := \left(S_{D_1,\mathrm{i}}^{-1/2}\right)^* : H^{1/2}(\partial D_1) \to L^2(\partial D_1) \tag{2.21b}$$

for the adjoint of the square root and the inverse of the latter. Accordingly, when replacing D_1 by D_2 in the definition (2.18) we obtain the operators $S_{D_2,\mathrm{i}}^{1/2}$, $S_{D_2,\mathrm{i}}^{-1/2}$, $S_{D_2,\mathrm{i}}^{*/2}$ and $S_{D_2,\mathrm{i}}^{-*/2}$. In the next lemma, we follow an idea from [DFS20] and apply these operators to show two estimates that we require in the proofs of the shape characterization results.

Lemma 2.15.

(a) Let $K_1 : H^{-1/2}(\partial D_1) \to H^{1/2}(\partial D_1)$ be some compact self-adjoint operator. Then, for any constant $c_1 > 0$, there exists a finite-dimensional subspace $V_1 \subseteq L^2(S^{d-1})$ such that

$$\left|\langle {G_{D_1}^{\mathrm{dir}}}^* \phi, K_1 {G_{D_1}^{\mathrm{dir}}}^* \phi\rangle_{\partial D_1}\right| \leq c_1 \|{G_{D_1}^{\mathrm{dir}}}^* \phi\|^2_{H^{-1/2}(\partial D_1)} \qquad \text{for all } \phi \in V_1^\perp\,.$$

(b) Let $K_2 : H^{1/2}(\partial D_2) \to H^{-1/2}(\partial D_2)$ be some compact self-adjoint operator. Then, for any constant $c_2 > 0$, there exists a finite-dimensional subspace $V_2 \subseteq L^2(S^{d-1})$ such that

$$\left|\langle K_2 {G_{D_2}^{\mathrm{neu}}}^* \phi, {G_{D_2}^{\mathrm{neu}}}^* \phi\rangle_{\partial D_2}\right| \leq c_2 \|{G_{D_2}^{\mathrm{neu}}}^*\|^2_{H^{1/2}(\partial D_2)} \qquad \text{for all } \phi \in V_2^\perp\,.$$

Proof. (a) Adding the identity operator from $H^{-1/2}(\partial D_1) \to H^{-1/2}(\partial D_1)$ in the form $S_{D_1,\mathrm{i}}^{-1/2} S_{D_1,\mathrm{i}}^{1/2}$ and from $H^{1/2}(\partial D_1) \to H^{1/2}(\partial D_1)$ in the form $S_{D_1,\mathrm{i}}^{*/2} S_{D_1,\mathrm{i}}^{-*/2}$ gives

$$\begin{aligned}\left|\langle {G_{D_1}^{\mathrm{dir}}}^* \phi, K_1 {G_{D_1}^{\mathrm{dir}}}^* \phi\rangle_{\partial D_1}\right| &= \left|\langle {G_{D_1}^{\mathrm{dir}}}^* \phi, S_{D_1,\mathrm{i}}^{*/2} S_{D_1,\mathrm{i}}^{-*/2} K_1 S_{D_1,\mathrm{i}}^{-1/2} S_{D_1,\mathrm{i}}^{1/2} {G_{D_1}^{\mathrm{dir}}}^* \phi\rangle_{\partial D_1}\right| \\ &= \left|\langle S_{D_1,\mathrm{i}}^{1/2} {G_{D_1}^{\mathrm{dir}}}^* \phi, \widetilde{K}_1 S_{D_1,\mathrm{i}}^{1/2} {G_{D_1}^{\mathrm{dir}}}^* \phi\rangle_{L^2(\partial D_1)}\right|, \end{aligned} \tag{2.22}$$

where $\widetilde{K}_1 := S_{D_1,\mathrm{i}}^{-*/2} K_1 S_{D_1,\mathrm{i}}^{-1/2} : L^2(\partial D_1) \to L^2(\partial D_1)$ is compact and self-adjoint. The spectral theorem for compact self-adjoint operators (see Remark 2.1) implies that the operator $\widetilde{K}_1$

has at most a countable number of eigenvalues with zero as the only accumulation point, and the corresponding eigenvalues form a complete orthonormal system of $L^2(\partial D_1)$. We define the subspace $\widetilde{V}_1 \subseteq L^2(\partial D_1)$ as the sum of eigenspaces of $\widetilde{K}_1$ associated to eigenvalues with an absolute value larger than $\widetilde{c}_1 := c_1/\|S_{D_1,\mathrm{i}}^{1/2}\|^2$, and we notice that $\widetilde{V}_1$ is finite dimensional. Moreover, we have

$$|\langle \widetilde{v}_1, \widetilde{K}_1 \widetilde{v}_1 \rangle_{L^2(\partial D_1)}| \leq \widetilde{c}_1 \|\widetilde{v}_1\|^2_{L^2(\partial D_1)} \qquad \text{for all } \widetilde{v}_1 \in \widetilde{V}_1^{\perp}. \tag{2.23}$$

Let $\phi \in L^2(S^{d-1})$. Then, it holds $S_{D_1,\mathrm{i}}^{1/2} G_{D_1}^{\mathrm{dir}\,*} \phi \in \widetilde{V}_1^{\perp}$ if and only if

$$0 = \langle S_{D_1,\mathrm{i}}^{1/2} G_{D_1}^{\mathrm{dir}\,*} \phi, \widetilde{v}_1 \rangle_{L^2(\partial D_1)} = \langle \phi, G_{D_1}^{\mathrm{dir}} S_{D_1,\mathrm{i}}^{*/2} \widetilde{v}_1 \rangle_{L^2(S^{d-1})} \qquad \text{for all } \widetilde{v}_1 \in \widetilde{V}_1.$$

Consequently, we find that

$$S_{D_1,\mathrm{i}}^{1/2} G_{D_1}^{\mathrm{dir}\,*} \phi \in \widetilde{V}_1^{\perp} \qquad \text{if and only if} \qquad \phi \in \big(G_{D_1}^{\mathrm{dir}} S_{D_1,\mathrm{i}}^{*/2} \widetilde{V}_1\big)^{\perp}.$$

Setting $V_1 := G_{D_1}^{\mathrm{dir}} S_{D_1,\mathrm{i}}^{*/2} \widetilde{V}_1 \subseteq L^2(S^{d-1})$, it follows that

$$\dim(V_1) = \dim(G_{D_1}^{\mathrm{dir}} S_{D_1,\mathrm{i}}^{*/2} \widetilde{V}_1) \leq \dim(\widetilde{V}_1) < \infty.$$

Finally, combining (2.22) and (2.23) gives

$$\begin{aligned} |\langle G_{D_1}^{\mathrm{dir}\,*} \phi, K_1 G_{D_1}^{\mathrm{dir}\,*} \phi \rangle_{\partial D_1}| &\leq \widetilde{c}_1 \|S_{D_1,\mathrm{i}}^{1/2} G_{D_1}^{\mathrm{dir}\,*} \phi\|^2_{L^2(\partial D_1)} \\ &\leq \widetilde{c}_1 \|S_{D_1,\mathrm{i}}^{1/2}\|^2 \|G_{D_1}^{\mathrm{dir}\,*} \phi\|^2_{H^{-1/2}(\partial D_1)} = c_1 \|G_{D_1}^{\mathrm{dir}\,*} \phi\|^2_{H^{-1/2}(\partial D_1)} \end{aligned}$$

for all $\phi \in V_1^{\perp}$.

(b) We observe that

$$\begin{aligned} |\langle K_2 G_{D_2}^{\mathrm{neu}*} \phi, G_{D_2}^{\mathrm{neu}*} \phi \rangle_{\partial D_2}| &= |\langle S_{D_2,\mathrm{i}}^{-1/2} S_{D_2,\mathrm{i}}^{1/2} K_2 S_{D_2,\mathrm{i}}^{*/2} S_{D_2,\mathrm{i}}^{-*/2} G_{D_2}^{\mathrm{neu}*} \phi, G_{D_2}^{\mathrm{neu}*} \phi \rangle_{\partial D_2}| \\ &= |\langle \widetilde{K}_2 S_{D_2,\mathrm{i}}^{-*/2} G_{D_2}^{\mathrm{neu}*} \phi, S_{D_2,\mathrm{i}}^{-*/2} G_{D_2}^{\mathrm{neu}*} \phi \rangle_{L^2(\partial D_2)}| \end{aligned} \tag{2.24}$$

with the operator $\widetilde{K}_2 := S_{D_2,\mathrm{i}}^{1/2} K_2 S_{D_2,\mathrm{i}}^{*/2} : L^2(\partial D_2) \to L^2(\partial D_2)$ which is compact and self-adjoint. We define the subspace $\widetilde{V}_2 \subseteq L^2(\partial D_2)$ as the sum of eigenspaces of $\widetilde{K}_2$ associated to eigenvalues with an absolute value larger than $\widetilde{c}_2 := c_2/\|S_{D_2,\mathrm{i}}^{-*/2}\|^2$. Then, the spectral theorem for compact self-adjoint operators guarantees that $\widetilde{V}_2$ is finite dimensional, and it is

$$|\langle \widetilde{K}_2 \widetilde{v}_2, \widetilde{v}_2 \rangle_{L^2(\partial D_2)}| \leq \widetilde{c}_2 \|\widetilde{v}_2\|^2_{L^2(\partial D_2)} \qquad \text{for all } \widetilde{v}_2 \in \widetilde{V}_2^{\perp}. \tag{2.25}$$

Besides, we find that

$$S_{D_2,\mathrm{i}}^{-*/2} G_{D_2}^{\mathrm{neu}*} \phi \in \widetilde{V}_2^{\perp} \qquad \text{if and only if} \qquad \phi \in \big(G_{D_2}^{\mathrm{neu}} S_{D_2,\mathrm{i}}^{-1/2} \widetilde{V}_2\big)^{\perp}.$$

Setting $V_2 := G_{D_2}^{\mathrm{neu}} S_{D_1,\mathrm{i}}^{-1/2} \widetilde{V}_2 \subseteq L^2(S^{d-1})$, the finite-dimensionality of $\widetilde{V}_2$ implies that V_2 is

finite dimensional as well. We plug (2.25) into (2.24) and obtain

$$\begin{aligned}\left|\langle K_2 G_{D_2}^{\mathrm{neu}*}\phi, G_{D_2}^{\mathrm{neu}*}\phi\rangle_{\partial D_2}\right| &\leq \widetilde{c}_2 \|S_{D_2,\mathrm{i}}^{-*/2} G_{D_2}^{\mathrm{neu}*}\phi\|_{L^2(\partial D_2)}^2 \\ &\leq \widetilde{c}_2 \|S_{D_2,\mathrm{i}}^{-*/2}\|^2 \|G_{D_2}^{\mathrm{neu}*}\phi\|_{H^{1/2}(\partial D_2)}^2 \;=\; c_2 \|G_{D_2}^{\mathrm{neu}*}\phi\|_{H^{1/2}(\partial D_2)}^2\end{aligned}$$

for all $\phi \in V_2^{\perp}$. □

The following result describes the factorizations of the far field operators for Dirichlet obstacles and Neumann obstacles, respectively. Since this theorem is crucial for our shape characterizations in Subsection 2.3.3 below, we give the proof. To this end, we follow [KG08, Thms. 1.15 and 1.26].

Theorem 2.16.

(a) The far field operator $F_{D_1}^{\mathrm{dir}} : L^2(S^{d-1}) \to L^2(S^{d-1})$ can be decomposed as

$$F_{D_1}^{\mathrm{dir}} \;=\; -G_{D_1}^{\mathrm{dir}} S_{D_1}^* G_{D_1}^{\mathrm{dir}\,*}\,. \tag{2.26}$$

(b) The far field operator $F_{D_2}^{\mathrm{neu}} : L^2(S^{d-1}) \to L^2(S^{d-1})$ can be decomposed as

$$F_{D_2}^{\mathrm{neu}} \;=\; -G_{D_2}^{\mathrm{neu}} N_{D_2}^* G_{D_2}^{\mathrm{neu}*}\,. \tag{2.27}$$

Proof. (a) We begin with defining the auxiliary operator $H_{D_1} : L^2(S^{d-1}) \to H^{1/2}(\partial D_1)$ by

$$(H_{D_1}\phi)(\boldsymbol{x}) \;:=\; \int_{S^{d-1}} e^{\mathrm{i}k\boldsymbol{x}\cdot\boldsymbol{\theta}}\phi(\boldsymbol{\theta})\,\mathrm{d}s(\boldsymbol{\theta})\,, \qquad \boldsymbol{x}\in\partial D_1\,,$$

and find that it is just the trace on ∂D_1 of the Herglotz wave function u_ϕ^i from (2.10) with density $\phi \in L^2(S^{d-1})$. For its adjoint operator $H_{D_1}^* : H^{-1/2}(\partial D_1) \to L^2(S^{d-1})$, it holds

$$(H_{D_1}^*\varphi)(\widehat{\boldsymbol{x}}) \;=\; \int_{\partial D_1} e^{-\mathrm{i}k\widehat{\boldsymbol{x}}\cdot\boldsymbol{y}}\varphi(\boldsymbol{y})\,\mathrm{d}s(\boldsymbol{y})\,, \qquad \widehat{\boldsymbol{x}}\in S^{d-1}\,.$$

The fundamental solution Φ_k has the asymptotic behavior

$$\Phi_k(\boldsymbol{x},\boldsymbol{y}) \;=\; \begin{cases} \dfrac{e^{\mathrm{i}\pi/4}}{\sqrt{8\pi k}}\dfrac{e^{\mathrm{i}k|\boldsymbol{x}|}}{\sqrt{|\boldsymbol{x}|}}\Big(e^{\mathrm{i}k\widehat{\boldsymbol{x}}\cdot\boldsymbol{y}} + \mathcal{O}\Big(\dfrac{1}{|\boldsymbol{x}|}\Big)\Big)\,, & |\boldsymbol{x}|\to\infty\,, \quad d=2\,, \\ \dfrac{1}{4\pi}\dfrac{e^{\mathrm{i}k|\boldsymbol{x}|}}{|\boldsymbol{x}|}\Big(e^{\mathrm{i}k\widehat{\boldsymbol{x}}\cdot\boldsymbol{y}} + \mathcal{O}\Big(\dfrac{1}{|\boldsymbol{x}|}\Big)\Big)\,, & |\boldsymbol{x}|\to\infty\,, \quad d=3\,, \end{cases}$$

for fixed $\boldsymbol{y}$ uniformly with respect to $\widehat{\boldsymbol{x}} = \boldsymbol{x}/|\boldsymbol{x}| \in S^{d-1}$ (see, e.g., [KH15, Lmm. 2.39] for $d=3$ and [CK19, Sec. 3.5] for $d=2$). Thus, we observe that $H_{D_1}^*\varphi$, $\varphi \in H^{-1/2}(\partial D_1)$, is just the far field pattern of the single layer potential SL_{D_1} from (2.16) with density φ. Results from the theory of layer potentials (see, e.g., [McL00, Equ. (7.6)]) show that $\mathrm{SL}_{D_1}\varphi|_{\pm} = S_{D_1}\varphi$ for all $\varphi \in H^{-1/2}(\partial D_1)$, where the index + denotes the trace from the exterior and − the trace from the interior, respectively. By the definition of the data-to-pattern operator (2.15a), it is

$$H_{D_1}^* \;=\; G_{D_1}^{\mathrm{dir}} S_{D_1} \qquad \text{or equivalently} \qquad H_{D_1} \;=\; S_{D_1}^* G_{D_1}^{\mathrm{dir}\,*}\,. \tag{2.28}$$

On the other hand, by linearity we have $F\phi = u_\phi^\infty$, where u_ϕ^i is again the Herglotz wave function from (2.10). This means that $F\phi$ is the far field pattern that corresponds to the solution of the exterior boundary value problem (2.11a)–(2.11b), where the boundary data coincide with the trace of $-u_\phi^i$ on ∂D_1. Recalling that $-H_{D_1}\phi$ is exactly this trace we end up with

$$F\phi \;=\; -G_{D_1}^{\mathrm{dir}} H_{D_1}\phi\,. \tag{2.29}$$

Combining (2.28) and (2.29) completes the proof.

(b) We proceed similarly as in part (a) and define the operator $\partial H_{D_2} : L^2(S^{d-1}) \to H^{-1/2}(\partial D_2)$ via

$$(\partial H_{D_2}\phi)(\boldsymbol{x}) \;:=\; \frac{\partial}{\partial \boldsymbol{\nu}(\boldsymbol{x})} \int_{S^{d-1}} e^{\mathrm{i}k\boldsymbol{x}\cdot\boldsymbol{\theta}}\phi(\boldsymbol{\theta})\,\mathrm{d}s(\boldsymbol{\theta}) \;=\; \mathrm{i}k \int_{S^{d-1}} e^{\mathrm{i}k\boldsymbol{x}\cdot\boldsymbol{\theta}}(\boldsymbol{\nu}(\boldsymbol{x})\cdot\boldsymbol{\theta})\phi(\boldsymbol{\theta})\,\mathrm{d}s(\boldsymbol{\theta})\,,$$

$\boldsymbol{x} \in \partial D_2$. We obtain its adjoint operator $(\partial H_{D_2})^* : H^{1/2}(\partial D_2) \to L^2(S^{d-1})$,

$$((\partial H_{D_2})^*\psi)(\widehat{\boldsymbol{x}}) \;=\; -\mathrm{i}k \int_{\partial D_2} e^{-\mathrm{i}k\widehat{\boldsymbol{x}}\cdot\boldsymbol{y}}(\boldsymbol{\nu}(\boldsymbol{y})\cdot\widehat{\boldsymbol{x}})\psi(\boldsymbol{y})\,\mathrm{d}s(\boldsymbol{y}) \;=\; \int_{\partial D_2} \frac{\partial e^{-\mathrm{i}k\widehat{\boldsymbol{x}}\cdot\boldsymbol{y}}}{\partial \boldsymbol{\nu}(\boldsymbol{y})}\psi(\boldsymbol{y})\,\mathrm{d}s(\boldsymbol{y})\,,$$

$\widehat{\boldsymbol{x}} \in S^{d-1}$. From the asymptotic behavior of the fundamental solution, it follows that $(\partial H_{D_2})^*\psi$, $\psi \in H^{1/2}(\partial D_2)$, is the far field pattern of the double layer potential DL_{D_2} from (2.17) with density ψ. For $\psi \in H^{1/2}(D_2)$, we have $\partial(\mathrm{DL}_{D_2}\psi)/\partial\boldsymbol{\nu}|_\pm = N_{D_2}\psi$ (see, e.g., [McL00, Equ. (7.6)]), and we deduce $\partial H_{D_2} = N_{D_2}^* G_{D_2}^{\mathrm{neu}}$. Moreover, an analogous argument as in (a) shows that $F\phi = -G_{D_2}^{\mathrm{neu}}(\partial H_{D_2})\phi$ which yields the assertion. □

The following result is a direct consequence of Theorem 2.16.

Corollary 2.17. *For the real parts of $F_{D_1}^{\mathrm{dir}}$ and $F_{D_2}^{\mathrm{neu}}$, it holds*

$$\mathrm{Re}(F_{D_1}^{\mathrm{dir}}) \;\leq_{\mathrm{fin}}\; 0 \qquad \textit{and} \qquad \mathrm{Re}(F_{D_2}^{\mathrm{neu}}) \;\geq_{\mathrm{fin}}\; 0\,.$$

Proof. From Theorem 2.16 (a), it follows that

$$\mathrm{Re}(F_{D_1}^{\mathrm{dir}}) \;=\; -\frac{1}{2} G_{D_1}^{\mathrm{dir}}(S_{D_1}^* + S_{D_1}) G_{D_1}^{\mathrm{dir}\,*}\,.$$

Furthermore, we calculate

$$\begin{aligned}\frac{1}{2}(S_{D_1}^* + S_{D_1}) \;&=\; \frac{1}{2}(2S_{D_1,\mathrm{i}} + S_{D_1}^* + S_{D_1} - 2S_{D_1,\mathrm{i}}) \\ &=\; S_{D_1,\mathrm{i}} + \frac{1}{2}\Big((S_{D_1}^* - S_{D_1,\mathrm{i}}) + (S_{D_1} - S_{D_1,\mathrm{i}})\Big)\,.\end{aligned}$$

Since adjoint operators of compact operators are compact as well (see, e.g., [McL00, Thm. 2.17]), using Theorem 2.12 (b)–(c) we find that $\frac{1}{2}(S_{D_1}^* + S_{D_1})$ is a compact perturbation of the self-adjoint and coercive operator $S_{D_1,\mathrm{i}}$, i.e.,

$$\frac{1}{2}(S_{D_1}^* + S_{D_1}) \;=\; S_{D_1,\mathrm{i}} + K^{\mathrm{dir}} \tag{2.30}$$

with the compact self-adjoint operator $K^{\mathrm{dir}} : H^{-1/2}(\partial D_1) \to H^{1/2}(\partial D_1)$ given by

$$K^{\mathrm{dir}} := \frac{1}{2}((S_{D_1}^* - S_{D_1,\mathrm{i}}) + (S_{D_1} - S_{D_1,\mathrm{i}}))\,.$$

Accordingly, we have

$$\begin{aligned}\langle \mathrm{Re}(F_{D_1}^{\mathrm{dir}})\phi, \phi\rangle &= -\langle G_{D_1}^{\mathrm{dir}\,*}\phi, (S_{D_1,\mathrm{i}} + K^{\mathrm{dir}})G_{D_1}^{\mathrm{dir}\,*}\phi\rangle_{\partial D_1} \\ &\leq -c_1\|G_{D_1}^{\mathrm{dir}\,*}\phi\|^2_{H^{-1/2}(\partial D_1)} - \langle G_{D_1}^{\mathrm{dir}\,*}\phi, K^{\mathrm{dir}}G_{D_1}^{\mathrm{dir}\,*}\phi\rangle_{\partial D_1} \end{aligned} \tag{2.31}$$

for all $\phi \in L^2(S^{d-1})$, where c_1 denotes the coercivity constant of $S_{D_1,\mathrm{i}}$ (see Theorem 2.12 (b)). Lemma 2.15 (a) implies that there exists a finite-dimensional subspace $V_1 \subseteq L^2(S^{d-1})$ such that

$$-\langle G_{D_1}^{\mathrm{dir}\,*}\phi, K^{\mathrm{dir}}G_{D_1}^{\mathrm{dir}\,*}\phi\rangle_{\partial D_1} \leq c_1\|G_{D_1}^{\mathrm{dir}\,*}\phi\|^2_{H^{-1/2}(\partial D_1)} \qquad \text{for all } \phi \in V_1^{\perp}\,. \tag{2.32}$$

Combining (2.31) and (2.32) we obtain

$$\langle (\mathrm{Re}(F_{D_1}^{\mathrm{dir}})\phi, \phi\rangle \leq 0 \qquad \text{for all } \phi \in V_1^{\perp}\,,$$

and Lemma 2.2 yields $\mathrm{Re}(F_{D_1}^{\mathrm{dir}}) \leq_{\mathrm{fin}} 0$.

For the real part of $F_{D_2}^{\mathrm{neu}}$, Theorem 2.16 (b) gives

$$F_{D_2}^{\mathrm{neu}} = -\frac{1}{2}G_{D_2}^{\mathrm{neu}}(N_{D_2}^* + N_{D_2})G_{D_2}^{\mathrm{neu}*}\,.$$

We proceed similarly as above and apply Theorem 2.13 (b)–(c) to find that $-\frac{1}{2}(N_{D_2}^* + N_{D_2})$ is a compact perturbation of the self-adjoint and coercive operator $-N_{D_2,\mathrm{i}}$, i.e.,

$$-\frac{1}{2}(N_{D_2}^* + N_{D_2}) = -N_{D_2,\mathrm{i}} + K^{\mathrm{neu}} \tag{2.33}$$

with a compact self-adjoint operator $K^{\mathrm{neu}} : H^{1/2}(\partial D_2) \to H^{-1/2}(\partial D_2)$. Accordingly,

$$\begin{aligned}\langle \mathrm{Re}(F_{D_2}^{\mathrm{neu}})\phi, \phi\rangle &= \langle (-N_{D_2,\mathrm{i}} + K^{\mathrm{neu}})G_{D_2}^{\mathrm{neu}*}\phi, G_{D_2}^{\mathrm{neu}*}\phi\rangle_{\partial D_2} \\ &\geq c_2\|G_{D_2}^{\mathrm{neu}*}\phi\|^2_{H^{1/2}(\partial D_2)} + \langle K^{\mathrm{neu}}G_{D_2}^{\mathrm{neu}*}\phi, G_{D_2}^{\mathrm{neu}*}\phi\rangle_{\partial D_2} \end{aligned} \tag{2.34}$$

for all $\phi \in L^2(S^{d-1})$, where c_2 denotes the coercivity constant of $-N_{D_2,\mathrm{i}}$ (see Theorem 2.13 (b)). From Lemma 2.15 (b), it follows that there exists a finite-dimensional subspace $V_2 \subseteq L^2(S^{d-1})$ such that

$$-\langle K^{\mathrm{neu}}G_{D_2}^{\mathrm{neu}*}\phi, G_{D_2}^{\mathrm{neu}*}\phi\rangle_{\partial D_2} \leq c_2\|G_{D_2}^{\mathrm{neu}*}\phi\|^2_{H^{1/2}(\partial D_2)} \qquad \text{for all } \phi \in V_2^{\perp}\,. \tag{2.35}$$

We insert (2.35) into (2.34) to see that

$$\langle (\mathrm{Re}(F_{D_2}^{\mathrm{neu}})\phi, \phi\rangle \geq 0 \qquad \text{for all } \phi \in V_2^{\perp}\,,$$

and Lemma 2.2 gives $\mathrm{Re}(F_{D_2}^{\mathrm{neu}}) \geq_{\mathrm{fin}} 0$. □

In the traditional Factorization Method (see, e.g., [Kir98, KG08]), one proceeds with characterizing the ranges of the data-to-pattern operators $G_{D_1}^{\mathrm{dir}}$ and $G_{D_2}^{\mathrm{neu}}$ by the obstacles D_1 and D_2, respectively. For some $\boldsymbol{z} \in \mathbb{R}^d$, let $\Psi_{\boldsymbol{z}}(\widehat{\boldsymbol{x}}) := e^{-\mathrm{i}k\widehat{\boldsymbol{x}}\cdot\boldsymbol{z}}$, $\widehat{\boldsymbol{x}} \in S^{d-1}$. Then, it can be shown that $\boldsymbol{z}$ lies in D_1 if and only if $\Psi_{\boldsymbol{z}} \in \mathcal{R}(G_{D_1}^{\mathrm{dir}})$. Analogously, $\boldsymbol{z}$ lies in D_2 if and only if $\Psi_{\boldsymbol{z}} \in \mathcal{R}(G_{D_2}^{\mathrm{neu}})$. Using the factorizations (2.26) and (2.27), we find that $\Psi_{\boldsymbol{z}} \in \mathcal{R}(F_{D_1}^{\mathrm{dir}})$ implies $\boldsymbol{z} \in D_1$, and $\Psi_{\boldsymbol{z}} \in \mathcal{R}(F_{D_2}^{\mathrm{neu}})$ implies $\boldsymbol{z} \in D_2$. This criterion is implemented in the Linear Sampling Method (see, e.g., [CK96]). For the Factorization Method, one continues with connecting the far field operators $F_{D_1}^{\mathrm{dir}}$ and $F_{D_2}^{\mathrm{neu}}$ with the ranges of the data-to-pattern operators $G_{D_1}^{\mathrm{dir}}$ and $G_{D_2}^{\mathrm{neu}}$. Using the representations

$$(F_{D_1}^{\mathrm{dir}*}F_{D_1}^{\mathrm{dir}})^{1/4}\phi = \sum_{i=1}^{\infty}\sqrt{|\lambda_i^{\mathrm{dir}}|}\langle\phi,\phi_i^{\mathrm{dir}}\rangle\phi_i^{\mathrm{dir}} \quad \text{and} \quad (F_{D_2}^{\mathrm{neu}*}F_{D_2}^{\mathrm{neu}})^{1/4}\phi = \sum_{i=1}^{\infty}\sqrt{|\lambda_i^{\mathrm{neu}}|}\langle\phi,\phi_i^{\mathrm{neu}}\rangle\phi_i^{\mathrm{neu}},$$

where $\lambda_i^{\mathrm{dir}}, \lambda_i^{\mathrm{neu}} \in \mathbb{C}$, $i = 1, 2, \ldots$, are the eigenvalues of the corresponding far field operator with normalized eigenvectors $\phi_i^{\mathrm{dir}}, \phi_i^{\mathrm{neu}} \in L^2(S^{d-1})$, one obtains

$$\begin{aligned}
\boldsymbol{z} \in D_1 &\iff \Psi_{\boldsymbol{z}} \in \mathcal{R}\big((F_{D_1}^{\mathrm{dir}*}F_{D_1}^{\mathrm{dir}})^{1/4}\big) \iff \sum_{i=1}^{\infty}\frac{|\langle\Psi_{\boldsymbol{z}},\phi_i^{\mathrm{dir}}\rangle|^2}{|\lambda_i^{\mathrm{dir}}|} < \infty \quad \text{and}\\
\boldsymbol{z} \in D_2 &\iff \Psi_{\boldsymbol{z}} \in \mathcal{R}\big((F_{D_2}^{\mathrm{neu}*}F_{D_2}^{\mathrm{neu}})^{1/4}\big) \iff \sum_{i=1}^{\infty}\frac{|\langle\Psi_{\boldsymbol{z}},\phi_i^{\mathrm{neu}}\rangle|^2}{|\lambda_i^{\mathrm{neu}}|} < \infty.
\end{aligned}$$

Plotting the inverse of the series on the right-hand side provides a good impression of the obstacles' shapes and positions.

In the monotonicity-based ansatz, we compare the real parts of the far field operators to certain probing operators approximating the far field operators corresponding to probing domains. More precisely, we show that suitable combinations of these operators are positive definite up to some finite-dimensional subspaces if and only if the probing domains are contained inside the obstacle. On the one hand, we employ the factorizations from Theorem 2.16, and on the other hand, we need localized wave functions that we introduce in the following subsection.

2.3.2. Localized Wave Functions

In this subsection, we develop the concept of *localized wave functions*. These are pairs of certain functions such that one component has arbitrarily large norm on some prescribed part of a boundary while the other component has arbitrarily small norm on some different part of a boundary. These localized wave functions are essential in the proof of the monotonicity-based shape characterizations in Subsection 2.3.3 below.

Before establishing the existence of localized wave functions, we need to introduce some more operators. Let $B \subseteq \mathbb{R}^d$ be open and Lipschitz bounded. First, from the proof of Theorem 2.16, we recall the definition of the *acoustic Herglotz operator*

$$H_B : L^2(S^{d-1}) \to H^{1/2}(\partial B), \quad (H_B\phi)(\boldsymbol{x}) := \int_{S^{d-1}} e^{\mathrm{i}k\boldsymbol{x}\cdot\boldsymbol{\theta}}\phi(\boldsymbol{\theta})\,\mathrm{d}s(\boldsymbol{\theta}), \qquad \boldsymbol{x} \in \partial B. \tag{2.36}$$

Let $\Gamma \subseteq \partial B$ be relatively open. We define the *restriction operator*

$$R_\Gamma : H^{1/2}(\partial B) \to H^{1/2}(\Gamma), \quad R_\Gamma f := f|_\Gamma,$$

and we note that its adjoint operator satisfies

$$R_\Gamma^* : \widetilde{H}^{-1/2}(\Gamma) \to H^{-1/2}(\partial B), \quad R_\Gamma^* f = \begin{cases} f & \text{on } \Gamma, \\ 0 & \text{on } \partial B \setminus \Gamma. \end{cases}$$

At this point, we recall that $\widetilde{H}^{-1/2}(\Gamma)$ is the dual space of $H^{1/2}(\Gamma)$ from (2.3a). Besides, we introduce

$$H_\Gamma := R_\Gamma H_B$$

and note that (2.28) implies

$$H_\Gamma^* = H_B^* R_\Gamma^* = G_B^{\mathrm{dir}} S_B R_\Gamma^*. \tag{2.37}$$

Moreover, we introduce the *Dirichlet-to-Neumann operator* given by

$$\Lambda_B^{\mathrm{dir}\to\mathrm{neu}} : H^{1/2}(\partial B) \to H^{-1/2}(\partial B), \quad \Lambda_B^{\mathrm{dir}\to\mathrm{neu}} f := \frac{\partial w}{\partial \boldsymbol{\nu}}\Big|_{\partial B},$$

where w is the unique radiating solution to the exterior Dirichlet boundary value problem (2.11a)–(2.11b) with B instead of D_1 (and $D_2 = \emptyset$). Then, $\Lambda_B^{\mathrm{dir}\to\mathrm{neu}}$ is a bounded linear operator (see, e.g., [KG08, Thm. 2.3]), and it holds that

$$G_B^{\mathrm{dir}} = G_B^{\mathrm{neu}} \Lambda_B^{\mathrm{dir}\to\mathrm{neu}}. \tag{2.38}$$

Conversely, we define the *Neumann-to-Dirichlet operator* by

$$\Lambda_B^{\mathrm{neu}\to\mathrm{dir}} : H^{-1/2}(\partial B) \to H^{1/2}(\partial B), \quad \Lambda_B^{\mathrm{neu}\to\mathrm{dir}} g := w|_{\partial B},$$

where w is the unique radiating solution to the exterior Neumann boundary value problem (2.11a) and (2.11c) with B instead of D_2 (and $D_1 = \emptyset$). The Neumann-to-Dirichlet operator $\Lambda_B^{\mathrm{neu}\to\mathrm{dir}}$ is the bounded inverse of the Dirichlet-to-Neumann operator (see, e.g., [KG08, Thm. 2.3]). Furthermore, it is

$$G_B^{\mathrm{neu}} = G_B^{\mathrm{dir}} \Lambda_B^{\mathrm{neu}\to\mathrm{dir}}. \tag{2.39}$$

Theorem 2.18 (Localized Wave Functions for Dirichlet Obstacles)**.** *Let $D_2 = \emptyset$, and let $B, D_1 \subseteq \mathbb{R}^d$ be open and Lipschitz bounded such that $\mathbb{R}^d \setminus \overline{D_1}$ is connected. Suppose that $B \not\subseteq D_1$. Then, for any finite-dimensional subspace $V \subseteq L^2(S^{d-1})$, there exists a sequence $(\phi_m)_{m\in\mathbb{N}} \subseteq V^\perp$ such that*

$$\|H_B \phi_m\|_{H^{1/2}(\partial B)} \to \infty \qquad \text{and} \qquad \|{G_{D_1}^{\mathrm{dir}}}^* \phi_m\|_{H^{-1/2}(\partial D_1)} \to 0 \qquad \text{as } m \to \infty.$$

Remark 2.19. Recalling (2.28), we have $H_B = S_B^* {G_B^{\mathrm{dir}}}^*$, and therefore, Theorem 2.18 remains true when replacing $\|H_B \phi_m\|_{H^{1/2}(\partial B)}$ with $\|{G_B^{\mathrm{dir}}}^* \phi_m\|_{H^{-1/2}(\partial B)}$. ◊

The proof of Theorem 2.18 relies on the following lemmas.

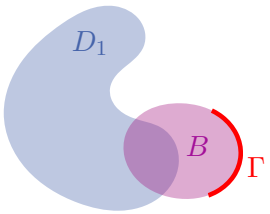

Figure 2.1. Visualization of an exemplary geometry from Lemma 2.20.

Lemma 2.20. *Let $D_2 = \emptyset$, and let $B, D_1 \subseteq \mathbb{R}^d$ be open and Lipschitz bounded. Suppose that $B \not\subseteq D_1$, and let $\Gamma \subseteq \partial B \setminus \overline{D_1}$ be relatively open such that $\mathbb{R}^d \setminus (\overline{\Gamma \cup D_1})$ is connected (see Figure 2.1 for an exemplary visualization of the geometry). Then,*

$$\mathcal{R}(H_\Gamma^*) \cap \mathcal{R}(G_{D_1}^{\mathrm{dir}}) \;=\; \{0\}\,.$$

Proof. Let $h \in \mathcal{R}(H_\Gamma^*) \cap \mathcal{R}(G_{D_1}^{\mathrm{dir}})$. Then, there exist $\psi_\Gamma \in \widetilde{H}^{-1/2}(\Gamma)$ and $f_1 \in H^{1/2}(\partial D_1)$ such that

$$h \;=\; H_\Gamma^* \psi_\Gamma \;=\; G_{D_1}^{\mathrm{dir}} f_1\,.$$

We observe that $H_\Gamma^*\psi_\Gamma$ is the far field pattern of the single layer potential SL_B from (2.16) with density $R_\Gamma^*\psi_\Gamma$. Recalling the definition (2.15a) of the data-to-pattern operator $G_{D_1}^{\mathrm{dir}}$, we find that

$$h \;=\; v_\Gamma^\infty \;=\; w_1^\infty\,,$$

where $v_\Gamma = \mathrm{SL}_B R_\Gamma^* \psi_\Gamma \in H^1_{\mathrm{loc}}(\mathbb{R}^d \setminus \overline{\Gamma})$ and $w_1 \in H^1_{\mathrm{loc}}(\mathbb{R}^d \setminus \overline{D_1})$ are radiating solutions to

$$\Delta v_\Gamma + k^2 v_\Gamma \;=\; 0 \quad \text{in } \mathbb{R}^d \setminus \overline{\Gamma} \qquad \text{and} \qquad \Delta w_1 + k^2 w_1 \;=\; 0 \quad \text{in } \mathbb{R}^d \setminus \overline{D_1}\,,$$

respectively. Thus, Rellich's lemma 2.9 guarantees that $v_\Gamma = w_1$ in $\mathbb{R}^d \setminus (\overline{\Gamma \cup D_1})$. We define $w \in H^1_{\mathrm{loc}}(\mathbb{R}^d)$ by

$$w \;:=\; \begin{cases} v_\Gamma = w_1 & \text{in } \mathbb{R}^d \setminus (\overline{\Gamma \cup D_1})\,, \\ w_1 & \text{on } \Gamma\,, \\ v_\Gamma & \text{in } D_1\,. \end{cases}$$

Then, w is an entire radiating solution to the Helmholtz equation, and from Lemma 2.4, we obtain that $w = 0$ in $\mathbb{R}^d$. This shows that $h = w^\infty = 0$. □

The next lemma is a consequence of the closed graph theorem. Since it plays an important role in this work, we present a proof which is taken from [TW09, Pro. 12.1.2].

Lemma 2.21. *Let X, Y and Z be Hilbert spaces, and let $A_1 : X \to Y$ and $A_2 : X \to Z$ be bounded linear operators. Then, the following statements are equivalent:*

(a) There exists a constant $C > 0$ such that

$$\|A_1 x\|_Y \;\leq\; C \|A_2 x\|_Z \qquad \text{for all } x \in X\,.$$

(b) $\mathcal{R}(A_1^*) \subseteq \mathcal{R}(A_2^*)$.

Proof. First, we prove that statement (a) is equivalent to the existence of a bounded linear operator $L : Y \to Z$ that satisfies $A_1^* = A_2^* L$. Afterward, we complete the proof by showing that such an operator exists if and only if statement (b) holds.

Suppose that there is a constant $C > 0$ such that $\|A_1 x\|_Y \leq C\|A_2 x\|_Z$ holds for all $x \in X$. We define the operator $Q : \mathcal{R}(A_2) \to \mathcal{R}(A_1)$ by $Q(A_2 x) := A_1 x$ for all $x \in X$. This operator is well defined, since (a) implies that for $A_2 x_1 = A_2 x_2$, $x_1, x_2 \in X$, it is

$$\|Q(A_2 x_1) - Q(A_2 x_2)\|_Y \;=\; \|A_1(x_1 - x_2)\|_Y \;\leq\; C\|A_2(x_1 - x_2)\|_Z \;=\; 0\,,$$

and thus, $Q(A_2 x_1) = Q(A_2 x_2)$. Moreover, Q is bounded because (a) yields that

$$\|Q A_2 x\|_Y \;=\; \|A_1 x\|_Y \;\leq\; C\|A_2 x\|_Z \qquad \text{for all } x \in X\,.$$

Consequently, Q has a unique extension to $\overline{\mathcal{R}(A_2)}$ (see, e.g., [KH15, Thm. A.1]). Setting $Qz := 0$ for all $z \in \mathcal{R}(A_2)^\perp$ we find that Q is still well defined and bounded. Furthermore, we have $QA_2 = A_1$ or equivalently $A_1^* = A_2^* Q^*$, and the operator $L := Q^*$ fulfills the requirements. Conversely, if there exists a bounded linear operator with $A_1^* = A_2^* L$, we have

$$\|A_1 x\|_Y \;=\; \|L^* A_2 x\|_Y \;\leq\; \|L^*\|\|A_2 x\|_Z \qquad \text{for all } x \in X\,,$$

and (a) is satisfied with $C = \|L^*\|$.

Now, let $\mathcal{R}(A_1^*) \subseteq \mathcal{R}(A_2^*)$, and let $y \in Y$. Then, $A_1^* y \in \mathcal{R}(A_2^*)$. Thus, there exists a unique $z \in \mathcal{N}(A_2^*)^\perp$ such that $A_2^* z = A_1^* y$. Therefore, setting $Ly := z$ is well defined. Therewith, we have constructed a linear operator L for all $y \in Y$, and it holds $A_1^* = A_2^* L$. To show that L is bounded, we use the closed graph theorem (see, e.g., [Lax02, p. 170]). Let $(y_n)_{n\in\mathbb{N}} \subseteq Y$ converge to $y \in Y$, and let $(Ly_n)_{n\in\mathbb{N}} \subseteq Z$ converge to $\widetilde{z} \in Z$. It follows that

$$A_2^* \widetilde{z} \;=\; \lim_{n\to\infty} A_2^* L y_n \;=\; \lim_{n\to\infty} A_1^* y_n \;=\; A_1^* y \;=\; A_2^* L y\,,$$

which yields $A_2^*(Ly - \widetilde{z}) = 0$. By definition, it holds $Ly \in \mathcal{N}(A_2^*)^\perp$. Since $\mathcal{N}(A_2^*)^\perp$ is closed, we further have $\widetilde{z} \in \mathcal{N}(A_2^*)^\perp$. Accordingly, we end up with $Ly = \widetilde{z}$ and thus, $\widetilde{z} \in \mathcal{R}(L)$. Finally, we assume that there exists a bounded linear operator $L : Y \to Z$ with $A_1^* = A_2^* L$. Then, $\mathcal{R}(A_1^*) = \mathcal{R}(A_2^* L) \subseteq \mathcal{R}(A_2^*)$. □

Remark 2.22. The result remains true when X, Y, Z are reflexive Banach spaces. A proof can be found in [Geb08, Lem. 2.5]. ◊

In the next lemma, we cite a dimensionality statement.

Lemma 2.23. *Let $V, Z_1, Z_2 \subset Z$ be subspaces of a vector space Z. If*

$$Z_1 \cap Z_2 \;=\; \{0\} \quad \textit{and} \quad Z_1 \;\subseteq\; Z_2 + V\,,$$

then $\dim(Z_1) \leq \dim(V)$.

Proof. This is shown in [HPS19b, Lem. 4.7]. □

Now, we give the proof of Theorem 2.18.

Proof of Theorem 2.18. Let $D_2 = \emptyset$, and let $B, D_1 \subseteq \mathbb{R}^d$ be open and Lipschitz bounded such that $\mathbb{R}^d \setminus \overline{D_1}$ is connected, and suppose that $B \not\subseteq D_1$. Let $V \subseteq L^2(S^{d-1})$ be a finite-dimensional subspace. Therefore, the orthogonal projection onto V is well defined, and we denote it by $P_V : L^2(S^{d-1}) \to L^2(S^{d-1})$.

Since $B \not\subseteq D_1$ and $\mathbb{R}^d \setminus \overline{D_1}$ is connected, there exists $\Gamma \subseteq \partial B \setminus \overline{D_1}$ relatively open such that $\mathbb{R}^d \setminus (\overline{\Gamma \cup D_1})$ is connected. Applying Lemma 2.20 we find that

$$\mathcal{R}(H_\Gamma^*) \cap \mathcal{R}(G_{D_1}^{\mathrm{dir}}) \,=\, \{0\}\,. \tag{2.40}$$

Moreover, (2.37) remains true if we modify ∂B away from Γ. Therefore, we can without loss of generality assume that k^2 is not a Dirichlet eigenvalue of $-\Delta$ in B. In this case, S_B and G_B^{dir} are injective operators (see Theorems 2.11 and 2.12 (a)). Furthermore, the extension operator R_Γ^* has infinite-dimensional range. This implies that the range $\mathcal{R}(H_\Gamma^*) = \mathcal{R}(G_B^{\mathrm{dir}} S_B R_\Gamma^*)$ is infinite dimensional as well since injective operators map linearly independent functions on linearly independent functions. Thus, we utilize Lemma 2.23 and (2.40) and obtain that

$$\mathcal{R}(H_\Gamma^*) \,\not\subseteq\, \mathcal{R}(G_{D_1}^{\mathrm{dir}}) + V \,=\, \mathcal{R}\Big(\begin{bmatrix} G_{D_1}^{\mathrm{dir}} & P_V \end{bmatrix}\Big)\,.$$

Accordingly, Lemma 2.21 implies that there is no constant $C > 0$ such that

$$\begin{aligned} \|H_\Gamma \phi\|_{H^{1/2}(\Gamma)}^2 \,&\leq\, C^2 \left\| \begin{bmatrix} {G_{D_1}^{\mathrm{dir}}}^* \\ P_V \end{bmatrix} \phi \right\|_{H^{-1/2}(\partial D_1) \times L^2(S^{d-1})}^2 \\ &=\, C^2 \big(\|{G_{D_1}^{\mathrm{dir}}}^* \phi\|_{H^{-1/2}(\partial D_1)}^2 + \|P_V \phi\|_{L^2(S^{d-1})}^2 \big)\,. \end{aligned}$$

We remind the reader of the notation from (2.6) that we use here. Besides, we utilized that $P_V^* = P_V$ since P_V is an orthogonal projector. We deduce that, for any $m \in \mathbb{N}$, there exists a $\psi_m \in L^2(S^{d-1})$ such that

$$\|H_\Gamma \psi_m\|_{H^{1/2}(\Gamma)}^2 \,>\, m^2 \big(\|{G_{D_1}^{\mathrm{dir}}}^* \psi_m\|_{H^{-1/2}(\partial D_1)}^2 + \|P_V \psi_m\|_{L^2(S^{d-1})}^2 \big)\,.$$

Without loss of generality, suppose that $c_m := \|{G_{D_1}^{\mathrm{dir}}}^* \psi_m\|_{H^{-1/2}(\partial D_1)}^2 + \|P_V \psi_m\|_{L^2(S^{d-1})}^2 = 1$. Otherwise, we replace ψ_m with $\psi_m / \sqrt{c_m}$. Now, let $\widetilde{\phi}_m := \psi_m / \sqrt{m}$, $m \in \mathbb{N}$. On the one hand, we obtain

$$\|H_\Gamma \widetilde{\phi}_m\|_{H^{1/2}(\Gamma)}^2 = \frac{1}{m} \|H_\Gamma \psi_m\|_{H^{1/2}(\Gamma)}^2 > m \big(\|{G_{D_1}^{\mathrm{dir}}}^* \psi_m\|_{H^{-1/2}(\partial D_1)}^2 + \|P_V \psi_m\|_{L^2(S^{d-1})}^2 \big) = m \to \infty$$

as $m \to \infty$. On the other hand, it follows

$$\|{G_{D_1}^{\mathrm{dir}}}^* \widetilde{\phi}_m\|_{H^{-1/2}(\partial D_1)}^2 + \|P_V \widetilde{\phi}_m\|_{L^2(S^{d-1})}^2 = \frac{1}{m} \big(\|{G_{D_1}^{\mathrm{dir}}}^* \psi_m\|_{H^{-1/2}(\partial D_1)}^2 + \|P_V \psi_m\|_{L^2(S^{d-1})}^2 \big) = \frac{1}{m} \to 0$$

as $m \to \infty$. This implies

$$\|H_\Gamma \widetilde{\phi}_m\|_{H^{1/2}(\Gamma)} \to \infty \qquad \text{and} \qquad \|{G_{D_1}^{\mathrm{dir}}}^* \widetilde{\phi}_m\|_{H^{-1/2}(\partial D_1)}\,,\, \|P_V \widetilde{\phi}_m\|_{L^2(S^{d-1})} \to 0$$

as $m \to \infty$. We define $\phi_m := \widetilde{\phi}_m - P_V \widetilde{\phi}_m \in V^\perp$ for any $m \in \mathbb{N}$. Using the reverse triangle

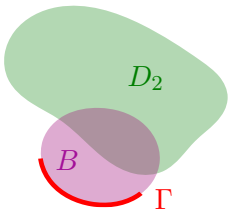

FIGURE 2.2. Visualization of an exemplary geometry from Lemma 2.26.

inequality and the triangle inequality we get

$$\begin{aligned}
\|H_\Gamma \phi_m\|_{H^{1/2}(\Gamma)} &\geq \big| \|H_\Gamma \widetilde{\phi}_m\|_{H^{1/2}(\Gamma)} - \|H_\Gamma P_V \widetilde{\phi}_m\|_{H^{1/2}(\Gamma)} \big| \\
&\geq \|H_\Gamma \widetilde{\phi}_m\|_{H^{1/2}(\Gamma)} - \|H_\Gamma\| \|P_V \widetilde{\phi}_m\|_{L^2(S^{d-1})} \to \infty \,, \\
\|{G_{D_1}^{\mathrm{dir}}}^* \phi_m\|_{H^{-1/2}(\partial D_1)} &\leq \|{G_{D_1}^{\mathrm{dir}}}^* \widetilde{\phi}_m\|_{H^{-1/2}(\partial D_1)} + \|{G_{D_1}^{\mathrm{dir}}}^*\| \|P_V \widetilde{\phi}_m\|_{L^2(S^{d-1})} \to 0
\end{aligned}$$

as $m \to \infty$. Recalling that $H_\Gamma = R_\Gamma H_B$ we obtain

$$\|R_\Gamma\| \|H_B \phi_m\|_{H^{1/2}(\partial B)} \geq \|H_\Gamma \phi_m\|_{H^{1/2}(\Gamma)} \,,$$

and the assertion follows. □

When there are only Neumann obstacles present we get the following result.

Theorem 2.24 (Localized Wave Functions for Neumann Obstacles)**.** *Let $D_1 = \emptyset$, and let $B, D_2 \subseteq \mathbb{R}^d$ be open and Lipschitz bounded such that $\mathbb{R}^d \setminus \overline{D_2}$ is connected. Suppose that $B \not\subseteq D_2$. Then, for any finite-dimensional subspace $V \subseteq L^2(S^{d-1})$, there exists a sequence $(\phi_m)_{m\in\mathbb{N}} \subseteq V^\perp$ such that*

$$\|H_B \phi_m\|_{H^{1/2}(\partial B)} \to \infty \qquad \text{and} \qquad \|G_{D_2}^{\mathrm{neu}*} \phi_m\|_{H^{1/2}(\partial D_2)} \to 0 \qquad \text{as } m \to \infty \,.$$

Remark 2.25. Combining (2.28) with (2.38) gives $H_B = S_B^* (\Lambda_B^{\mathrm{neu}\to\mathrm{dir}})^* G_B^{\mathrm{neu}*}$, and therefore, Theorem 2.24 remains true when replacing $\|H_B \phi_m\|_{H^{1/2}(\partial B)}$ with $\|G_B^{\mathrm{neu}*} \phi_m\|_{H^{1/2}(\partial B)}$. ◊

For the proof of Theorem 2.24, we need an analog of Lemma 2.20.

Lemma 2.26. *Let $D_1 = \emptyset$, and let $B, D_2 \subseteq \mathbb{R}^d$ be open and Lipschitz bounded. Suppose that $B \not\subseteq D_2$, and let $\Gamma \subseteq \partial B \setminus \overline{D_2}$ be relatively open such that $\mathbb{R}^d \setminus (\overline{\Gamma \cup D_2})$ is connected (see Figure 2.2 for an exemplary visualization of the geometry). Then,*

$$\mathcal{R}(H_\Gamma^*) \cap \mathcal{R}(G_{D_2}^{\mathrm{neu}}) = \{0\} \,.$$

Proof. Let $h \in \mathcal{R}(H_\Gamma^*) \cap \mathcal{R}(G_{D_2}^{\mathrm{neu}})$. Then, there exist $\psi_\Gamma \in \widetilde{H}^{-1/2}(\Gamma)$ and $g_2 \in H^{-1/2}(\partial D_2)$ such that

$$h = H_\Gamma^* \psi_\Gamma = G_{D_2}^{\mathrm{neu}} g_2 \,.$$

We already know that $H_\Gamma^* \psi_\Gamma$ is the far field pattern of the single layer potential SL_B from (2.16) with density $R_\Gamma^* \psi_\Gamma$. Accordingly,

$$h = v_\Gamma^\infty = w_2^\infty \,,$$

where $v_\Gamma = \mathrm{SL}_B R_\Gamma^* \psi_\Gamma \in H^1_{\mathrm{loc}}(\mathbb{R}^d \setminus \overline{\Gamma})$ and $w_2 \in H^1_{\mathrm{loc}}(\mathbb{R}^d \setminus \overline{D_2})$ are radiating solutions to

$$\Delta v_\Gamma + k^2 v_\Gamma = 0 \quad \text{in } \mathbb{R}^d \setminus \overline{\Gamma} \qquad \text{and} \qquad \Delta w_2 + k^2 w_2 = 0 \quad \text{in } \mathbb{R}^d \setminus \overline{D_2}\,,$$

respectively. Again, Rellich's lemma 2.9 guarantees that $v_\Gamma = w_2$ in $\mathbb{R}^d \setminus (\overline{\Gamma \cup D_2})$. We define $w \in H^1_{\mathrm{loc}}(\mathbb{R}^d)$ by

$$w := \begin{cases} v_\Gamma = w_2 & \text{in } \mathbb{R}^d \setminus (\overline{\Gamma \cup D_2})\,, \\ w_2 & \text{on } \Gamma\,, \\ v_\Gamma & \text{in } D_2\,. \end{cases}$$

Then, w is an entire radiating solution to the Helmholtz equation, and from Lemma 2.4, we obtain $w = 0$ in $\mathbb{R}^d$. This shows that $h = w^\infty = 0$. □

Now, we give the proof of Theorem 2.24 proceeding similarly as in the proof of Theorem 2.18.

Proof of Theorem 2.24. Let $D_1 = \emptyset$, and let $B, D_2 \subseteq \mathbb{R}^d$ be open and Lipschitz bounded such that $\mathbb{R}^d \setminus \overline{D_2}$ is connected, and suppose that $B \not\subseteq D_2$. Let $V \subseteq L^2(S^{d-1})$ be a finite-dimensional subspace. As before, we use the notation $P_V : L^2(S^{d-1}) \to L^2(S^{d-1})$ for the orthogonal projector onto V.

Since $B \not\subseteq D_2$ and $\mathbb{R}^d \setminus \overline{D_2}$ is connected, there exists $\Gamma \subseteq \partial B \setminus \overline{D_2}$ relatively open such that $\mathbb{R}^d \setminus (\overline{\Gamma \cup D_2})$ is connected. Applying Lemma 2.26 we find that

$$\mathcal{R}(H_\Gamma^*) \cap \mathcal{R}(G_{D_2}^{\mathrm{neu}}) = \{0\}\,. \tag{2.41}$$

We have seen earlier that $\mathcal{R}(H_\Gamma^*)$ is infinite dimensional. Using Lemma 2.23 and (2.41) it follows that

$$\mathcal{R}(H_\Gamma^*) \not\subseteq \mathcal{R}(G_{D_2}^{\mathrm{neu}}) + V = \mathcal{R}\big(\begin{bmatrix} G_{D_2}^{\mathrm{neu}} & P_V \end{bmatrix}\big)\,.$$

Accordingly, Lemma 2.21 implies that there is no constant $C > 0$ such that

$$\begin{aligned} \|H_\Gamma \phi\|^2_{H^{1/2}(\Gamma)} &\leq C^2 \left\| \begin{bmatrix} G_{D_2}^{\mathrm{neu}*} \\ P_V \end{bmatrix} \phi \right\|^2_{H^{1/2}(\partial D_2) \times L^2(S^{d-1})} \\ &= C^2 \big(\|G_{D_2}^{\mathrm{neu}*} \phi\|^2_{H^{1/2}(\partial D_2)} + \|P_V \phi\|^2_{L^2(S^{d-1})} \big)\,. \end{aligned}$$

Thus, there exists a sequence $(\widetilde{\phi}_m)_{m \in \mathbb{N}} \subseteq L^2(S^{d-1})$ satisfying

$$\|H_\Gamma \widetilde{\phi}_m\|^2_{H^{1/2}(\Gamma)} \to \infty \qquad \text{and} \qquad \|G_{D_2}^{\mathrm{neu}*} \widetilde{\phi}_m\|^2_{H^{1/2}(\partial D_2)} + \|P_V \widetilde{\phi}_m\|^2_{L^2(S^{d-1})} \to 0$$

as $m \to \infty$. We define $\phi_m := \widetilde{\phi}_m - P_V \widetilde{\phi}_m \in V^\perp$ for any $m \in \mathbb{N}$. Therewith, it follows that

$$\begin{aligned} \|H_\Gamma \phi_m\|_{H^{1/2}(\Gamma)} &\geq \big| \|H_\Gamma \widetilde{\phi}_m\|_{H^{1/2}(\Gamma)} - \|H_\Gamma P_V \widetilde{\phi}_m\|_{H^{1/2}(\Gamma)} \big| \\ &\geq \|H_\Gamma \widetilde{\phi}_m\|_{H^{1/2}(\Gamma)} - \|H_\Gamma\| \|P_V \widetilde{\phi}_m\|_{L^2(S^{d-1})} \to \infty\,, \\ \|G_{D_2}^{\mathrm{dir}\,*} \phi_m\|_{H^{1/2}(\partial D_2)} &\leq \|G_{D_2}^{\mathrm{dir}\,*} \widetilde{\phi}_m\|_{H^{1/2}(\partial D_2)} + \|G_{D_2}^{\mathrm{dir}\,*}\| \|P_V \widetilde{\phi}_m\|_{L^2(S^{d-1})} \to 0 \end{aligned}$$

as $m \to \infty$. Recalling that $H_\Gamma = R_\Gamma H_B$ we obtain

$$\|R_\Gamma\| \|H_B \phi_m\|_{H^{1/2}(\partial B)} \geq \|H_\Gamma \phi_m\|_{H^{1/2}(\Gamma)},$$

and the assertion follows. □

2.3.3. Monotonicity-Based Shape Reconstruction

In this subsection, we establish monotonicity relations for far field operators in terms of the extended Loewner order from (2.7). First, we compare the far field operator corresponding to the obstacle D to far field operators corresponding to probing domains B. To begin with, we discuss the case when only Dirichlet obstacles are present. The criterion that we establish in the next theorems describes whether the probing domain B is contained inside the obstacle D_1 or not.

Theorem 2.27. *Let $D_2 = \emptyset$, and let $B, D_1 \subseteq \mathbb{R}^d$ be open and Lipschitz bounded such that $\mathbb{R}^d \setminus \overline{D_1}$ is connected.*

(a) If $\overline{B} \subseteq D_1$, then $\operatorname{Re}(F^{\mathrm{dir}}_{D_1}) \leq_{\mathrm{fin}} \operatorname{Re}(F^{\mathrm{dir}}_{B})$.

(b) If $B \not\subseteq D_1$, then $\operatorname{Re}(F^{\mathrm{dir}}_{D_1}) \not\leq_{\mathrm{fin}} \operatorname{Re}(F^{\mathrm{dir}}_{B})$.

Proof. (a) Let $\overline{B} \subseteq D_1$. We define the operator

$$P^{\mathrm{dir}}_{B\to D_1} : H^{1/2}(\partial B) \to H^{1/2}(\partial D_1), \quad P^{\mathrm{dir}}_{B\to D_1} f_B := w^{\mathrm{dir}}_B|_{\partial D_1}, \tag{2.42}$$

where $w^{\mathrm{dir}}_B \in H^1_{\mathrm{loc}}(\mathbb{R}^d \setminus \overline{B})$ is the unique radiating solution to the exterior Dirichlet boundary value problem (2.11a)–(2.11b) with D_1 replaced by B and f by f_B (and $D_2 = \emptyset$). From (2.15a), it follows that $G^{\mathrm{dir}}_{D_1} P^{\mathrm{dir}}_{B\to D_1} f_B = w^{\mathrm{dir},\infty}_{D_1}$, where $w^{\mathrm{dir}}_{D_1} \in H^1_{\mathrm{loc}}(\mathbb{R}^d \setminus \overline{D_1})$ is the unique radiating solution to the exterior Dirichlet boundary value problem (2.11a)–(2.11b) with boundary data $w^{\mathrm{dir}}_B|_{\partial D_1} = P^{\mathrm{dir}}_{B\to D_1} f_B$. Since $\overline{B} \subseteq D_1$, we get $w^{\mathrm{dir},\infty}_B = w^{\mathrm{dir},\infty}_{D_1}$ and obtain

$$G^{\mathrm{dir}}_B = G^{\mathrm{dir}}_{D_1} P^{\mathrm{dir}}_{B\to D_1}. \tag{2.43}$$

Furthermore, the operator $P^{\mathrm{dir}}_{B\to D_1}$ is compact. In order to show this we use [GT01, Thm. 8.8] which in particular states that every solution $v \in H^1(\Omega)$ to the Helmholtz equation on some domain Ω even lies in $H^2(\widetilde{\Omega})$ for any subdomain $\widetilde{\Omega} \subset\subset \Omega$. We choose a subset $\widetilde{D}_1 \subseteq \mathbb{R}^d$ such that $\overline{D_1} \subseteq \widetilde{D}_1$ and note that w satisfies the Helmholtz equation in $\widetilde{D}_1 \setminus \overline{B}$. Since $\overline{B} \subseteq D_1$, there exists a $\widetilde{\Omega} \subset\subset \widetilde{D}_1 \setminus \overline{B}$ such that $\partial D_1 \subseteq \widetilde{\Omega}$ (see Figure 2.3 for a visualization). Thus, w lies in $H^2(\widetilde{\Omega})$ and the trace theorem (see, e.g., [Néd01, Thm. 2.5.3]) implies $w|_{\partial D_1} \in H^{3/2}(\partial D_1)$. This allows us to write the operator $P^{\mathrm{dir}}_{B\to D_1}$ in the form $P^{\mathrm{dir}}_{B\to D_1} = J \circ \widetilde{P}^{\mathrm{dir}}_{B\to D_1}$ with $\widetilde{P}^{\mathrm{dir}}_{B\to D_1} : H^{1/2}(\partial B) \to H^{3/2}(\partial D_1)$, given by $\widetilde{P}^{\mathrm{dir}}_{B\to D_1} f_B := w^{\mathrm{dir}}_B|_{\partial D_1}$, and $J : H^{3/2}(\partial D_1) \hookrightarrow H^{1/2}(\partial D_1)$ is the compact embedding operator. This proves the compactness of $P^{\mathrm{dir}}_{B\to D_1}$.

We plug in the factorization (2.26) of $F^{\mathrm{dir}}_{D_1}$ and obtain

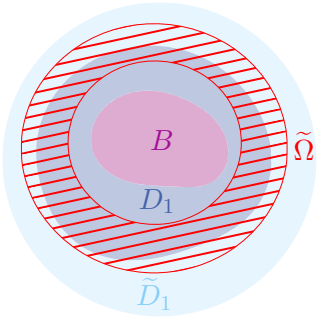

Figure 2.3. Visualization of an exemplary geometry from the proof of Theorem 2.27 (a).

$$\begin{aligned}\operatorname{Re}(F_{D_1}^{\mathrm{dir}} - F_B^{\mathrm{dir}}) &= -\frac{1}{2} G_{D_1}^{\mathrm{dir}} (S_{D_1}^* + S_{D_1}) G_{D_1}^{\mathrm{dir}\,*} + \frac{1}{2} G_B^{\mathrm{dir}} (S_B^* + S_B) G_B^{\mathrm{dir}\,*} \\ &= -G_{D_1}^{\mathrm{dir}} \Big(\frac{1}{2}(S_{D_1}^* + S_{D_1}) - \frac{1}{2} P_{B\to D_1}^{\mathrm{dir}} (S_B^* + S_B)(P_{B\to D_1}^{\mathrm{dir}})^* \Big) G_{D_1}^{\mathrm{dir}\,*} .\end{aligned}$$

From (2.30), we have that $\frac{1}{2}(S_{D_1}^* + S_{D_1})$ is a compact perturbation of the self-adjoint and coercive operator $S_{D_1,\mathrm{i}}$. Thus, it holds

$$\operatorname{Re}(F_{D_1}^{\mathrm{dir}} - F_B^{\mathrm{dir}}) = -G_{D_1}^{\mathrm{dir}} (S_{D_1,\mathrm{i}} + K) G_{D_1}^{\mathrm{dir}\,*}$$

with the compact self-adjoint operator $K : H^{-1/2}(\partial D_1) \to H^{1/2}(\partial D_1)$ given by

$$K := \frac{1}{2}((S_{D_1}^* - S_{D_1,\mathrm{i}}) + (S_{D_1} - S_{D_1,\mathrm{i}})) - P_{B\to D_1}^{\mathrm{dir}} (S_B^* + S_B)(P_{B\to D_1}^{\mathrm{dir}})^* .$$

Therewith, we get

$$\begin{aligned}\langle \operatorname{Re}(F_{D_1}^{\mathrm{dir}} - F_B^{\mathrm{dir}})\phi, \phi\rangle &= -\langle G_{D_1}^{\mathrm{dir}\,*}\phi, (S_{D_1,\mathrm{i}} + K) G_{D_1}^{\mathrm{dir}\,*}\phi\rangle_{\partial D_1} \\ &\le -c_1 \|G_{D_1}^{\mathrm{dir}\,*}\phi\|^2_{H^{-1/2}(\partial D_1)} - \langle G_{D_1}^{\mathrm{dir}\,*}\phi, K G_{D_1}^{\mathrm{dir}\,*}\phi\rangle_{\partial D_1}\end{aligned}$$

for all $\phi \in L^2(S^{d-1})$, where c_1 is the coercivity constant of $S_{D_1,\mathrm{i}}$ (see Theorem 2.12 (b)). We apply Lemma 2.15 (a) which shows the existence of a finite-dimensional subspace $V \subseteq L^2(S^{d-1})$ such that

$$-\langle G_{D_1}^{\mathrm{dir}\,*}\phi, K G_{D_1}^{\mathrm{dir}\,*}\phi\rangle_{\partial D_1} \le c_1 \|G_{D_1}^{\mathrm{dir}\,*}\phi\|^2_{H^{-1/2}(\partial D_1)} \qquad \text{for all } \phi \in V^\perp .$$

It follows that

$$\langle \operatorname{Re}(F_{D_1}^{\mathrm{dir}} - F_B^{\mathrm{dir}})\phi, \phi\rangle \le 0 \qquad \text{for all } \phi \in V^\perp ,$$

and Lemma 2.2 yields the result.

(b) Let $B \not\subseteq D_1$. We suppose that there exists a finite-dimensional subspace $V_1 \subseteq L^2(S^{d-1})$ such that

$$\langle \operatorname{Re}(F_{D_1}^{\mathrm{dir}})\phi, \phi\rangle \le \langle \operatorname{Re}(F_B^{\mathrm{dir}})\phi, \phi\rangle \qquad \text{for all } \phi \in V_1^\perp .$$

On the one hand, using the factorization (2.26) of $F_{D_1}^{\mathrm{dir}}$, we find that, for all $\phi \in L^2(S^{d-1})$,

$$\begin{aligned} -\langle \mathrm{Re}(F_{D_1}^{\mathrm{dir}})\phi, \phi\rangle &\leq |\langle \mathrm{Re}(F_{D_1}^{\mathrm{dir}})\phi, \phi\rangle| \\ &\leq \frac{1}{2}\|S_{D_1} + S_{D_1}^*\| \|G_{D_1}^{\mathrm{dir}\,*}\phi\|_{H^{-1/2}(\partial D_1)}^2 \leq C\|G_{D_1}^{\mathrm{dir}\,*}\phi\|_{H^{-1/2}(\partial D_1)}^2 \end{aligned} \tag{2.44}$$

for some $C > 0$. Analogously to (2.30), it follows that $\frac{1}{2}(S_B^* + S_B)$ is a compact perturbation of the self-adjoint and coercive operator $S_{B,\mathrm{i}}$. We combine this with the factorization (2.26) of F_B^{dir} and see that, on the other hand,

$$\begin{aligned} \langle \mathrm{Re}(F_B^{\mathrm{dir}})\phi, \phi\rangle &= -\langle G_B^{\mathrm{dir}\,*}\phi, (S_{B,\mathrm{i}} + \widetilde{K})G_B^{\mathrm{dir}\,*}\phi\rangle_{\partial B} \\ &\leq -\widetilde{c}_1\|G_B^{\mathrm{dir}\,*}\phi\|_{H^{-1/2}(\partial B)}^2 - \langle G_B^{\mathrm{dir}\,*}\phi, \widetilde{K}G_B^{\mathrm{dir}\,*}\phi\rangle_{\partial B}\,, \end{aligned}$$

where $\widetilde{K} : H^{-1/2}(\partial B) \to H^{1/2}(\partial B)$ is a compact self-adjoint operator, and $\widetilde{c}_1$ denotes the coercivity constant of $S_{B,\mathrm{i}}$ (see Theorem 2.12 (b)). Accordingly, Lemma 2.15 (a) guarantees that there exists a finite-dimensional subspace $V_2 \subseteq L^2(S^{d-1})$ such that

$$-\langle G_B^{\mathrm{dir}\,*}\phi, \widetilde{K}G_B^{\mathrm{dir}\,*}\phi\rangle_{\partial B} \leq \frac{\widetilde{c}_1}{2}\|G_B^{\mathrm{dir}\,*}\phi\|_{H^{-1/2}(\partial B)}^2 \qquad \text{for all } \phi \in V_2^{\perp}\,.$$

Therefore, it holds

$$\langle \mathrm{Re}(F_B^{\mathrm{dir}})\phi, \phi\rangle \leq -\frac{\widetilde{c}_1}{2}\|G_B^{\mathrm{dir}\,*}\phi\|_{H^{-1/2}(\partial B)}^2 \qquad \text{for all } \phi \in V_2^{\perp}\,.$$

Finally, we obtain

$$0 \geq \langle \mathrm{Re}(F_{D_1}^{\mathrm{dir}} - F_B^{\mathrm{dir}})\phi, \phi\rangle \geq -C\|G_{D_1}^{\mathrm{dir}\,*}\phi\|_{H^{-1/2}(\partial D_1)}^2 + \frac{\widetilde{c}_1}{2}\|G_B^{\mathrm{dir}\,*}\phi\|_{H^{-1/2}(\partial B)}^2$$

for all $\phi \in V^{\perp}$, where $V := V_1 + V_2$ is finite dimensional, and thus $V^{\perp} \neq \{0\}$. Accordingly, Remark 2.19 gives a contradiction. □

Now, we replace the real part $\mathrm{Re}(F_B^{\mathrm{dir}})$ of the far field operator corresponding to the probing domain B with the negative of the *probing operator* $H_B^* H_B$, where H_B is the Herglotz operator from (2.36). Precisely, we would have to write $H_B^* J H_B$, where $J : H^{1/2}(\partial B) \hookrightarrow H^{-1/2}(\partial B)$ is the compact embedding operator. For the sake of simplicity, we omit the operator J in our notation. Since $H_B^* H_B$ is self-adjoint, this operator is positive semi-definite. Moreover, this integral operator is rather easy to implement as we demonstrate in Section 2.5 below. In Corollary 2.17, we have seen that $\mathrm{Re}(F_{D_1}^{\mathrm{dir}})$ is negative definite up to some finite-dimensional subspace. In the following theorem, we show that this property stays true even if we add the positive semi-definite operator $H_B^* H_B$ as long as the probing domain B is contained within D_1. On the contrary, if B is not contained within D_1, then the operator $F_{D_1}^{\mathrm{dir}} + H_B^* H_B$ fails to be negative definite up to some finite-dimensional subspace.

Theorem 2.28 (Shape Characterization for Dirichlet Obstacles)**.** *Let $D_2 = \emptyset$, and let $B, D_1 \subseteq \mathbb{R}^d$ be open and Lipschitz bounded such that $\mathbb{R}^d \setminus \overline{D_1}$ is connected.*

(a) If $\overline{B} \subseteq D_1$, then $\mathrm{Re}(F_{D_1}^{\mathrm{dir}}) \leq_{\mathrm{fin}} -H_B^* H_B$.

(b) If $B \not\subseteq D_1$, then $\mathrm{Re}(F_{D_1}^{\mathrm{dir}}) \not\leq_{\mathrm{fin}} -H_B^* H_B$.

Proof. (a) Let $\overline{B} \subseteq D_1$. We recall the definition (2.42) of the compact operator $P_{B\to D_1}^{\mathrm{dir}}$. Combining (2.28) with B instead of D and (2.43), we obtain

$$H_B \;=\; S_B^*(P_{B\to D_1}^{\mathrm{dir}})^* {G_{D_1}^{\mathrm{dir}}}^* . \tag{2.45}$$

Substituting the factorization (2.26) of $F_{D_1}^{\mathrm{dir}}$ gives

$$\mathrm{Re}(F_{D_1}^{\mathrm{dir}}) + H_B^* H_B \;=\; -G_{D_1}^{\mathrm{dir}}\Big(\frac{1}{2}(S_{D_1}^* + S_{D_1}) - P_{B\to D_1}^{\mathrm{dir}} S_B {S_B}^* (P_{B\to D_1}^{\mathrm{dir}})^*\Big){G_{D_1}^{\mathrm{dir}}}^* .$$

Since $\frac{1}{2}(S_{D_1}^* + S_{D_1})$ is a compact perturbation of the self-adjoint and coercive operator $S_{D_1,\mathrm{i}}$ by (2.30), we get

$$\mathrm{Re}(F_{D_1}^{\mathrm{dir}}) + H_B^* H_B \;=\; -G_{D_1}^{\mathrm{dir}}(S_{D_1,\mathrm{i}} + K){G_{D_1}^{\mathrm{dir}}}^*$$

with the compact self-adjoint operator $K : H^{-1/2}(\partial D_1) \to H^{1/2}(\partial D_1)$ given by

$$K \;:=\; \frac{1}{2}\big((S_{D_1}^* - S_{D_1,\mathrm{i}}) + (S_{D_1} - S_{D_1,\mathrm{i}})\big) - P_{B\to D_1}^{\mathrm{dir}} S_B {S_B}^* (P_{B\to D_1}^{\mathrm{dir}})^* .$$

Accordingly,

$$\begin{aligned}\langle(\mathrm{Re}(F_{D_1}^{\mathrm{dir}}) + H_B^* H_B)\phi, \phi\rangle \;&=\; -\langle {G_{D_1}^{\mathrm{dir}}}^*\phi, (S_{D_1,\mathrm{i}} + K){G_{D_1}^{\mathrm{dir}}}^*\phi\rangle_{\partial D_1} \\ &\leq\; -c_1 \|{G_{D_1}^{\mathrm{dir}}}^*\phi\|^2_{H^{-1/2}(\partial D_1)} - \langle {G_{D_1}^{\mathrm{dir}}}^*\phi, K {G_{D_1}^{\mathrm{dir}}}^*\phi\rangle_{\partial D_1}\end{aligned}$$

for all $\phi \in L^2(S^{d-1})$, where c_1 denotes the coercivity constant of $S_{D_1,\mathrm{i}}$ (see Theorem 2.12 (b)). We use Lemma 2.15 (a) to find that there exists a finite-dimensional subspace $V \subseteq L^2(S^{d-1})$ such that

$$-\langle {G_{D_1}^{\mathrm{dir}}}^*\phi, K {G_{D_1}^{\mathrm{dir}}}^*\phi\rangle_{\partial D_1} \;\leq\; c_1 \|{G_{D_1}^{\mathrm{dir}}}^*\phi\|^2_{H^{-1/2}(\partial D_1)} \qquad \text{for all } \phi \in V^\perp .$$

Therewith, it is

$$\langle(\mathrm{Re}(F_{D_1}^{\mathrm{dir}}) + H_B^* H_B)\phi, \phi\rangle \;\leq\; 0 \qquad \text{for all } \phi \in V^\perp ,$$

and the assertion follows from Lemma 2.2.

(b) Let $B \not\subseteq D_1$. We suppose that there exists a finite-dimensional subspace $V \subseteq L^2(S^{d-1})$ such that

$$\langle \mathrm{Re}(F_{D_1}^{\mathrm{dir}})\phi, \phi\rangle \;\leq\; -\langle H_B^* H_B \phi, \phi\rangle \qquad \text{for all } \phi \in V^\perp .$$

Further, we have

$$\langle H_B^* H_B \phi, \phi\rangle \;=\; \|H_B\phi\|^2_{H^{1/2}(\partial B)} .$$

Together with (2.44), we obtain

$$0 \geq \langle (\operatorname{Re}(F_{D_1}^{\mathrm{dir}}) + H_B^* H_B)\phi, \phi\rangle \geq -C\|G_{D_1}^{\mathrm{dir}\,*}\phi\|^2_{H^{-1/2}(\partial D_1)} + \|H_B\phi\|^2_{H^{1/2}(\partial B)},$$

where $C > 0$ is a constant. Finally, Theorem 2.18 gives a contradiction. □

We investigate the case when there are only Neumann obstacles present. As for the Dirichlet obstacles, we begin with deriving a monotonicity relation in terms of the far field operators corresponding to the obstacle D_2 and a certain probing domain B.

Theorem 2.29. *Let $D_1 = \emptyset$, and let $B, D_2 \subseteq \mathbb{R}^d$ be open and Lipschitz bounded such that $\mathbb{R}^d \setminus \overline{D_2}$ is connected.*

(a) If $\overline{B} \subseteq D_2$, then $\operatorname{Re}(F_B^{\mathrm{neu}}) \leq_{\mathrm{fin}} \operatorname{Re}(F_{D_2}^{\mathrm{neu}})$.

(b) If $B \not\subseteq D_2$, then $\operatorname{Re}(F_B^{\mathrm{neu}}) \not\leq_{\mathrm{fin}} \operatorname{Re}(F_{D_2}^{\mathrm{neu}})$.

Proof. (a) Let $\overline{B} \subseteq D_2$. We replace D_1 with D_2 in (2.42) and define the operator $P_{B\to D_2}^{\mathrm{dir}}$. We have seen before that this operator is compact. Combining (2.43) with (2.38) and (2.39), we obtain

$$G_B^{\mathrm{neu}} = G_{D_2}^{\mathrm{neu}} \Lambda_{D_2}^{\mathrm{dir}\to\mathrm{neu}} P_{B\to D_2}^{\mathrm{dir}} \Lambda_B^{\mathrm{neu}\to\mathrm{dir}}.$$

We set $P_{B\to D_2}^{\mathrm{neu}} := \Lambda_{D_2}^{\mathrm{dir}\to\mathrm{neu}} P_{B\to D_2}^{\mathrm{dir}} \Lambda_B^{\mathrm{neu}\to\mathrm{dir}}$ and substitute the factorization (2.27) of $F_{D_2}^{\mathrm{neu}}$. This implies

$$\begin{aligned}\operatorname{Re}(F_{D_2}^{\mathrm{neu}} - F_B^{\mathrm{neu}}) &= -\frac{1}{2} G_{D_2}^{\mathrm{neu}}(N_{D_2}^* + N_{D_2}) G_{D_2}^{\mathrm{neu}\,*} + \frac{1}{2} G_B^{\mathrm{neu}}(N_B^* + N_B) G_B^{\mathrm{neu}\,*} \\ &= -G_{D_2}^{\mathrm{neu}}\Big(\frac{1}{2}(N_{D_2}^* + N_{D_2}) - \frac{1}{2} P_{B\to D_2}^{\mathrm{neu}}(N_B^* + N_B)(P_{B\to D_2}^{\mathrm{neu}})^*\Big) G_{D_2}^{\mathrm{neu}\,*}.\end{aligned}$$

From (2.33), we already know that $-\frac{1}{2}(N_{D_2}^* + N_{D_2})$ is a compact perturbation of the operator $-N_{D_2,\mathrm{i}}$. Thus, we have

$$\operatorname{Re}(F_{D_2}^{\mathrm{neu}} - F_B^{\mathrm{neu}}) = G_{D_2}^{\mathrm{neu}}(-N_{D_2,\mathrm{i}} + K) G_{D_2}^{\mathrm{neu}\,*}$$

with some compact self-adjoint operator $K : H^{1/2}(\partial D_2) \to H^{-1/2}(\partial D_2)$. As $-N_{D_2,\mathrm{i}}$ is coercive with coercivity constant c_2 (see Theorem 2.13 (b)) we obtain

$$\langle (\operatorname{Re}(F_{D_2}^{\mathrm{neu}} - F_B^{\mathrm{neu}})\phi, \phi\rangle \geq c_2 \|G_{D_2}^{\mathrm{neu}\,*}\phi\|^2_{H^{1/2}(\partial D_2)} + \langle K G_{D_2}^{\mathrm{neu}\,*}\phi, G_{D_2}^{\mathrm{neu}\,*}\phi\rangle_{\partial D_2}$$

for all $\phi \in L^2(S^{d-1})$. Lemma 2.15 (b) implies the existence of a finite-dimensional subspace $V \subseteq L^2(S^{d-1})$ such that

$$-\langle K G_{D_2}^{\mathrm{neu}\,*}\phi, G_{D_2}^{\mathrm{neu}\,*}\phi\rangle_{\partial D_2} \leq c_2 \|G_{D_2}^{\mathrm{neu}\,*}\phi\|^2_{H^{1/2}(\partial D_2)} \qquad \text{for all } \phi \in V^\perp.$$

Consequently, it follows

$$\langle (\operatorname{Re}(F_{D_2}^{\mathrm{neu}}) - \operatorname{Re}(F_B^{\mathrm{neu}}))\phi, \phi\rangle \geq 0 \qquad \text{for all } \phi \in V^\perp,$$

and Lemma 2.2 yields the result.

(b) Let $B \not\subseteq D_2$. We suppose that there exists a finite-dimensional subspace $V_1 \subseteq L^2(S^{d-1})$ such that

$$\langle \mathrm{Re}(F_B^{\mathrm{neu}})\phi, \phi\rangle \;\leq\; \langle \mathrm{Re}(F_{D_2}^{\mathrm{neu}})\phi, \phi\rangle \qquad \text{for all } \phi \in V_1^{\perp}\,.$$

Using the factorization (2.27) of $F_{D_2}^{\mathrm{neu}}$, we find that, for all $\phi \subseteq L^2(S^{d-1})$,

$$\begin{aligned}\langle \mathrm{Re}(F_{D_2}^{\mathrm{neu}})\phi, \phi\rangle \;&\leq\; |\langle \mathrm{Re}(F_{D_2}^{\mathrm{neu}})\phi, \phi\rangle| \\ &\leq\; \frac{1}{2}\|N_{D_2} + N_{D_2}^*\|\|G_{D_2}^{\mathrm{neu}*}\phi\|^2_{H^{1/2}(\partial D_2)} \;\leq\; C\|G_{D_2}^{\mathrm{neu}*}\phi\|^2_{H^{1/2}(\partial D_2)} \qquad (2.46)\end{aligned}$$

for some $C > 0$. Moreover, from (2.33), we have that $-\frac{1}{2}(N_B^* + N_B)$ is a compact perturbation of the self-adjoint and coercive operator $-N_{B,\mathrm{i}}$. Together with the factorization (2.27) of F_B^{neu}, this gives

$$\begin{aligned}\langle \mathrm{Re}(F_B^{\mathrm{neu}})\phi, \phi\rangle \;&=\; -\langle (N_{B,\mathrm{i}} + \widetilde{K})G_B^{\mathrm{neu}*}\phi, G_B^{\mathrm{neu}*}\phi\rangle_{\partial B} \\ &\geq\; \widetilde{c}_2\|G_B^{\mathrm{neu}*}\phi\|^2_{H^{1/2}(\partial B)} - \langle \widetilde{K}G_B^{\mathrm{neu}*}\phi, G_B^{\mathrm{neu}*}\phi\rangle_{\partial B}\,,\end{aligned}$$

where $\widetilde{K} : H^{1/2}(\partial B) \to H^{-1/2}(\partial B)$ is a compact self-adjoint operator, and $\widetilde{c}_2$ denotes the coercivity constant of $-N_{B,\mathrm{i}}$ (see Theorem 2.13 (b)). From Lemma 2.15, it follows that there exists a finite-dimensional subspace $V_2 \subseteq L^2(S^{d-1})$ such that

$$\langle \widetilde{K}G_B^{\mathrm{neu}*}\phi, G_B^{\mathrm{neu}*}\phi\rangle_{\partial B} \;\leq\; \frac{\widetilde{c}_2}{2}\|G_B^{\mathrm{neu}*}\phi\|^2_{H^{1/2}(\partial B)} \qquad \text{for all } \phi \in V_2^{\perp}\,.$$

Therefore, we have

$$\langle \mathrm{Re}(F_B^{\mathrm{neu}})\phi, \phi\rangle \;\geq\; \frac{\widetilde{c}_2}{2}\|G_B^{\mathrm{neu}*}\phi\|^2_{H^{1/2}(\partial B)} \qquad \text{for all } \phi \in V_2^{\perp}\,.$$

Finally, we obtain

$$0 \;\leq\; \langle \mathrm{Re}(F_{D_2}^{\mathrm{neu}} - F_B^{\mathrm{neu}})\phi, \phi\rangle \;\leq\; C\|G_{D_2}^{\mathrm{neu}*}\phi\|^2_{H^{1/2}(\partial D_2)} - \frac{\widetilde{c}_2}{2}\|G_B^{\mathrm{neu}*}\phi\|^2_{H^{1/2}(\partial B)}$$

for all $\phi \in V^{\perp}$, where $V := V_1 + V_2$ is finite dimensional, and thus $V^{\perp} \neq \{0\}$. Accordingly, Remark 2.25 gives a contradiction. □

The following result represents the monotonicity relation that we obtain when replacing the real part of the far field operator F_B^{neu} with the probing operator $H_B^* H_B$.

Theorem 2.30 (Shape Characterization for Neumann Obstacles)**.** *Let $D_1 = \emptyset$, and let $B, D_2 \subseteq \mathbb{R}^d$ be open and Lipschitz bounded such that $\mathbb{R}^d \setminus \overline{D_2}$ is connected.*

(a) If $\overline{B} \subseteq D_2$, then $H_B^* H_B \leq_{\mathrm{fin}} \mathrm{Re}(F_{D_2}^{\mathrm{neu}})$.

(b) If $B \not\subseteq D_2$, then $H_B^* H_B \not\leq_{\mathrm{fin}} \mathrm{Re}(F_{D_2}^{\mathrm{neu}})$.

Proof. (a) Let $\overline{B} \subseteq D_2$. As before, we use the notation $P^{\mathrm{dir}}_{B\to D_2}$ for the compact operator from (2.42) with D_1 replaced with D_2. Using the factorization (2.27) of $F_{D_2}^{\mathrm{neu}}$ and identity (2.45)

with D_2 instead of D_1 as well as (2.38) with D_2 instead of B, we get

$$\begin{aligned}&\mathrm{Re}(F_{D_2}^{\mathrm{neu}}) - H_B^* H_B \\ &= -G_{D_2}^{\mathrm{neu}}\big(\frac{1}{2}(N_{D_2}^* + N_{D_2}) + \Lambda^{\mathrm{dir}\to\mathrm{neu}} P_{B\to D_2}^{\mathrm{dir}} S_B S_B^* (P_{B\to D_2}^{\mathrm{dir}})^* (\Lambda^{\mathrm{dir}\to\mathrm{neu}})^*\big) G_{D_2}^{\mathrm{neu}*}\,.\end{aligned}$$

Since $-\frac{1}{2}(N_{D_2}^* + N_{D_2})$ is a compact perturbation of the operator $-N_{D_2,\mathrm{i}}$, this shows that

$$\mathrm{Re}(F_{D_2}^{\mathrm{neu}}) - H_B^* H_B \;=\; G_{D_2}^{\mathrm{neu}}(-N_{D_2,\mathrm{i}} + K) G_{D_2}^{\mathrm{neu}*}$$

with some compact self-adjoint operator $K : H^{1/2}(\partial D_2) \to H^{-1/2}(\partial D_2)$. As $-N_{D_2,\mathrm{i}}$ is coercive with coercivity constant c_2 (see Theorem 2.13 (b)) we obtain

$$\langle(\mathrm{Re}(F_{D_2}^{\mathrm{neu}}) - H_B^* H_B)\phi, \phi\rangle \;\geq\; c_2 \|G_{D_2}^{\mathrm{neu}*}\phi\|_{H^{1/2}(\partial D_2)}^2 + \langle K G_{D_2}^{\mathrm{neu}*}\phi, G_{D_2}^{\mathrm{neu}*}\phi\rangle_{\partial D_2}$$

for all $\phi \in L^2(S^{d-1})$. Lemma 2.15 yields the existence of a finite-dimensional subspace $V \subseteq L^2(S^{d-1})$ such that

$$-\langle K G_{D_2}^{\mathrm{neu}*}\phi, G_{D_2}^{\mathrm{neu}*}\phi\rangle_{\partial D_2} \;\leq\; c_2 \|G_{D_2}^{\mathrm{neu}*}\phi\|_{H^{1/2}(\partial D_2)}^2 \qquad \text{for all } \phi \in V^\perp\,.$$

Therewith, it holds

$$\langle(\mathrm{Re}(F_{D_2}^{\mathrm{neu}}) - H_B^* H_B)\phi, \phi\rangle \;\geq\; 0 \qquad \text{for all } \phi \in V^\perp\,,$$

and applying Lemma 2.2 completes the proof.

(b) Let $B \not\subseteq D_2$. We suppose that there exists a finite-dimensional subspace $V \subseteq L^2(S^{d-1})$ such that

$$\langle H_B^* H_B \phi, \phi\rangle \;\leq\; \langle \mathrm{Re}(F_{D_2}^{\mathrm{neu}})\phi, \phi\rangle \qquad \text{for all } \phi \in V^\perp\,.$$

Using (2.46), we obtain

$$0 \;\geq\; \langle(H_B^* H_B - \mathrm{Re}(F_{D_2}^{\mathrm{neu}}))\phi, \phi\rangle \;\geq\; \|H_B\phi\|_{H^{1/2}(\partial B)}^2 - C\|G_{D_2}^{\mathrm{neu}*}\phi\|_{H^{1/2}(\partial D_2)}^2\,.$$

Finally, Theorem 2.24 gives a contradiction. □

2.4. Mixed Obstacles

In this section, we consider the mixed case when the obstacle $D = D_1 \cup D_2$ consists of two bounded components and carries Dirichlet boundary conditions on ∂D_1 and Neumann boundary conditions on ∂D_2. We proceed in the same manner as in the previous section and begin with deducing a factorization of the far field operator F_D^{mix} in Subsection 2.4.1. Afterward, we establish an extension of the localized wave functions from Theorems 2.18 and 2.24 in Subsection 2.4.2, and finally, we present a shape characterization result in Subsection 2.4.3.

2.4.1. Factorization of the Far Field Operator

Again, the starting point is the definition of the *data-to-pattern operator*

$$G_D^{\mathrm{mix}} : H^{1/2}(\partial D_1) \times H^{-1/2}(\partial D_2) \to L^2(S^{d-1}), \quad G_D^{\mathrm{mix}}(f,g) := w^{\mathrm{mix},\infty}, \tag{2.47}$$

where $w^{\mathrm{mix},\infty}$ is the far field pattern of the unique radiating solution to the exterior mixed boundary value problem (2.11a)–(2.11c).

Theorem 2.31. *The operator G_D^{mix} is compact and one-to-one with dense range in $L^2(S^{d-1})$.*

Proof. For a proof, we refer to [KG08, Thm. 3.2]. □

In the next lemma, we derive an estimate that is similar to the ones from Lemma 2.15. To this end, we introduce the duality pairing $\langle \cdot, \cdot \rangle_{\partial D_1 \times \partial D_2}$ between $H^{1/2}(\partial D_1) \times H^{-1/2}(\partial D_2)$ and $H^{-1/2}(\partial D_1) \times H^{1/2}(\partial D_2)$ via

$$\left\langle \begin{pmatrix} \psi_1 \\ \varphi_2 \end{pmatrix}, \begin{pmatrix} \varphi_1 \\ \psi_2 \end{pmatrix} \right\rangle_{\partial D_1 \times \partial D_2} = \overline{\langle \varphi_1, \psi_1 \rangle_{\partial D_1}} + \langle \varphi_2, \psi_2 \rangle_{\partial D_2},$$
$$\begin{pmatrix} \psi_1 \\ \varphi_2 \end{pmatrix} \in H^{1/2}(\partial D_1) \times H^{-1/2}(\partial D_2), \begin{pmatrix} \varphi_1 \\ \psi_2 \end{pmatrix} \in H^{-1/2}(\partial D_1) \times H^{1/2}(\partial D_2).$$

Lemma 2.32. *Let $K : H^{-1/2}(\partial D_1) \times H^{1/2}(\partial D_2) \to H^{1/2}(\partial D_1) \times H^{-1/2}(\partial D_2)$ be some compact self-adjoint operator. Then, for any constant $c > 0$, there exists a finite-dimensional subspace $V \subseteq L^2(S^{d-1})$ such that*

$$\left| \langle K G_D^{\mathrm{mix}^*} \phi, G_D^{\mathrm{mix}^*} \phi \rangle_{\partial D_1 \times \partial D_2} \right| \leq c \, \| G_D^{\mathrm{mix}^*} \phi \|^2_{H^{-1/2}(\partial D_1) \times H^{1/2}(\partial D_2)} \qquad \text{for all } \phi \in V^\perp .$$

Proof. First, we recall the square root $S_{D_j,\mathrm{i}}^{1/2}$, $j = 1, 2$, from Lemma 2.14 as well as the mapping properties of the operators $S_{D_j,\mathrm{i}}^{-1/2}$, $S_{D_j,\mathrm{i}}^{*/2}$ and $S_{D_j,\mathrm{i}}^{-*/2}$ from (2.20)–(2.21). Therewith, we write

$$\begin{aligned} \left| \langle K G_D^{\mathrm{mix}^*} \phi, G_D^{\mathrm{mix}^*} \phi \rangle_{\partial D_1 \times \partial D_2} \right| &= \left| \left\langle \begin{bmatrix} S_{D_1,\mathrm{i}}^{*/2} S_{D_1,\mathrm{i}}^{-*/2} & \\ & S_{D_2,\mathrm{i}}^{-1/2} S_{D_2,\mathrm{i}}^{1/2} \end{bmatrix} K \begin{bmatrix} S_{D_1,\mathrm{i}}^{-1/2} S_{D_1,\mathrm{i}}^{1/2} & \\ & S_{D_2,\mathrm{i}}^{*/2} S_{D_2,\mathrm{i}}^{-*/2} \end{bmatrix} G_D^{\mathrm{mix}^*} \phi, G_D^{\mathrm{mix}^*} \phi \right\rangle_{\partial D_1 \times \partial D_2} \right| \\ &= \left| \left\langle \widetilde{K} \begin{bmatrix} S_{D_1,\mathrm{i}}^{1/2} & \\ & S_{D_2,\mathrm{i}}^{-*/2} \end{bmatrix} G_D^{\mathrm{mix}^*} \phi, \begin{bmatrix} S_{D_1,\mathrm{i}}^{1/2} & \\ & S_{D_2,\mathrm{i}}^{-*/2} \end{bmatrix} G_D^{\mathrm{mix}^*} \phi \right\rangle_{L^2(\partial D_1) \times L^2(\partial D_2)} \right|, \end{aligned} \tag{2.48}$$

where $\widetilde{K} : L^2(\partial D_1) \times L^2(\partial D_2) \to L^2(\partial D_1) \times L^2(\partial D_2)$, given by

$$\widetilde{K} := \begin{bmatrix} S_{D_1,\mathrm{i}}^{-*/2} & \\ & S_{D_2,\mathrm{i}}^{1/2} \end{bmatrix} K \begin{bmatrix} S_{D_1,\mathrm{i}}^{-1/2} & \\ & S_{D_2,\mathrm{i}}^{*/2} \end{bmatrix},$$

is a compact self-adjoint operator. Let $\widetilde{V} \subseteq L^2(\partial D_1) \times L^2(\partial D_2)$ be the sum of eigenspaces of $\widetilde{K}$ associated to eigenvalues with an absolute value larger than $\widetilde{c} := c / \| \begin{bmatrix} S_{D_1,\mathrm{i}}^{*/2} & S_{D_2,\mathrm{i}}^{-1/2} \end{bmatrix} \|^2$. Applying

the spectral theorem for compact self-adjoint operators (see Remark 2.1) we find that $\widetilde{V}$ is finite dimensional, and we have

$$\left|\langle K\widetilde{v},\widetilde{v}\rangle_{L^2(\partial D_1)\times L^2(\partial D_2)}\right| \leq \widetilde{c}\,\|\widetilde{v}\|^2_{L^2(\partial D_1)\times L^2(\partial D_2)} \qquad \text{for all } \widetilde{v}\in\widetilde{V}^\perp\,. \tag{2.49}$$

Besides, we observe that

$$\begin{bmatrix} S^{1/2}_{D_1,\mathrm{i}} \\ S^{-*/2}_{D_2,\mathrm{i}} \end{bmatrix} G_D^{\mathrm{mix}*}\phi \in \widetilde{V}^\perp \qquad \text{if and only if} \qquad \phi \in (G_D^{\mathrm{mix}} \begin{bmatrix} S^{*/2}_{D_1,\mathrm{i}} \\ S^{-1/2}_{D_2,\mathrm{i}} \end{bmatrix} \widetilde{V})^\perp\,.$$

We define

$$V := G_D^{\mathrm{mix}} \begin{bmatrix} S^{*/2}_{D_1,\mathrm{i}} \\ S^{-1/2}_{D_2,\mathrm{i}} \end{bmatrix} \widetilde{V} \subseteq L^2(S^{d-1})$$

and find that $\dim(V)\leq\dim(\widetilde{V})<\infty$. Thus, combining (2.49) with (2.48) yields

$$\begin{aligned}\left|\langle KG_D^{\mathrm{mix}*}\phi, G_D^{\mathrm{mix}*}\phi\rangle_{\partial D_1\times\partial D_2}\right| &\leq \widetilde{c}\left\| \begin{bmatrix} S^{1/2}_{D_1,\mathrm{i}} \\ S^{-*/2}_{D_2,\mathrm{i}} \end{bmatrix} G_D^{\mathrm{mix}*}\phi\right\|^2_{L^2(\partial D_1)\times L^2(\partial D_2)} \\ &\leq \widetilde{c}\left\| \begin{bmatrix} S^{1/2}_{D_1,\mathrm{i}} \\ S^{-*/2}_{D_2,\mathrm{i}} \end{bmatrix}\right\|^2 \|G_D^{\mathrm{mix}*}\phi\|^2_{H^{-1/2}(\partial D_1)\times H^{1/2}(\partial D_2)} = c\,\|G_D^{\mathrm{mix}*}\phi\|^2_{H^{-1/2}(\partial D_1)\times H^{1/2}(\partial D_2)}\end{aligned}$$

for all $\phi\in V^\perp$. □

The following theorem describes the factorization of the far field operator for mixed obstacles. Since the factorization is an essential tool in the proof of our shape characterization result, we give a complete proof which is taken from [KG08, Thm. 3.4].

Theorem 2.33. *The far field operator $F_D^{\mathrm{mix}} : L^2(S^{d-1})\to L^2(S^{d-1})$ can be decomposed as*

$$F_D^{\mathrm{mix}} = -G_D^{\mathrm{mix}} T_D^{\mathrm{mix}*} G_D^{\mathrm{mix}*}\,. \tag{2.50}$$

The operator $T_D^{\mathrm{mix}} : H^{-1/2}(\partial D_1)\times H^{1/2}(\partial D_2)\to H^{1/2}(\partial D_1)\times H^{-1/2}(\partial D_2)$ is of the form

$$T_D^{\mathrm{mix}} = \left(\begin{bmatrix} S_{D_1} & 0 \\ 0 & N_{D_2}\end{bmatrix} + K_D^{\mathrm{mix}}\right), \tag{2.51}$$

and $K_D^{\mathrm{mix}} : H^{-1/2}(\partial D_1)\times H^{1/2}(\partial D_2)\to H^{1/2}(\partial D_1)\times H^{-1/2}(\partial D_2)$ is compact.

If k^2 is neither a Dirichlet eigenvalue of $-\Delta$ in D_1 nor a Neumann eigenvalue of $-\Delta$ in D_2, then the operators T_D^{mix} and $T_D^{\mathrm{mix}*}$ are isomorphisms.

Proof. Recalling the operators H_{D_1} and ∂H_{D_2} that have been introduced in the proof of Theorem 2.16, we start with calculating the adjoint operator

$$\begin{bmatrix} H_{D_1} \\ \partial H_{D_2}\end{bmatrix}^* \begin{pmatrix}\varphi\\ \psi\end{pmatrix}(\widehat{\boldsymbol{x}}) = \int_{\partial D_1} e^{-\mathrm{i}k\widehat{\boldsymbol{x}}\cdot\boldsymbol{y}}\varphi(\boldsymbol{y})\,\mathrm{d}s(\boldsymbol{y}) + \int_{\partial D_2}\frac{\partial e^{-\mathrm{i}k\widehat{\boldsymbol{x}}\cdot\boldsymbol{y}}}{\partial\boldsymbol{\nu}(\boldsymbol{y})}\psi(\boldsymbol{y})\,\mathrm{d}s(\boldsymbol{y})\,, \qquad \widehat{\boldsymbol{x}}\in S^{d-1}\,. \tag{2.52}$$

We note that the right-hand side of (2.52) is just the far field pattern of

$$w(\boldsymbol{x}) \;=\; (\mathrm{SL}_{D_1}\varphi)(\boldsymbol{x}) + (\mathrm{DL}_{D_2}\psi)(\boldsymbol{x})\,, \qquad \boldsymbol{x} \in \mathbb{R}^d \setminus \partial D\,.$$

where SL_{D_1} and DL_{D_2} are the single and the double layer potentials from (2.16) and (2.17), respectively. Furthermore, we define the operators $D_{D_2\to D_1} : H^{1/2}(\partial D_2) \to H^{1/2}(\partial D_1)$ and $D'_{D_1\to D_2} : H^{-1/2}(\partial D_1) \to H^{-1/2}(\partial D_2)$ by

$$\begin{aligned}
(D_{D_2\to D_1}\psi)(\boldsymbol{x}) &:= \int_{\partial D_2} \frac{\partial \Phi_k}{\partial \boldsymbol{\nu}(\boldsymbol{y})}(\boldsymbol{x},\boldsymbol{y})\psi(\boldsymbol{y})\,\mathrm{d}s(\boldsymbol{y})\,, \qquad \boldsymbol{x} \in \partial D_1\,,\\
(D'_{D_1\to D_2}\varphi)(\boldsymbol{x}) &:= \int_{\partial D_1} \frac{\partial \Phi_k}{\partial \boldsymbol{\nu}(\boldsymbol{x})}(\boldsymbol{x},\boldsymbol{y})\varphi(\boldsymbol{y})\,\mathrm{d}s(\boldsymbol{y})\,, \qquad \boldsymbol{x} \in \partial D_2\,.
\end{aligned}$$

Using the jump relations for layer potentials (see, e.g., [McL00, Equ. (7.6)]) we obtain that on the boundary ∂D_1 it holds

$$w|_{\pm} \;=\; S_{D_1}\varphi + D_{D_2\to D_1}\psi$$

for all $\varphi \in H^{-1/2}(\partial D_1)$, $\psi \in H^{1/2}(\partial D_2)$, and on the boundary ∂D_2 it holds

$$\frac{\partial w}{\partial \boldsymbol{\nu}}\Big|_{\pm} \;=\; D'_{D_1\to D_2}\varphi + N_{D_2}\psi$$

for all $\varphi \in H^{-1/2}(\partial D_1)$, $\psi \in H^{1/2}(\partial D_2)$. Thus, by definition (2.47) we have

$$\begin{bmatrix} H_{D_1} \\ \partial H_{D_2} \end{bmatrix}^* \begin{pmatrix} \varphi \\ \psi \end{pmatrix} \;=\; G_D^{\mathrm{mix}} T_D^{\mathrm{mix}} \begin{pmatrix} \varphi \\ \psi \end{pmatrix} \tag{2.53}$$

for all $\varphi \in H^{-1/2}(\partial D_1)$, $\psi \in H^{1/2}(\partial D_2)$, where

$$T_D^{\mathrm{mix}} \;=\; \begin{bmatrix} S_{D_1} & 0 \\ 0 & N_{D_2} \end{bmatrix} + \begin{bmatrix} 0 & D_{D_2\to D_1} \\ D'_{D_1\to D_2} & 0 \end{bmatrix} =: \begin{bmatrix} S_{D_1} & 0 \\ 0 & N_{D_2} \end{bmatrix} + K_D^{\mathrm{mix}}\,.$$

Since $D_{D_2\to D_1}$ and $D'_{D_1\to D_2}$ are integral operators with analytic kernels, these operators are compact (see, e.g., [Kre14, Thm. 2.28]). This implies that K_D^{mix} is compact as well. Eventually, we deduce from (2.53) that

$$\begin{bmatrix} H_{D_1} \\ \partial H_{D_2} \end{bmatrix} \;=\; T_D^{\mathrm{mix}*} G_D^{\mathrm{mix}*}\,. \tag{2.54}$$

On the other side, the definition (2.14) of F_D^{mix} implies that $F_D^{\mathrm{mix}}\phi$ is the far field pattern of the solution to the exterior mixed boundary value problem (2.11a)–(2.11d) with boundary data

$$\begin{aligned}
f(\boldsymbol{x}) &\;=\; -\int_{S^{d-1}} u^i(\boldsymbol{x},\boldsymbol{\theta})\phi(\boldsymbol{\theta})\,\mathrm{d}s(\boldsymbol{\theta})\,, \qquad \boldsymbol{x} \in \partial D_1\,,\\
g(\boldsymbol{x}) &\;=\; -\frac{\partial}{\partial \boldsymbol{\nu}} \int_{S^{d-1}} u^i(\boldsymbol{x},\boldsymbol{\theta})\phi(\boldsymbol{\theta})\,\mathrm{d}s(\boldsymbol{\theta})\,, \qquad \boldsymbol{x} \in \partial D_2\,.
\end{aligned}$$

We see that f is the trace of the Herglotz function $-u^i_\phi$ from (2.10) and g the trace of its normal

derivative. Accordingly,

$$F_D^{\mathrm{mix}}\phi \;=\; -G_D^{\mathrm{mix}} \begin{bmatrix} H_{D_1} \\ \partial H_{D_2} \end{bmatrix} \phi \,. \tag{2.55}$$

Substituting (2.54) into (2.55) yields the assertion.

For a proof that T_D^{mix} and $T_D^{\mathrm{mix}*}$ are isomorphisms, we refer to [KG08, Thm. 3.4(b)]. □

In the proofs of the shape characterization results in Subsection 2.3.3, it was essential to decompose the real part of the isomorphism T, appearing in the middle of the factorizations of the far field operators, into a coercive and a compact part. However, the previous theorem gives $T_D^{\mathrm{mix}} = \mathrm{diag}(S_{D_1}, N_{D_2}) + K_D^{\mathrm{mix}}$, and Theorems 2.12 and 2.13 imply that the real part of this operator fails to be the sum of a coercive and a compact operator. This fact is the reason why the proof of the classical Factorization Method cannot be carried over from the case when there are either only Dirichlet or either only Neumann obstacles present to the mixed case without making any restrictions. Indeed, there exist approaches, for instance proposed by N. Grinberg and A. Kirsch in [Gri02, GK04]. Here, one assumes that the Dirichlet and the Neumann obstacles are a priori geometrically separated, i.e., there exist two a priori known non-intersecting open and bounded domains $\widetilde{D}_1$ and $\widetilde{D}_2$ such that D_1 and D_2 are each completely contained within $\widetilde{D}_1$ and $\widetilde{D}_2$, respectively. Consequently, the domain containing D_1 is often referred to as the Dirichlet separator and the domain containing D_2 as the Neumann separator, respectively. Broadly speaking, this assumption means that we have a priori an idea about where the Dirichlet and the Neumann parts are located. For more details, we also recommend reading the third chapter in [KG08]. In contrast to the Factorization Method for a priori separated mixed obstacles, we do not need any a priori information about the location of the Dirichlet and the Neumann parts when following the monotonicity-based shape reconstruction ansatz.

In the next lemma, it is shown that there exist factorizations of some modified far field operators. For the proof, we follow the arguments from [KG08, Lem. 3.5].

Lemma 2.34. *Let $B, D_1, D_2 \subseteq \mathbb{R}^d$ be open and Lipschitz bounded. Assume that k^2 is neither a Dirichlet eigenvalue of $-\Delta$ in D_1 and B nor a Neumann eigenvalue of $-\Delta$ in D_2.*

(a) If $\overline{D_1} \subseteq B$, then

$$F_D^{\mathrm{mix}} + H_B^* H_B \;=\; -\begin{bmatrix} H_B \\ \partial H_{D_2} \end{bmatrix}^* \left(\begin{bmatrix} -J_B & 0 \\ 0 & N_{D_2}^{-1} \end{bmatrix} + K_1 \right) \begin{bmatrix} H_B \\ \partial H_{D_2} \end{bmatrix},$$

where $K_1 : H^{1/2}(\partial B) \times H^{-1/2}(\partial D_2) \to H^{-1/2}(\partial B) \times H^{1/2}(\partial D_2)$ is some compact operator, and $J_B : H^{1/2}(\partial B) \hookrightarrow H^{-1/2}(\partial B)$ denotes the compact embedding operator.

(b) If $\overline{D_2} \subseteq B$, then

$$F_D^{\mathrm{mix}} - H_B^* H_B \;=\; -\begin{bmatrix} H_{D_1} \\ H_B \end{bmatrix}^* \left(\begin{bmatrix} S_{D_1}^{-1} & 0 \\ 0 & J_B \end{bmatrix} + K_2 \right) \begin{bmatrix} H_{D_1} \\ H_B \end{bmatrix},$$

where $K_2 : H^{1/2}(\partial D_1) \times H^{1/2}(\partial B) \to H^{-1/2}(\partial D_1) \times H^{-1/2}(\partial B)$ is some compact operator, and $J_B : H^{1/2}(\partial B) \hookrightarrow H^{-1/2}(\partial B)$ is again the compact embedding operator.

Proof. First, from Theorems 2.16 and 2.33, we know that the operators S_{D_1}, N_{D_2} and T_D^{mix} are isomorphisms. Moreover, using (2.51) we observe that

$$I = \left(\begin{bmatrix} S_{D_1} & 0 \\ 0 & N_{D_2} \end{bmatrix} + K_D^{\mathrm{mix}} - K_D^{\mathrm{mix}} \right) \begin{bmatrix} S_{D_1}^{-1} & 0 \\ 0 & N_{D_2}^{-1} \end{bmatrix} = (T_D^{\mathrm{mix}} - K_D^{\mathrm{mix}}) \begin{bmatrix} S_{D_1}^{-1} & 0 \\ 0 & N_{D_2}^{-1} \end{bmatrix},$$

where $I : H^{1/2}(\partial D_1) \times H^{-1/2}(\partial D_2) \to H^{1/2}(\partial D_1) \times H^{-1/2}(\partial D_2)$ is the identity operator. This implies

$$(T_D^{\mathrm{mix}})^{-1} = \begin{bmatrix} S_{D_1}^{-1} & 0 \\ 0 & N_{D_2}^{-1} \end{bmatrix} - (T_D^{\mathrm{mix}})^{-1} K_D^{\mathrm{mix}} \begin{bmatrix} S_{D_1}^{-1} & 0 \\ 0 & N_{D_2}^{-1} \end{bmatrix}.$$

Next, we recall the factorization (2.50) of F_D^{mix} and combine it with equality (2.54). Therewith, we get

$$\begin{aligned} F_D^{\mathrm{mix}} &= -G_D^{\mathrm{mix}} T_D^{\mathrm{mix}*} G_D^{\mathrm{mix}*} = - \begin{bmatrix} H_{D_1} \\ \partial H_{D_2} \end{bmatrix}^* (T_D^{\mathrm{mix}})^{-1} \begin{bmatrix} H_{D_1} \\ \partial H_{D_2} \end{bmatrix} \\ &= - \begin{bmatrix} H_{D_1} \\ \partial H_{D_2} \end{bmatrix}^* \left(\begin{bmatrix} S_{D_1}^{-1} & 0 \\ 0 & N_{D_2}^{-1} \end{bmatrix} - (T_D^{\mathrm{mix}})^{-1} K_D^{\mathrm{mix}} \begin{bmatrix} S_{D_1}^{-1} & 0 \\ 0 & N_{D_2}^{-1} \end{bmatrix} \right) \begin{bmatrix} H_{D_1} \\ \partial H_{D_2} \end{bmatrix}. \end{aligned} \tag{2.56}$$

(a) Let $\overline{D_1} \subseteq B$. We define the operator $P_1 : H^{1/2}(\partial B) \to H^{1/2}(\partial D_1)$ via $P_1\varphi = w|_{\partial D_1}$, where w solves the interior Dirichlet boundary value problem

$$\Delta w + k^2 w = 0 \quad \text{in } B, \qquad w = f \quad \text{on } \partial B. \tag{2.57}$$

We observe that

$$P_1 H_B = H_{D_1}. \tag{2.58}$$

Besides, P_1 is compact by interior regularity results. More precisely, since $\overline{D_1} \subseteq B$ there exists a $\widetilde{B} \subset\subset B$ such that $\partial D_1 \subseteq \widetilde{B}$. Applying [GT01, Thm. 8.8] yields that the unique solution $w \in H^1(B)$ to the boundary value problem (2.57) even lies in $H^2(\widetilde{B})$, and therefore, $w|_{\partial D_1} \in H^{3/2}(\partial D_1)$ (see, e.g., [Néd01, Thm. 2.5.3]). Thus, we can rewrite P_1 in the way $P_1 = J \circ \widetilde{P}_1$ with $\widetilde{P}_1 : H^{1/2}(\partial B) \to H^{3/2}(\partial D_1)$, and $J : H^{3/2}(\partial D_1) \hookrightarrow H^{1/2}(\partial D_1)$ is the compact embedding operator.

Now, we plug in (2.56) and (2.58) to obtain

$$\begin{aligned} &F_D^{\mathrm{mix}} + H_B^* H_B \\ &= - \begin{bmatrix} P_1 H_B \\ \partial H_{D_2} \end{bmatrix}^* \left(\begin{bmatrix} S_{D_1}^{-1} & 0 \\ 0 & N_{D_2}^{-1} \end{bmatrix} - (T_D^{\mathrm{mix}})^{-1} K_D^{\mathrm{mix}} \begin{bmatrix} S_{D_1}^{-1} & 0 \\ 0 & N_{D_2}^{-1} \end{bmatrix} \right) \begin{bmatrix} P_1 H_B \\ \partial H_{D_2} \end{bmatrix} \\ &\qquad + \begin{bmatrix} H_B \\ \partial H_{D_2} \end{bmatrix}^* \begin{bmatrix} J_B & 0 \\ 0 & 0 \end{bmatrix} \begin{bmatrix} H_B \\ \partial H_{D_2} \end{bmatrix} \\ &= - \begin{bmatrix} H_B \\ \partial H_{D_2} \end{bmatrix}^* \left(\begin{bmatrix} -J_B & 0 \\ 0 & N_{D_2}^{-1} \end{bmatrix} + \begin{bmatrix} P_1^* S_{D_1}^{-1} P_1 & 0 \\ 0 & 0 \end{bmatrix} \right. \end{aligned}$$

$$
\begin{aligned}
&\quad - \begin{bmatrix} P_1^* & 0 \\ 0 & I_{D_2} \end{bmatrix} (T_D^{\mathrm{mix}})^{-1} K_D^{\mathrm{mix}} \begin{bmatrix} S_{D_1}^{-1} & 0 \\ 0 & N_{D_2}^{-1} \end{bmatrix} \begin{bmatrix} P_1 & 0 \\ 0 & \widetilde{I}_{D_2} \end{bmatrix} \Bigg) \begin{bmatrix} H_B \\ \partial H_{D_2} \end{bmatrix} \\
&=: - \begin{bmatrix} H_B \\ \partial H_{D_2} \end{bmatrix}^* \left(\begin{bmatrix} -J_B & 0 \\ 0 & N_{D_2}^{-1} \end{bmatrix} + K_1 \right) \begin{bmatrix} H_B \\ \partial H_{D_2} \end{bmatrix},
\end{aligned}
$$

where $I_{D_2} : H^{1/2}(\partial D_2) \to H^{1/2}(\partial D_2)$ and $\widetilde{I}_{D_2} : H^{-1/2}(\partial D_2) \to H^{-1/2}(\partial D_2)$ are identity operators. Since P_1 and K_D^{mix} are compact operators, K_1 is compact as well.

(b) Let $\overline{D_2} \subseteq B$. We define the operator $P_2 : H^{1/2}(\partial B) \to H^{-1/2}(\partial D_2)$ via $P_2\psi = (\partial w/\partial \boldsymbol{\nu})|_{\partial D_2}$, where w solves the interior Dirichlet boundary value problem (2.57). We note that

$$
P_2 H_B \,=\, \partial H_{D_2}\,.
$$

As in part (a), the interior regularity result [GT01, Thm. 8.8] guarantees the compactness of P_2. Recalling (2.56), we end up with

$$
\begin{aligned}
&F_D^{\mathrm{mix}} - H_B^* H_B \\
&= - \begin{bmatrix} H_{D_1} \\ H_B \end{bmatrix}^* \left(\begin{bmatrix} S_{D_1}^{-1} & 0 \\ 0 & J_B \end{bmatrix} + \begin{bmatrix} 0 & 0 \\ 0 & P_2^* N_{D_2}^{-1} P_2 \end{bmatrix} \right. \\
&\qquad \left. - \begin{bmatrix} \widetilde{I}_{D_1} & 0 \\ 0 & P_2^* \end{bmatrix} (T_D^{\mathrm{mix}})^{-1} K_D^{\mathrm{mix}} \begin{bmatrix} S_{D_1}^{-1} & 0 \\ 0 & N_{D_2}^{-1} \end{bmatrix} \begin{bmatrix} I_{D_1} & 0 \\ 0 & P_2 \end{bmatrix} \right) \begin{bmatrix} H_{D_1} \\ H_B \end{bmatrix} \\
&=: - \begin{bmatrix} H_{D_1} \\ H_B \end{bmatrix}^* \left(\begin{bmatrix} S_{D_1}^{-1} & 0 \\ 0 & J_B \end{bmatrix} + K_2 \right) \begin{bmatrix} H_{D_1} \\ H_B \end{bmatrix},
\end{aligned}
$$

where $I_{D_1} : H^{1/2}(\partial D_1) \to H^{1/2}(\partial D_1)$ and $\widetilde{I}_{D_1} : H^{-1/2}(\partial D_1) \to H^{-1/2}(\partial D_1)$ are identity operators, and K_2 is a compact operator. □

2.4.2. Simultaneously Localized Wave Functions

For the shape characterization result in the mixed case, we require a refined version of the localized wave functions that we introduced in Subsection 2.3.2. More precisely, we generalize the results obtained in Theorems 2.18 and 2.24 in a way such that we not only control the total field but also the incident field. The established functions are called *simultaneously localized wave functions*.

To begin with, we define additional *restriction operators*. Let

$$
R_{D_1} : H^{-1/2}(\partial D_1) \times H^{1/2}(\partial D_2) \to H^{-1/2}(\partial D_1)\,, \quad R_{D_1}(f,g) \,:=\, f\,, \tag{2.59a}
$$

$$
R_{D_2} : H^{-1/2}(\partial D_1) \times H^{1/2}(\partial D_2) \to H^{1/2}(\partial D_2)\,, \quad R_{D_2}(f,g) \,:=\, g\,. \tag{2.59b}
$$

Then, the adjoint operators satisfy

$$
R_{D_1}^* : H^{1/2}(\partial D_1) \to H^{1/2}(\partial D_1) \times H^{-1/2}(\partial D_2)\,, \quad R_{D_1}^* f \,=\, (f,0)\,, \tag{2.60a}
$$

$$
R_{D_2}^* : H^{-1/2}(\partial D_2) \to H^{1/2}(\partial D_1) \times H^{-1/2}(\partial D_2)\,, \quad R_{D_2}^* g \,=\, (0,g)\,. \tag{2.60b}
$$

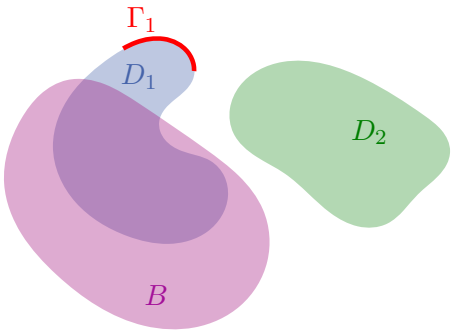

Figure 2.4. Visualization of an exemplary geometry from Lemma 2.36.

Furthermore, given an open and Lipschitz bounded $D_1 \subseteq \mathbb{R}^d$ and $\Gamma_1 \subseteq \partial D_1$ relatively open we define

$$\widetilde{R}_{\Gamma_1} : H^{-1/2}(\partial D_1) \to H^{-1/2}(\Gamma_1), \quad \widetilde{R}_{\Gamma_1} f := f|_{\Gamma_1},$$
$$\widetilde{R}_{\Gamma_2} : H^{1/2}(\partial D_2) \to H^{1/2}(\Gamma_2), \quad \widetilde{R}_{\Gamma_2} g := g|_{\Gamma_2}.$$

We note that the adjoint operators satisfy

$$\widetilde{R}^*_{\Gamma_1} : \widetilde{H}^{1/2}(\Gamma_1) \to H^{1/2}(\partial D_1), \quad \widetilde{R}^*_{\Gamma_1} f = \begin{cases} f & \text{on } \Gamma_1, \\ 0 & \text{on } \partial D_1 \setminus \Gamma_1, \end{cases} \tag{2.61a}$$

$$\widetilde{R}^*_{\Gamma_2} : \widetilde{H}^{-1/2}(\Gamma_2) \to H^{-1/2}(\partial D_2), \quad \widetilde{R}^*_{\Gamma_2} g = \begin{cases} g & \text{on } \Gamma_2, \\ 0 & \text{on } \partial D_2 \setminus \Gamma_2. \end{cases} \tag{2.61b}$$

In the first theorem, we establish simultaneously localized wave functions for the case when $D_1 \not\subseteq B$.

Theorem 2.35 (Simultaneously Localized Wave Functions)**.** *Let $B, D_1, D_2 \subseteq \mathbb{R}^d$ be open and Lipschitz bounded such that $\mathbb{R}^d \setminus (\overline{B \cup D_1 \cup D_2})$ is connected. Suppose that ∂D_1 is piecewise C^1 smooth and that $D_1 \not\subseteq B$. Then, for any finite-dimensional subspace $V \subseteq L^2(S^{d-1})$, there exists a sequence $(\phi_m)_{m\in\mathbb{N}} \subseteq V^\perp$ such that*

$$\|(R_{D_1} G_D^{\mathrm{mix}*})\phi_m\|_{H^{-1/2}(\partial D_1)} \to \infty \quad \text{and} \quad \|(R_{D_2} G_D^{\mathrm{mix}*})\phi_m\|_{H^{1/2}(\partial D_2)} + \|H_B \phi_m\|_{H^{1/2}(\partial B)} \to 0$$

as $m \to \infty$.

The proof of Theorem 2.35 relies on the following lemma.

Lemma 2.36. *Let $B, D_1, D_2 \subseteq \mathbb{R}^d$ be open and Lipschitz bounded. Suppose that $D_1 \not\subseteq B$ and $\mathbb{R}^d \setminus (\overline{B \cup D_1 \cup D_2})$ is connected. Assume furthermore that there exists a connected subset $\Gamma_1 \subseteq \partial D_1 \setminus \overline{B}$ that is relatively open and such that $\overline{\Gamma_1}$ is C^1 smooth (see Figure 2.4 for an exemplary visualization of the geometry). Then,*

$$\mathcal{R}(G_D^{\mathrm{mix}} R^*_{D_1} \widetilde{R}^*_{\Gamma_1}) \not\subseteq \mathcal{R}(\begin{bmatrix} G_D^{\mathrm{mix}} R^*_{D_2} & H^*_B \end{bmatrix}),$$

and there exists an infinite-dimensional subspace $Z \subseteq \mathcal{R}(G_D^{\mathrm{mix}} R_{D_1}^* \widetilde{R}_{\Gamma_1}^*)$ *such that*

$$Z \cap \mathcal{R}\Big(\begin{bmatrix} G_D^{\mathrm{mix}} R_{D_2}^* & H_B^* \end{bmatrix}\Big) \;=\; \{0\}\,.$$

Proof. We assume that $h \in \mathcal{R}(G_D^{\mathrm{mix}} R_{D_1}^* \widetilde{R}_{\Gamma_1}^*) \cap \mathcal{R}([G_D^{\mathrm{mix}} R_{D_2}^* \; H_B^*])$. Then, there are $f_{\Gamma_1} \in \widetilde{H}^{1/2}(\Gamma_1)$, $g_2 \in H^{-1/2}(\partial D_2)$ and $\psi_B \in H^{-1/2}(\partial B)$ such that

$$h \;=\; (G_D^{\mathrm{mix}} R_{D_1}^* \widetilde{R}_{\Gamma_1}^*) f_{\Gamma_1} \;=\; (G_D^{\mathrm{mix}} R_{D_2}^*) g_2 + H_B^* \psi_B\,. \tag{2.62}$$

Recalling the definitions (2.47) of the data-to-pattern operator G_D^{mix} and (2.60)–(2.61) of the extension operators $R_{D_1}^*$, $R_{D_2}^*$ and $\widetilde{R}_{\Gamma_1}^*$, we find that $(G_D^{\mathrm{mix}} R_{D_1}^* \widetilde{R}_{\Gamma_1}^*) f_{\Gamma_1} = w_1^\infty$ and $(G_D^{\mathrm{mix}} R_{D_2}^*) g_2 = w_2^\infty$, where $w_1, w_2 \in H^1_{\mathrm{loc}}(\mathbb{R}^d \setminus (\overline{D_1 \cup D_2}))$ are radiating solutions to

$$\begin{aligned} &\Delta w_1 + k^2 w_1 \;=\; 0 \quad \text{in } \mathbb{R}^d \setminus (\overline{D_1 \cup D_2})\,, \quad w_1 \;=\; \widetilde{R}_{\Gamma_1}^* f_{\Gamma_1} \quad \text{on } \partial D_1\,, \quad \frac{\partial w_1}{\partial \boldsymbol{\nu}} \;=\; 0 \quad \text{on } \partial D_2\,,\\ &\Delta w_2 + k^2 w_2 \;=\; 0 \quad \text{in } \mathbb{R}^d \setminus (\overline{D_1 \cup D_2})\,, \quad w_2 \;=\; 0 \quad \text{on } \partial D_1\,, \qquad\quad \frac{\partial w_2}{\partial \boldsymbol{\nu}} \;=\; g_2 \quad \text{on } \partial D_2\,. \end{aligned}$$

Besides, we have seen before that $H_B^* \psi_B$ is the far field pattern of the single layer potential SL_B from (2.16) with density ψ_B. Thus, $H_B^* \psi_B = v_B^\infty$, where $v_B = \mathrm{SL}_B \psi_B \in H^1_{\mathrm{loc}}(\mathbb{R}^d \setminus \overline{\partial B})$ is a radiating solution to

$$\Delta v_B + k^2 v_B \;=\; 0 \quad \text{in } \mathbb{R}^d \setminus \overline{\partial B}\,.$$

Accordingly, (2.62) implies

$$h \;=\; w_1^\infty \;=\; w_2^\infty + v_B^\infty\,,$$

and Rellich's lemma 2.9 gives $w_1 = w_2 + v_B$ in $\mathbb{R}^d \setminus (\overline{B \cup D_1 \cup D_2})$. Therefore,

$$f_{\Gamma_1} \;=\; w_1|_{\Gamma_1} \;=\; (w_2 + v_B)|_{\Gamma_1} \;=\; v_B|_{\Gamma_1} \;=\; (\mathrm{SL}_B f_B)|_{\Gamma_1}\,.$$

Since $\overline{\Gamma_1}$ is C^1 smooth, this and the smoothness of $\mathrm{SL}_B \psi_B$ away from ∂B imply that $f_{\Gamma_1} \in C^1(\overline{\Gamma_1})$. Let $X \subseteq \widetilde{H}^{1/2}(\Gamma_1)$ be the subspace of continuous piecewise linear functions on Γ_1 that vanish on $\partial\Gamma_1$ constructed in Lemma A.1. This subspace is infinite dimensional, and zero is the only C^1-smooth function contained in it. That is, $X \cap C^1(\overline{\Gamma_1}) = \{0\}$. From our above considerations, it follows that $Z := G_D^{\mathrm{mix}} R_{D_1}^* \widetilde{R}_{\Gamma_1}^*(X)$ satisfies

$$Z \cap \mathcal{R}\Big(\begin{bmatrix} G_D^{\mathrm{mix}} R_{D_2}^* & H_B^* \end{bmatrix}\Big) \;=\; \{0\}\,.$$

The extension operators $R_{D_1}^*$ and $\widetilde{R}_{\Gamma_1}^*$ are injective, and the operator G_D^{mix} is injective as well (see Theorem 2.31). Besides, the space X is infinite dimensional. Since Z is the image of X under the injective operator $G_D^{\mathrm{mix}} R_{D_1}^* \widetilde{R}_{\Gamma_1}^*$, Z is also infinite dimensional. Accordingly,

$$\mathcal{R}(G_D^{\mathrm{mix}} R_{D_1}^* \widetilde{R}_{\Gamma_1}^*) \not\subseteq \mathcal{R}\Big(\begin{bmatrix} G_D^{\mathrm{mix}} R_{D_2}^* & H_B^* \end{bmatrix}\Big)\,. \qquad \square$$

Remark 2.37. The only argument, where we need the additional smoothness assumption on $\Gamma_1 \subseteq \partial D_1$, is the step where we conclude that $f_{\Gamma_1} \in C^1(\overline{\Gamma_1})$. $\lozenge$

Now, we give the proof of Theorem 2.35.

Proof of Theorem 2.35. Let $B, D_1, D_2 \subseteq \mathbb{R}^d$ be open and Lipschitz bounded such that the complement $\mathbb{R}^d \setminus (\overline{B \cup D_1 \cup D_2})$ is connected. Suppose that ∂D_1 is piecewise C^1 smooth and that $D_1 \not\subseteq B$. Let $V \subseteq L^2(S^{d-1})$ be a finite-dimensional subspace. We denote by $P_V : L^2(S^{d-1}) \to L^2(S^{d-1})$ the orthogonal projection onto V.

Since $D_1 \not\subseteq B$ and ∂D_1 is piecewise C^1 smooth, there exists $\Gamma_1 \subseteq \partial D_1 \setminus \overline{B}$ connected and relatively open such that $\overline{\Gamma_1}$ is C^1 smooth. Thus, as $\mathbb{R}^d \setminus (\overline{B \cup D_1 \cup D_2})$ is connected, it follows from Lemma 2.36 that

$$Z \cap \mathcal{R}(\begin{bmatrix} G_D^{\mathrm{mix}} R_{D_2}^* & H_B^* \end{bmatrix}) = \{0\},$$

where $Z \subseteq \mathcal{R}(G_D^{\mathrm{mix}} R_{D_1}^* \widetilde{R}_{\Gamma_1}^*)$ denotes the infinite-dimensional subspace in Lemma 2.36. We apply Lemma 2.23 and find that

$$Z \not\subseteq \mathcal{R}(\begin{bmatrix} G_D^{\mathrm{mix}} R_{D_2}^* & H_B^* \end{bmatrix}) + V = \mathcal{R}(\begin{bmatrix} G_D^{\mathrm{mix}} R_{D_2}^* & H_B^* & P_V \end{bmatrix}).$$

Thus, we have

$$\mathcal{R}(G_D^{\mathrm{mix}} R_{D_1}^* \widetilde{R}_{\Gamma_1}^*) \not\subseteq \mathcal{R}(\begin{bmatrix} G_D^{\mathrm{mix}} R_{D_2}^* & H_B^* & P_V \end{bmatrix}).$$

Accordingly, Lemma 2.21 implies that there is no constant $C > 0$ such that

$$\begin{aligned} \|(\widetilde{R}_{\Gamma_1} R_{D_1} G_D^{\mathrm{mix}^*})\phi\|_{H^{-1/2}(\Gamma_1)}^2 &\leq C^2 \left\| \begin{bmatrix} R_{D_2} G_D^{\mathrm{mix}^*} \\ H_B \\ P_V \end{bmatrix} \phi \right\|_{H^{1/2}(\partial D_2) \times H^{1/2}(\partial B) \times L^2(S^{d-1})}^2 \\ &= C^2 \big(\|(R_{D_2} G_D^{\mathrm{mix}^*})\phi\|_{H^{1/2}(\partial D_2)}^2 + \|H_B \phi\|_{H^{1/2}(\partial B)}^2 + \|P_V \phi\|_{L^2(S^{d-1})}^2 \big). \end{aligned}$$

Therefore, there exists a sequence $(\widetilde{\phi}_m)_{m \in \mathbb{N}} \subseteq L^2(S^{d-1})$ satisfying

$$\|(\widetilde{R}_{\Gamma_1} R_{D_1} G_D^{\mathrm{mix}^*})\widetilde{\phi}_m\|_{H^{-1/2}(\Gamma_1)}^2 \to \infty$$

and

$$\|(R_{D_2} G_D^{\mathrm{mix}^*})\widetilde{\phi}_m\|_{H^{1/2}(\partial D_2)}^2 + \|H_B \widetilde{\phi}_m\|_{H^{1/2}(\partial B)}^2 + \|P_V \widetilde{\phi}_m\|_{L^2(S^{d-1})}^2 \to 0$$

as $m \to \infty$. We define $\phi_m := \widetilde{\phi}_m - P_V \widetilde{\phi}_m \in V^\perp$ for any $m \in \mathbb{N}$. As $\|\widetilde{R}_{\Gamma_1}\| = 1$, using the reverse triangle inequality and the triangle inequality we obtain

$$\begin{aligned} \|(R_{D_1} G_D^{\mathrm{mix}^*})\phi_m\|_{H^{-1/2}(\partial D_1)} &= \|\widetilde{R}_{\Gamma_1}\| \|(R_{D_1} G_D^{\mathrm{mix}^*})\phi_m\|_{H^{-1/2}(\partial D_1)} \\ &\geq \|(\widetilde{R}_{\Gamma_1} R_{D_1} G_D^{\mathrm{mix}^*})\phi_m\|_{H^{-1/2}(\Gamma_1)} \\ &\geq \big| \|(\widetilde{R}_{\Gamma_1} R_{D_1} G_D^{\mathrm{mix}^*})\widetilde{\phi}_m\|_{H^{-1/2}(\Gamma_1)} - \|\widetilde{R}_{\Gamma_1} R_{D_1} G_D^{\mathrm{mix}^*} P_V \widetilde{\phi}_m\|_{H^{-1/2}(\Gamma_1)} \big| \\ &\geq \|(\widetilde{R}_{\Gamma_1} R_{D_1} G_D^{\mathrm{mix}^*})\widetilde{\phi}_m\|_{H^{-1/2}(\Gamma_1)} \\ &\quad - \|\widetilde{R}_{\Gamma_1} R_{D_1} G_D^{\mathrm{mix}^*}\| \|P_V \widetilde{\phi}_m\|_{L^2(S^{d-1})} \to \infty, \\ \|(R_{D_2} G_D^{\mathrm{mix}^*})\phi_m\|_{H^{1/2}(\partial D_2)} &\leq \|(R_{D_2} G_D^{\mathrm{mix}^*})\widetilde{\phi}_m\|_{H^{1/2}(\partial D_2)} + \|R_{D_2} G_D^{\mathrm{mix}^*}\| \|P_V \widetilde{\phi}_m\|_{L^2(S^{d-1})} \to 0, \\ \|H_B \phi_m\|_{H^{1/2}(\partial B)} &\leq \|H_B \widetilde{\phi}_m\|_{H^{1/2}(\partial B)} + \|H_B\| \|P_V \widetilde{\phi}_m\|_{L^2(S^{d-1})} \to 0 \end{aligned}$$

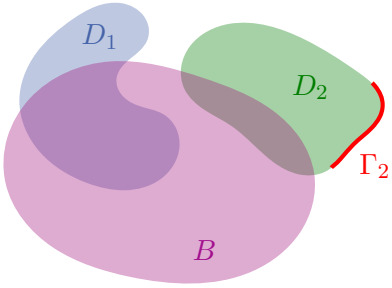

FIGURE 2.5. Visualization of an exemplary geometry from Lemma 2.39.

as $m \to \infty$. This ends the proof. □

The following result states the existence of simultaneously localized wave functions for the case when $D_2 \not\subseteq B$.

Theorem 2.38 (Simultaneously Localized Wave Functions)**.** *Let $B, D_1, D_2 \subseteq \mathbb{R}^d$ be open and Lipschitz bounded such that $\mathbb{R}^d \setminus (\overline{B \cup D_1 \cup D_2})$ is connected. Suppose that ∂D_2 is piecewise C^1 smooth and that $D_2 \not\subseteq B$. Then, for any finite-dimensional subspace $V \subseteq L^2(S^{d-1})$, there exists a sequence $(\phi_m)_{m\in\mathbb{N}} \subseteq V^\perp$ such that*

$$\|(R_{D_1} G_D^{\text{mix}^*})\phi_m\|_{H^{-1/2}(\partial D_1)} + \|H_B \phi_m\|_{H^{1/2}(\partial B)} \to 0 \quad \text{and} \quad \|(R_{D_2} G_D^{\text{mix}^*})\phi_m\|_{H^{1/2}(\partial D_2)} \to \infty$$

as $m \to \infty$.

Again, we need to show an auxiliary result before we can prove the theorem.

Lemma 2.39. *Let $B, D_1, D_2 \subseteq \mathbb{R}^d$ be open and Lipschitz bounded. Suppose that $D_2 \not\subseteq B$ and $\mathbb{R}^d \setminus (\overline{B \cup D_1 \cup D_2})$ is connected. Assume furthermore that there exists a connected subset $\Gamma_2 \subseteq \partial D_2 \setminus \overline{B}$ that is relatively open and such that $\overline{\Gamma_2}$ is C^1 smooth (see Figure 2.5 for an exemplary visualization of the geometry). Then,*

$$\mathcal{R}(G_D^{\text{mix}} R_{D_2}^* \widetilde{R}_{\Gamma_2}^*) \not\subseteq \mathcal{R}\left(\begin{bmatrix} G_D^{\text{mix}} R_{D_1}^* & H_B^* \end{bmatrix}\right),$$

and there exists an infinite-dimensional subspace $Z \subseteq \mathcal{R}(G_D^{\text{mix}} R_{D_2}^* \widetilde{R}_{\Gamma_2}^*)$ such that

$$Z \cap \mathcal{R}\left(\begin{bmatrix} G_D^{\text{mix}} R_{D_1}^* & H_B^* \end{bmatrix}\right) = \{0\}.$$

Proof. We assume that $h \in \mathcal{R}(G_D^{\text{mix}} R_{D_2}^* \widetilde{R}_{\Gamma_2}^*) \cap \mathcal{R}([G_D^{\text{mix}} R_{D_1}^* \; H_B^*])$. Then, there are $g_{\Gamma_2} \in \widetilde{H}^{-1/2}(\Gamma_2)$, $f_1 \in H^{1/2}(\partial D_1)$ and $\psi_B \in H^{-1/2}(\partial B)$ such that

$$h = (G_D^{\text{mix}} R_{D_2}^* \widetilde{R}_{\Gamma_2}^*) g_{\Gamma_2} = (G_D^{\text{mix}} R_{D_1}^*) f_1 + H_B^* \psi_B .$$

Proceeding similarly to the proof of Lemma 2.36 we find that

$$h = w_2^\infty = w_1^\infty + v_B^\infty ,$$

where $w_1, w_2 \in H^1_{\mathrm{loc}}(\mathbb{R}^d \setminus (\overline{D_1 \cup D_2}))$ and $v_B = \mathrm{SL}_B\psi_B \in H^1_{\mathrm{loc}}(\mathbb{R}^d \setminus \overline{\partial B})$ are radiating solutions to

$$\begin{aligned}
&\Delta w_1 + k^2 w_1 = 0 \quad \text{in } \mathbb{R}^d \setminus (\overline{D_1 \cup D_2}), \quad w_1 = f_1 \quad \text{on } \partial D_1, \quad \frac{\partial w_1}{\partial \boldsymbol{\nu}} = 0 \quad \text{on } \partial D_2,\\
&\Delta w_2 + k^2 w_2 = 0 \quad \text{in } \mathbb{R}^d \setminus (\overline{D_1 \cup D_2}), \quad w_2 = 0 \quad \text{on } \partial D_1, \quad \frac{\partial w_2}{\partial \boldsymbol{\nu}} = \widetilde{R}^*_{\Gamma_1} g_{\Gamma_2} \quad \text{on } \partial D_2,\\
&\Delta v_B + k^2 v_B = 0 \quad \text{in } \mathbb{R}^d \setminus \overline{\partial B}.
\end{aligned}$$

Applying Rellich's lemma 2.9 we see that $w_2 = w_1 + v_B$ in $\mathbb{R}^d \setminus (\overline{B \cup D_1 \cup D_2})$. Therefore,

$$g_{\Gamma_2} = \frac{\partial w_2}{\partial \boldsymbol{\nu}}\Big|_{\Gamma_2} = \Big(\frac{\partial w_1}{\partial \boldsymbol{\nu}} + \frac{\partial v_B}{\partial \boldsymbol{\nu}}\Big)\Big|_{\Gamma_2} = \frac{\partial v_B}{\partial \boldsymbol{\nu}}\Big|_{\Gamma_2} = \frac{\partial}{\partial \boldsymbol{\nu}}(\mathrm{SL}_B\psi_B)|_{\Gamma_2}.$$

Since $\overline{\Gamma_2}$ is C^1 smooth, this and the smoothness of $\mathrm{SL}_B\psi_B$ away from ∂B imply that $g_{\Gamma_2} \in C^1(\overline{\Gamma_2})$. Let $X \subseteq \widetilde{H}^{1/2}(\Gamma_2)$ be the infinite-dimensional subspace of continuous piecewise linear functions from Lemma A.1. Since X does not contain any C^1-smooth functions except zero, it follows that $Z := G^{\mathrm{mix}}_D R^*_{D_2} \widetilde{R}^*_{\Gamma_2}(X)$ satisfies

$$Z \cap \mathcal{R}\Big(\begin{bmatrix} G^{\mathrm{mix}}_D R^*_{D_1} & H^*_B \end{bmatrix}\Big) = \{0\}.$$

As Z is the image of the infinite-dimensional space X under the injective operator $G^{\mathrm{mix}}_D R^*_{D_2} \widetilde{R}^*_{\Gamma_2}$, Z is infinite dimensional as well. Accordingly,

$$\mathcal{R}(G^{\mathrm{mix}}_D R^*_{D_2} \widetilde{R}^*_{\Gamma_2}) \not\subseteq \mathcal{R}\Big(\begin{bmatrix} G^{\mathrm{mix}}_D R^*_{D_1} & H^*_B \end{bmatrix}\Big). \qquad \square$$

Finally, we give the proof of Theorem 2.38

Proof of Theorem 2.38. Let $B, D_1, D_2 \subseteq \mathbb{R}^d$ be open and Lipschitz bounded such that the complement $\mathbb{R}^d \setminus (\overline{B \cup D_1 \cup D_2})$ is connected. Suppose that ∂D_2 is piecewise C^1 smooth and that $D_2 \not\subseteq B$. Let $V \subseteq L^2(S^{d-1})$ be a finite-dimensional subspace. As before, $P_V : L^2(S^{d-1}) \to L^2(S^{d-1})$ denotes the orthogonal projection onto V.

Since $D_2 \not\subseteq B$ and ∂D_2 is piecewise C^1 smooth, there exists $\Gamma_2 \subseteq \partial D_2 \setminus \overline{B}$ connected and relatively open such that $\overline{\Gamma_2}$ is C^1 smooth. Thus, as $\mathbb{R}^d \setminus (\overline{B \cup D_1 \cup D_2})$ is connected, it follows from Lemma 2.36 that

$$Z \cap \mathcal{R}\Big(\begin{bmatrix} G^{\mathrm{mix}}_D R^*_{D_1} & H^*_B \end{bmatrix}\Big) = \{0\},$$

where $Z \subseteq \mathcal{R}(G^{\mathrm{mix}}_D R^*_{D_2} \widetilde{R}^*_{\Gamma_2})$ denotes the infinite-dimensional subspace in Lemma 2.39. We apply Lemma 2.23 and find that

$$Z \not\subseteq \mathcal{R}\Big(\begin{bmatrix} G^{\mathrm{mix}}_D R^*_{D_1} & H^*_B \end{bmatrix}\Big) + V = \mathcal{R}\Big(\begin{bmatrix} G^{\mathrm{mix}}_D R^*_{D_1} & H^*_B & P_V \end{bmatrix}\Big).$$

Thus, we have

$$\mathcal{R}(G^{\mathrm{mix}}_D R^*_{D_2} \widetilde{R}^*_{\Gamma_2}) \not\subseteq \mathcal{R}\Big(\begin{bmatrix} G^{\mathrm{mix}}_D R^*_{D_1} & H^*_B & P_V \end{bmatrix}\Big).$$

Accordingly, Lemma 2.21 implies that there is no constant $C > 0$ such that

$$\begin{aligned}\|(\widetilde{R}_{\Gamma_2} R_{D_2} G_D^{\mathrm{mix}^*})\phi\|^2_{H^{1/2}(\Gamma_2)} &\leq C^2 \left\| \begin{bmatrix} R_{D_1} G_D^{\mathrm{mix}^*} \\ H_B \\ P_V \end{bmatrix} \phi \right\|^2_{H^{-1/2}(\partial D_1)\times H^{1/2}(\partial B)\times L^2(S^{d-1})} \\ &= C^2 \big(\|(R_{D_1} G_D^{\mathrm{mix}^*})\phi\|^2_{H^{-1/2}(\partial D_1)} + \|H_B\phi\|^2_{H^{1/2}(\partial B)} + \|P_V\phi\|^2_{L^2(S^{d-1})} \big) .\end{aligned}$$

Therefore, there exists a sequence $(\widetilde{\phi}_m)_{m\in\mathbb{N}} \subseteq L^2(S^{d-1})$ satisfying

$$\|(\widetilde{R}_{\Gamma_2} R_{D_2} G_D^{\mathrm{mix}^*})\widetilde{\phi}_m\|^2_{H^{1/2}(\Gamma_2)} \to \infty$$

and

$$\|(R_{D_1} G_D^{\mathrm{mix}^*})\widetilde{\phi}_m\|^2_{H^{1/2}(\partial D_2)} + \|H_B\widetilde{\phi}_m\|^2_{H^{1/2}(\partial B)} + \|P_V\widetilde{\phi}_m\|^2_{L^2(S^{d-1})} \to 0$$

as $m \to \infty$. We define $\phi_m := \widetilde{\phi}_m - P_V\widetilde{\phi}_m \in V^\perp$ for any $m \in \mathbb{N}$. As $\|\widetilde{R}_{\Gamma_2}\| = 1$, we obtain

$$\begin{aligned}\|(R_{D_2} G_D^{\mathrm{mix}^*})\phi_m\|_{H^{1/2}(\partial D_2)} &= \|\widetilde{R}_{\Gamma_2}\| \|(R_{D_2} G_D^{\mathrm{mix}^*})\phi_m\|_{H^{1/2}(\partial D_2)} \\ &\geq \|(\widetilde{R}_{\Gamma_2} R_{D_2} G_D^{\mathrm{mix}^*})\phi_m\|_{H^{1/2}(\Gamma_2)} \\ &\geq \big| \|(\widetilde{R}_{\Gamma_2} R_{D_2} G_D^{\mathrm{mix}^*})\widetilde{\phi}_m\|_{H^{1/2}(\Gamma_2)} - \|\widetilde{R}_{\Gamma_2} R_{D_2} G_D^{\mathrm{mix}^*} P_V\widetilde{\phi}_m\|_{H^{1/2}(\Gamma_2)} \big| \\ &\geq \|(\widetilde{R}_{\Gamma_2} R_{D_2} G_D^{\mathrm{mix}^*})\widetilde{\phi}_m\|_{H^{1/2}(\Gamma_2)} \\ &\quad - \|\widetilde{R}_{\Gamma_2} R_{D_2} G_D^{\mathrm{mix}^*}\| \|P_V\widetilde{\phi}_m\|_{L^2(S^{d-1})} \to \infty , \\ \|(R_{D_1} G_D^{\mathrm{mix}^*})\phi_m\|_{H^{-1/2}(\partial D_1)} &\leq \|(R_{D_1} G_D^{\mathrm{mix}^*})\widetilde{\phi}_m\|_{H^{-1/2}(\partial D_1)} + \|R_{D_1} G_D^{\mathrm{mix}^*}\| \|P_V\widetilde{\phi}_m\|_{L^2(S^{d-1})} \to 0 , \\ \|H_B\phi_m\|_{H^{1/2}(\partial B)} &\leq \|H_B\widetilde{\phi}_m\|_{H^{1/2}(\partial B)} + \|H_B\| \|P_V\widetilde{\phi}_m\|_{L^2(S^{d-1})} \to 0\end{aligned}$$

as $m \to \infty$. This ends the proof. □

2.4.3. Monotonicity-Based Shape Reconstruction

While the criteria developed in Theorems 2.28 and 2.30 determine whether a certain probing domain B is contained inside the obstacle D or not, the criterion for the mixed case established in Theorem 2.40 below characterizes whether a certain probing domain B contains the obstacle D or not.

Theorem 2.40 (Shape Characterization for Mixed Obstacles)**.** *Let $B, D_1, D_2 \subseteq \mathbb{R}^d$ be open and Lipschitz bounded. Assume that k^2 is neither a Dirichlet eigenvalue of $-\Delta$ in D_1 and B nor a Neumann eigenvalue of $-\Delta$ in D_2.*

(a) If $\overline{D_1} \subseteq B$, then $-H_B^* H_B \leq_{\mathrm{fin}} \mathrm{Re}(F_D^{\mathrm{mix}})$.

(b) Suppose that $\mathbb{R}^d \setminus (\overline{B \cup D_1 \cup D_2})$ is connected and that ∂D_1 is piecewise C^1 smooth. If $D_1 \not\subseteq B$, then $-H_B^* H_B \not\leq_{\mathrm{fin}} \mathrm{Re}(F_D^{\mathrm{mix}})$.

(c) If $\overline{D_2} \subseteq B$, then $\mathrm{Re}(F_D^{\mathrm{mix}}) \leq_{\mathrm{fin}} H_B^* H_B$.

(d) Suppose that $\mathbb{R}^d \setminus (\overline{B \cup D_1 \cup D_2})$ is connected and that ∂D_2 is piecewise C^1 smooth. If $D_2 \not\subseteq B$, then $\mathrm{Re}(F_D^{\mathrm{mix}}) \not\leq_{\mathrm{fin}} H_B^* H_B$.

Remark 2.41. The results in Theorem 2.40 remain true in the special case when $D_2 = \emptyset$ and $F_D^{\mathrm{mix}} = F_{D_1}^{\mathrm{dir}}$, and also in the special case when $D_1 = \emptyset$ and $F_D^{\mathrm{mix}} = F_{D_2}^{\mathrm{neu}}$. The corresponding shape characterizations complement the results established in Theorems 2.28 and 2.30. ◊

Proof. (a) First, we observe that the operator $-N_{D_2,\mathrm{i}}^{-1}$ is self-adjoint because $-N_{D_2,\mathrm{i}}$ is self-adjoint by Theorem 2.13 (b). Besides, this theorem implies that $-N_{D_2,\mathrm{i}}^{-1}$ is coercive. In detail, we calculate

$$\begin{aligned} -\langle \varphi, N_{D_2,\mathrm{i}}^{-1}\varphi\rangle_{\partial D_2} &= -\langle \varphi, N_{D_2,\mathrm{i}}^{-1}N_{D_2,\mathrm{i}}N_{D_2,\mathrm{i}}^{-1}\varphi\rangle_{\partial D_2} = -\langle N_{D_2,\mathrm{i}}N_{D_2,\mathrm{i}}^{-1}\varphi, N_{D_2,\mathrm{i}}^{-1}\varphi\rangle_{\partial D_2} \\ &\geq c_2\|N_{D_2,\mathrm{i}}^{-1}\varphi\|_{H^{1/2}(\partial D_2)}^2 \geq \frac{c_2}{\|N_{D_2}\|^2}\|\varphi\|_{H^{-1/2}(\partial D_2)}^2 =: \underline{c}_2\|\varphi\|_{H^{-1/2}(\partial D_2)}^2 \end{aligned}$$

for all $\varphi \in H^{-1/2}(\partial D_2)$, where we used the self-adjointness of $N_{D_2,\mathrm{i}}$ and $N_{D_2,\mathrm{i}}^{-1}$ as well as the coercivity of $N_{D_2,\mathrm{i}}$. It follows that $\mathrm{diag}(J_B, -N_{D_2,\mathrm{i}}^{-1})$, where J_B again denotes the compact embedding operator $J_B : H^{1/2}(\partial B) \hookrightarrow H^{-1/2}(\partial B)$, is also self-adjoint and coercive, and we write $\widehat{c}_2$ for its coercivity constant.

Let $\overline{D_1} \subseteq B$. From Lemma 2.34 (a), it follows that

$$\mathrm{Re}(F_D^{\mathrm{mix}}) + H_B^* H_B = \begin{bmatrix} H_B \\ \partial H_{D_2} \end{bmatrix}^* \left(\begin{bmatrix} J_B & 0 \\ 0 & -\mathrm{Re}(N_{D_2}^{-1}) \end{bmatrix} - \mathrm{Re}(K_1) \right) \begin{bmatrix} H_B \\ \partial H_{D_2} \end{bmatrix}$$

with some compact operator $K_1 : H^{1/2}(\partial B) \times H^{-1/2}(\partial D_2) \to H^{-1/2}(\partial B) \times H^{1/2}(\partial D_2)$. We calculate

$$\begin{aligned} \mathrm{Re}(N_{D_2}^{-1}) &= \frac{1}{2}(N_{D_2}^{-1} + (N_{D_2}^{-1})^*) \\ &= N_{D_2,\mathrm{i}}^{-1} + \frac{1}{2}\Big((N_{D_2}^{-1} - N_{D_2,\mathrm{i}}^{-1}) + ((N_{D_2}^{-1})^* + (N_{D_2,\mathrm{i}}^{-1})^*)\Big). \end{aligned} \tag{2.63}$$

Since $N_{D_2} - N_{D_2,\mathrm{i}}$ and $N_{D_2}^* - N_{D_2,\mathrm{i}}$ are compact by Theorem 2.13 (c), this implies that

$$\mathrm{Re}(F_D^{\mathrm{mix}}) + H_B^* H_B = \begin{bmatrix} H_B \\ \partial H_{D_2} \end{bmatrix}^* \left(\begin{bmatrix} J_B & 0 \\ 0 & -N_{D_2,\mathrm{i}}^{-1} \end{bmatrix} + C_1 \right) \begin{bmatrix} H_B \\ \partial H_{D_2} \end{bmatrix}$$

with a compact self-adjoint operator $C_1 : H^{1/2}(\partial B) \times H^{-1/2}(\partial D_2) \to H^{-1/2}(\partial B) \times H^{1/2}(\partial D_2)$. Thus, $\mathrm{Re}(F_D^{\mathrm{mix}}) + H_B^* H_B$ is a compact perturbation of a self-adjoint and coercive operator. Accordingly,

$$\begin{aligned} \langle (\mathrm{Re}(F_D^{\mathrm{mix}}) + H_B^* H_B)\phi, \phi\rangle &\geq \widehat{c}_2 \left\| \begin{bmatrix} H_B \\ \partial H_{D_2} \end{bmatrix} \phi \right\|_{H^{1/2}(\partial B) \times H^{-1/2}(\partial D_2)}^2 \\ &\quad + \left\langle \begin{bmatrix} H_B \\ \partial H_{D_2} \end{bmatrix}^* C_1 \begin{bmatrix} H_B \\ \partial H_{D_2} \end{bmatrix} \phi, \phi \right\rangle \end{aligned} \tag{2.64}$$

for all $\phi \in L^2(S^{d-1})$. We proceed similarly as in the proof of Lemma 2.32 and employ the square root of the single layer operator from Lemma 2.14 and the associated operators from

(2.20)–(2.21) to see that

$$\Big\langle \begin{bmatrix} H_B \\ \partial H_{D_2} \end{bmatrix}^* C_1 \begin{bmatrix} H_B \\ \partial H_{D_2} \end{bmatrix} \phi,\phi \Big\rangle = \Big\langle \begin{bmatrix} H_B^* S_{B,\mathrm{i}}^{-1/2} S_{B,\mathrm{i}}^{1/2} \\ (\partial H_{D_2})^* S_{D_2,\mathrm{i}}^{*/2} S_{D_2,\mathrm{i}}^{-*/2} \end{bmatrix} C_1 \begin{bmatrix} S_{B,\mathrm{i}}^{*/2} S_{B,\mathrm{i}}^{-*/2} H_B \\ S_{D_2,\mathrm{i}}^{-1/2} S_{D_2,\mathrm{i}}^{1/2} \partial H_{D_2} \end{bmatrix} \phi, \phi \Big\rangle$$
$$= \Big\langle \widetilde{C}_1 \begin{bmatrix} S_{B,\mathrm{i}}^{-*/2} H_B \\ S_{D_2,\mathrm{i}}^{1/2} (\partial H_{D_2}) \end{bmatrix} \phi, \begin{bmatrix} S_{B,\mathrm{i}}^{-*/2} H_B \\ S_{D_2,\mathrm{i}}^{1/2} (\partial H_{D_2}) \end{bmatrix} \phi \Big\rangle_{L^2(\partial B)\times L^2(\partial D_2)}, \quad (2.65)$$

where the operator $\widetilde{C}_1 : L^2(\partial B) \times L^2(\partial D_2) \to L^2(\partial B) \times L^2(\partial D_2)$,

$$\widetilde{C}_1 := \begin{bmatrix} S_{B,\mathrm{i}}^{1/2} \\ S_{D_2,\mathrm{i}}^{-*/2} \end{bmatrix} C_1 \begin{bmatrix} S_{B,\mathrm{i}}^{*/2} \\ S_{D_2,\mathrm{i}}^{-1/2} \end{bmatrix},$$

is compact and self-adjoint. Let $\widetilde{V}_1 \subseteq L^2(\partial B) \times L^2(\partial D_2)$ be the sum of eigenspaces of $\widetilde{C}_1$ associated to eigenvalues smaller than $-\widetilde{c}_2 := -\widehat{c}_2 / \| \begin{bmatrix} S_{B,\mathrm{i}}^{-*/2} & S_{D_2,\mathrm{i}}^{1/2} \end{bmatrix} \|^2$. From the spectral theorem for compact self-adjoint operators (see Remark 2.1), it follows that $\widetilde{V}_1$ is finite dimensional. Besides, we observe that

$$\langle \widetilde{C}_1 \widetilde{v}_1, \widetilde{v}_1 \rangle_{L^2(\partial B)\times L^2(\partial D_2)} \geq -\widetilde{c}_2 \|\widetilde{v}_1\|^2_{L^2(\partial B)\times L^2(\partial D_2)} \qquad \text{for all } \widetilde{v}_1 \in \widetilde{V}_1^{\perp}. \quad (2.66)$$

Moreover, we have

$$\begin{bmatrix} S_{B,\mathrm{i}}^{-*/2} H_B \\ S_{D_2,\mathrm{i}}^{1/2} (\partial H_{D_2}) \end{bmatrix} \phi \in \widetilde{V}_1^{\perp} \qquad \text{if and only if} \qquad \phi \in \left(\begin{bmatrix} H_B^* S_{B,\mathrm{i}}^{-1/2} \\ (\partial H_{D_2})^* S_{D_2,\mathrm{i}}^{*/2} \end{bmatrix} \widetilde{V}_1 \right)^{\perp}.$$

Setting

$$V_1 := \begin{bmatrix} H_B^* S_{B,\mathrm{i}}^{-1/2} \\ (\partial H_{D_2})^* S_{D_2,\mathrm{i}}^{*/2} \end{bmatrix} \widetilde{V}_1 \subseteq L^2(S^{d-1})$$

yields $\dim(V_1) \leq \dim(\widetilde{V}_1) < \infty$, and combining (2.66) with (2.65) gives

$$\Big\langle \begin{bmatrix} H_B \\ \partial H_{D_2} \end{bmatrix}^* C_1 \begin{bmatrix} H_B \\ \partial H_{D_2} \end{bmatrix} \phi, \phi \Big\rangle \geq -\widetilde{c}_2 \Big\| \begin{bmatrix} S_{B,\mathrm{i}}^{-*/2} H_B \\ S_{D_2,\mathrm{i}}^{1/2} (\partial H_{D_2}) \end{bmatrix} \phi \Big\|^2_{L^2(\partial B)\times L^2(\partial D_2)}$$
$$\geq -\widetilde{c}_2 \Big\| \begin{bmatrix} S_{B,\mathrm{i}}^{-*/2} \\ S_{D_2,\mathrm{i}}^{1/2} \end{bmatrix} \Big\|^2 \Big\| \begin{bmatrix} H_B \\ \partial H_{D_2} \end{bmatrix} \phi \Big\|^2_{H^{1/2}(\partial B)\times H^{-1/2}(\partial D_2)} = -\widehat{c}_2 \Big\| \begin{bmatrix} H_B \\ \partial H_{D_2} \end{bmatrix} \phi \Big\|^2_{H^{1/2}(\partial B)\times H^{-1/2}(\partial D_2)}$$

for all $\phi \in V_1^{\perp}$. Finally, (2.64) implies

$$\langle (\mathrm{Re}(F_D^{\mathrm{mix}}) + H_B^* H_B)\phi, \phi \rangle \geq 0 \qquad \text{for all } \phi \in V_1^{\perp},$$

and Lemma 2.2 yields the result.

(b) Let $\mathbb{R}^d \setminus (\overline{B \cup D_1 \cup D_2})$ be connected, and let ∂D_1 be piecewise C^1 smooth. We suppose that there exists a finite-dimensional subspace $V_2 \subseteq L^2(S^{d-1})$ such that

$$-\langle H_B^* H_B \phi, \phi\rangle \;\leq\; \langle \mathrm{Re}(F_D^{\mathrm{mix}})\phi, \phi\rangle \qquad \text{for all } \phi \in V_2^{\perp}\,.$$

Theorem 2.33 gives

$$\mathrm{Re}(F_D^{\mathrm{mix}}) \;=\; -G_D^{\mathrm{mix}}\Bigg(\begin{bmatrix}\mathrm{Re}(S_{D_1}) & 0\\ 0 & \mathrm{Re}(N_{D_2})\end{bmatrix} + \mathrm{Re}(K_D^{\mathrm{mix}})\Bigg)G_D^{\mathrm{mix}*}\,.$$

We already know that $\mathrm{Re}(S_{D_1}) = \frac{1}{2}(S_{D_1}^* + S_{D_1})$ and $\mathrm{Re}(N_{D_2}) = \frac{1}{2}(N_{D_2}^* + N_{D_2})$ are compact perturbations of $S_{D_1,\mathrm{i}}$ and $N_{D_2,\mathrm{i}}$, respectively (see, e.g., in the proof of Corollary 2.17). Therewith, we deduce

$$\mathrm{Re}(F_D^{\mathrm{mix}}) \;=\; -G_D^{\mathrm{mix}}\Bigg(\begin{bmatrix}S_{D_1,\mathrm{i}} & 0\\ 0 & N_{D_2,\mathrm{i}}\end{bmatrix} + K\Bigg)G_D^{\mathrm{mix}*}$$

with some compact self-adjoint operator K that maps from $H^{-1/2}(\partial D_1) \times H^{1/2}(\partial D_2)$ to $H^{1/2}(\partial D_1) \times H^{-1/2}(\partial D_2)$. Accordingly, Lemma 2.32 guarantees the existence of a finite-dimensional subspace $V_3 \subseteq L^2(S^{d-1})$ such that

$$\big|\langle K G_D^{\mathrm{mix}*}\phi, G_D^{\mathrm{mix}*}\phi\rangle_{\partial D_1 \times \partial D_2}\big| \;\leq\; \frac{c_1}{2}\|G_D^{\mathrm{mix}*}\phi\|^2_{H^{-1/2}(\partial D_1)\times H^{1/2}(\partial D_2)} \qquad \text{for all } \phi \in V_3^{\perp}\,,$$

where c_1 denotes the coercivity constant of $S_{D_1,\mathrm{i}}$ (see Theorem 2.12 (b)). We find that the subspace $V_2 + V_3 \subseteq L^2(S^{d-1})$ is finite dimensional, and thus $(V_2 + V_3)^{\perp} \neq \{0\}$. Using the definitions of the restriction operators R_{D_1} and R_{D_2} from (2.59), it follows that, for all $\phi \in (V_2 + V_3)^{\perp}$,

$$\begin{aligned}
0 \;&\leq\; \langle \mathrm{Re}(F_D^{\mathrm{mix}})\phi, \phi\rangle + \langle H_B^* H_B \phi, \phi\rangle\\
&=\; -\langle (G_D^{\mathrm{mix}} R_{D_1}^*) S_{D_1,\mathrm{i}} (G_D^{\mathrm{mix}} R_{D_1}^*)^* \phi, \phi\rangle - \langle (G_D^{\mathrm{mix}} R_{D_2}^*) N_{D_2,\mathrm{i}} (G_D^{\mathrm{mix}} R_{D_2}^*)^* \phi, \phi\rangle\\
&\quad - \langle G_D^{\mathrm{mix}} K G_D^{\mathrm{mix}*}\phi, \phi\rangle + \langle H_B^* H_B \phi, \phi\rangle\\
&\leq\; -\langle (R_{D_1} G_D^{\mathrm{mix}*})\phi, S_{D_1,\mathrm{i}}(R_{D_1} G_D^{\mathrm{mix}*})\phi\rangle_{\partial D_1} + |\langle N_{D_2,\mathrm{i}}(R_{D_2} G_D^{\mathrm{mix}*})\phi, (R_{D_2} G_D^{\mathrm{mix}*})\phi\rangle_{\partial D_2}|\\
&\quad + |\langle K G_D^{\mathrm{mix}*}\phi, G_D^{\mathrm{mix}*}\phi\rangle_{\partial D_1 \times \partial D_2}| + \langle H_B^* H_B \phi, \phi\rangle\\
&\leq -c_1 \|(R_{D_1} G_D^{\mathrm{mix}*})\phi\|^2_{H^{-1/2}(\partial D_1)} + \|N_{D_2,\mathrm{i}}\|\|(R_{D_2} G_D^{\mathrm{mix}*})\phi\|^2_{H^{1/2}(\partial D_2)}\\
&\quad + \frac{c_1}{2}\|G_D^{\mathrm{mix}*}\phi\|^2_{H^{-1/2}(\partial D_1)\times H^{1/2}(\partial D_2)} + \|H_B\phi\|^2_{H^{1/2}(\partial B)}\\
&=\; \Big(\|N_{D_2,\mathrm{i}}\| + \frac{c_1}{2}\Big)\|(R_{D_2} G_D^{\mathrm{mix}*})\phi\|^2_{H^{1/2}(\partial D_2)} + \|H_B\phi\|^2_{H^{1/2}(\partial B)}\\
&\quad - \frac{c_1}{2}\|(R_{D_1} G_D^{\mathrm{mix}*})\phi\|^2_{H^{-1/2}(\partial D_1)}\\
&\leq\; \max\{\|N_{D_2,\mathrm{i}}\| + \frac{c_1}{2}, 1\}\Big(\|(R_{D_2} G_D^{\mathrm{mix}*})\phi\|^2_{H^{1/2}(\partial D_2)} + \|H_B\phi\|^2_{H^{1/2}(\partial B)}\Big)\\
&\quad - \frac{c_1}{2}\|(R_{D_1} G_D^{\mathrm{mix}*})\phi\|^2_{H^{-1/2}(\partial D_1)}\,.
\end{aligned}$$

Applying Theorem 2.35 with $V = V_2 + V_3$ gives a contradiction.

(c) Proceeding similarly as in part (a), it can be shown that the operator $\operatorname{diag}(S_{D_1,\mathrm{i}}^{-1}, J_B)$ is self-adjoint and coercive with a positive coercivity constant that we denote by $\widetilde{c}_1$.

Let $\overline{D_2} \subseteq B$. Lemma 2.34 (b) gives

$$\operatorname{Re}(F_D^{\mathrm{mix}}) - H_B^* H_B \;=\; -\begin{bmatrix} H_{D_1} \\ H_B \end{bmatrix}^* \left(\begin{bmatrix} \operatorname{Re}(S_{D_1}^{-1}) & 0 \\ 0 & J_B \end{bmatrix} + \operatorname{Re}(K_2) \right) \begin{bmatrix} H_{D_1} \\ H_B \end{bmatrix},$$

where $K_2 : H^{1/2}(\partial D_1) \times H^{1/2}(\partial B) \to H^{-1/2}(\partial D_1) \times H^{-1/2}(\partial B)$ is compact. Analogous to (2.63) we observe that $\operatorname{Re}(S_{D_1}^{-1})$ is a compact perturbation of the self-adjoint and coercive operator $S_{D_1,\mathrm{i}}^{-1}$. Therewith, we get

$$\operatorname{Re}(F_D^{\mathrm{mix}}) - H_B^* H_B \;=\; -\begin{bmatrix} H_{D_1} \\ H_B \end{bmatrix}^* \left(\begin{bmatrix} S_{D_1,\mathrm{i}}^{-1} & 0 \\ 0 & J_B \end{bmatrix} + C_2 \right) \begin{bmatrix} H_{D_1} \\ H_B \end{bmatrix},$$

where $C_2 : H^{1/2}(\partial D_1) \times H^{1/2}(\partial B) \to H^{-1/2}(\partial D_1) \times H^{-1/2}(\partial B)$ is a compact self-adjoint operator. It follows that

$$\langle (\operatorname{Re}(F_D^{\mathrm{mix}}) - H_B^* H_B)\phi, \phi \rangle \;\leq\; -\widetilde{c}_1 \left\| \begin{bmatrix} H_{D_1} \\ H_B \end{bmatrix} \phi \right\|^2_{H^{1/2}(\partial D_1) \times H^{1/2}(\partial B)} - \left\langle \begin{bmatrix} H_{D_1} \\ H_B \end{bmatrix}^* C_2 \begin{bmatrix} H_{D_1} \\ H_B \end{bmatrix} \phi, \phi \right\rangle$$

for all $\phi \in L^2(S^{d-1})$. We rewrite the inner product on the right-hand side in the form

$$\left\langle \begin{bmatrix} H_{D_1} \\ H_B \end{bmatrix}^* C_2 \begin{bmatrix} H_{D_1} \\ H_B \end{bmatrix} \phi, \phi \right\rangle \;=\; \left\langle \begin{bmatrix} H_{D_1}^* S_{D_1,\mathrm{i}}^{-1/2} S_{D_1,\mathrm{i}}^{1/2} \\ H_B^* S_{B,\mathrm{i}}^{-1/2} S_{B,\mathrm{i}}^{1/2} \end{bmatrix} C_2 \begin{bmatrix} S_{D_1,\mathrm{i}}^{*/2} S_{D_1,\mathrm{i}}^{-*/2} H_{D_1} \\ S_{B,\mathrm{i}}^{*/2} S_{B,\mathrm{i}}^{-*/2} H_B \end{bmatrix} \phi, \phi \right\rangle.$$

Then, similar reasoning as in part (a) shows that there exists a finite-dimensional subspace $V_4 \subseteq L^2(S^{d-1})$ such that

$$\langle (\operatorname{Re}(F_D^{\mathrm{mix}}) - H_B^* H_B)\phi, \phi \rangle \;\leq\; 0 \qquad \text{for all } \phi \in V_4^{\perp},$$

and Lemma 2.2 yields the result.

(d) Let $\mathbb{R}^d \setminus (\overline{B \cup D_1 \cup D_2})$ be connected, and let ∂D_2 be piecewise C^1 smooth. We suppose that there exists a finite-dimensional subspace $V_5 \subseteq L^2(S^{d-1})$ such that

$$\langle \operatorname{Re}(F_D^{\mathrm{mix}})\phi, \phi \rangle \;\leq\; \langle H_B^* H_B \phi, \phi \rangle \qquad \text{for all } \phi \in V_5^{\perp}.$$

We recall from part (b) that

$$\operatorname{Re}(F_D^{\mathrm{mix}}) \;=\; -G_D^{\mathrm{mix}} \left(\begin{bmatrix} S_{D_1,\mathrm{i}} & 0 \\ 0 & N_{D_2,\mathrm{i}} \end{bmatrix} + K \right) G_D^{\mathrm{mix}*}$$

with some compact self-adjoint operator K that maps from $H^{-1/2}(\partial D_1) \times H^{1/2}(\partial D_2)$ to $H^{1/2}(\partial D_1) \times H^{-1/2}(\partial D_2)$. Consequently, from Lemma 2.32, it follows that there exists a

finite-dimensional subspace $V_6 \subseteq L^2(S^{d-1})$ such that

$$\left|\langle K G_D^{\mathrm{mix}^*}\phi, G_D^{\mathrm{mix}^*}\phi\rangle_{\partial D_1\times\partial D_2}\right| \leq \frac{c_2}{2}\|G_D^{\mathrm{mix}^*}\phi\|^2_{H^{-1/2}(\partial D_1)\times H^{1/2}(\partial D_2)} \qquad \text{for all } \phi \in V_6^{\perp},$$

where c_2 denotes the coercivity constant of $N_{D_2,\mathrm{i}}$ (see Theorem 2.13 (b)). We observe that $V_5 + V_6 \subseteq L^2(S^{d-1})$ is finite dimensional, and thus $(V_5+V_6)^{\perp} \neq \{0\}$. Using the definitions of the restriction operators R_{D_1} and R_{D_2} from (2.59), we find that, for all $\phi \in (V_5+V_6)^{\perp}$,

$$\begin{aligned}
0 &\leq \langle H_B^* H_B\phi,\phi\rangle - \langle \mathrm{Re}(F_D^{\mathrm{mix}})\phi,\phi\rangle\\
&= \langle H_B^* H_B\phi,\phi\rangle + \langle (G_D^{\mathrm{mix}} R_{D_1}^*) S_{D_1,\mathrm{i}} (G_D^{\mathrm{mix}} R_{D_1}^*)^*\phi,\phi\rangle\\
&\quad + \langle (G_D^{\mathrm{mix}} R_{D_2}^*) N_{D_2,\mathrm{i}} (G_D^{\mathrm{mix}} R_{D_2}^*)^*\phi,\phi\rangle + \langle G_D^{\mathrm{mix}} K G_D^{\mathrm{mix}^*}\phi,\phi\rangle\\
&\leq \langle H_B^* H_B\phi,\phi\rangle + |\langle (R_{D_1} G_D^{\mathrm{mix}^*})\phi, S_{D_1,\mathrm{i}}(R_{D_1} G_D^{\mathrm{mix}^*})\phi\rangle_{\partial D_1}|\\
&\quad + \langle N_{D_2,\mathrm{i}}(R_{D_2} G_D^{\mathrm{mix}^*})\phi, (R_{D_2} G_D^{\mathrm{mix}^*}\phi\rangle_{\partial D_2} + |\langle K G_D^{\mathrm{mix}^*}\phi, G_D^{\mathrm{mix}^*}\phi\rangle_{\partial D_1\times\partial D_2}|\\
&\leq \|H_B\phi\|^2_{H^{1/2}(\partial B)} + \|S_{D_1,\mathrm{i}}\|\|(R_{D_1} G_D^{\mathrm{mix}^*})\phi\|^2_{H^{-1/2}(\partial D_1)}\\
&\quad - c_2\|(R_{D_2} G_D^{\mathrm{mix}^*})\phi\|^2_{H^{1/2}(\partial D_2)} + \frac{c_2}{2}\|G_D^{\mathrm{mix}^*}\phi\|^2_{H^{-1/2}(\partial D_1)\times H^{1/2}(\partial D_2)}\\
&= \|H_B\phi\|^2_{H^{1/2}(\partial B)} + \Big(\|S_{D_1,\mathrm{i}}\| + \frac{c_2}{2}\Big)\|(R_{D_1} G_D^{\mathrm{mix}^*})\phi\|^2_{H^{-1/2}(\partial D_1)}\\
&\quad - \frac{c_2}{2}\|(R_{D_2} G_D^{\mathrm{mix}^*})\phi\|^2_{H^{1/2}(\partial D_2)}\\
&\leq \max\{\|S_{D_1,\mathrm{i}}\| + \frac{c_2}{2}, 1\}\Big(\|H_B\phi\|^2_{H^{1/2}(\partial B)} + \|(R_{D_1} G_D^{\mathrm{mix}^*})\phi\|^2_{H^{-1/2}(\partial D_1)}\Big)\\
&\quad - \frac{c_2}{2}\|(R_{D_2} G_D^{\mathrm{mix}^*})\phi\|^2_{H^{1/2}(\partial D_2)}.
\end{aligned}$$

Applying Theorem 2.38 with $V = V_5 + V_6$ gives a contradiction. □

2.5. Numerical Examples

We aim to illustrate our theoretical findings from Subsections 2.3.3 and 2.4.3 and are now working toward numerical implementations of the developed shape characterizations. The main issue here is that numerical approximations of the operators $F_{D_1}^{\mathrm{dir}}$, $F_{D_2}^{\mathrm{neu}}$, F_D^{mix} and H_B are necessarily finite dimensional. Accordingly, the question of whether suitable combinations of these operators as considered in Theorems 2.28, 2.30 and 2.40 are positive or negative definite up to some finite-dimensional subspace, needs to be carefully relaxed to obtain reliable numerical algorithms. We present some preliminary ideas in this direction, restricting the discussion to the two-dimensional case. First, we consider the case when there are either only Dirichlet or only Neumann obstacles present. In Subsection 2.5.1, we examine radially symmetric obstacles. Thereafter, we derive a reconstruction procedure for arbitrary shapes in Subsection 2.5.2. To conclude, we consider mixed obstacles in Subsection 2.5.3 and propose a strategy to separate the Dirichlet and the Neumann parts.

2.5.1. AN EXPLICIT RADIALLY SYMMETRIC EXAMPLE

We consider a single radially symmetric obstacle. More precisely, we assume that the obstacle is a disk of radius $r > 0$ centered at the origin. Besides, we suppose the probing domains B to be disks of radius $R > 0$ with the same center. In this case, it is possible to compute the eigenvalue decompositions of the far field operators $F_{D_1}^{\mathrm{dir}}$ and $F_{D_2}^{\mathrm{neu}}$, respectively, and of the probing operator $H_B^* H_B$ explicitly. Therewith, we illustrate the shape characterization results from Theorems 2.28, 2.30 and 2.40.

We start with a single Dirichlet obstacle and present the scenario of a single Neumann obstacle afterward. Hence, let $D_2 = \emptyset$, and let $D_1 = B_r(0) \subseteq \mathbb{R}^2$ be the disk of radius $r > 0$ centered at the origin.

First, we derive series expansions for the incident and scattered fields and utilize them to compute the eigenvalue decomposition of the far field operator $F_{D_1}^{\mathrm{dir}}$. We use the Jacobi-Anger expansion (C.7) and obtain that for each incident direction $\boldsymbol{\theta} = (\cos t, \sin t)^\top \in S^1$, the incident field satisfies

$$u^i(\boldsymbol{x};\boldsymbol{\theta}) \;=\; e^{\mathrm{i}k\boldsymbol{x}\cdot\boldsymbol{\theta}} \;=\; e^{\mathrm{i}k|\boldsymbol{x}|(\cos\xi\cos t+\sin\xi\sin t)} \;=\; e^{\mathrm{i}k|\boldsymbol{x}|\cos(t-\xi)} \;=\; \sum_{n\in\mathbb{Z}} \mathrm{i}^n e^{-\mathrm{i}n\xi} J_n(k|\boldsymbol{x}|) e^{\mathrm{i}nt} \tag{2.67}$$

in every point $\boldsymbol{x} = |\boldsymbol{x}|(\cos\xi, \sin\xi)^\top \in \mathbb{R}^2$. From Theorem C.1, it follows that there exist uniquely determined coefficients a_n, $n \in \mathbb{Z}$, such that

$$u^s(\boldsymbol{x};\boldsymbol{\theta}) \;=\; \sum_{n\in\mathbb{Z}} a_n H_n^{(1)}(k|\boldsymbol{x}|) e^{-\mathrm{i}n\xi}\,, \qquad \boldsymbol{x} = |\boldsymbol{x}|(\cos\xi,\sin\xi)^\top \in \mathbb{R}^2 \setminus \overline{D_1}\,.$$

We plug in the boundary condition $u^s(\boldsymbol{x};\boldsymbol{\theta}) = -u^i(\boldsymbol{x};\boldsymbol{\theta})$ on ∂D_1 and get

$$a_n \;=\; -\mathrm{i}^n \frac{J_n(kr)}{H_n^{(1)}(kr)} e^{\mathrm{i}nt}\,,$$

and therefore, it holds

$$u^s(\boldsymbol{x};\boldsymbol{\theta}) \;=\; -\sum_{n\in\mathbb{Z}} \mathrm{i}^n \frac{J_n(kr)}{H_n^{(1)}(kr)} e^{-\mathrm{i}n\xi} H_n^{(1)}(k|\boldsymbol{x}|) e^{\mathrm{i}nt}\,, \qquad \boldsymbol{x} = |\boldsymbol{x}|(\cos\xi,\sin\xi)^\top \in \mathbb{R}^2 \setminus \overline{D_1}\,.$$

Substituting the asymptotic behavior (C.3) of the Hankel functions, we find that

$$\begin{aligned} H_n^{(1)}(k|\boldsymbol{x}|) \;&=\; \sqrt{\frac{2}{\pi k|\boldsymbol{x}|}} e^{\mathrm{i}(k|\boldsymbol{x}|-\frac{n\pi}{2}-\frac{\pi}{4})} \Big(1 + \mathcal{O}\Big(\frac{1}{k|\boldsymbol{x}|}\Big)\Big) \\ &=\; \frac{4}{\sqrt{8\pi k|\boldsymbol{x}|}} e^{\mathrm{i}k|\boldsymbol{x}|} e^{(-n-1)\frac{\pi}{2}\mathrm{i}} e^{\mathrm{i}\frac{\pi}{4}} + \mathcal{O}\big((k|\boldsymbol{x}|)^{-3/2}\big) \\ &=\; \frac{e^{\mathrm{i}\frac{\pi}{4}}}{\sqrt{8\pi k}} \frac{e^{\mathrm{i}k|\boldsymbol{x}|}}{\sqrt{|\boldsymbol{x}|}} 4\mathrm{i}^{-n-1} + \mathcal{O}\big((k|\boldsymbol{x}|)^{-3/2}\big) \end{aligned} \tag{2.68}$$

as $|\boldsymbol{x}| \to \infty$. We recall Lemma 2.8 to see that the far field pattern of u^s is

$$u^\infty(\widehat{\boldsymbol{x}};\boldsymbol{\theta}) \;=\; \sum_{n\in\mathbb{Z}} 4\mathrm{i}\frac{J_n(kr)}{H_n^{(1)}(kr)} e^{-\mathrm{i}n\xi} e^{\mathrm{i}nt}\,, \qquad \widehat{\boldsymbol{x}} = (\cos\xi,\sin\xi)^\top \in S^1\,.$$

Let $\phi \in L^2(S^1)$ with Fourier expansion

$$\phi(\boldsymbol{\theta}) \;=\; \sum_{m\in\mathbb{Z}} \phi_m e^{\mathrm{i}mt}\,, \qquad \boldsymbol{\theta} = (\cos t,\sin t)^\top \in S^1\,. \tag{2.69}$$

Then, the far field operator $F_{D_1}^{\mathrm{dir}}:\; L^2(S^1) \to L^2(S^1)$ from (2.14) satisfies

$$\begin{aligned}
(F_{D_1}^{\mathrm{dir}}\phi)(\widehat{\boldsymbol{x}}) \;&=\; \int_0^{2\pi} \Big(\sum_{n\in\mathbb{Z}} 4\mathrm{i}\frac{J_n(kr)}{H_n^{(1)}(kr)} e^{-\mathrm{i}n\xi} e^{\mathrm{i}nt}\Big)\Big(\sum_{m\in\mathbb{Z}} \phi_m e^{\mathrm{i}mt}\Big)\,\mathrm{d}t \\
&=\; \sum_{n\in\mathbb{Z}}\sum_{m\in\mathbb{Z}} 4\mathrm{i}\frac{J_n(kr)}{H_n^{(1)}(kr)} \Big(\int_0^{2\pi} \phi_m e^{\mathrm{i}(n+m)t}\,\mathrm{d}t\Big) e^{-\mathrm{i}n\xi} \\
&=\; \sum_{n\in\mathbb{Z}} 8\pi\mathrm{i}\frac{J_n(kr)}{H_n^{(1)}(kr)} \phi_n e^{\mathrm{i}n\xi}\,,
\end{aligned}$$

$\widehat{\boldsymbol{x}} = (\cos\xi,\sin\xi)^\top \in S^1$. Accordingly, the eigenvalues and eigenvectors of $F_{D_1}^{\mathrm{dir}}$ are given by $(\lambda_{n,r}^{\mathrm{dir}}, \upsilon_n)_{n\in\mathbb{Z}}$ with

$$\lambda_{n,r}^{\mathrm{dir}} \;:=\; 8\pi\mathrm{i}\frac{J_n(kr)}{H_n^{(1)}(kr)}\,, \quad \upsilon_n(\widehat{\boldsymbol{x}}) \;:=\; \frac{1}{\sqrt{2\pi}} e^{\mathrm{i}n\xi}\,, \qquad \widehat{\boldsymbol{x}} = (\cos\xi,\sin\xi)^\top \in S^1\,. \tag{2.70}$$

Now, we turn to the probing operator $H_B^* H_B:\; L^2(S^1) \to L^2(S^1)$, where H_B is the Herglotz operator from (2.36). It holds

$$\begin{aligned}
(H_B^* H_B\phi)(\boldsymbol{\theta}) \;&=\; \int_{\partial B} e^{-\mathrm{i}k\boldsymbol{\theta}\cdot\boldsymbol{y}} \Big(\int_{S_1} e^{\mathrm{i}k\boldsymbol{y}\cdot\boldsymbol{\vartheta}} \phi(\boldsymbol{\vartheta})\,\mathrm{d}s(\boldsymbol{\vartheta})\Big)\,\mathrm{d}s(\boldsymbol{y}) \\
&=\; \int_{S^1} \Big(\int_{\partial B} e^{\mathrm{i}k\boldsymbol{y}\cdot(\boldsymbol{\vartheta}-\boldsymbol{\theta})}\,\mathrm{d}s(\boldsymbol{y})\Big)\phi(\boldsymbol{\vartheta})\,\mathrm{d}s(\boldsymbol{\vartheta})\,.
\end{aligned}$$

Let $B = B_R(0)$ be the disk of radius $R > 0$ centered at the origin. We set $\widehat{\boldsymbol{y}} = (\cos\upsilon,\sin\upsilon)^\top \in S^1$ and $\boldsymbol{\vartheta} - \boldsymbol{\theta} = |\boldsymbol{\vartheta} - \boldsymbol{\theta}|(\cos\sigma,\sin\sigma)^\top \in \mathbb{R}^2$. Therewith, using (C.7) we arrive at

$$\begin{aligned}
&\int_{\partial B} e^{\mathrm{i}k\boldsymbol{y}\cdot(\boldsymbol{\vartheta}-\boldsymbol{\theta})}\,\mathrm{d}s(\boldsymbol{y}) \;=\; \int_{S^1} e^{\mathrm{i}kR\widehat{\boldsymbol{y}}\cdot(\boldsymbol{\vartheta}-\boldsymbol{\theta})} R\,\mathrm{d}s(\widehat{\boldsymbol{y}}) \\
&=\; R\int_0^{2\pi} e^{\mathrm{i}kR|\boldsymbol{\vartheta}-\boldsymbol{\theta}|\cos(\upsilon-\sigma)}\,\mathrm{d}\upsilon \;=\; R\int_0^{2\pi} \Big(\sum_{n\in\mathbb{Z}} \mathrm{i}^n J_n(kR|\boldsymbol{\vartheta}-\boldsymbol{\theta}|) e^{\mathrm{i}n(\upsilon-\sigma)}\Big)\,\mathrm{d}\upsilon \\
&=\; R\int_0^{2\pi} J_0(kR|\boldsymbol{\vartheta}-\boldsymbol{\theta}|)\,\mathrm{d}\upsilon + R\Big(\sum_{\substack{n\in\mathbb{Z}\\ n\neq 0}} \mathrm{i}^n J_n(kR|\boldsymbol{\vartheta}-\boldsymbol{\theta}|) e^{-\mathrm{i}n\sigma} \int_0^{2\pi} e^{\mathrm{i}n\upsilon}\,\mathrm{d}\upsilon\Big) \\
&=\; 2\pi R J_0(kR|\boldsymbol{\vartheta}-\boldsymbol{\theta}|)\,.
\end{aligned} \tag{2.71}$$

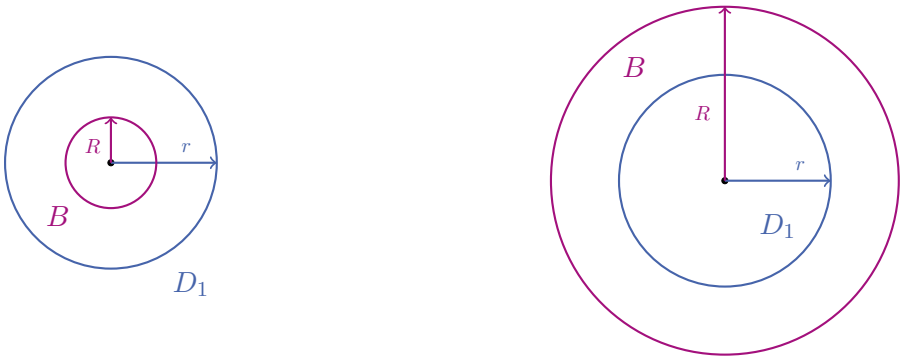

FIGURE 2.6. Visualization of the geometries of D_1 and B for $R < r$ (left) and $R > r$ (right).

Thus, we have

$$(H_B^* H_B \phi)(\boldsymbol{\theta}) = \int_{S^1} 2\pi R J_0(kR|\boldsymbol{\theta} - \boldsymbol{\vartheta}|)\phi(\boldsymbol{\vartheta}) \, \mathrm{d}s(\boldsymbol{\vartheta}) \,, \qquad \boldsymbol{\theta} = (\cos t, \sin t)^\top \in S^1 \,. \tag{2.72}$$

We write $\boldsymbol{\vartheta} = (\cos\tau, \sin\tau)^\top$ and substitute the Fourier expansion (2.69) of ϕ. Moreover, we apply (C.6) and calculate

$$\begin{aligned}(H_B^* H_B \phi)(\boldsymbol{\theta}) &= 2\pi R \int_0^{2\pi} \left(\sum_{n\in\mathbb{Z}} J_n^2(kR) e^{\mathrm{i}n(t-\tau)} \right) \left(\sum_{m\in\mathbb{Z}} \phi_m e^{\mathrm{i}m\tau} \right) \mathrm{d}\tau \\ &= 2\pi R \sum_{n\in\mathbb{Z}} \sum_{m\in\mathbb{Z}} J_n^2(kR) \left(\int_0^{2\pi} \phi_m e^{\mathrm{i}(m-n)\tau} \, \mathrm{d}\tau \right) e^{\mathrm{i}nt} = 4\pi^2 R \sum_{n\in\mathbb{Z}} J_n^2(kR) \phi_n e^{\mathrm{i}nt} \,.\end{aligned}$$

Accordingly, the eigenvalues and eigenvectors of the operator $H_B^* H_B$ are given by $(\mu_{n,R}, v_n)_{n\in\mathbb{Z}}$ with

$$\mu_{n,R} := 4\pi^2 R J_n^2(kR) \,, \quad v_n(\boldsymbol{\theta}) = \frac{1}{\sqrt{2\pi}} e^{\mathrm{i}nt} \,, \qquad \boldsymbol{\theta} = (\cos t, \sin t)^\top \in S^1 \,. \tag{2.73}$$

From (2.70) and (2.73), we conclude that in the special case when $D_1 = B_r(0)$ and $B = B_R(0)$, the eigenvalues and eigenvectors of $\mathrm{Re}(F_{D_1}^{\mathrm{dir}}) + H_B^* H_B$ are given by $(\mathrm{Re}(\lambda_{n,r}^{\mathrm{dir}}) + \mu_{n,R}, v_n)_{n\in\mathbb{Z}}$ with

$$\begin{aligned}\mathrm{Re}(\lambda_{n,r}^{\mathrm{dir}}) + \mu_{n,R} &= 8\pi \frac{J_n(kr) Y_n(kr)}{|H_n^{(1)}(kr)|^2} + 4\pi^2 R J_n^2(kR) \,, \\ v_n(\widehat{\boldsymbol{x}}) &= \frac{1}{\sqrt{2\pi}} e^{\mathrm{i}n\xi} \,, \qquad \widehat{\boldsymbol{x}} = (\cos\xi, \sin\xi)^\top \in S^1 \,.\end{aligned} \tag{2.74}$$

We return to the shape characterization results that we established in Subsections 2.3.3 and 2.4.3 and observe the following.

(a) If $R < r$, then $\overline{B} \subseteq D_1$ and $D_1 \not\subseteq B$, respectively (see picture on the left in Figure 2.6). Thus, Theorem 2.28 (a) implies that $\mathrm{Re}(F_{D_1}^{\mathrm{dir}}) + H_B^* H_B \leq_{\mathrm{fin}} 0$ whereas Theorem 2.40 (b) yields that $\mathrm{Re}(F_{D_1}^{\mathrm{dir}}) + H_B^* H_B \not\geq_{\mathrm{fin}} 0$. This means that $\mathrm{Re}(F_{D_1}^{\mathrm{dir}}) + H_B^* H_B$ has only finitely many positive but infinitely many negative eigenvalues.

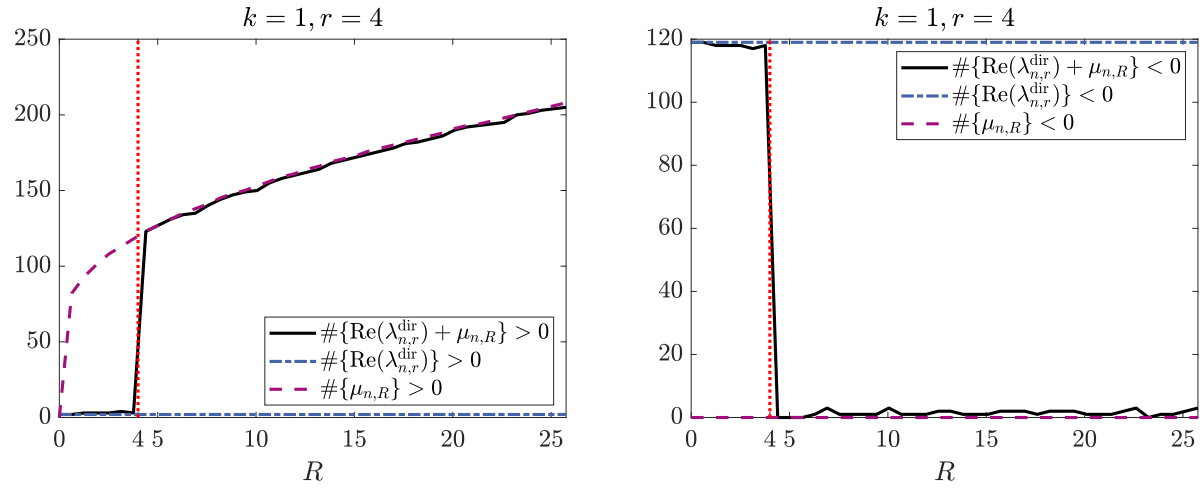

Figure 2.7. Number of positive eigenvalues (left) and number of negative eigenvalues (right) $\mathrm{Re}(\lambda_{n,r}^{\mathrm{dir}}) + \mu_{n,R}$ (black, solid), $\mathrm{Re}(\lambda_{n,r}^{\mathrm{dir}})$ (blue, dash-dotted) and $\mu_{n,R}$ (purple, dashed) from Example 2.42 within the range $n = 0, \dots, 1000$ as function of R.

(b) If $R > r$, then $\overline{D_1} \subseteq B$ and $B \not\subseteq D_1$, respectively (see picture on the right in Figure 2.6). Thus, Theorem 2.40 (a) implies that $\mathrm{Re}(F_{D_1}^{\mathrm{dir}}) + H_B^* H_B \geq_{\mathrm{fin}} 0$ whereas Theorem 2.28 (b) yields that $\mathrm{Re}(F_{D_1}^{\mathrm{dir}}) + H_B^* H_B \not\leq_{\mathrm{fin}} 0$. This means that $\mathrm{Re}(F_{D_1}^{\mathrm{dir}}) + H_B^* H_B$ has only finitely many negative but infinitely many positive eigenvalues.

In the following numerical example, we illustrate how this can be utilized to reconstruct the radius of the scatterer $D_1 = B_r(0)$ from observations of $F_{D_1}^{\mathrm{dir}}$.

Example 2.42. We consider a single Dirichlet obstacle $D_1 = B_r(0)$ with radius $r = 4$. We evaluate the eigenvalues $\mathrm{Re}(\lambda_{n,r}^{\mathrm{dir}})$ of the far field operator $F_{D_1}^{\mathrm{dir}}$, $\mu_{n,R}$ of the probing operator $H_B^* H_B$ and $\mathrm{Re}(\lambda_{n,r}^{\mathrm{dir}}) + \mu_{n,R}$ of the operator $\mathrm{Re}(F_{D_1}^{\mathrm{dir}}) + H_B^* H_B$ with wave number $k = 1$ for $n = 0, \dots, 1000$. For the radii R of the probing domains $B = B_R(0)$, we use different values within the interval $(0, 26]$. Figure 2.7 shows plots of the number of positive eigenvalues (left) and of the number of negative eigenvalues (right) $\mathrm{Re}(\lambda_{n,r}^{\mathrm{dir}})$ (blue, dash-dotted), $\mu_{n,R}$ (purple, dashed) and $\mathrm{Re}(\lambda_{n,r}^{\mathrm{dir}}) + \mu_{n,R}$ (black, solid) within the range $n = 0, \dots, 1000$ as a function of R. These plots are created with Matlab using the explicit formulas given in (2.70), (2.73) and (2.74).

As suggested by Theorems 2.28 and 2.40 there is a sharp transition in the behavior of the eigenvalues of $\mathrm{Re}(F_{D_1}^{\mathrm{dir}}) + H_B^* H_B$ at $R = r = 4$, that is when the radii of the obstacle and the probing domain coincide. In Figure 2.7, we inserted a red dotted line for $R = r$, and we notice that the sharp transition in the number of the eigenvalues can be used to estimate the value of r. On the left-hand side of the red dotted line, the obstacle D_1 contains the probing domain B (compare picture on the left in Figure 2.6) whereas on the right-hand side, the obstacle D_1 is contained inside the probing domain B (compare picture on the right in Figure 2.6). In these plots, the contribution of the far field operator $\mathrm{Re}(F_{D_1}^{\mathrm{dir}})$ dominates in the superposition $\mathrm{Re}(F_{D_1}^{\mathrm{dir}}) + H_B^* H_B$ as long as $R < r$ (i.e., $B \subseteq D_1$), while the contribution of the probing operator $H_B^* H_B$ dominates when $R > r$ (i.e., $D_1 \subseteq B$).

Since the radius of D_1 does not depend on R, the number of positive and negative eigenvalues

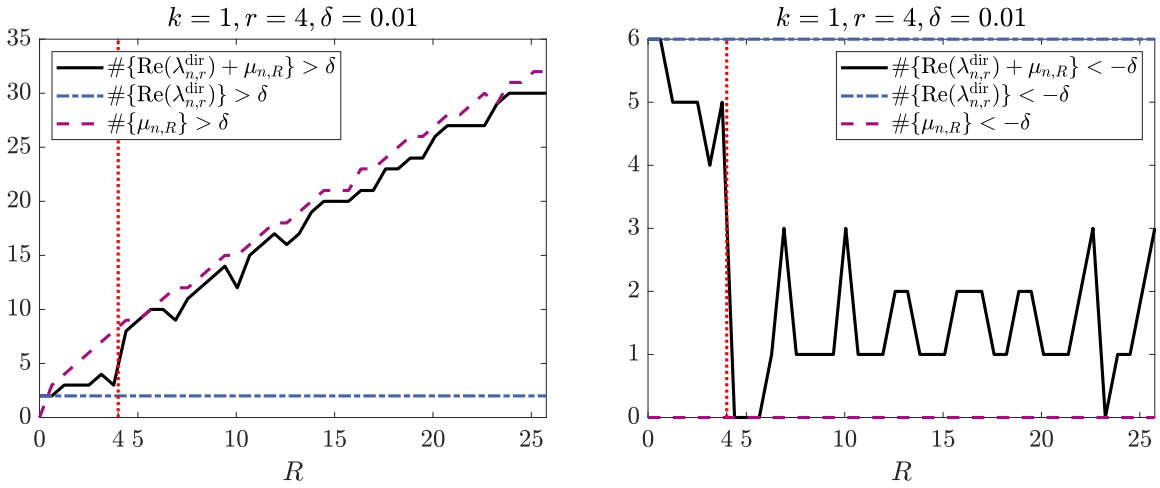

FIGURE 2.8. Same as Figure 2.7, but with $\delta = 0.01$ instead of $\delta = 0$.

$\mathrm{Re}(\lambda^{\mathrm{dir}}_{n,r})$ of $F^{\mathrm{dir}}_{D_1}$ is constant in these plots. The number of positive eigenvalues is equal to two and thus quite low as Corollary 2.17 suggests. However, one might expect the number of negative eigenvalues to be higher. From the asymptotic expansions (C.4)–(C.5) for Bessel functions for large order, we see that

$$\mathrm{Re}(\lambda^{\mathrm{dir}}_{n,r}) \sim -4\pi\Big(\frac{ekr}{2n}\Big)^{2n} \qquad \text{as } n \to \infty\,.$$

Therefore, the sequence $(\mathrm{Re}(\lambda^{\mathrm{dir}}_{n,r}))_{n\in\mathbb{Z}}$ tends rapidly to zero once the value of $|n|$ is sufficiently large. Eigenvalues below some threshold are rounded to zero in Matlab. Consequently, this explains the somewhat low number of negative eigenvalues. Similarly, using (C.4) we obtain

$$\mu_{n,R} \sim \frac{2\pi R}{n}\Big(\frac{ekR}{2n}\Big)^{2n} \qquad \text{as } n \to \infty\,.$$

Accordingly, the sequence $(\mu_{n,R})_{n\in\mathbb{Z}}$ decays rapidly for sufficiently large $|n|$. Besides, the eigenvalues $\mu_{n,R}$ are on average increasing with respect to the radius R. This is the reason for the increasing but somewhat low numbers of positive eigenvalues of $H_B^* H_B$ in the left plot in Figure 2.7. The number of negative eigenvalues is zero.

In practice, the far field data is usually corrupted by measurement errors, and therefore, it is not possible to compute the eigenvalues of $\mathrm{Re}(F^{\mathrm{dir}}_{D_1}) + H_B^* H_B$ with very high precision, as done in this example so far. This implies that we cannot trust eigenvalues with an absolute value below some threshold. This threshold depends on the quality of the given far field data. If there are good reasons to believe that these are known up to a perturbation of size $\delta > 0$ with respect to the spectral norm, then we discard those eigenvalues with a magnitude smaller than δ (see, e.g., [GVL13, Thm. 7.2.2]). To see how this influences the numerical results, we repeat the previous computations but consider only those eigenvalues with an absolute value larger than a threshold $\delta = 0.01$. For comparison, we note that the eigenvalue of the largest magnitude of $\mathrm{Re}(F^{\mathrm{dir}}_{D_1})$ in this example is $\mathrm{Re}(\lambda^{(r)}_2) \approx 11.03$. In Figure 2.8, we show plots of the number of positive eigenvalues $\mathrm{Re}(\lambda^{\mathrm{dir}}_{n,r})$ (blue, dash-dotted), $\mu_{n,R}$ (purple, dashed) and $\mathrm{Re}(\lambda^{\mathrm{dir}}_{n,r}) + \mu_{n,R}$ (black, solid) within the

range $n = 0, \dots, 1000$ that are larger than δ (left) and of the number of negative eigenvalues that are smaller than $-\delta$ (right) as a function of R. The transition in the behavior of the eigenvalues of $\mathrm{Re}(F_{D_1}^{\mathrm{dir}}) + H_B^* H_B$ at $R = r = 4$ is not nearly as pronounced as before. The reason for this behavior is the rapid decay of the sequences of eigenvalues for larger values of $|n|$, which implies that only a few eigenvalues remain above the threshold δ. However, a rough estimate of r would still be possible by visual inspection of these plots, in particular from the plot on the right-hand side of Figure 2.8. △

We move on to the special case of a single radially symmetric Neumann obstacle. Thus, let $D_1 = \emptyset$, and let $D_2 = B_r(0) \subseteq \mathbb{R}^2$ be the disk of radius $r > 0$ centered at the origin. For the probing domains, we still have $B = B_R(0) \subseteq \mathbb{R}^2$.

We begin with deriving series expansions for the normal derivatives of the incident and scattered fields. Using (2.67) we obtain

$$\frac{\partial u^i}{\partial \boldsymbol{\nu}}(\boldsymbol{x};\boldsymbol{\theta}) \;=\; \frac{\partial u^i}{\partial |\boldsymbol{x}|}(\boldsymbol{x};\boldsymbol{\theta}) \;=\; \sum_{n\in\mathbb{Z}} \mathrm{i}^n e^{-\mathrm{i}n\xi} k J_n'(k|\boldsymbol{x}|) e^{\mathrm{i}nt}$$

for each direction $\boldsymbol{\theta} = (\cos t, \sin t)^\top \in S^1$ and every point $\boldsymbol{x} = |\boldsymbol{x}|(\cos\xi, \sin\xi)^\top \in \mathbb{R}^2$. Similarly to the Dirichlet case, Theorem C.1 gives

$$\frac{\partial u^s}{\partial \boldsymbol{\nu}}(\boldsymbol{x};\boldsymbol{\theta}) \;=\; \sum_{n\in\mathbb{Z}} a_n k \big(H_n^{(1)}\big)'(k|\boldsymbol{x}|) e^{-\mathrm{i}n\xi}\,, \qquad \boldsymbol{x} = |\boldsymbol{x}|(\cos\xi, \sin\xi)^\top \in \mathbb{R}^2 \setminus \overline{D_2}$$

with uniquely determined coefficients a_n, $n \in \mathbb{Z}$. We substitute the boundary condition $\partial u^s(\boldsymbol{x};\boldsymbol{\theta})/\partial\boldsymbol{\nu} = -\partial u^i(\boldsymbol{x};\boldsymbol{\theta})/\partial\boldsymbol{\nu}$ on ∂D_2 and derive that

$$a_n \;=\; -\mathrm{i}^n \frac{J_n(kr)'}{\big(H_n^{(1)}\big)'(kr)} e^{\mathrm{i}nt}\,.$$

Therewith, we get

$$u^s(\boldsymbol{x};\boldsymbol{\theta}) \;=\; -\sum_{n\in\mathbb{Z}} \mathrm{i}^n \frac{J_n'(kr)}{\big(H_n^{(1)}\big)'(kr)} e^{-\mathrm{i}n\xi} H_n^{(1)}(k|\boldsymbol{x}|) e^{\mathrm{i}nt}\,, \qquad \boldsymbol{x} = |\boldsymbol{x}|(\cos\xi, \sin\xi)^\top \in \mathbb{R}^2 \setminus \overline{D_2}\,.$$

We use (2.68) and see that the far field pattern of u^s is

$$u^\infty(\widehat{\boldsymbol{x}};\boldsymbol{\theta}) \;=\; \sum_{n\in\mathbb{Z}} 4\mathrm{i} \frac{J_n'(kr)}{\big(H_n^{(1)}\big)'(kr)} e^{-\mathrm{i}n\xi} e^{\mathrm{i}nt}\,, \qquad \widehat{\boldsymbol{x}} = (\cos\xi, \sin\xi)^\top \in S^1\,.$$

Consequently, the far field operator $F_{D_2}^{\mathrm{neu}} \colon L^2(S^1) \to L^2(S^1)$ from (2.14) satisfies

$$(F_{D_2}^{\mathrm{neu}}\phi)(\widehat{\boldsymbol{x}}) \;=\; \sum_{n\in\mathbb{Z}} 8\pi\mathrm{i} \frac{J_n'(kr)}{\big(H_n^{(1)}\big)'(kr)} \phi_n e^{\mathrm{i}n\xi}\,, \qquad \widehat{\boldsymbol{x}} = (\cos\xi, \sin\xi)^\top \in S^1\,,$$

where $\phi \in L^2(S^1)$ has the Fourier expansion (2.69). Accordingly, the eigenvalues and eigenvectors

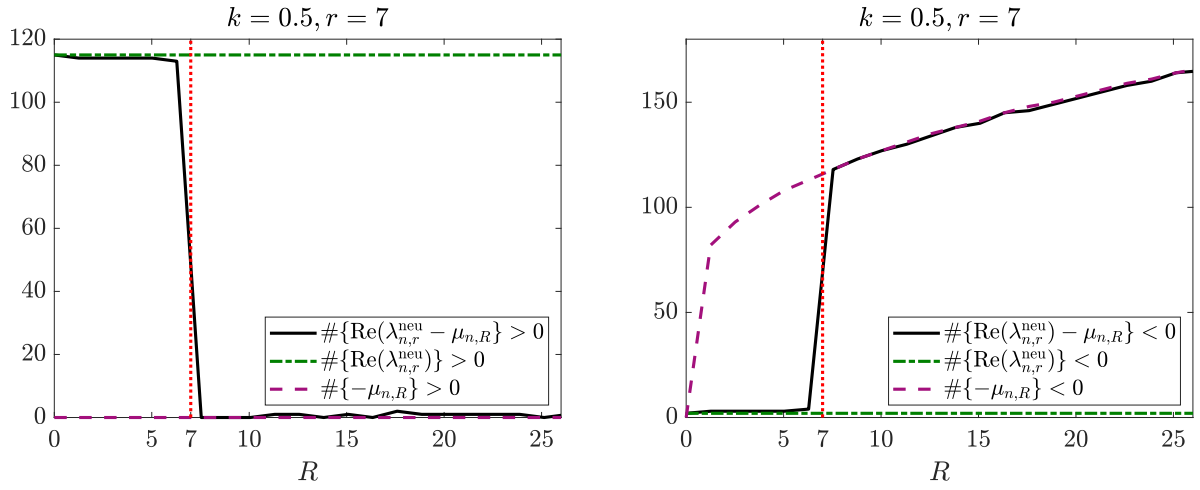

FIGURE 2.9. Number of positive eigenvalues (left) and number of negative eigenvalues (right) $\mathrm{Re}(\lambda^{\mathrm{neu}}_{n,r}) - \mu_{n,R}$ (black, solid), $\mathrm{Re}(\lambda^{\mathrm{neu}}_{n,r})$ (green, dash-dotted) and $-\mu_{n,R}$ (purple, dashed) from Example 2.43 within the range $n = 0, \ldots, 1000$ as function of R.

of $F^{\mathrm{neu}}_{D_2}$ are given by $(\lambda^{\mathrm{neu}}_{n,r}, v_n)_{n\in\mathbb{Z}}$ with

$$\lambda^{\mathrm{neu}}_{n,r} := 8\pi \mathrm{i} \frac{J_n'(kr)}{(H_n^{(1)})'(kr)}, \quad v_n(\widehat{\boldsymbol{x}}) := \frac{1}{\sqrt{2\pi}} e^{\mathrm{i}n\xi}, \qquad \widehat{\boldsymbol{x}} = (\cos\xi, \sin\xi)^\top \in S^1 . \tag{2.75}$$

Inserting the eigenvalue decomposition (2.73) of $H_B^* H_B$, we find that in the special case when $D_2 = B_r(0)$ and $B = B_R(0)$, the eigenvalues and eigenvectors of $\mathrm{Re}(F^{\mathrm{neu}}_{D_2}) - H_B^* H_B$ are given by $(\mathrm{Re}(\lambda^{\mathrm{neu}}_{n,r}) - \mu_{n,R}, v_n)_{n\in\mathbb{Z}}$ with

$$\begin{aligned} \mathrm{Re}(\lambda^{\mathrm{neu}}_{n,r}) - \mu_{n,R} &= 8\pi \frac{J_n'(kr) Y_n'(kr)}{|(H_n^{(1)})'(kr)|^2} - 4\pi^2 R J_n^2(kR), \\ v_n(\widehat{\boldsymbol{x}}) &= \frac{1}{\sqrt{2\pi}} e^{\mathrm{i}n\xi}, \quad \widehat{\boldsymbol{x}} = (\cos\xi, \sin\xi)^\top \in S^1 . \end{aligned} \tag{2.76}$$

The shape characterization results that we established in Subsections 2.3.3 and 2.4.3 yield the following.

(a) If $R < r$, then $\overline{B} \subseteq D_2$ and $D_2 \not\subseteq B$, respectively. Thus, Theorem 2.30 (a) implies that $\mathrm{Re}(F^{\mathrm{neu}}_{D_2}) - H_B^* H_B$ has only finitely many negative eigenvalues whereas Theorem 2.40 (d) yields that $\mathrm{Re}(F^{\mathrm{neu}}_{D_2}) - H_B^* H_B$ has infinitely many positive eigenvalues.

(b) If $R > r$, then $\overline{D_2} \subseteq B$ and $B \not\subseteq D_2$, respectively. Thus, Theorem 2.40 (c) implies that $\mathrm{Re}(F^{\mathrm{neu}}_{D_2}) - H_B^* H_B$ has only finitely many positive eigenvalues whereas Theorem 2.30 (b) yields that $\mathrm{Re}(F^{\mathrm{neu}}_{D_2}) - H_B^* H_B$ has infinitely many negative eigenvalues.

The following numerical example shows similar results as we presented in Example 2.42.

Example 2.43. In the second example, the scatterer is a disk of radius 7 and we assume a Neumann boundary condition, i.e., $D_2 = B_r(0)$ with $r = 7$. Exactly as in Example 2.42, we

evaluate the eigenvalues of the far field operator $F_{D_2}^{\text{neu}}$, of the probing operator $H_B^* H_B$ and of the operator $\operatorname{Re}(F_{D_2}^{\text{neu}}) - H_B^* H_B$ for $n = 0, \dots, 1000$ and different values R within the interval $(0, 26]$ by means of the explicit formulas (2.75), (2.73) and (2.76). The wave number k is set to 0.5. In Figure 2.9, we present plots of the number of positive eigenvalues (left) and of the number of negative eigenvalues (right) $\operatorname{Re}(\lambda_{n,r}^{\text{neu}})$ (green, dash-dotted), $-\mu_{n,R}$ (purple, dashed) and $\operatorname{Re}(\lambda_{n,r}^{\text{neu}}) - \mu_{n,R}$ (black, solid) within the range $n = 0, \dots, 1000$ as a function of R. Again, we observe a sharp transition in the behavior of the eigenvalues of $\operatorname{Re}(F_{D_2}^{\text{neu}}) - H_B^* H_B$ at $R = r = 7$. Therewith, it would be possible to estimate the radius of the obstacle D_2. Just like in the previous example, the contribution of the far field operator dominates in the superposition $\operatorname{Re}(F_{D_2}^{\text{neu}}) - H_B^* H_B$ as long as $R < r$ while the contribution of the probing operator $H_B^* H_B$ dominates when $R > r$. Besides, similar reasoning as in Example 2.6 explains the somewhat low numbers of positive eigenvalues of $\operatorname{Re}(F_{D_2}^{\text{neu}})$ and negative eigenvalues of $-H_B^* H_B$, respectively. △

2.5.2. A Sampling Strategy for Dirichlet or Neumann Obstacles

After having studied radially symmetric obstacles, we now allow for arbitrary shapes. However, we assume that the scatterer consists either only of Dirichlet or only of Neumann obstacles. In the special case when only Dirichlet obstacles are present, Theorem 2.28 suggests that the number of positive eigenvalues of $\operatorname{Re}(F_{D_1}^{\text{dir}}) + H_B^* H_B$ can be utilized to decide whether a probing domain $B \subseteq \mathbb{R}^2$ is contained inside the scatterer D_1 or not. We discuss this approach in the following and comment on the special case when only Neumann obstacles are present at the end of this subsection.

Let $D_2 = \emptyset$, and let $D_1 \subseteq \mathbb{R}^2$ be open and Lipschitz bounded such that $\mathbb{R}^d \setminus \overline{D_1}$ is connected. We assume that far field observations $u^\infty(\widehat{\boldsymbol{x}}_l; \boldsymbol{\theta}_m)$ are available for N equidistant observation and incident directions

$$\widehat{\boldsymbol{x}}_l \;=\; (\cos\xi_l, \sin\xi_l) \in S^1\,, \qquad \xi_l \;:=\; (n-1)\frac{2\pi}{N}\,, \quad 1 \le l \le N\,, \tag{2.77a}$$

$$\boldsymbol{\theta}_m \;=\; (\cos t_m, \sin t_m) \in S^1\,, \quad t_m \;:=\; (n-1)\frac{2\pi}{N}\,, \quad 1 \le m \le N\,. \tag{2.77b}$$

Applying the trapezoidal rule to (2.14) gives

$$(F_{D_1}^{\text{dir}}\phi)(\widehat{\boldsymbol{x}}) \;\approx\; \frac{2\pi}{N} \sum_{m=1}^{N} u^\infty(\widehat{\boldsymbol{x}}; \boldsymbol{\theta}_m)\phi(\boldsymbol{\theta}_m)\,.$$

Accordingly, the matrix

$$\boldsymbol{F}_{D_1}^{\text{dir}} \;:=\; \frac{2\pi}{N}[u^\infty(\widehat{\boldsymbol{x}}_l; \boldsymbol{\theta}_m)]_{1\le l,m\le N} \in \mathbb{C}^{N\times N} \tag{2.78}$$

approximates the far field operator $F_{D_1}^{\text{dir}}$. Assuming that the obstacle D_1 is contained within the disk $B_R(0)$ for some $R > 0$, we require

$$N \;\gtrsim\; 2kR\,, \tag{2.79}$$

where as before k denotes the wave number, to fully resolve the relevant information contained

in the far field patterns (see, e.g., [GS17b]).

We define an equidistant grid of points

$$\Delta := \{\boldsymbol{z}_{ij} = (ih, jh) \mid -J \leq i, j \leq J\} \subseteq [-R, R]^2 \tag{2.80}$$

with step size $h = R/J$ in the *region of interest* $[-R, R]^2$. For each $\boldsymbol{z}_{ij} \in \Delta$, we consider the probing operator $H_{B_{ij}}^* H_{B_{ij}}$ with $B_{ij} = B_h(\boldsymbol{z}_{ij})$. We have

$$\begin{aligned}(H_{B_{ij}}^* H_{B_{ij}} \phi)(\boldsymbol{\theta}) &= \int_{S^1} \Big(\int_{\partial B_{ij}} e^{\mathrm{i}k\boldsymbol{y}\cdot(\boldsymbol{\vartheta}-\boldsymbol{\theta})} \, \mathrm{d}s(\boldsymbol{y}) \Big) \phi(\boldsymbol{\vartheta}) \, \mathrm{d}s(\boldsymbol{\vartheta}) \\ &= \int_{S^1} e^{\mathrm{i}k\boldsymbol{z}_{ij}\cdot(\boldsymbol{\vartheta}-\boldsymbol{\theta})} \Big(\int_{\partial B_h(0)} e^{\mathrm{i}k\boldsymbol{y}\cdot(\boldsymbol{\vartheta}-\boldsymbol{\theta})} \, \mathrm{d}s(\boldsymbol{y}) \Big) \phi(\boldsymbol{\vartheta}) \, \mathrm{d}s(\boldsymbol{\vartheta}) \, .\end{aligned}$$

We substitute (2.71) and obtain

$$(H_{B_{ij}}^* H_{B_{ij}} \phi)(\boldsymbol{\theta}) = 2\pi h \int_{S^1} e^{\mathrm{i}k\boldsymbol{z}_{ij}\cdot(\boldsymbol{\vartheta}-\boldsymbol{\theta})} J_0(kh|\boldsymbol{\vartheta}-\boldsymbol{\theta}|) \phi(\boldsymbol{\vartheta}) \, \mathrm{d}s(\boldsymbol{\vartheta}) \, .$$

With

$$\boldsymbol{\vartheta}_m = (\cos\tau_m, \sin\tau_m) \in S^1 \, , \quad \tau_m := (m-1)\frac{2\pi}{N} \, , \quad 1 \leq m \leq N \, ,$$

applying the trapezoidal rule to (2.72) yields

$$(H_{B_{ij}}^* H_{B_{ij}} \phi)(\boldsymbol{\theta}) \approx \frac{2\pi}{N} 2\pi h \sum_{m=1}^{N} e^{\mathrm{i}k\boldsymbol{z}_{ij}\cdot(\boldsymbol{\vartheta}_m-\boldsymbol{\theta})} J_0(kh|\boldsymbol{\vartheta}_m-\boldsymbol{\theta}|) \phi(\boldsymbol{\vartheta}_m)$$

for each $\boldsymbol{z}_{ij} \in \Delta$. Thus, the matrix

$$\boldsymbol{T}_{B_{ij}} := \frac{4\pi^2}{N} h \Big[e^{\mathrm{i}k\boldsymbol{z}_{ij}\cdot(\boldsymbol{\vartheta}_m-\boldsymbol{\theta}_l)} J_0\Big(kh|\boldsymbol{\vartheta}_m-\boldsymbol{\theta}_l|\Big) \Big]_{1\leq l,m\leq N} \in \mathbb{C}^{N\times N} \tag{2.81}$$

approximates the probing operator. Therewith, we compute the eigenvalues $\lambda_{1,(ij)}^{\mathrm{dir}}, \ldots, \lambda_{N,(ij)}^{\mathrm{dir}} \in \mathbb{R}$ of the self-adjoint matrices

$$\boldsymbol{A}_{B_{ij}}^{\mathrm{dir}} := \mathrm{Re}(\boldsymbol{F}_{D_1}^{\mathrm{dir}}) + \boldsymbol{T}_{B_{ij}} \in \mathbb{C}^{N\times N} \, , \qquad -J \leq i, j \leq J \, , \tag{2.82}$$

approximating the operator $\mathrm{Re}(F_{D_1}^{\mathrm{dir}}) + H_{B_{ij}}^* H_{B_{ij}}$.

For numerical stabilization, we discard eigenvalues with absolute values smaller than some threshold $\delta > 0$. This threshold should correspond to the error of $\boldsymbol{A}_{B_{ij}}^{\mathrm{dir}}$, as [GVL13, Thm. 7.2.2]) suggests. To obtain a reasonable estimate for δ, we use the magnitude of the non-unitary part of $\boldsymbol{S}_{D_1}^{\mathrm{dir}} := \boldsymbol{I}_N + \mathrm{i}/(4\pi)\boldsymbol{F}_{D_1}^{\mathrm{dir}}$, i.e., we take $\delta \approx \|(\boldsymbol{S}_{D_1}^{\mathrm{dir}})^* \boldsymbol{S}_{D_1}^{\mathrm{dir}} - \boldsymbol{I}_N\|_2$ since this quantity should be zero for exact data and be of the order of the data error, otherwise.

The shape characterization of Dirichlet obstacles given in Theorem 2.28 states that

(a) if $\overline{B} \subseteq D_1$, then $\mathrm{Re}(F_{D_1}^{\mathrm{dir}}) + H_B^* H_B$ has only finitely many positive eigenvalues, and

(b) if $B \not\subseteq D_1$, then $\mathrm{Re}(F_{D_1}^{\mathrm{dir}}) + H_B^* H_B$ has infinitely many positive eigenvalues.

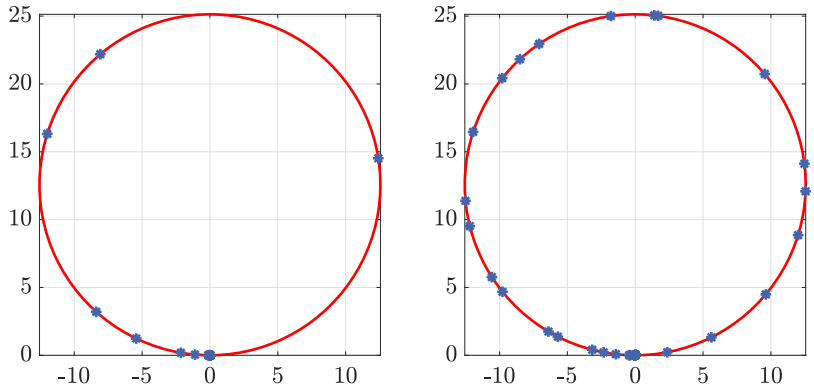

Figure 2.10. Eigenvalues of $F_{D_1}^{\mathrm{dir}}$ (blue) from Example 2.44 for two different wave numbers $k = 1$ with $N = 32$ (left) and $k = 5$ with $N = 128$ (right).

Together with our observations from Subsection 2.5.1, this suggests that the number of positive eigenvalues of $\boldsymbol{A}_{B_{ij}}^{\mathrm{dir}}$ corresponding to a sampling point $\boldsymbol{z}_{ij} \in \Delta$ should be smaller if $\boldsymbol{z}_{ij}$ lies inside the obstacle than if it lies outside. We define the *indicator function* $I_{\mathrm{dir}} : \Delta \to \mathbb{N}$,

$$I_{\mathrm{dir}}(\boldsymbol{z}_{ij}) := \#\{\lambda_{n,(ij)}^{\mathrm{dir}} \mid \lambda_{n,(ij)}^{\mathrm{dir}} > \delta\,,\ 1 \leq n \leq N\}\,, \qquad -J \leq i,j \leq J\,. \tag{2.83}$$

that counts the number of positive eigenvalues for each sampling point. Accordingly, we expect that I_{dir} admits smaller values at sampling points $\boldsymbol{z}_{ij}$ inside D_1 than at sampling points outside of D_1.

Example 2.44. We consider a single Dirichlet obstacle that has the shape of a kite as sketched in Figure 2.11 (left) and simulate the corresponding far field matrix $\boldsymbol{F}_{D_1}^{\mathrm{dir}} \in \mathbb{C}^{N\times N}$ for N incident and observation directions as in (2.77) using a Nyström method for a boundary integral formulation of the scattering problem (2.11a), (2.11b) and (2.11d). There, the appearing boundary integrals are approximated by quadrature formulas. For details about the utilized quadrature rules and weights, we recommend reading [CK19, Sec. 3.6]. We use two different wave numbers $k = 1$ and $k = 5$, and we choose the number of observation and incident directions to be $N = 32$ and $N = 128$, respectively, in compliance with the sampling condition (2.79). Since we do not incorporate any noise in the data, we use a threshold $\delta = 10^{-14}$. Consequently, we discard all eigenvalues with an absolute value smaller than δ.

Figure 2.10 shows the eigenvalues of the matrix $\boldsymbol{F}_{D_1}^{\mathrm{dir}}$ from (2.78). We notice that the eigenvalues lie on a circle and that they converge to zero. More precisely, they converge to zero from the left side as we expect from Corollary 2.17. In fact, the real part of $\boldsymbol{F}_{D_1}^{\mathrm{dir}}$ counts 22 negative eigenvalues and one positive eigenvalue for $k = 1$, and 38 negative eigenvalues and nine positive eigenvalues for $k = 5$.

In Figure 2.11, we show color-coded plots of the indicator function I_{dir} from (2.83) in the region of interest $[-10, 10]^2 \subseteq \mathbb{R}^2$. This means that we assign the number of positive eigenvalues of the matrix $\boldsymbol{A}_{B_{ij}}^{\mathrm{dir}}$ from (2.82) that are larger than $\delta = 10^{-14}$ to each sampling point $\boldsymbol{z}_{ij} \in \Delta$. The step size of the equidistant rectangular sampling grid Δ from (2.80) is $h = 0.1$. Thus, it consists of $2J + 1 = 201$ grid points in each direction.

The number of positive eigenvalues of the matrix $\boldsymbol{A}_{B_{ij}}^{\mathrm{dir}}$ increases with increasing wave number,

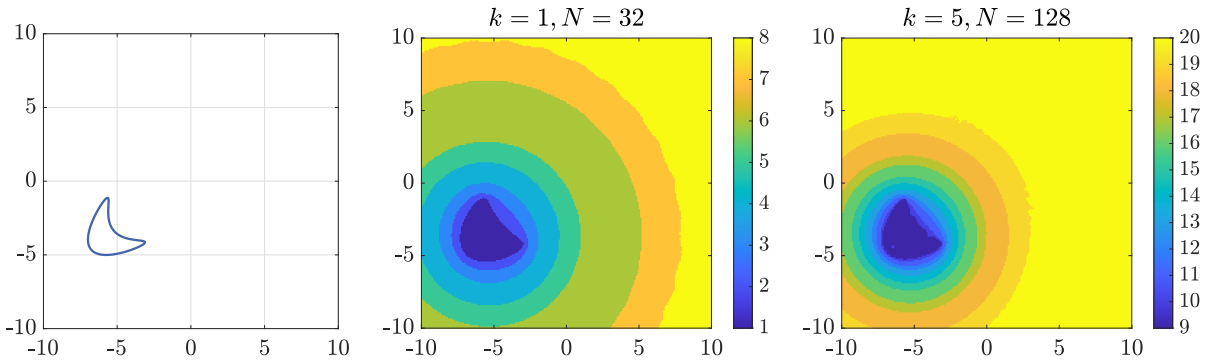

FIGURE 2.11. Exact shape of the Dirichlet obstacle from Example 2.44 (left), Visualization of the indicator function I_{dir} for two different wave numbers $k = 1$ with $N = 32$ (middle) and $k = 5$ with $N = 128$ (right).

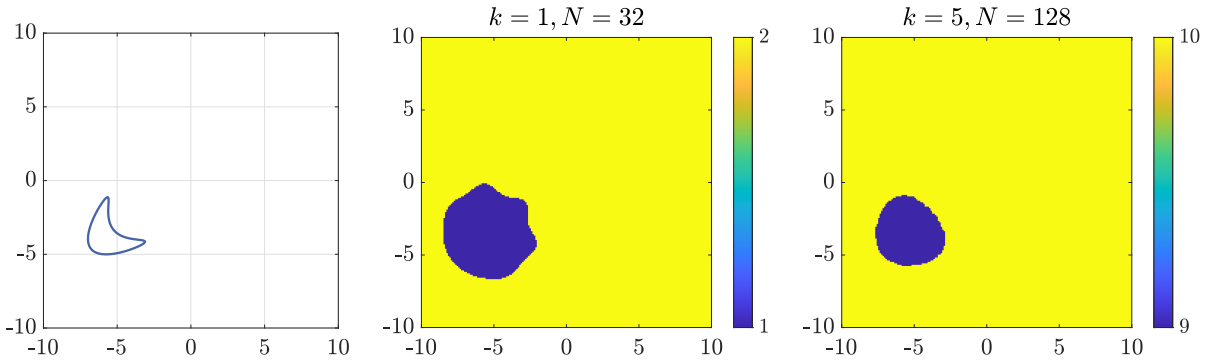

FIGURE 2.12. Same as in Figure 2.11, but with 0.1% complex-valued uniformly distributed error on the far field data.

and it is larger at sampling points $\boldsymbol{z}_{ij}$ sufficiently far away from the obstacle than at sampling points $\boldsymbol{z}_{ij}$ inside of it, as suggested by Theorem 2.28. The lower value always coincides with the number of positive eigenvalues of the real part $\text{Re}(\boldsymbol{F}_{D_1}^{\text{dir}})$ of the far field matrix from (2.78) that are larger than the threshold δ. The total number of eigenvalues of $\boldsymbol{A}_{B_{ij}}^{\text{dir}}$, $i, j = 1, \ldots, J$, whose absolute values are larger than δ is approximately (on average over all grid points) 26 for $k = 1$ and 56 for $k = 5$. Depending on the wave number, the lowest level set of the indicator function I_{dir} nicely approximates the shape of the obstacle.

Next, we repeat the previous computation but add 0.1% complex-valued uniformly distributed error to the far field matrix $\boldsymbol{F}_{D_1}^{\text{dir}}$. We estimate the non-unitarity error of the corresponding scattering operator and accordingly, we choose $\delta = 0.1$ for the threshold in the reconstruction algorithm. Figure 2.12 visualizes the indicator function I_{dir} from (2.83) as color-coded plots for the wave numbers $k = 1$ (with $N = 32$) and $k = 5$ (with $N = 128$). The total number of eigenvalues of $\boldsymbol{A}_{B_{ij}}^{\text{dir}}$, $j = 1, \ldots, J$, whose absolute values are larger than δ is approximately (on average over all grid points) nine for $k = 1$ and 26 for $k = 5$. In comparison with the values we achieved with noise-free data, we see that the numbers of used eigenvalues are lower. The reconstruction for $k = 5$ is better than the reconstruction for $k = 1$ because more eigenvectors are stably propagated into the far field for larger wave numbers (the number of eigenvalues with

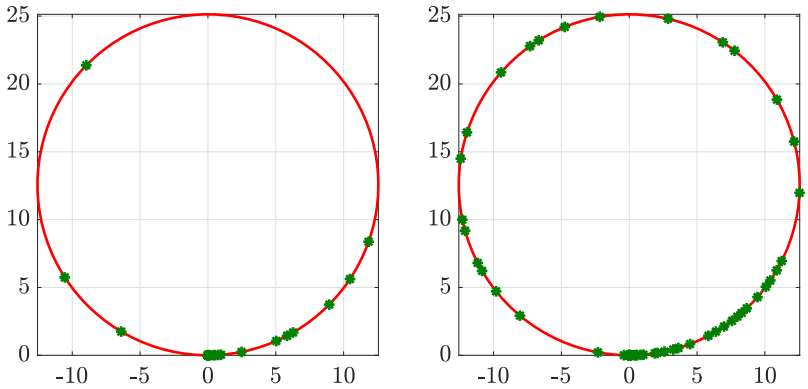

Figure 2.13. Eigenvalues of $F^{\text{neu}}_{D_2}$ (green) from Example 2.45 for two different wave numbers $k = 1$ with $N = 32$ (left) and $k = 5$ with $N = 128$ (right).

absolute values above the threshold δ increases with k). However, despite the low noise level, the shape of the obstacle is not reconstructed very well. Hence, we observe that the reconstruction algorithm is rather sensitive to noise in the far field data. △

If only Neumann obstacles are present, i.e., $D_1 = \emptyset$ and $D_2 \subseteq \mathbb{R}^2$ is open and Lipschitz bounded such that $\mathbb{R}^d \setminus \overline{D_2}$ is connected, then we use the corresponding far field matrix $\boldsymbol{F}^{\text{neu}}_{D_2} \in \mathbb{C}^{N\times N}$ as in (2.78) and the matrix $\boldsymbol{T}_{B_{ij}} \in \mathbb{C}^{N\times N}$ from (2.81) to compute the eigenvalues $\lambda^{\text{neu}}_{1,(ij)}, \dots, \lambda^{\text{neu}}_{N,(ij)} \in \mathbb{R}$ of the self-adjoint matrices

$$\boldsymbol{A}^{\text{neu}}_{B_{ij}} := \operatorname{Re}(\boldsymbol{F}^{\text{neu}}_{D_2}) - \boldsymbol{T}_{B_{ij}} \in \mathbb{C}^{N\times N}, \qquad -J \le i, j \le J,$$

for each sampling point $\boldsymbol{z}_{ij} \in \Delta$. The shape characterization of Neumann obstacles given in Theorem 2.30 states that

(a) if $\overline{B} \subseteq D_2$, then $\operatorname{Re}(F^{\text{neu}}_{D_2}) - H^*_B H_B$ has only finitely many negative eigenvalues, and

(b) if $B \not\subseteq D_1$, then $\operatorname{Re}(F^{\text{neu}}_{D_2}) - H^*_B H_B$ has infinitely many negative eigenvalues.

This suggests that we count the number of negative eigenvalues of $\boldsymbol{A}^{\text{neu}}_{B_{ij}}$ for each sampling point $\boldsymbol{z}_{ij} \in \Delta$. We define the *indicator function* $I_{\text{neu}} : \Delta \to \mathbb{N}$,

$$I_{\text{neu}}(z_{ij}) := \#\{\lambda^{\text{neu}}_{n,(ij)} \mid \lambda^{\text{neu}}_{n,(ij)} < -\delta,\ 1 \le n \le N\}, \qquad -J \le i, j \le J. \tag{2.84}$$

Consequently, Theorem 2.30 suggests that I_{neu} admits smaller values at test points $\boldsymbol{z}_{ij}$ inside D_2 than at sampling points outside of D_2.

Example 2.45. In this example, the scatterer consists of a peanut and an ellipse, and it carries a Neumann boundary condition. The corresponding geometry is plotted in Figure 2.14 (left). As in Example 2.44, we simulate the corresponding far field matrix $\boldsymbol{F}^{\text{neu}}_{D_2} \in \mathbb{C}^{N\times N}$ for N incident and observation directions by means of a Nyström method. We refer to [Kre95] for a deeper insight into the parameterization of the underlying boundary integral equation as well as the used quadrature rules. Again, we examine two different wave numbers $k = 1$ (with $N = 32$) and $k = 5$ (with $N = 128$) and choose the threshold parameter $\delta = 10^{-14}$. Figure 2.13 shows

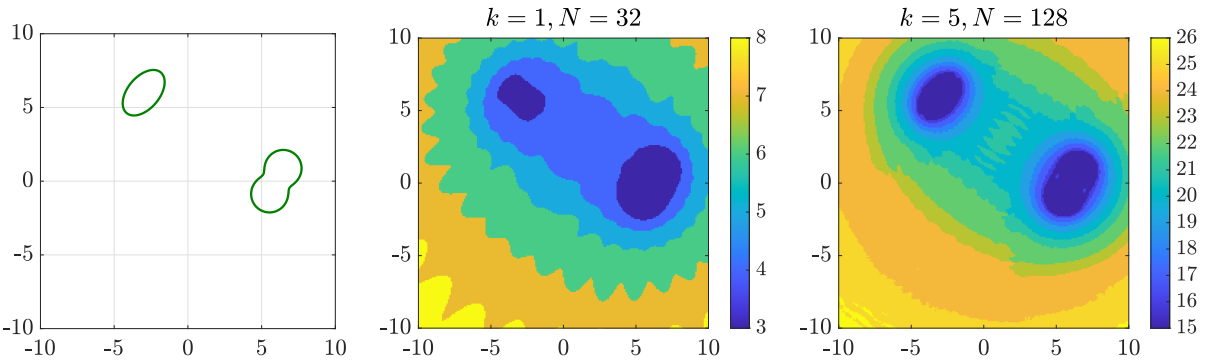

FIGURE 2.14. Exact shape of the Neumann obstacle from Example 2.45 (left), Visualization of the indicator function I_{neu} for two different wave numbers $k = 1$ with $N = 32$ (middle) and $k = 5$ with $N = 128$ (right).

the eigenvalues of the matrix $\boldsymbol{F}_{D_2}^{\text{neu}}$. As seen for the Dirichlet obstacle, the eigenvalues lie on a circle and converge to zero. However, in contrast to Figure 2.10, they converge to zero from the right side. This is the behavior that we expect from Corollary 2.17. More precisely, the real part of $\boldsymbol{F}_{D_2}^{\text{neu}}$ has 29 positive eigenvalues and three negative eigenvalues for $k = 1$, and 70 positive eigenvalues and 15 negative eigenvalues for $k = 5$.

In Figure 2.14, we present color-coded plots of the indicator function I_{neu} from (2.84) in the region of interest $[-10, 10]^2 \subseteq \mathbb{R}^2$. The sampling grid is the same as in Example 2.42, i.e. we use 201 sampling points in each direction.

We note that the number of negative eigenvalues of the matrix $\boldsymbol{A}_{B_{ij}}$ is higher for $k = 5$. Regardless of the wave number, the farther away a sampling point $\boldsymbol{z}_{ij}$ is located from the obstacle the higher the number of negative eigenvalues becomes, in compliance with Theorem 2.30. As seen in the previous example, the number of negative eigenvalues of the matrix $\text{Re}(\boldsymbol{F}_{D_2}^{\text{neu}})$ that are smaller than the threshold $-\delta$ is exactly the lowest number of negative eigenvalues that we observe in Figure 2.14. The number of eigenvalues of $\boldsymbol{A}_{B_{ij}}^{\text{neu}}$, $j = 1, \ldots, J$, whose absolute values are larger than δ is approximately (on average over all grid points) 32 for $k = 1$ and 90 for $k = 5$. In both plots, the lowest level set of the indicator function I_{neu} is a good approximation of the scatterer. Especially, the two components of the obstacle are reconstructed separately. △

2.5.3. SEPARATING MIXED OBSTACLES

We return to the general mixed case, i.e., when both Dirichlet and Neumann obstacles are present. While the algorithm developed for Dirichlet or Neumann obstacles in the previous subsection determines whether a sufficiently small probing domain B is contained inside the unknown scattering obstacle D or not, the shape characterization for mixed obstacles established in Theorem 2.40 describes whether a sufficiently large probing domain B contains the scatterer D or not. A corresponding numerical algorithm that implements a similar criterion for the inverse conductivity problem has recently been proposed in [GS19]. However, since in contrast to the inverse conductivity problem, the monotonicity relations in Theorem 2.40 only hold up to certain finite-dimensional subspaces of unknown dimension, an extension of the reconstruction algorithm from [GS19] to the mixed inverse obstacle problem is not straightforward. In the following, we do

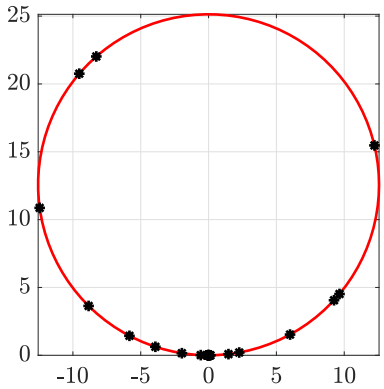

Figure 2.15. Eigenvalues of F_D^{mix} (black) from Example 2.46 for $k = 1$ with $N = 64$.

not perform a full shape reconstruction but we utilize Theorem 2.40 to develop an algorithm to recover the convex hulls of the Dirichlet obstacle D_1 and of the Neumann obstacle D_2 separately. We will see that our results confirm that we can separate Dirichlet and Neumann obstacles given the far field data, at least when their convex hulls do not overlap. After having separated the Dirichlet and the Neumann parts, one could, for instance, use them as a priori information that is required in the Factorization Method for mixed obstacles from [Gri02, GK04, KG08] to obtain an improved shape reconstruction.

We treat the Dirichlet part first and comment on the Neumann part afterward. The idea is to consider a sufficiently large number of probing disks $B = B_R(\boldsymbol{z}) \subseteq \mathbb{R}^2$, where for each center $\boldsymbol{z} \in \mathbb{R}^2$ the radius $R > 0$ is chosen as small as possible but such that B still completely covers D_1. Intersecting those disks then gives an approximation of the convex hull of D_1. To determine the optimal radius R for each of these disks, we use Theorem 2.40, which (under some additional assumptions) says that

(a) if $\overline{D_1} \subseteq B$, then $\operatorname{Re}(F_D^{\text{mix}}) + H_B^* H_B$ has only finitely many negative eigenvalues, and

(b) if $D_1 \not\subseteq B$, then $\operatorname{Re}(F_D^{\text{mix}}) + H_B^* H_B$ has infinitely many negative eigenvalues.

We define the matrix $\boldsymbol{T}_{B_R(\boldsymbol{z})} \in \mathbb{C}^{N \times N}$ analogously to (2.81). Then, we evaluate the eigenvalues of the matrix

$$\boldsymbol{A}_{B_R(\boldsymbol{z})}^{\text{mix},-} := \operatorname{Re}(\boldsymbol{F}_D^{\text{mix}}) + \boldsymbol{T}_{B_R(\boldsymbol{z})} \tag{2.85}$$

on a whole interval of radii R. As in our previous examples, we choose a threshold parameter δ and count the number of negative eigenvalues of $\boldsymbol{A}_{B_R(\boldsymbol{z})}^{\text{mix},-}$ that are smaller than $-\delta$. Of course, this number is always finite in our necessarily finite-dimensional numerical setting. Thus, the difficulty is to decide which number is high enough such that we consider it to be "infinite".

Example 2.46. We consider a kite-shaped Dirichlet obstacle and a peanut-shaped Neumann obstacle as shown in Figure 2.18 (left). We simulate the corresponding far field matrix $\boldsymbol{F}_D^{\text{mix}} \in \mathbb{C}^{N \times N}$ analogously to (2.78) for a wave number $k = 1$ and $N = 64$ observation and incident directions by means of a Nyström method. Figure 2.15 shows the eigenvalues of the matrix $\boldsymbol{F}_D^{\text{mix}}$, and we notice that they lie on a circle and converge to zero. As opposed to the previous examples, when we considered either only Dirichlet or only Neumann obstacles, there does not seem to

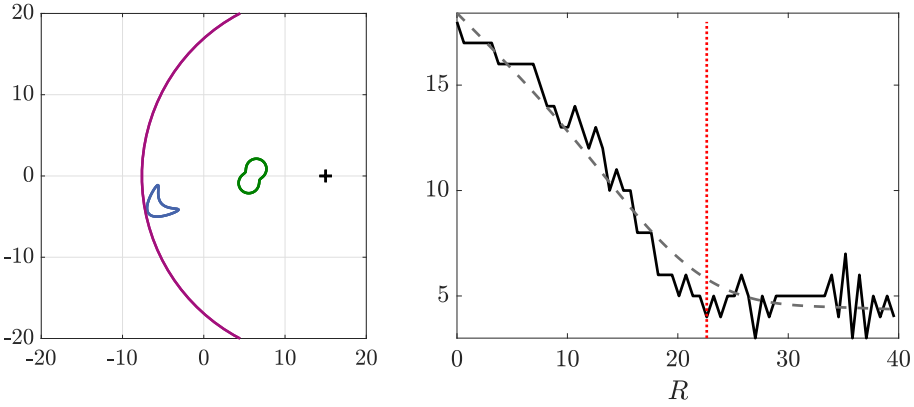

FIGURE 2.16. Exact shape of the mixed obstacles from Example 2.46 and smallest disk around $\boldsymbol{z} = (15, 0)$ containing the Dirichlet obstacle (left), Number of negative eigenvalues (right) of $\boldsymbol{A}^{\mathrm{mix},-}_{B_R(\boldsymbol{z})}$ smaller than $-\delta$ as function of radius R (black, solid), smoothing spline (gray, dashed) and estimated radius of smallest disk around $\boldsymbol{z} = (15, 0)$ containing the Dirichlet obstacle (red, dotted).

exist a direction from which the eigenvalues converge to zero. This emphasizes that, in contrast to $\mathrm{Re}(F^{\mathrm{dir}}_{D_1})$ and $\mathrm{Re}(F^{\mathrm{neu}}_{D_2})$, the operator $\mathrm{Re}(F^{\mathrm{mix}}_{D})$ is neither negative nor positive definite up to some finite-dimensional subspace.

To begin with, we fix the center $\boldsymbol{z} = (15, 0)$ of a single probing disk $B = B_R(\boldsymbol{z})$ and evaluate the matrix $\boldsymbol{A}^{\mathrm{mix},-}_{B_R(\boldsymbol{z})}$ from (2.85) for 64 radii in $(0, 40)$. As in our previous examples, we choose a threshold parameter $\delta = 10^{-14}$, and in Figure 2.16 (right) we show the number of negative eigenvalues of $\boldsymbol{A}^{\mathrm{mix},-}_{B_R(\boldsymbol{z})}$ that are smaller than $-\delta$ as a function of the radius R (black, solid).

In the plot on the right-hand side of Figure 2.16, we observe a similar behavior as for the concentric disks studied in Subsection 2.5.1 (cf. the plots on the right-hand side of Figures 2.7–2.8). The number of negative eigenvalues of $\boldsymbol{A}^{\mathrm{mix},-}_{B_R(\boldsymbol{z})}$ decreases with increasing R until it becomes stationary up to small oscillations around $R \approx 22.6$. Our theoretical results suggest that the radius R, where this transition from decreasing to almost stationary appears, corresponds to the radius of the smallest disk that still completely covers the Dirichlet obstacle D_1. To evaluate this transition numerically, we fit a smoothing spline curve through the number of negative eigenvalues of $\boldsymbol{A}^{\mathrm{mix},-}_{B_R(\boldsymbol{z})}$ as shown on the right-hand side of Figure 2.16 (gray, dashed). We determine the point of maximum signed curvature of this smoothing spline and use the corresponding value of R as an approximation of the radius of the smallest disk around $\boldsymbol{z}$ that still completely covers the Dirichlet obstacle D_1. The result of this strategy is shown as a dotted red vertical line, and the corresponding disk $B_R(\boldsymbol{z})$ is shown on the left-hand side of Figure 2.16 (purple). △

We proceed with the Neumann part. Theorem 2.40 states that

(a) if $\overline{D_2} \subseteq B$, then $\mathrm{Re}(F^{\mathrm{mix}}_{D}) - H^*_B H_B$ has only finitely many positive eigenvalues, and

(b) if $D_2 \not\subseteq B$, then $\mathrm{Re}(F^{\mathrm{mix}}_{D}) - H^*_B H_B$ has infinitely many positive eigenvalues.

Counting the numbers of eigenvalues larger than the threshold $\delta > 0$ of

$$\boldsymbol{A}^{\mathrm{mix},+}_{B_R(\boldsymbol{z})} := \mathrm{Re}(\boldsymbol{F}^{\mathrm{mix}}_{D}) - \boldsymbol{T}_{B_R(\boldsymbol{z})}$$

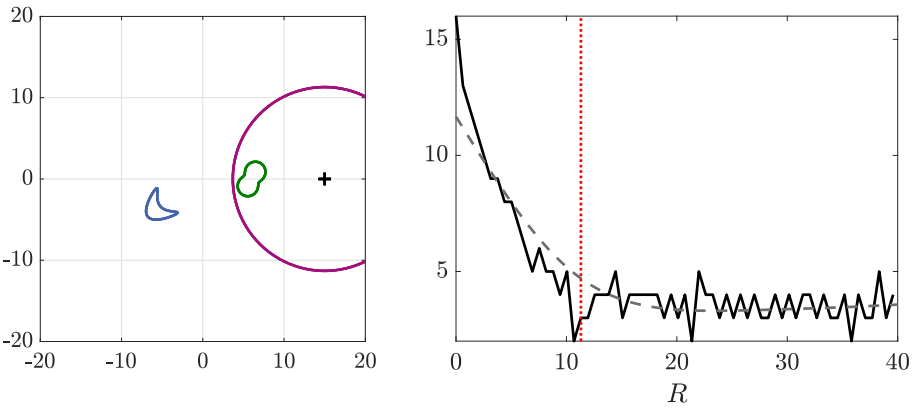

FIGURE 2.17. Exact shape of the mixed obstacles from Example 2.46 and smallest disk around $\boldsymbol{z} = (15, 0)$ containing the Neumann obstacle (left), Number of negative eigenvalues (right) of $\boldsymbol{A}^{\mathrm{mix},+}_{B_R(\boldsymbol{z})}$ smaller than $-\delta$ as function of radius R (black, solid), smoothing spline (gray, dashed) and estimated radius of smallest disk around $\boldsymbol{z} = (15, 0)$ containing the Neumann obstacle (red, dotted).

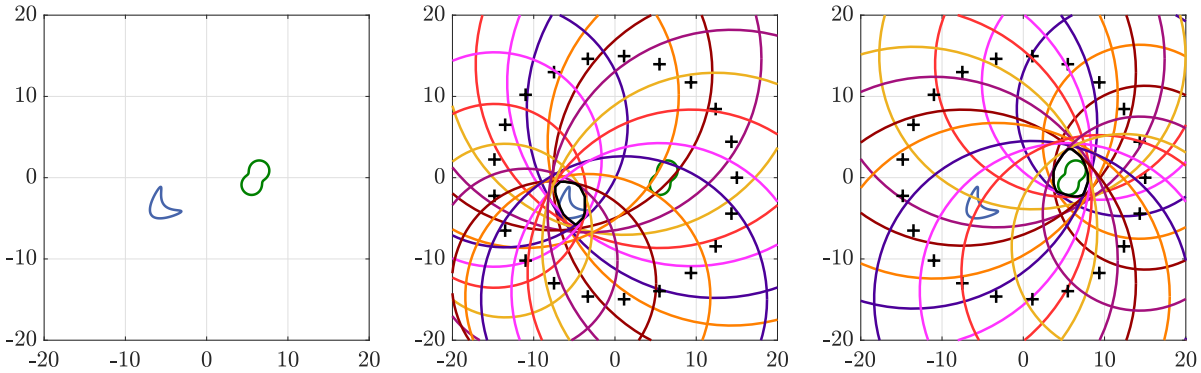

FIGURE 2.18. Exact shape of the mixed obstacles from Example 2.47 (left), Visualization of the reconstructions of the convex hulls of the Dirichlet obstacle (middle) and of the Neumann obstacle (right) for $k = 1$ (with $N = 64$).

for different radii R, we can use the strategy proposed in Example 2.46 for the Dirichlet obstacle to determine minimal radii of probing disks $B_R(\boldsymbol{z})$ containing the Neumann obstacle. The plots in Figure 2.17 show the corresponding result.

Example 2.47. We continue with Example 2.46 and pick 21 evenly spaced points $\boldsymbol{z}_1, \ldots, \boldsymbol{z}_{21}$ on a circle of radius 15 around the origin, which are shown as solid pluses in the two plots on the right-hand side of Figure 2.18. The points $\boldsymbol{z}_\ell$, $\ell = 1, \ldots, 21$, are the centers of 21 probing disks that are used to approximate the convex hulls of the Dirichlet obstacle and of the Neumann obstacle separately. For each center $\boldsymbol{z}_\ell$, we estimate the radii R^{dir}_ℓ and R^{neu}_ℓ of the smallest disks $B_{R^{\mathrm{dir}}_\ell}(\boldsymbol{z}_\ell)$ and $B_{R^{\mathrm{neu}}_\ell}(\boldsymbol{z}_\ell)$ centered at $\boldsymbol{z}_\ell$ that completely cover the Dirichlet obstacle and the Neumann obstacle, respectively. These estimates are obtained as described in Example 2.46.

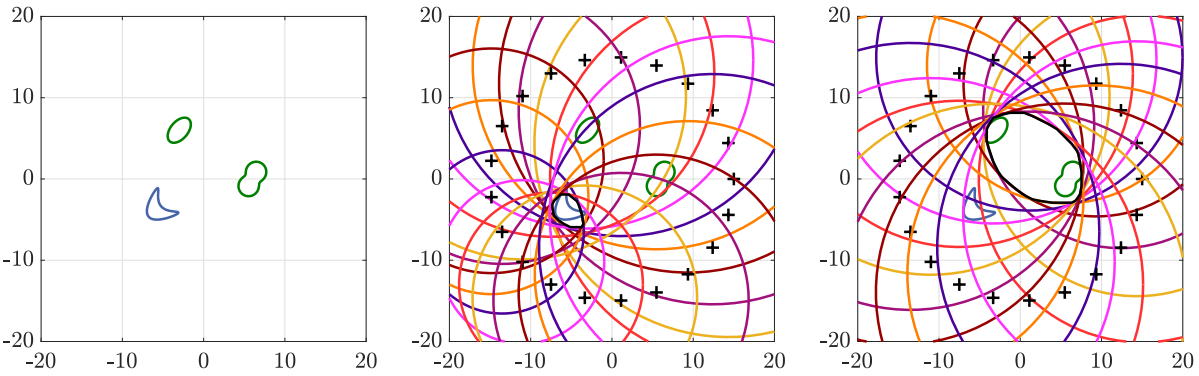

FIGURE 2.19. Exact shape of the mixed obstacles from Example 2.48 (left), Visualization of the reconstructions of the convex hulls of the Dirichlet obstacle (middle) and of the Neumann obstacles (right) for $k = 1$ (with $N = 64$).

Therewith, we compute approximations

$$\mathscr{C}^{\mathrm{dir}} = \bigcap_{\ell=1}^{21} B_{R_\ell^{\mathrm{dir}}}(\boldsymbol{z}_\ell) \qquad \text{and} \qquad \mathscr{C}^{\mathrm{neu}} = \bigcap_{\ell=1}^{21} B_{R_\ell^{\mathrm{neu}}}(\boldsymbol{z}_\ell)$$

of the convex hulls of D_1 and of D_2, respectively. The results are shown in Figure 2.18 (middle and right).

Reasonable approximations of the convex hulls of the Dirichlet obstacle and of the Neumann obstacle are recovered by the algorithm. As already pointed out, the separated regions could, e.g., be used as the a priori information required in the Factorization Method for mixed obstacles from [Gri02, GK04, KG08] to better reconstruct the shapes of the obstacles. △

Example 2.48. We add an ellipse with a Neumann boundary to the scattering configuration from Example 2.47 as shown in Figure 2.19 (left). As before, we simulate the corresponding far field matrix $\boldsymbol{F}_D^{\mathrm{mix}} \in \mathbb{C}^{N\times N}$ for a wave number $k = 1$ and $N = 64$ observation and incident directions using a Nyström method, and we apply the reconstruction scheme to approximate the convex hulls of the Dirichlet obstacle D_1 and of the Neumann obstacles D_2 with the same parameters as in the previous example. The reconstructions $\mathscr{C}^{\mathrm{dir}}$ and $\mathscr{C}^{\mathrm{neu}}$ are shown in Figure 2.19 (middle and right).

Again, the approximations of the convex hulls of the Dirichlet obstacle and of the Neumann obstacles are satisfactory in the sense that they do not overlap and allow separating the two components of the scatterer. Accordingly, they could be used as a priori information for the Factorization Method for mixed obstacles. △

Both examples illustrate that we can classify and separate the Dirichlet and Neumann obstacles without having any a priori knowledge about the boundary conditions. Different configurations for the centers of the probing disks that are used to approximate the convex hulls (i.e., of the solid pluses in the two plots on the right-hand side of Figures 2.18–2.19) are possible. However, arranging them on a circle around the region of interest worked well in all examples that we considered. Moreover, one could consider scattering configurations where the convex hulls of the Dirichlet and the Neumann obstacles intersect. Indeed, we did perform some numerical examples

and observed that we can still reconstruct the convex hulls. However, since the convex hulls intersect, we cannot separate the Dirichlet and the Neumann parts in this case.

CHAPTER 3

Monotonicity in Inverse Medium Scattering for Maxwell's Equations

3.1. Preliminaries

First, we establish some further notation and give several definitions. Thereby, we stick to the notation introduced in Section 2.1 and extend it by the terminology that additionally appears in the context of Maxwell's equations.

In contrast to the previous chapter, from now on we only consider the space $\mathbb{R}^3$. For $\boldsymbol{x}, \boldsymbol{y} \in \mathbb{R}^3$, we write $\boldsymbol{x} \times \boldsymbol{y}$ for the vector product of $\boldsymbol{x}$ and $\boldsymbol{y}$. The divergence of a vector field $\boldsymbol{F} : \mathbb{R}^3 \to \mathbb{C}^3$ is denoted by $\operatorname{div} \boldsymbol{F}$ and its rotation by $\mathbf{curl}\, \boldsymbol{F}$. Spaces of vector fields are indicated by an additional argument $\mathbb{C}^3$ inside the brackets as, for instance, in $L^2(\Omega, \mathbb{C}^3)$ or $L^2(\partial\Omega, \mathbb{C}^3)$. This means that every component of the vector field belongs to $L^2(\Omega)$ or $L^2(\partial\Omega)$, respectively. We introduce the tangential space

$$L_t^2(\partial\Omega, \mathbb{C}^3) := \{\boldsymbol{F} \in L^2(\partial\Omega, \mathbb{C}^3) \mid \boldsymbol{\nu} \cdot \boldsymbol{F} = 0 \text{ almost everywhere on } \partial\Omega\},$$

where $\boldsymbol{\nu}$ still denotes the exterior unit normal on $\partial\Omega$. In particular, we often make use of the space $L_t^2(S^2, \mathbb{C}^3)$.

Let $\Omega \subseteq \mathbb{R}^3$ be open. A vector field $\boldsymbol{F} \in L^2(\Omega, \mathbb{C}^3)$ is said to possess a weak curl $\mathbf{curl}\, \boldsymbol{F}$ in $L^2(\Omega, \mathbb{C}^3)$ if there exists a $\boldsymbol{G} \in L^2(\Omega, \mathbb{C}^3)$ such that

$$\int_\Omega \boldsymbol{G} \cdot \boldsymbol{\psi} \, \mathrm{d}\boldsymbol{x} = \int_\Omega \boldsymbol{F} \cdot \mathbf{curl}\, \boldsymbol{\psi} \, \mathrm{d}\boldsymbol{x} \qquad \text{for all } \boldsymbol{\psi} \in C_0^\infty(\Omega, \mathbb{C}^3),$$

and we set $\mathbf{curl}\, \boldsymbol{F} := \boldsymbol{G}$. Therewith, we are in the position to introduce the Sobolev spaces

$$\begin{aligned} H(\mathbf{curl}; \Omega) &:= \{\boldsymbol{F} \in L^2(\Omega, \mathbb{C}^3) \mid \mathbf{curl}\, \boldsymbol{F} \in L^2(\Omega, \mathbb{C}^3)\}, \\ H_{\mathrm{loc}}(\mathbf{curl}; \Omega) &:= \{\boldsymbol{F} \in L^2_{\mathrm{loc}}(\Omega, \mathbb{C}^3) \mid \mathbf{curl}\, \boldsymbol{F} \in L^2_{\mathrm{loc}}(\Omega, \mathbb{C}^3)\}. \end{aligned}$$

In these two spaces, we naturally seek solutions to Maxwell's equations. Equipped with the inner

product

$$\langle \boldsymbol{F}, \boldsymbol{G} \rangle_{H(\mathbf{curl};\Omega)} := \langle \mathbf{curl}\, \boldsymbol{F}, \mathbf{curl}\, \boldsymbol{G} \rangle_{L^2(\Omega,\mathbb{C}^3)} + \langle \boldsymbol{F}, \boldsymbol{G} \rangle_{L^2(\Omega,\mathbb{C}^3)}\,, \tag{3.1}$$

the space $H(\mathbf{curl};\Omega)$ is a Hilbert space. The dual space of $H(\mathbf{curl};\Omega)$ is denoted by $H(\mathbf{curl};\Omega)^*$. We write $\langle \boldsymbol{G}, \boldsymbol{F} \rangle_*$ for the value of a functional $\boldsymbol{G} \in H(\mathbf{curl};\Omega)^*$ evaluated at $\boldsymbol{F} \in H(\mathbf{curl};\Omega)$.

Similar to the definition of the weak curl, one introduces the weak divergence $\operatorname{div} \boldsymbol{F}$ of a vector field $\boldsymbol{F} \in L^2(\Omega,\mathbb{C}^3)$ via a variational formulation. To be more precise, $g \in L^2(\Omega)$ is the weak divergence of $\boldsymbol{F}$ if

$$\int_\Omega g\psi \,\mathrm{d}\boldsymbol{x} = -\int_\Omega \boldsymbol{F} \cdot \nabla\psi \,\mathrm{d}\boldsymbol{x} \qquad \text{for all } \psi \in C_0^\infty(\Omega)\,.$$

As above, the spaces $H(\operatorname{div};\Omega)$ and $H_{\mathrm{loc}}(\operatorname{div};\Omega)$ are given by

$$\begin{aligned} H(\operatorname{div};\Omega) &:= \{\boldsymbol{F} \in L^2(\Omega,\mathbb{C}^3) \mid \operatorname{div} \boldsymbol{F} \in L^2(\Omega)\}\,,\\ H_{\mathrm{loc}}(\operatorname{div};\Omega) &:= \{\boldsymbol{F} \in L^2_{\mathrm{loc}}(\Omega,\mathbb{C}^3) \mid \operatorname{div} \boldsymbol{F} \in L^2_{\mathrm{loc}}(\Omega)\}\,. \end{aligned}$$

The following diagram (see, e.g., [Arn18, Sec. 4.3]) shows the connections between different Sobolev spaces with respect to taking the gradient, curl and divergence of the functions and vector fields included therein. It reads

$$\begin{aligned} H^1(\Omega) &\xrightarrow{\nabla} H(\mathbf{curl};\Omega) \xrightarrow{\mathbf{curl}} H(\operatorname{div};\Omega) \xrightarrow{\operatorname{div}} L^2(\Omega)\,,\\ H^1_{\mathrm{loc}}(\Omega) &\xrightarrow{\nabla} H_{\mathrm{loc}}(\mathbf{curl};\Omega) \xrightarrow{\mathbf{curl}} H_{\mathrm{loc}}(\operatorname{div};\Omega) \xrightarrow{\operatorname{div}} L^2_{\mathrm{loc}}(\Omega)\,. \end{aligned} \tag{3.2}$$

In fact, these sequences are exact, meaning that the ranges of the spaces to the left of the arrows equal the null spaces of the spaces to the right.

Next, we aim to establish trace theorems for the space $H(\mathbf{curl};\Omega)$. Our starting point is the following classical identity. Let Ω be Lipschitz bounded and assume that $\boldsymbol{F}, \boldsymbol{G} \in C^1(\overline{\Omega},\mathbb{C}^3)$. Then, we have

$$\int_\Omega (\mathbf{curl}\, \boldsymbol{F}) \cdot \boldsymbol{G} \,\mathrm{d}\boldsymbol{x} - \int_\Omega \boldsymbol{F} \cdot (\mathbf{curl}\, \boldsymbol{G}) \,\mathrm{d}\boldsymbol{x} = \int_{\partial\Omega} (\boldsymbol{\nu} \times \boldsymbol{F}) \cdot \boldsymbol{G} \,\mathrm{d}s = \int_{\partial\Omega} (\boldsymbol{\nu} \times \boldsymbol{F}) \cdot ((\boldsymbol{\nu} \times \boldsymbol{G}) \times \boldsymbol{\nu}) \,\mathrm{d}s$$

(see, e.g., [Mon03, Cor. 3.20]), where we applied (B.4). Taking $\boldsymbol{G}$ as a test function motivates the definition $\gamma_t(\boldsymbol{F}) := \boldsymbol{\nu} \times \boldsymbol{F}|_{\partial\Omega}$ of the *tangential trace*. Accordingly, considering $\boldsymbol{F}$ as a test function, we define the *projection on the tangent plane* $\pi_t(\boldsymbol{G}) := (\boldsymbol{\nu} \times \boldsymbol{G}|_{\partial\Omega}) \times \boldsymbol{\nu}$. In [KH15, Thm. 5.24], it is shown that these traces have bounded extensions

$$\gamma_t : H(\mathbf{curl};\Omega) \to H^{-1/2}(\mathrm{Div};\partial\Omega)\,, \qquad \pi_t : H(\mathbf{curl};\Omega) \to H^{-1/2}(\mathrm{Curl};\partial\Omega)\,. \tag{3.3}$$

Besides, the operators γ_t and π_t possess bounded right inverses. For a precise definition of the spaces $H^{-1/2}(\mathrm{Div};\partial\Omega)$ and $H^{-1/2}(\mathrm{Curl};\partial\Omega)$, we refer the reader to [KH15, pp. 245–255], where the authors employ Sobolev spaces of periodic functions on a square. The space $H^{-1/2}(\mathrm{Div};\partial\Omega)$ can be identified with the dual space of $H^{-1/2}(\mathrm{Curl};\partial\Omega)$ (see, e.g., [KH15, Thm. 5.26]). Throughout, we write the dual pairing between $H^{-1/2}(\mathrm{Div};\partial\Omega)$ and $H^{-1/2}(\mathrm{Curl};\partial\Omega)$ as an integral for notational convenience. For the matter of readability, we further use the classical notation $\boldsymbol{\nu} \times \cdot$ and

$(\boldsymbol{\nu} \times \cdot) \times \boldsymbol{\nu}$ for the trace operators in (3.3). In addition, we introduce the map r, which is given by $r(\boldsymbol{\phi}) := \boldsymbol{\nu} \times \boldsymbol{\phi}$ for any continuously differentiable vector field on $\partial\Omega$. It can be extended to an isomorphism $r : H^{-1/2}(\mathrm{Div}; \partial\Omega) \to H^{-1/2}(\mathrm{Curl}; \partial\Omega)$. Respecting these specifications, we obtain the integration by parts formula that reads

$$\int_\Omega (\mathbf{curl}\, \boldsymbol{F}) \cdot \boldsymbol{G} \, \mathrm{d}\boldsymbol{x} - \int_\Omega \boldsymbol{F} \cdot (\mathbf{curl}\, \boldsymbol{G}) \, \mathrm{d}\boldsymbol{x} = \int_{\partial\Omega} (\boldsymbol{\nu} \times \boldsymbol{F}) \cdot ((\boldsymbol{\nu} \times \boldsymbol{G}) \times \boldsymbol{\nu}) \, \mathrm{d}s \tag{3.4}$$

for all $\boldsymbol{F}, \boldsymbol{G} \in H(\mathbf{curl}; \Omega)$ (see, e.g., [KH15, Thm. 5.26]). It is also known as *Green's formula*. The subspace of $H(\mathbf{curl}; \Omega)$-functions with vanishing tangential traces is denoted by

$$H_0(\mathbf{curl}; \Omega) := \left\{ \boldsymbol{F} \in H(\mathbf{curl}; \Omega) \mid \boldsymbol{\nu} \times \boldsymbol{F}|_{\partial\Omega} = 0 \right\},$$

where $\boldsymbol{F}$ has compact support. It can be equivalently defined as the closure of $C_0^\infty(\Omega, \mathbb{C}^3)$ in $H(\mathbf{curl}; \Omega)$ (see, e.g., [KH15, Def. 4.19 and Thm. 5.25]).

We continue with presenting four surface operators that are related to tangential vector fields. The *surface divergence* $\mathrm{Div}_{\partial\Omega} : H^{-1/2}(\mathrm{Div}; \partial\Omega) \to H^{-1/2}(\partial\Omega)$ is defined via the variational equation

$$\langle \mathrm{Div}_{\partial\Omega}\, \boldsymbol{\phi}, \varphi \rangle_{\partial\Omega} := -\int_{\partial\Omega} \boldsymbol{\phi} \cdot ((\boldsymbol{\nu} \times \nabla\widetilde{\varphi}) \times \boldsymbol{\nu}) \, \mathrm{d}s \qquad \text{for all } \varphi \in H^{1/2}(\partial\Omega),$$

where $\widetilde{\varphi} \in H^1(\Omega)$ is any extension of φ. Since $\widetilde{\varphi} \in H^1(\Omega)$ implies that $\nabla\widetilde{\varphi} \in H(\mathbf{curl}; \Omega)$ (see (3.2)), the application of the trace operator in the duality pairing on the right-hand side is admissible. Besides, we remind the reader of the notation $\langle \cdot, \cdot \rangle_{\partial\Omega}$ for the duality pairing between $H^{-1/2}(\partial\Omega)$ and $H^{1/2}(\partial\Omega)$. Analogously, we introduce the second surface operator called *surface scalar curl* $\mathrm{Curl}_{\partial\Omega} : H^{-1/2}(\mathrm{Curl}; \partial\Omega) \to H^{-1/2}(\partial\Omega)$ by

$$\langle \mathrm{Curl}_{\partial\Omega}\, \boldsymbol{\phi}, \varphi \rangle_{\partial\Omega} := -\int_{\partial\Omega} (\boldsymbol{\nu} \times \nabla\widetilde{\varphi}) \cdot \boldsymbol{\phi} \, \mathrm{d}s \qquad \text{for all } \varphi \in H^{1/2}(\partial\Omega)$$

(see, e.g., [KH15, Def. 5.29]). The remaining operators are given by duality. To be more precise, for the *surface gradient* $\mathbf{Grad}_{\partial\Omega} : H^{1/2}(\partial\Omega) \to H^{-1/2}(\mathrm{Curl}; \partial\Omega)$, it holds

$$\int_{\partial\Omega} \boldsymbol{\phi} \cdot \mathbf{Grad}_{\partial\Omega}\, \varphi \, \mathrm{d}s = -\langle \mathrm{Div}_{\partial\Omega}\, \boldsymbol{\phi}, \varphi \rangle_{\partial\Omega} \, \mathrm{d}s \qquad \text{for all } \boldsymbol{\phi} \in H^{-1/2}(\mathrm{Div}; \partial\Omega).$$

The last surface operator is the *surface vector curl* $\mathbf{Curl}_{\partial\Omega} : H^{1/2}(\partial\Omega) \to H^{-1/2}(\mathrm{Div}; \partial\Omega)$, and we have

$$\int_{\partial\Omega} \mathbf{Curl}_{\partial\Omega}\, \varphi \cdot \boldsymbol{\phi} \, \mathrm{d}s = \langle \mathrm{Curl}_{\partial\Omega}\, \boldsymbol{\phi}, \varphi \rangle_{\partial\Omega} \qquad \text{for all } \boldsymbol{\phi} \in H^{-1/2}(\mathrm{Curl}; \partial\Omega).$$

Eventually, we introduce the tangential space $H_t^{1/2}(\partial\Omega, \mathbb{C}^3)$ for smooth boundaries $\partial\Omega$ via

$$H_t^{1/2}(\partial\Omega, \mathbb{C}^3) := \left\{ \boldsymbol{F} \in H^{1/2}(\partial\Omega, \mathbb{C}^3) \mid \boldsymbol{\nu} \cdot \boldsymbol{F} = 0 \text{ almost everywhere on } \partial\Omega \right\}.$$

Therewith, we get the characterizations

$$H^{-1/2}(\mathrm{Div};\partial\Omega) \;=\; \{\boldsymbol{\phi} \in H_t^{-1/2}(\partial\Omega,\mathbb{C}^3) \mid \mathrm{Div}_{\partial\Omega}\,\boldsymbol{\phi} \in H^{-1/2}(\partial\Omega)\}\,,$$
$$H^{-1/2}(\mathrm{Curl};\partial\Omega) \;=\; \{\boldsymbol{\phi} \in H_t^{-1/2}(\partial\Omega,\mathbb{C}^3) \mid \mathrm{Curl}_{\partial\Omega}\,\boldsymbol{\phi} \in H^{-1/2}(\partial\Omega)\}\,,$$

where $H_t^{-1/2}(\partial\Omega,\mathbb{C}^3)$ denotes the dual space of $H_t^{1/2}(\partial\Omega,\mathbb{C}^3)$. Moreover, we require the space $H_t^{3/2}(\partial\Omega,\mathbb{C}^3)$ which is given as the image $\gamma_t(H^2(\Omega,\mathbb{C}^3))$.

Similar to the previous chapter, we use Sobolev spaces on a relatively open subset Γ of the boundary $\partial\Omega$. To this end, we introduce the notation

$$\widetilde{H}^{-1/2}(\mathrm{Div};\Gamma) \;=\; \{\boldsymbol{\phi} \in H^{-1/2}(\mathrm{Div};\partial\Omega) \mid \mathrm{supp}\,\boldsymbol{\phi} \subseteq \overline{\Gamma}\}\,.$$

We recall the definition (2.4) of the local parameterization of Γ and extend the notion (2.5) of piecewise linear functions to vector fields. For a vector field $\boldsymbol{F} = (F_1,F_2,F_3)^\top$, we define $\boldsymbol{F}_\zeta$ by

$$\boldsymbol{F}_\zeta(\boldsymbol{x}') \;:=\; \begin{pmatrix} F_{1,\zeta}(\boldsymbol{x}') \\ F_{2,\zeta}(\boldsymbol{x}') \\ F_{3,\zeta}(\boldsymbol{x}') \end{pmatrix} \;:=\; \begin{pmatrix} F_1(\boldsymbol{x}',\zeta(\boldsymbol{x}')) \\ F_2(\boldsymbol{x}',\zeta(\boldsymbol{x}')) \\ F_3(\boldsymbol{x}',\zeta(\boldsymbol{x}')) \end{pmatrix}$$

and call $\boldsymbol{F}$ *piecewise linear* if the functions $F_{i,\zeta}$, $i=1,2,3$, are piecewise linear on the domain $B_r'(0) \subseteq \mathbb{R}^2$ of the local parameterization. In Appendix A, we construct a special subspace of tangential continuous piecewise linear vector fields.

3.2. Electromagnetic Scattering by an Inhomogeneous Medium

In this section, we will give a short overview of the scattering of electromagnetic waves. Thereby, we concentrate on results that are relevant for the inverse scattering problem we are interested in. More details can, e.g., be found in [CK19, KH15, Mon03].

We consider electromagnetic waves in inhomogeneous isotropic dielectric media in $\mathbb{R}^3$. Their propagation is characterized by the space-dependent *electric permittivity* $\varepsilon = \varepsilon(\boldsymbol{x})$ and the *magnetic permeability* $\mu = \mu(\boldsymbol{x})$. We denote by $\varepsilon_0 > 0$ and $\mu_0 > 0$ the electric permittivity and the magnetic permeability in free space. Then, the *electric field* $\mathcal{E}$ and the *magnetic field* $\mathcal{H}$ satisfy the time-dependent *Maxwell equations*

$$\mathbf{curl}_{\boldsymbol{x}}\,\mathcal{E}(\boldsymbol{x},t) + \mu\frac{\partial\mathcal{H}(\boldsymbol{x},t)}{\partial t} \;=\; 0\,, \quad \mathbf{curl}_{\boldsymbol{x}}\,\mathcal{H}(\boldsymbol{x},t) - \varepsilon\frac{\partial\mathcal{E}(\boldsymbol{x},t)}{\partial t} \;=\; 0\,, \qquad \boldsymbol{x}\in\mathbb{R}^3\,,\, t>0\,.$$

The *relative electric permittivity* of the medium is defined by $\varepsilon_r := \varepsilon/\varepsilon_0$ and we suppose that $\mu = \mu_0$. Thus, the considered media are non-magnetic. Throughout, we assume that the electromagnetic waves are time-harmonic in the form

$$\mathcal{E}(\boldsymbol{x},t) \;=\; \mathrm{Re}\left(\boldsymbol{E}(\boldsymbol{x})e^{-\mathrm{i}\omega t}\right), \quad \mathcal{H}(\boldsymbol{x},t) \;=\; \mathrm{Re}\left(\boldsymbol{H}(\boldsymbol{x})e^{-\mathrm{i}\omega t}\right)$$

with *frequency* $\omega > 0$. The complex-valued space-dependent vector fields $\boldsymbol{E}$ and $\boldsymbol{H}$ satisfy the

time-harmonic Maxwell equations

$$\mathbf{curl}\,\boldsymbol{E} - \mathrm{i}\omega\mu_0\boldsymbol{H} \;=\; 0\,, \quad \mathbf{curl}\,\boldsymbol{H} + \mathrm{i}\omega\varepsilon\boldsymbol{E} \;=\; 0 \qquad \text{in } \mathbb{R}^3\,.$$

An *incident field* $(\boldsymbol{E}^i, \boldsymbol{H}^i)$ is a solution to the Maxwell equations

$$\mathbf{curl}\,\boldsymbol{E}^i - \mathrm{i}\omega\mu_0\boldsymbol{H}^i \;=\; 0\,, \quad \mathbf{curl}\,\boldsymbol{H}^i + \mathrm{i}\omega\varepsilon_0\boldsymbol{E}^i \;=\; 0 \qquad \text{in } \mathbb{R}^3\,, \tag{3.5}$$

and it gets scattered by the inhomogeneous medium with relative electric permittivity ε_r. We suppose that $\varepsilon_r^{-1} = 1 - q$ for some real-valued contrast function

$$q \in \mathcal{Y}_D \;:=\; \left\{ f \in L^\infty(\mathbb{R}^3) \;\middle|\; f|_D \in W^{1,\infty}(D,\mathbb{R})\,,\; \operatorname{supp}(f) = \overline{D}\,,\; \operatorname{ess\,inf}(1-f) > 0 \right\}, \tag{3.6}$$

where $D \subseteq \mathbb{R}^3$ is open and Lipschitz bounded. Since $\overline{D}$ is the support of the inhomogeneity, D is the scattering object that deviates the incident field. The *scattered field* is denoted by $(\boldsymbol{E}_q^s, \boldsymbol{H}_q^s)$, and its dependence on the inhomogeneity is indicated by the index q. To ensure that the scattered field propagates outwards, we require an analog to the Sommerfeld radiation condition corresponding to the Helmholtz equation. The appropriate condition is the *Silver-Müller radiation condition*. We suppose that $(\boldsymbol{E}_q^s, \boldsymbol{H}_q^s)$ satisfies

$$\lim_{|\boldsymbol{x}|\to\infty} \left(\sqrt{\varepsilon_0}\,\boldsymbol{x} \times \boldsymbol{E}_q^s(\boldsymbol{x}) - |\boldsymbol{x}|\sqrt{\mu_0}\boldsymbol{H}_q^s(\boldsymbol{x}) \right) \;=\; 0 \tag{3.7}$$

uniformly with respect to all directions $\widehat{\boldsymbol{x}} := \boldsymbol{x}/|\boldsymbol{x}| \in S^2$. As before, we refer to solutions to Maxwell's equations in the connected complement $\mathbb{R}^d \setminus \overline{D}$ satisfying the radiation condition as *radiating solutions*. The *total field*

$$(\boldsymbol{E}_q, \boldsymbol{H}_q) \;:=\; (\boldsymbol{E}^i, \boldsymbol{H}^i) + (\boldsymbol{E}_q^s, \boldsymbol{H}_q^s) \tag{3.8}$$

is defined as the superposition of the incident and the scattered field, and it fulfills

$$\mathbf{curl}\,\boldsymbol{E}_q - \mathrm{i}\omega\mu_0\boldsymbol{H}_q \;=\; 0\,, \quad \mathbf{curl}\,\boldsymbol{H}_q + \mathrm{i}\omega\varepsilon\boldsymbol{E}_q \;=\; 0 \qquad \text{in } \mathbb{R}^3\,. \tag{3.9}$$

It is often convenient to eliminate either the electric field or the magnetic field from (3.5)–(3.9) and to work with second-order formulations. Introducing the *wave number* $k := \omega\sqrt{\varepsilon_0\mu_0}$ we obtain

$$\begin{aligned}
\mathbf{curl}\,\mathbf{curl}\,\boldsymbol{E}^i - k^2\boldsymbol{E}^i \;&=\; 0 && \text{in } \mathbb{R}^3\,, && \text{(3.10a)}\\
\mathbf{curl}\,\mathbf{curl}\,\boldsymbol{E}_q - k^2\varepsilon_r\boldsymbol{E}_q \;&=\; 0 && \text{in } \mathbb{R}^3\,, && \text{(3.10b)}\\
\boldsymbol{E}^i + \boldsymbol{E}_q^s \;&=\; \boldsymbol{E}_q && \text{in } \mathbb{R}^3\,, && \text{(3.10c)}\\
\lim_{|\boldsymbol{x}|\to\infty} \left(\boldsymbol{x} \times \mathbf{curl}\,\boldsymbol{E}_q^s(\boldsymbol{x}) + \mathrm{i}k|\boldsymbol{x}|\boldsymbol{E}_q^s(\boldsymbol{x}) \right) \;&=\; 0 && && \text{(3.10d)}
\end{aligned}$$

and

$$\begin{aligned}
\mathbf{curl}\,\mathbf{curl}\,\boldsymbol{H}^i - k^2\boldsymbol{H}^i &= 0 && \text{in } \mathbb{R}^3\,, && (3.11a)\\
\mathbf{curl}(\varepsilon_r^{-1}\,\mathbf{curl}\,\boldsymbol{H}_q) - k^2\boldsymbol{H}_q &= 0 && \text{in } \mathbb{R}^3\,, && (3.11b)\\
\boldsymbol{H}^i + \boldsymbol{H}_q^s &= \boldsymbol{H}_q && \text{in } \mathbb{R}^3\,, && (3.11c)\\
\lim_{|\boldsymbol{x}|\to\infty}(\boldsymbol{x}\times\mathbf{curl}\,\boldsymbol{H}_q^s(\boldsymbol{x}) + \mathrm{i}k|\boldsymbol{x}|\boldsymbol{H}_q^s(\boldsymbol{x})) &= 0\,, && && (3.11d)
\end{aligned}$$

respectively. Throughout this work, Maxwell's equations are always to be understood in the variational sense. More precisely, we call $(\boldsymbol{E}_q, \boldsymbol{H}_q) \in H_{\mathrm{loc}}(\mathbf{curl};\mathbb{R}^3)$ a *variational solution* to (3.10b) or (3.11b) (or equivalently to (3.9)) if

$$\int_{\mathbb{R}^3}(\mathbf{curl}\,\boldsymbol{E}_q\cdot\mathbf{curl}\,\boldsymbol{\psi} - k^2\varepsilon_r\boldsymbol{E}_q\cdot\boldsymbol{\psi})\,\mathrm{d}\boldsymbol{x} = 0 \qquad \text{for all } \boldsymbol{\psi}\in H_0(\mathbf{curl};\mathbb{R}^3)\,, \tag{3.12a}$$

or

$$\int_{\mathbb{R}^3}(\varepsilon_r^{-1}\,\mathbf{curl}\,\boldsymbol{H}_q\cdot\mathbf{curl}\,\boldsymbol{\psi} - k^2\boldsymbol{H}_q\cdot\boldsymbol{\psi})\,\mathrm{d}\boldsymbol{x} = 0 \qquad \text{for all } \boldsymbol{\psi}\in H_0(\mathbf{curl};\mathbb{R}^3)\,. \tag{3.12b}$$

Remark 3.1. Standard regularity results (see, e.g., [Web81]) yield smoothness of $(\boldsymbol{E}_q, \boldsymbol{H}_q)$ and $(\boldsymbol{E}_q^s, \boldsymbol{H}_q^s)$ in $\mathbb{R}^3\setminus\overline{B_R(0)}$, whenever $B_R(0)$ contains the scatterer D, and similarly the solution $(\boldsymbol{E}^i, \boldsymbol{H}^i)$ is smooth throughout $\mathbb{R}^3$. In particular, the Silver-Müller radiation condition (3.7) is well defined. ◊

Sometimes, it is necessary to allow for more general right-hand sides $\boldsymbol{f}\in L^2(\Omega,\mathbb{C}^3)$ or even $\boldsymbol{f}\in H(\mathbf{curl};\Omega)^*$ in (3.10b) and (3.11b), where $\Omega\subseteq\mathbb{R}^3$ is open and bounded. The corresponding variational formulations read

$$\int_{\mathbb{R}^3}(\mathbf{curl}\,\boldsymbol{E}_q\cdot\mathbf{curl}\,\boldsymbol{\psi} - k^2\varepsilon_r\boldsymbol{E}_q\cdot\boldsymbol{\psi})\,\mathrm{d}\boldsymbol{x} = \langle\boldsymbol{f},\boldsymbol{\psi}\rangle_* \quad \text{for all } \boldsymbol{\psi}\in H_0(\mathbf{curl};\mathbb{R}^3) \tag{3.13a}$$

or

$$\int_{\mathbb{R}^3}(\varepsilon_r^{-1}\,\mathbf{curl}\,\boldsymbol{H}_q\cdot\mathbf{curl}\,\boldsymbol{\psi} - k^2\boldsymbol{H}_q\cdot\boldsymbol{\psi})\,\mathrm{d}\boldsymbol{x} = \langle\boldsymbol{f},\boldsymbol{\psi}\rangle_* \quad \text{for all } \boldsymbol{\psi}\in H_0(\mathbf{curl};\mathbb{R}^3)\,, \tag{3.13b}$$

where $\boldsymbol{f}\in H(\mathbf{curl};\Omega)^*$ is extended by zero for all of $\mathbb{R}^3$.

The following lemma illustrates the behavior of radiating solutions to Maxwell's equations far away from the scatterer.

Lemma 3.2. *Every radiating solution $(\boldsymbol{E}_q^s, \boldsymbol{H}_q^s)$ to the Maxwell equations* (3.9) *in $\mathbb{R}^3\setminus\overline{D}$ has the asymptotic behavior*

$$\boldsymbol{E}_q^s(\boldsymbol{x}) = \frac{e^{\mathrm{i}k|\boldsymbol{x}|}}{4\pi|\boldsymbol{x}|}(\boldsymbol{E}_q^\infty(\widehat{\boldsymbol{x}}) + \mathcal{O}(|\boldsymbol{x}|^{-1}))\,, \quad \boldsymbol{H}_q^s(\boldsymbol{x}) = \frac{e^{\mathrm{i}k|\boldsymbol{x}|}}{4\pi|\boldsymbol{x}|}(\boldsymbol{H}_q^\infty(\widehat{\boldsymbol{x}}) + \mathcal{O}(|\boldsymbol{x}|^{-1})) \tag{3.14}$$

as $|\boldsymbol{x}|\to\infty$, uniformly in $\widehat{\boldsymbol{x}} = \boldsymbol{x}/|\boldsymbol{x}|\in S^2$, and $\boldsymbol{E}_q^\infty, \boldsymbol{H}_q^\infty\in L_t^2(S^2,\mathbb{C}^3)$ are called electric *and* magnetic far field patterns. *They are given by*

$$\begin{aligned}
\boldsymbol{E}_q^\infty(\widehat{\boldsymbol{x}}) &= \widehat{\boldsymbol{x}}\times\int_{\partial B_R(0)}(\mathrm{i}k(\boldsymbol{\nu}\times\boldsymbol{E}_q^s)(\boldsymbol{y}) + (\boldsymbol{\nu}\times\mathbf{curl}\,\boldsymbol{E}_q^s)(\boldsymbol{y})\times\widehat{\boldsymbol{x}})e^{-\mathrm{i}k\widehat{\boldsymbol{x}}\cdot\boldsymbol{y}}\,\mathrm{d}s(\boldsymbol{y})\,, && (3.15a)\\
\boldsymbol{H}_q^\infty(\widehat{\boldsymbol{x}}) &= \widehat{\boldsymbol{x}}\times\int_{\partial B_R(0)}(\mathrm{i}k(\boldsymbol{\nu}\times\boldsymbol{H}_q^s)(\boldsymbol{y}) + (\boldsymbol{\nu}\times\mathbf{curl}\,\boldsymbol{H}_q^s)(\boldsymbol{y})\times\widehat{\boldsymbol{x}})e^{-\mathrm{i}k\widehat{\boldsymbol{x}}\cdot\boldsymbol{y}}\,\mathrm{d}s(\boldsymbol{y})\,. && (3.15b)
\end{aligned}$$

In particular,

$$\boldsymbol{E}_q^\infty(\widehat{\boldsymbol{x}}) = -\sqrt{\frac{\mu_0}{\varepsilon_0}}\widehat{\boldsymbol{x}} \times \boldsymbol{H}_q^\infty(\widehat{\boldsymbol{x}}) \qquad \text{and} \qquad \widehat{\boldsymbol{x}} \cdot \boldsymbol{E}_q^\infty(\widehat{\boldsymbol{x}}) = \widehat{\boldsymbol{x}} \cdot \boldsymbol{H}_q^\infty(\widehat{\boldsymbol{x}}) = 0$$

for all $\widehat{\boldsymbol{x}} \in S^2$, i.e. the far field patterns are tangential to the unit sphere.

Proof. For a proof, we refer the reader to [Mon03, Cor. 9.5 and Rem. 9.6]. □

Rellich's lemma guarantees a one-to-one correspondence between radiating solutions to the Maxwell equations and their far field patterns.

Lemma 3.3 (Rellich)**.** *Let $R > 0$ such that $B_R(0)$ contains the scatterer D, and let $(\boldsymbol{E}_q^s, \boldsymbol{H}_q^s)$ be a radiating solution to the Maxwell equations* (3.9) *in $\mathbb{R}^3 \setminus \overline{B_R(0)}$. If $\boldsymbol{E}_q^\infty = 0$ or $\boldsymbol{H}_q^\infty = 0$, then $\boldsymbol{E}_q^s = \boldsymbol{H}_q^s = 0$ in $\mathbb{R}^3 \setminus \overline{B_R(0)}$.*

Proof. A proof can be found in [Mon03, Cor. 9.29]. □

The unique continuation principle stated in the following theorem is used to prove uniqueness of the scattering problem (3.5)–(3.9), and it serves as an important tool in the proofs in Subsections 3.4.1 and 3.5.1.

Theorem 3.4 (Unique Continuation Principle)**.** *Let $\Omega \subseteq \mathbb{R}^3$ be connected, and let $q \in \mathcal{Y}_D$. If $(\boldsymbol{E}_q, \boldsymbol{H}_q) \in H_{\mathrm{loc}}(\mathbf{curl}; \Omega) \times H_{\mathrm{loc}}(\mathbf{curl}; \Omega)$ satisfies the Maxwell equations* (3.12) *and $\boldsymbol{E}_q$ or $\boldsymbol{H}_q$ vanishes in a neighborhood of some $\boldsymbol{x}_0 \in \Omega$, then $\boldsymbol{E}_q = \boldsymbol{H}_q = 0$ in Ω.*

Proof. This is a direct consequence of [NW12, Cor. 1.2]. □

The following theorem gives the well-posedness of the scattering problem (3.5)–(3.9), i.e., it guarantees existence and uniqueness of solutions. Beforehand, we introduce the auxiliary boundary value problem

$$\mathbf{curl}\,\mathbf{curl}\,\boldsymbol{w} - k^2\boldsymbol{w} = 0 \quad \text{in } \mathbb{R}^3 \setminus \overline{B_R(0)}\,, \qquad \boldsymbol{\nu} \times \boldsymbol{w} = \boldsymbol{\psi} \quad \text{on } \partial B_R(0)\,. \tag{3.16}$$

There exists a unique radiating solution $\boldsymbol{w} \in H(\mathbf{curl}; \mathbb{R}^3 \setminus \overline{B_R(0)})$ to (3.16) (see, e.g., [Mon03, Thm. 9.30]). Thus, we can define the *exterior Calderon operator*

$$\Lambda : H^{-1/2}(\mathrm{Div}; \partial B_R(0)) \to H^{-1/2}(\mathrm{Curl}; \partial B_R(0))\,, \quad \Lambda\boldsymbol{\psi} := (\boldsymbol{\nu} \times \mathbf{curl}\,\boldsymbol{w}|_{\partial B_R(0)}) \times \boldsymbol{\nu}\,, \tag{3.17}$$

which maps boundary data $\boldsymbol{\psi}$ to the projection on the tangent plane of $\mathbf{curl}\,\boldsymbol{w}$, where $\boldsymbol{w}$ is the unique radiating solution to the exterior boundary value problem (3.16). For more details, we refer the reader to [Mon03, pp. 248–250] (please note that in contrast to the definition in [Mon03] the Calderon considered in this work includes an additional $\times\boldsymbol{\nu}$).

Theorem 3.5. *Let $q \in \mathcal{Y}_D$ and suppose that the incident field $(\boldsymbol{E}^i, \boldsymbol{H}^i)$ satisfies* (3.5)*. Then, there exists a unique radiating solution $(\boldsymbol{E}_q, \boldsymbol{H}_q)$ to* (3.12)*.*

Proof. Suppose that the incident field $(\boldsymbol{E}^i, \boldsymbol{H}^i)$ satisfies (3.5), and let $R > 0$ such that $B_R(0)$ contains D. Using either a volume integral equation approach (see, e.g., [KG08, pp. 113–118]) or

a variational formulation on $B_R(0)$ involving the exterior Calderon operator (see, e.g., [Mon03, pp. 262–272]), Riesz-Fredholm theory can be applied to show existence of a solution to (3.12), provided uniqueness holds. Outside $B_R(0)$, uniqueness of radiating solutions to (3.12) or equivalently to (3.8)–(3.9) is guaranteed by Rellich's lemma in the form [Mon03, Lem. 9.28]. Under our assumptions on the coefficients, uniqueness in the whole space $\mathbb{R}^3$ follows, e.g., from [BCTX12, Thm. 2.1]. □

Remark 3.6. Existence and uniqueness carry over when replacing the right-hand sides in (3.10b) and (3.11b), respectively, by an arbitrary function $\boldsymbol{f} \in L^2(\Omega;\mathbb{C}^3)$, where $\Omega \subseteq \mathbb{R}^3$ is open and bounded. If we allow for even more general right-hand sides $\boldsymbol{f} \in H(\mathbf{curl};\Omega)^*$, we still get existence and uniqueness since the right-hand sides of the variational formulations (3.13) yield linear forms on $H(\mathbf{curl}, B_R(0))$ for any ball $B_R(0) \subseteq \mathbb{R}^3$ containing Ω. Thus, combining the uniqueness result from [BCTX12, Thm. 2.1] with Riesz-Fredholm theory guarantees existence. ◊

We define *plane wave incident fields* with *direction of propagation* $\boldsymbol{\theta} \in S^2$ and *polarization* $\boldsymbol{p} \in \mathbb{C}^3$ such that $\boldsymbol{p} \cdot \boldsymbol{\theta} = 0$. They are given by matrix-valued functions $(\boldsymbol{E}^i(\boldsymbol{x};\boldsymbol{\theta}), \boldsymbol{H}^i(\boldsymbol{x};\boldsymbol{\theta}))$ satisfying

$$\boldsymbol{E}^i(\boldsymbol{x};\boldsymbol{\theta})\boldsymbol{p} := -\sqrt{\frac{\mu_0}{\varepsilon_0}}(\boldsymbol{\theta}\times\boldsymbol{p})\, e^{\mathrm{i}k\boldsymbol{\theta}\cdot\boldsymbol{x}}\,, \quad \boldsymbol{H}^i(\boldsymbol{x};\boldsymbol{\theta})\boldsymbol{p} := \boldsymbol{p}\, e^{\mathrm{i}k\boldsymbol{\theta}\cdot\boldsymbol{x}}\,, \qquad \boldsymbol{x}\in\mathbb{R}^3\,.$$

Then, $(\boldsymbol{E}^i(\cdot;\boldsymbol{\theta})\boldsymbol{p}, \boldsymbol{H}^i(\cdot;\boldsymbol{\theta})\boldsymbol{p})$ are *entire solutions* to Maxwell's equations (3.5), i.e. solving the Maxwell equations in the whole of $\mathbb{R}^3$. However, these are not radiating. In fact, the next lemma shows that radiating entire solutions have to vanish identically

Lemma 3.7. *Every entire solution to Maxwell's equations* (3.5) *that satisfies the Silver-Müller radiation condition* (3.7) *must vanish identically.*

Proof. Let $(\boldsymbol{E}^i, \boldsymbol{H}^i)$ be a solution to Maxwell's equations (3.5). Then, $(\boldsymbol{E}^i, \boldsymbol{H}^i)$ is twice differentiable according to Remark 3.1. Taking the divergence in (3.5) and using that $\operatorname{div}\mathbf{curl} = 0$ (see (B.2)) shows that $\operatorname{div}\boldsymbol{E}^i = \operatorname{div}\boldsymbol{H}^i = 0$. Moreover, we apply (B.1) in the second-order formulations (3.10a) and (3.11a). Therewith, we obtain

$$\Delta\boldsymbol{E}^i + k^2\boldsymbol{E}^i = 0\,, \quad \Delta\boldsymbol{H}^i + k^2\boldsymbol{H}^i = 0 \qquad \text{in } \mathbb{R}^3\,.$$

Since the Silver-Müller radiation condition is equivalent to the Sommerfeld radiation condition for the Cartesian components of $\boldsymbol{E}^i, \boldsymbol{H}^i$ (see, e.g., [CK19, Thm. 6.8]), Lemma 2.4 ensures the assertion. □

Since (3.5)–(3.9) is linear with respect to the incident field, the scattered field, the total field and the far field patterns can also be expressed by matrix-valued functions. In order to underline their dependence on the direction of propagation, we denote them by $(\boldsymbol{E}_q^s(\cdot;\boldsymbol{\theta}), \boldsymbol{H}_q^s(\cdot;\boldsymbol{\theta}))$, $(\boldsymbol{E}_q(\cdot;\boldsymbol{\theta}), \boldsymbol{H}_q(\cdot;\boldsymbol{\theta}))$ and $(\boldsymbol{E}_q^\infty(\cdot;\boldsymbol{\theta}), \boldsymbol{H}_q^\infty(\cdot;\boldsymbol{\theta}))$. These map the polarization $\boldsymbol{p} \in \mathbb{C}^3$ to the scattered field $(\boldsymbol{E}_q^s(\cdot;\boldsymbol{\theta})\boldsymbol{p}, \boldsymbol{H}_q^s(\cdot;\boldsymbol{\theta})\boldsymbol{p})$, the total field $(\boldsymbol{E}_q(\cdot;\boldsymbol{\theta})\boldsymbol{p}, \boldsymbol{H}_q(\cdot;\boldsymbol{\theta})\boldsymbol{p})$, and the far field patterns $(\boldsymbol{E}_q^\infty(\cdot;\boldsymbol{\theta})\boldsymbol{p}, \boldsymbol{H}_q^\infty(\cdot;\boldsymbol{\theta})\boldsymbol{p})$.

Analogous to the previous chapter, we define the *magnetic far field operator* as the operator mapping superpositions of plane wave incident fields to the far field patterns of the corresponding

scattered fields. Thus, we have

$$F_q : L_t^2(S^2, \mathbb{C}^3) \to L_t^2(S^2, \mathbb{C}^3), \quad (F_q \boldsymbol{p})(\widehat{\boldsymbol{x}}) := \int_{S^2} \boldsymbol{H}_q^\infty(\widehat{\boldsymbol{x}}; \boldsymbol{\theta}) \boldsymbol{p}(\boldsymbol{\theta}) \, \mathrm{d}s(\boldsymbol{\theta}) . \tag{3.18}$$

From Lemma 3.2, we have that the magnetic far field pattern is analytic. Thus, F_q is compact from $L_t^2(S^2, \mathbb{C}^3)$ to $L_t^2(S^2, \mathbb{C}^3)$ since it is an integral operator with smooth kernel (see, e.g., [Kre14, Thm. 2.28]). Furthermore, the magnetic far field operator is normal (see, e.g., [KG08, Thm. 5.7]). Besides, the *magnetic scattering operator*

$$\mathcal{S}_q := I + \frac{\mathrm{i}k}{8\pi^2} F_q : L_t^2(S^2, \mathbb{C}^3) \to L_t^2(S^2, \mathbb{C}^3) \tag{3.19}$$

is unitary (see, e.g., [KG08, Thm. 5.7]). This implies that the eigenvalues of $\mathcal{S}_q$ lie on the unit circle. Consequently, the eigenvalues of F_q lie on the circle of radius $8\pi^2/k$ centered in $8\pi^2 \, \mathrm{i}/k$ in the complex plane.

For any given $\boldsymbol{p} \in L_t^2(S^2, \mathbb{C}^3)$, the tangential vector field $F_q \boldsymbol{p} \in L_t^2(S^2, \mathbb{C}^3)$ is the far field pattern of the scattered magnetic field generated by the incident field

$$\boldsymbol{E}_{\boldsymbol{p}}^i(\boldsymbol{x}) := -\sqrt{\frac{\mu_0}{\varepsilon_0}} \int_{S^2} (\boldsymbol{\theta} \times \boldsymbol{p}(\boldsymbol{\theta})) e^{\mathrm{i}k\boldsymbol{\theta}\cdot\boldsymbol{x}} \, \mathrm{d}s(\boldsymbol{\theta}) , \; \boldsymbol{H}_{\boldsymbol{p}}^i(\boldsymbol{x}) := \int_{S^2} \boldsymbol{p}(\boldsymbol{\theta}) e^{\mathrm{i}k\boldsymbol{\theta}\cdot\boldsymbol{x}} \, \mathrm{d}s(\boldsymbol{\theta}) , \quad \boldsymbol{x} \in \mathbb{R}^3 . \tag{3.20}$$

The latter is called a *Herglotz wave pair* with density $\boldsymbol{p}$, and we observe that it represents an entire solution to Maxwell's equations. We write $(\boldsymbol{E}_{q,\boldsymbol{p}}^s, \boldsymbol{H}_{q,\boldsymbol{p}}^s)$, $(\boldsymbol{E}_{q,\boldsymbol{p}}, \boldsymbol{H}_{q,\boldsymbol{p}})$ and $(\boldsymbol{E}_{q,\boldsymbol{p}}^\infty, \boldsymbol{H}_{q,\boldsymbol{p}}^\infty)$ for the corresponding scattered field, total field and far field patterns, respectively. By linearity we have

$$\boldsymbol{E}_{q,\boldsymbol{p}}(\boldsymbol{x}) = \int_{S^2} \boldsymbol{E}_q(\boldsymbol{x}; \boldsymbol{\theta}) \boldsymbol{p}(\boldsymbol{\theta}) \, \mathrm{d}s(\boldsymbol{\theta}) , \quad \boldsymbol{H}_{q,\boldsymbol{p}}(\boldsymbol{x}) = \int_{S^2} \boldsymbol{H}_q(\boldsymbol{x}; \boldsymbol{\theta}) \boldsymbol{p}(\boldsymbol{\theta}) \, \mathrm{d}s(\boldsymbol{\theta}) , \quad \boldsymbol{x} \in \mathbb{R}^3 , \tag{3.21a}$$

$$\boldsymbol{E}_{q,\boldsymbol{p}}^s(\boldsymbol{x}) = \int_{S^2} \boldsymbol{E}_q^s(\boldsymbol{x}; \boldsymbol{\theta}) \boldsymbol{p}(\boldsymbol{\theta}) \, \mathrm{d}s(\boldsymbol{\theta}) , \quad \boldsymbol{H}_{q,\boldsymbol{p}}^s(\boldsymbol{x}) = \int_{S^2} \boldsymbol{H}_q^s(\boldsymbol{x}; \boldsymbol{\theta}) \boldsymbol{p}(\boldsymbol{\theta}) \, \mathrm{d}s(\boldsymbol{\theta}) , \quad \boldsymbol{x} \in \mathbb{R}^3 , \tag{3.21b}$$

$$\boldsymbol{E}_{q,\boldsymbol{p}}^\infty(\widehat{\boldsymbol{x}}) = \int_{S^2} \boldsymbol{E}_q^\infty(\widehat{\boldsymbol{x}}; \boldsymbol{\theta}) \boldsymbol{p}(\boldsymbol{\theta}) \, \mathrm{d}s(\boldsymbol{\theta}) , \quad \boldsymbol{H}_{q,\boldsymbol{p}}^\infty(\widehat{\boldsymbol{x}}) = \int_{S^2} \boldsymbol{H}_q^\infty(\widehat{\boldsymbol{x}}; \boldsymbol{\theta}) \boldsymbol{p}(\boldsymbol{\theta}) \, \mathrm{d}s(\boldsymbol{\theta}) , \quad \widehat{\boldsymbol{x}} \in S^2 . \tag{3.21c}$$

Comparing (3.18) and (3.21c) we note that $F_q \boldsymbol{p} = \boldsymbol{H}_{q,\boldsymbol{p}}^\infty$ for all $\boldsymbol{p} \in L_t^2(S^2, \mathbb{C}^3)$.

As already pointed out in the previous chapter, the *direct scattering problem* consists of finding the scattered field that satisfies the system (3.7)–(3.9) given an incident field and the contrast function. The purpose of our work is to reconstruct the shape and position of the scatterer, i.e. the support of the contrast function, from the knowledge of the far field operator. This is known as the *inverse scattering problem*. Our reconstruction ansatz builds again on monotonicity properties in terms of the modified Loewner order from (2.7). Thereby, we distinguish sign-definite scatterers where the contrast function q needs to be strictly positive or strictly negative throughout D and indefinite scatterers where we omit the definiteness assumptions on q. Beforehand, we derive a monotonicity relation for the magnetic far field operator that holds for all contrast functions $q \in \mathcal{Y}_D$.

3.3. A MONOTONICITY RELATION FOR THE MAGNETIC FAR FIELD OPERATOR

We begin with establishing a monotonicity relation for the magnetic far field operator.

Theorem 3.8 (Monotonicity Relation)**.** *Let $D_1, D_2 \subseteq \mathbb{R}^3$ be open and Lipschitz bounded, and let $q_1 \in \mathcal{Y}_{D_1}$ and $q_2 \in \mathcal{Y}_{D_2}$. Then, there exists a finite-dimensional subspace $V \subseteq L_t^2(S^2, \mathbb{C}^3)$ such that*

$$\operatorname{Re}\Big(\int_{S^2} \boldsymbol{p} \cdot \overline{\mathcal{S}_{q_1}^*(F_{q_2} - F_{q_1})\boldsymbol{p}}\, \mathrm{d}s\Big) \geq \int_{\mathbb{R}^3} (q_2 - q_1)\, |\operatorname{\mathbf{curl}} \boldsymbol{H}_{q_1,\boldsymbol{p}}|^2\, \mathrm{d}\boldsymbol{x} \qquad \text{for all } \boldsymbol{p} \in V^\perp. \tag{3.22}$$

In particular,

$$q_1 \leq q_2 \qquad \text{implies that} \qquad \operatorname{Re}(\mathcal{S}_{q_1}^* F_{q_1}) \leq_{\mathrm{fin}} \operatorname{Re}(\mathcal{S}_{q_1}^* F_{q_2})\,. \tag{3.23}$$

Remark 3.9. Recalling (3.19) and using that $\mathcal{S}_1$ and $\mathcal{S}_2$ are unitary operators, we find that

$$\begin{aligned}
\mathcal{S}_{q_1}^*(F_{q_2} - F_{q_1}) &= \frac{8\pi^2}{\mathrm{i}k}\mathcal{S}_{q_1}^*(\mathcal{S}_{q_2} - \mathcal{S}_{q_1}) = \frac{8\pi^2}{\mathrm{i}k}(\mathcal{S}_{q_1}^*\mathcal{S}_{q_2} - I) \\
&= \Big(\frac{8\pi^2}{\mathrm{i}k}(I - \mathcal{S}_{q_2}^*\mathcal{S}_{q_1})\Big)^* = \Big(\frac{8\pi^2}{\mathrm{i}k}\mathcal{S}_{q_2}^*(\mathcal{S}_{q_2} - \mathcal{S}_{q_1})\Big)^* = \big(\mathcal{S}_{q_2}^*(F_{q_2} - F_{q_1})\big)^*.
\end{aligned}$$

Accordingly, we have $\operatorname{Re}(\mathcal{S}_{q_1}^*(F_{q_2} - F_{q_1})) = \operatorname{Re}(\mathcal{S}_{q_2}^*(F_{q_2} - F_{q_1}))$, and therefore, the monotonicity relations (3.22)–(3.23) remain valid, if we replace $\mathcal{S}_{q_1}^*$ with $\mathcal{S}_{q_2}^*$ in these formulas. ◊

The subsequent result follows by interchanging the roles of q_1 and q_2 in Theorem 3.8, except for $\mathcal{S}_{q_1}^*$.

Corollary 3.10. *Let $D_1, D_2 \subseteq \mathbb{R}^3$ be open and Lipschitz bounded, and let $q_1 \in \mathcal{Y}_{D_1}$ and $q_2 \in \mathcal{Y}_{D_2}$. Then, there exists a finite-dimensional subspace $V \subseteq L_t^2(S^2, \mathbb{C}^3)$ such that*

$$\operatorname{Re}\Big(\int_{S^2} \boldsymbol{p} \cdot \overline{\mathcal{S}_{q_1}^*(F_{q_2} - F_{q_1})\boldsymbol{p}}\, \mathrm{d}s\Big) \leq \int_{\mathbb{R}^3} (q_2 - q_1)\, |\operatorname{\mathbf{curl}} \boldsymbol{H}_{q_2,\boldsymbol{p}}|^2\, \mathrm{d}\boldsymbol{x} \qquad \text{for all } \boldsymbol{p} \in V^\perp.$$

Proof. Combining Remark 3.9 with Theorem 3.8 guarantees the existence of a finite-dimensional subspace $V \subseteq L_t^2(S^2, \mathbb{C}^3)$ such that

$$\begin{aligned}
\operatorname{Re}\Big(\int_{S^2} \boldsymbol{p} \cdot \overline{\mathcal{S}_{q_1}^*(F_{q_2} - F_{q_1})\boldsymbol{p}}\, \mathrm{d}s\Big) &= -\operatorname{Re}\Big(\int_{S^2} \boldsymbol{p} \cdot \overline{\mathcal{S}_{q_2}^*(F_{q_1} - F_{q_2})\boldsymbol{p}}\, \mathrm{d}s\Big) \\
&\leq -\int_{\mathbb{R}^3} (q_1 - q_2)\, |\operatorname{\mathbf{curl}} \boldsymbol{H}_{q_2,\boldsymbol{p}}|^2\, \mathrm{d}\boldsymbol{x}
\end{aligned}$$

for all $\boldsymbol{p} \in V^\perp$. □

Before we establish the proof of Theorem 3.8, we discuss three preparatory lemmas. In the first of these lemmas, we collect several integral identities for the magnetic field. These will be utilized in Lemma 3.12 below, where we derive an integral identity for the left-hand side of inequality (3.22).

Lemma 3.11. *Let $D \subset\subset B_R(0)$ be open and Lipschitz bounded, and let $q \in \mathcal{Y}_D$. Then,*

$$\int_{S^2} \boldsymbol{p} \cdot \overline{F_q \boldsymbol{p}} \, \mathrm{d}s = \int_{B_R(0)} q \, \mathbf{curl}\, \boldsymbol{H}^i_{\boldsymbol{p}} \cdot \overline{\mathbf{curl}\, \boldsymbol{H}_{q,\boldsymbol{p}}} \, \mathrm{d}\boldsymbol{y} \qquad \text{for all } \boldsymbol{p} \in L^2_t(S^2, \mathbb{C}^3)\,, \tag{3.24}$$

and, for any $\boldsymbol{\psi} \in H(\mathbf{curl}; B_R(0))$,

$$\int_{B_R(0)} (\varepsilon_r^{-1} \, \mathbf{curl}\, \boldsymbol{H}^s_{q,\boldsymbol{p}} \cdot \mathbf{curl}\, \boldsymbol{\psi} - k^2 \boldsymbol{H}^s_{q,\boldsymbol{p}} \cdot \boldsymbol{\psi}) \, \mathrm{d}\boldsymbol{x} + \int_{\partial B_R(0)} (\boldsymbol{\nu} \times \mathbf{curl}\, \boldsymbol{H}^s_{q,\boldsymbol{p}}) \cdot \boldsymbol{\psi} \, \mathrm{d}s = \int_{B_R(0)} q \, \mathbf{curl}\, \boldsymbol{H}^i_{\boldsymbol{p}} \cdot \mathbf{curl}\, \boldsymbol{\psi} \, \mathrm{d}\boldsymbol{x}\,. \tag{3.25}$$

Moreover, if $q_1 \in \mathcal{Y}_{D_1}$ and $q_2 \in \mathcal{Y}_{D_2}$ for some $D_1, D_2 \subset\subset B_R(0)$ that are open and Lipschitz bounded, then

$$\int_{\partial B_R(0)} \Big(\boldsymbol{H}^s_{q_j,\boldsymbol{p}} \cdot (\boldsymbol{\nu} \times \overline{\mathbf{curl}\, \boldsymbol{H}^s_{q_l,\boldsymbol{p}}}) - \overline{\boldsymbol{H}^s_{q_l,\boldsymbol{p}}} \cdot (\boldsymbol{\nu} \times \mathbf{curl}\, \boldsymbol{H}^s_{q_j,\boldsymbol{p}}) \Big) \, \mathrm{d}s = \frac{\mathrm{i}k}{8\pi^2} \int_{S^2} F_{q_j} \boldsymbol{p} \cdot \overline{F_{q_l} \boldsymbol{p}} \, \mathrm{d}s \tag{3.26}$$

for any $j, l \in \{1, 2\}$.

Proof. Let $\boldsymbol{p} \in L^2_t(S^2, \mathbb{C}^3)$. Then, the scattered field $\boldsymbol{H}^s_{q,\boldsymbol{p}} = \boldsymbol{H}_{q,\boldsymbol{p}} - \boldsymbol{H}^i_{\boldsymbol{p}} \in H_{\mathrm{loc}}(\mathbf{curl}; \mathbb{R}^3)$ satisfies

$$\mathbf{curl}(\varepsilon_r^{-1} \, \mathbf{curl}\, \boldsymbol{H}^s_{q,\boldsymbol{p}}) - k^2 \boldsymbol{H}^s_{q,\boldsymbol{p}} = -\mathbf{curl}(\varepsilon_r^{-1} \, \mathbf{curl}\, \boldsymbol{H}^i_{\boldsymbol{p}}) + k^2 \boldsymbol{H}^i_{\boldsymbol{p}} = \mathbf{curl}(q \, \mathbf{curl}\, \boldsymbol{H}^i_{\boldsymbol{p}}) \tag{3.27}$$

in $\mathbb{R}^3$. Using the variational formulation of (3.27) with test function $\boldsymbol{\psi} \in H(\mathbf{curl}; B_R(0))$ yields

$$\int_{B_R(0)} \varepsilon_r^{-1} \, \mathbf{curl}\, \boldsymbol{H}^s_{q,\boldsymbol{p}} \cdot \mathbf{curl}\, \boldsymbol{\psi} \, \mathrm{d}\boldsymbol{x} = \int_{B_R(0)} q \, \mathbf{curl}\, \boldsymbol{H}^i_{\boldsymbol{p}} \cdot \mathbf{curl}\, \boldsymbol{\psi} \, \mathrm{d}\boldsymbol{x} + k^2 \int_{B_R(0)} \boldsymbol{H}^s_{q,\boldsymbol{p}} \cdot \boldsymbol{\psi} \, \mathrm{d}\boldsymbol{x} - \int_{\partial B_R(0)} (\boldsymbol{\nu} \times \mathbf{curl}\, \boldsymbol{H}^s_{q,\boldsymbol{p}}) \cdot \boldsymbol{\psi} \, \mathrm{d}s\,, \tag{3.28}$$

where we used that $\varepsilon_r = 1$ and $q = 0$ on the boundary $\partial B_R(0)$. This implies (3.25).

Likewise, we get

$$\int_{B_R(0)} \varepsilon_r^{-1} \, \mathbf{curl}\, \boldsymbol{H}^i_{\boldsymbol{p}} \cdot \mathbf{curl}\, \boldsymbol{\psi} \, \mathrm{d}\boldsymbol{x} = -\int_{B_R(0)} q \, \mathbf{curl}\, \boldsymbol{H}^i_{\boldsymbol{p}} \cdot \mathbf{curl}\, \boldsymbol{\psi} \, \mathrm{d}\boldsymbol{x} + k^2 \int_{B_R(0)} \boldsymbol{H}^i_{\boldsymbol{p}} \cdot \boldsymbol{\psi} \, \mathrm{d}\boldsymbol{x} - \int_{\partial B_R(0)} (\boldsymbol{\nu} \times \mathbf{curl}\, \boldsymbol{H}^i_{\boldsymbol{p}}) \cdot \boldsymbol{\psi} \, \mathrm{d}s \tag{3.29}$$

for any $\boldsymbol{\psi} \in H(\mathbf{curl}; B_R(0))$. Subtracting (3.29) with $\boldsymbol{\psi} = \overline{\boldsymbol{H}^s_{q,\boldsymbol{p}}}$ from the complex conjugate of (3.28) with $\boldsymbol{\psi} = \overline{\boldsymbol{H}^i_{\boldsymbol{p}}}$ gives

$$0 = \int_{B_R(0)} q \, \overline{\mathbf{curl}\, \boldsymbol{H}_{q,\boldsymbol{p}}} \cdot \mathbf{curl}\, \boldsymbol{H}^i_{\boldsymbol{p}} \, \mathrm{d}\boldsymbol{x} - \int_{\partial B_R(0)} \Big((\boldsymbol{\nu} \times \overline{\mathbf{curl}\, \boldsymbol{H}^s_{q,\boldsymbol{p}}}) \cdot \boldsymbol{H}^i_{\boldsymbol{p}} - (\boldsymbol{\nu} \times \mathbf{curl}\, \boldsymbol{H}^i_{\boldsymbol{p}}) \cdot \overline{\boldsymbol{H}^s_{q,\boldsymbol{p}}} \Big) \, \mathrm{d}s\,. \tag{3.30}$$

We employ (B.3) to calculate the curl of $\boldsymbol{H}^i_{\boldsymbol{p}}$, given by (3.20), and find that

$$\mathbf{curl}\, \boldsymbol{H}^i_{\boldsymbol{p}}(\boldsymbol{x}) = \int_{S^2} (\nabla e^{\mathrm{i}k\boldsymbol{x}\cdot\boldsymbol{\theta}} \times \boldsymbol{p}(\boldsymbol{\theta}))\, \mathrm{d}s(\boldsymbol{\theta}) = \mathrm{i}k \int_{S^2} (\boldsymbol{\theta} \times \boldsymbol{p}(\boldsymbol{\theta})) e^{\mathrm{i}k\boldsymbol{x}\cdot\boldsymbol{\theta}}\, \mathrm{d}s(\boldsymbol{\theta}), \qquad \boldsymbol{x} \in \mathbb{R}^3.$$

Therewith, we obtain using (3.15) that

$$\begin{aligned}
&\int_{\partial B_R(0)} \Big((\boldsymbol{\nu} \times \overline{\mathbf{curl}\, \boldsymbol{H}^s_{q,\boldsymbol{p}}}) \cdot \boldsymbol{H}^i_{\boldsymbol{p}} - (\boldsymbol{\nu} \times \mathbf{curl}\, \boldsymbol{H}^i_{\boldsymbol{p}}) \cdot \overline{\boldsymbol{H}^s_{q,\boldsymbol{p}}} \Big)\, \mathrm{d}s \\
&= \int_{\partial B_R(0)} \Big((\boldsymbol{\nu} \times \overline{\mathbf{curl}\, \boldsymbol{H}^s_{q,\boldsymbol{p}}}) \cdot \boldsymbol{H}^i_{\boldsymbol{p}} + (\boldsymbol{\nu} \times \overline{\boldsymbol{H}^s_{q,\boldsymbol{p}}}) \cdot \mathbf{curl}\, \boldsymbol{H}^i_{\boldsymbol{p}} \Big)\, \mathrm{d}s \\
&= \int_{S^2} \int_{\partial B_R(0)} \Big((\boldsymbol{\nu} \times \overline{\mathbf{curl}\, \boldsymbol{H}^s_{q,\boldsymbol{p}}})(\boldsymbol{x}) \cdot \boldsymbol{p}(\boldsymbol{\theta}) e^{\mathrm{i}k\boldsymbol{\theta}\cdot\boldsymbol{x}} \\
&\qquad\qquad + (\boldsymbol{\nu} \times \overline{\boldsymbol{H}^s_{q,\boldsymbol{p}}})(\boldsymbol{x}) \cdot \Big(\mathrm{i}k (\boldsymbol{\theta} \times \boldsymbol{p}(\boldsymbol{\theta})) e^{\mathrm{i}k\boldsymbol{\theta}\cdot\boldsymbol{x}} \Big) \Big)\, \mathrm{d}s(\boldsymbol{x})\, \mathrm{d}s(\boldsymbol{\theta}) \\
&= \int_{S^2} \boldsymbol{p}(\boldsymbol{\theta}) \cdot \int_{\partial B_R(0)} \Big((\boldsymbol{\nu} \times \overline{\mathbf{curl}\, \boldsymbol{H}^s_{q,\boldsymbol{p}}})(\boldsymbol{x}) + \mathrm{i}k \Big((\boldsymbol{\nu} \times \overline{\boldsymbol{H}^s_{q,\boldsymbol{p}}})(\boldsymbol{x}) \times \boldsymbol{\theta} \Big) \Big) e^{\mathrm{i}k\boldsymbol{\theta}\cdot\boldsymbol{x}}\, \mathrm{d}s(\boldsymbol{x})\, \mathrm{d}s(\boldsymbol{\theta}) \\
&= \int_{S^2} \boldsymbol{p}(\boldsymbol{\theta}) \cdot \Big(\boldsymbol{\theta} \times \int_{\partial B_R(0)} \Big(\Big((\boldsymbol{\nu} \times \mathbf{curl}\, \overline{\boldsymbol{H}^s_{q,\boldsymbol{p}}})(\boldsymbol{x}) \times \boldsymbol{\theta} \Big) \Big) \\
&\qquad\qquad - \mathrm{i}k (\boldsymbol{\nu} \times \overline{\boldsymbol{H}^s_{q,\boldsymbol{p}}})(\boldsymbol{x}) \Big) e^{\mathrm{i}k\boldsymbol{\theta}\cdot\boldsymbol{x}}\, \mathrm{d}s(\boldsymbol{x}) \Big)\, \mathrm{d}s(\boldsymbol{\theta}) \\
&= \int_{S^2} \boldsymbol{p}(\boldsymbol{\theta}) \cdot \overline{\boldsymbol{H}^\infty_{q,\boldsymbol{p}}(\boldsymbol{\theta})}\, \mathrm{d}s(\boldsymbol{\theta}) = \int_{S^2} \boldsymbol{p} \cdot \overline{F_q \boldsymbol{p}}\, \mathrm{d}s.
\end{aligned}$$

Together with (3.30) this shows (3.24).

Now, let $q_1 \in \mathcal{Y}_{D_1}$ and $q_2 \in \mathcal{Y}_{D_2}$ for some $D_1, D_2 \subset\subset B_R(0)$ that are open and Lipschitz bounded, and let $r > R$. Then, $\boldsymbol{H}^s_{q_j,\boldsymbol{p}}, \boldsymbol{H}^s_{q_l,\boldsymbol{p}} \in H_{\mathrm{loc}}(\mathbf{curl}; \mathbb{R}^3)$ fulfill

$$\mathbf{curl}\, \mathbf{curl}\, \boldsymbol{H}^s_{q_j,\boldsymbol{p}} - k^2 \boldsymbol{H}^s_{q_j,\boldsymbol{p}} = 0 \qquad \text{in } B_r(0) \setminus \overline{B_R(0)}, \tag{3.31a}$$

$$\mathbf{curl}\, \mathbf{curl}\, \boldsymbol{H}^s_{q_l,\boldsymbol{p}} - k^2 \boldsymbol{H}^s_{q_l,\boldsymbol{p}} = 0 \qquad \text{in } B_r(0) \setminus \overline{B_R(0)}. \tag{3.31b}$$

We subtract (3.31a) multiplied with $\overline{\boldsymbol{H}^s_{q_l,\boldsymbol{p}}}$ from the complex conjugate of (3.31b) multiplied with $\boldsymbol{H}^s_{q_j,\boldsymbol{p}}$. This implies

$$\overline{\boldsymbol{H}^s_{q_l,\boldsymbol{p}}} \cdot \mathbf{curl}\, \mathbf{curl}\, \boldsymbol{H}^s_{q_j,\boldsymbol{p}} - \boldsymbol{H}^s_{q_j,\boldsymbol{p}} \cdot \mathbf{curl}\, \mathbf{curl}\, \overline{\boldsymbol{H}^s_{q_l,\boldsymbol{p}}} = 0 \qquad \text{in } B_r(0) \setminus \overline{B_R(0)}.$$

Thus, the integration by parts formula (3.4) gives

$$\begin{aligned}
0 &= \int_{B_r(0)\setminus\overline{B_R(0)}} \overline{\boldsymbol{H}^s_{q_l,\boldsymbol{p}}} \cdot \mathbf{curl}\, \mathbf{curl}\, \boldsymbol{H}^s_{q_j,\boldsymbol{p}} - \boldsymbol{H}^s_{q_j,\boldsymbol{p}} \cdot \mathbf{curl}\, \mathbf{curl}\, \overline{\boldsymbol{H}^s_{q_l,\boldsymbol{p}}}\, \mathrm{d}\boldsymbol{x} \\
&= \int_{\partial B_r(0)} ((\boldsymbol{\nu} \times \mathbf{curl}\, \boldsymbol{H}^s_{q_j,\boldsymbol{p}}) \cdot \overline{\boldsymbol{H}^s_{q_l,\boldsymbol{p}}} - (\boldsymbol{\nu} \times \overline{\mathbf{curl}\, \boldsymbol{H}^s_{q_l,\boldsymbol{p}}}) \cdot \boldsymbol{H}^s_{q_j,\boldsymbol{p}})\, \mathrm{d}s \\
&\quad - \int_{\partial B_R(0)} ((\boldsymbol{\nu} \times \mathbf{curl}\, \boldsymbol{H}^s_{q_j,\boldsymbol{p}}) \cdot \overline{\boldsymbol{H}^s_{q_l,\boldsymbol{p}}} - (\boldsymbol{\nu} \times \overline{\mathbf{curl}\, \boldsymbol{H}^s_{q_l,\boldsymbol{p}}}) \cdot \boldsymbol{H}^s_{q_j,\boldsymbol{p}})\, \mathrm{d}s.
\end{aligned} \tag{3.32}$$

Applying the Silver-Müller radiation condition (3.11d) and inserting the far field expansion (3.14)

we obtain that

$$\begin{aligned}
&\int_{\partial B_r(0)} \Big((\boldsymbol{\nu} \times \overline{\operatorname{\mathbf{curl}} \boldsymbol{H}^s_{q_l,\boldsymbol{p}}}) \cdot \boldsymbol{H}^s_{q_j,\boldsymbol{p}} - (\boldsymbol{\nu} \times \operatorname{\mathbf{curl}} \boldsymbol{H}^s_{q_j,\boldsymbol{p}}) \cdot \overline{\boldsymbol{H}^s_{q_l,\boldsymbol{p}}} \Big) \, \mathrm{d}s \\
&= 2\mathrm{i}k \int_{\partial B_r(0)} \boldsymbol{H}^s_{q_j,\boldsymbol{p}} \cdot \overline{\boldsymbol{H}^s_{q_l,\boldsymbol{p}}} \, \mathrm{d}s + o(1) = \frac{\mathrm{i}k}{8\pi^2} \int_{S^2} \boldsymbol{H}^\infty_{q_j,\boldsymbol{p}} \cdot \overline{\boldsymbol{H}^\infty_{q_l,\boldsymbol{p}}} \, \mathrm{d}s + o(1) \\
&= \frac{\mathrm{i}k}{8\pi^2} \int_{S^2} F_{q_j} \boldsymbol{p} \cdot \overline{F_{q_l} \boldsymbol{p}} \, \mathrm{d}s + o(1)
\end{aligned}$$

as $r \to \infty$. In combination with (3.32) this yields (3.26). □

We focus on the left-hand side of (3.22), and in a first step, we observe that it is possible to rewrite the term found there. Using the definition (3.19) of the scattering operator we see that

$$\mathcal{S}^*_{q_1}(F_{q_2} - F_{q_1}) = F_{q_2} - F_{q_1} - \frac{\mathrm{i}k}{8\pi^2}(F^*_{q_1} F_{q_2} - F^*_{q_1} F_{q_1}) \, .$$

Since $\operatorname{Re}(F^*_{q_1} F_{q_1}) = F^*_{q_1} F_{q_1}$, it follows that $\operatorname{Re}(\frac{\mathrm{i}k}{8\pi^2} F^*_{q_1} F_{q_1}) = 0$, and thus,

$$\operatorname{Re}(\mathcal{S}^*_{q_1}(F_{q_2} - F_{q_1})) = \operatorname{Re}\Big(F_{q_2} - F_{q_1} - \frac{\mathrm{i}k}{8\pi^2} F^*_{q_1} F_{q_2} \Big) \, .$$

Accordingly, we arrive at

$$\begin{aligned}
&\operatorname{Re}\Big(\int_{S^2} \boldsymbol{p} \cdot \overline{\mathcal{S}^*_{q_1}(F_{q_2} - F_{q_1}) \boldsymbol{p}} \, \mathrm{d}s \Big) = \operatorname{Re}\Big(\int_{S^2} \boldsymbol{p} \cdot \overline{\Big(F_{q_2} - F_{q_1} - \frac{\mathrm{i}k}{8\pi^2} F^*_{q_1} F_{q_2} \Big) \boldsymbol{p}} \, \mathrm{d}s \Big) \\
&= \operatorname{Re}\Big(\int_{S^2} (\boldsymbol{p} \cdot \overline{F_{q_2} \boldsymbol{p}} - \overline{\boldsymbol{p}} \cdot F_{q_1} \boldsymbol{p}) \, \mathrm{d}s + \frac{\mathrm{i}k}{8\pi^2} \int_{S^2} F_{q_1} \boldsymbol{p} \cdot \overline{F_{q_2} \boldsymbol{p}} \, \mathrm{d}s \Big) \, .
\end{aligned} \tag{3.33}$$

Since F_{q_1} and F_{q_2} are compact, the operator $\mathcal{S}^*_{q_1}(F_{q_2} - F_{q_1})$ is compact as well. Utilizing (3.19) once more together with the unitarity of the scattering operator, we calculate

$$\begin{aligned}
\mathcal{S}^*_{q_1}(F_{q_2} - F_{q_1})(F^*_{q_2} - F^*_{q_1}) \mathcal{S}_{q_1} &= -\frac{(8\pi^2)^2}{k^2} \mathcal{S}^*_{q_1}(\mathcal{S}_{q_2} - \mathcal{S}_{q_1})(\mathcal{S}^*_{q_2} - \mathcal{S}^*_{q_1}) \mathcal{S}_{q_1} \\
&= -\frac{(8\pi^2)^2}{k^2}(2I - \mathcal{S}^*_{q_1} \mathcal{S}_{q_2} - \mathcal{S}^*_{q_2} \mathcal{S}_{q_1}) = -\frac{(8\pi^2)^2}{k^2}(\mathcal{S}^*_{q_2} - \mathcal{S}^*_{q_1})(\mathcal{S}_{q_2} - \mathcal{S}_{q_1}) \\
&= (F^*_{q_2} - F^*_{q_1}) \mathcal{S}_{q_1} \mathcal{S}^*_{q_1}(F_{q_2} - F_{q_1}) \, .
\end{aligned}$$

Consequently, we find that $\mathcal{S}^*_{q_1}(F_{q_2} - F_{q_1})$ is normal.

Taking (3.33) as a starting point, we show an integral identity for the left-hand side of (3.22).

Lemma 3.12. *Let $D_1, D_2 \subset\subset B_R(0)$ be open and Lipschitz bounded, and let $q_1 \in \mathcal{Y}_{D_1}$ and $q_2 \in \mathcal{Y}_{D_2}$. Then, for any $\boldsymbol{p} \in L^2_t(S^2, \mathbb{C}^3)$,*

$$\begin{aligned}
&\int_{S^2} (\boldsymbol{p} \cdot \overline{F_{q_2} \boldsymbol{p}} - \overline{\boldsymbol{p}} \cdot F_{q_1} \boldsymbol{p}) \, \mathrm{d}s + \frac{\mathrm{i}k}{8\pi^2} \int_{S^2} F_{q_1} \boldsymbol{p} \cdot \overline{F_{q_2} \boldsymbol{p}} \, \mathrm{d}s + \int_{B_R(0)} (q_1 - q_2) |\operatorname{\mathbf{curl}} \boldsymbol{H}_{q_1,\boldsymbol{p}}|^2 \, \mathrm{d}\boldsymbol{x} \\
&= \int_{B_R(0)} (\varepsilon^{-1}_{r,2} |\operatorname{\mathbf{curl}}(\boldsymbol{H}^s_{q_2,\boldsymbol{p}} - \boldsymbol{H}^s_{q_1,\boldsymbol{p}})|^2 - k^2 |\boldsymbol{H}^s_{q_2,\boldsymbol{p}} - \boldsymbol{H}^s_{q_1,\boldsymbol{p}}|^2) \, \mathrm{d}\boldsymbol{x} \\
&\quad + \int_{\partial B_R(0)} \overline{(\boldsymbol{H}^s_{q_2,\boldsymbol{p}} - \boldsymbol{H}^s_{q_1,\boldsymbol{p}})} \cdot (\boldsymbol{\nu} \times \operatorname{\mathbf{curl}}(\boldsymbol{H}^s_{q_2,\boldsymbol{p}} - \boldsymbol{H}^s_{q_1,\boldsymbol{p}})) \, \mathrm{d}s \, .
\end{aligned} \tag{3.34}$$

Proof. Let $\boldsymbol{p} \in L_t^2(S^2, \mathbb{C}^3)$. Using (3.26) with $j = 1$ and $l = 2$ we find that

$$\int_{\partial B_R(0)} \Big(\overline{\boldsymbol{H}^s_{q_1,\boldsymbol{p}}} \cdot (\boldsymbol{\nu} \times \mathbf{curl}\, \boldsymbol{H}^s_{q_2,\boldsymbol{p}}) + \overline{\boldsymbol{H}^s_{q_2,\boldsymbol{p}}} \cdot (\boldsymbol{\nu} \times \mathbf{curl}\, \boldsymbol{H}^s_{q_1,\boldsymbol{p}}) \Big)\, \mathrm{d}s + \frac{\mathrm{i}k}{8\pi^2} \int_{S^2} F_{q_1}\boldsymbol{p} \cdot \overline{F_{q_2}\boldsymbol{p}}\, \mathrm{d}s$$
$$= 2\,\mathrm{Re}\Big(\int_{\partial B_R(0)} \overline{\boldsymbol{H}^s_{q_1,\boldsymbol{p}}} \cdot (\boldsymbol{\nu} \times \mathbf{curl}\, \boldsymbol{H}^s_{q_2,\boldsymbol{p}})\, \mathrm{d}s \Big).$$

Therewith, we deduce that

$$\begin{aligned}
&\int_{B_R(0)} \big(\varepsilon_{r,2}^{-1} |\,\mathbf{curl}(\boldsymbol{H}^s_{q_2,\boldsymbol{p}} - \boldsymbol{H}^s_{q_1,\boldsymbol{p}})|^2 - k^2 |\boldsymbol{H}^s_{q_2,\boldsymbol{p}} - \boldsymbol{H}^s_{q_1,\boldsymbol{p}}|^2\big)\, \mathrm{d}\boldsymbol{x} \\
&\quad + \int_{\partial B_R(0)} \overline{(\boldsymbol{H}^s_{q_2,\boldsymbol{p}} - \boldsymbol{H}^s_{q_1,\boldsymbol{p}})} \cdot (\boldsymbol{\nu} \times \mathbf{curl}(\boldsymbol{H}^s_{q_2,\boldsymbol{p}} - \boldsymbol{H}^s_{q_1,\boldsymbol{p}}))\, \mathrm{d}s \\
&= \int_{B_R(0)} \big(\varepsilon_{r,2}^{-1} |\,\mathbf{curl}\, \boldsymbol{H}^s_{q_2,\boldsymbol{p}}|^2 - k^2 |\boldsymbol{H}^s_{q_2,\boldsymbol{p}}|^2\big)\, \mathrm{d}\boldsymbol{x} + \int_{B_R(0)} \big(\varepsilon_{r,2}^{-1} |\,\mathbf{curl}\, \boldsymbol{H}^s_{q_1,\boldsymbol{p}}|^2 - k^2 |\boldsymbol{H}^s_{q_1,\boldsymbol{p}}|^2\big)\, \mathrm{d}\boldsymbol{x} \\
&\quad - 2\,\mathrm{Re}\Big(\int_{B_R(0)} \Big(\varepsilon_{r,2}^{-1}\, \mathbf{curl}\, \boldsymbol{H}^s_{q_2,\boldsymbol{p}} \cdot \overline{\mathbf{curl}\, \boldsymbol{H}^s_{q_1,\boldsymbol{p}}} - k^2 \boldsymbol{H}^s_{q_2,\boldsymbol{p}} \cdot \overline{\boldsymbol{H}^s_{q_1,\boldsymbol{p}}} \Big)\, \mathrm{d}\boldsymbol{x} \\
&\qquad\quad + \int_{\partial B_R(0)} \overline{\boldsymbol{H}^s_{q_1,\boldsymbol{p}}} \cdot (\boldsymbol{\nu} \times \mathbf{curl}\, \boldsymbol{H}^s_{q_2,\boldsymbol{p}})\, \mathrm{d}s \Big) \\
&\quad + \int_{\partial B_R(0)} \Big(\overline{\boldsymbol{H}^s_{q_2,\boldsymbol{p}}} \cdot (\boldsymbol{\nu} \times \mathbf{curl}\, \boldsymbol{H}^s_{q_2,\boldsymbol{p}}) + \overline{\boldsymbol{H}^s_{q_1,\boldsymbol{p}}} \cdot (\boldsymbol{\nu} \times \mathbf{curl}\, \boldsymbol{H}^s_{q_1,\boldsymbol{p}}) \Big)\, \mathrm{d}s \\
&\quad + \frac{\mathrm{i}k}{8\pi^2} \int_{S^2} F_{q_1}\boldsymbol{p} \cdot \overline{F_{q_2}\boldsymbol{p}}\, \mathrm{d}s\,.
\end{aligned}$$

Applying (3.25) three times gives

$$\begin{aligned}
&\int_{B_R(0)} \big(\varepsilon_{r,2}^{-1} |\,\mathbf{curl}(\boldsymbol{H}^s_{q_2,\boldsymbol{p}} - \boldsymbol{H}^s_{q_1,\boldsymbol{p}})|^2 - k^2 |\boldsymbol{H}^s_{q_2,\boldsymbol{p}} - \boldsymbol{H}^s_{q_1,\boldsymbol{p}}|^2\big)\, \mathrm{d}\boldsymbol{x} \\
&\quad + \int_{\partial B_R(0)} \overline{(\boldsymbol{H}^s_{q_2,\boldsymbol{p}} - \boldsymbol{H}^s_{q_1,\boldsymbol{p}})} \cdot (\boldsymbol{\nu} \times \mathbf{curl}(\boldsymbol{H}^s_{q_2,\boldsymbol{p}} - \boldsymbol{H}^s_{q_1,\boldsymbol{p}}))\, \mathrm{d}s \\
&= \int_{B_R(0)} q_2\, \mathbf{curl}\, \boldsymbol{H}^i_{\boldsymbol{p}} \cdot \overline{\mathbf{curl}\, \boldsymbol{H}^s_{q_2,\boldsymbol{p}}}\, \mathrm{d}\boldsymbol{x} + \int_{B_R(0)} q_1\, \mathbf{curl}\, \boldsymbol{H}^i_{\boldsymbol{p}} \cdot \overline{\mathbf{curl}\, \boldsymbol{H}^s_{q_1,\boldsymbol{p}}}\, \mathrm{d}\boldsymbol{x} \\
&\quad + \int_{B_R(0)} (q_1 - q_2) |\,\mathbf{curl}\, \boldsymbol{H}^s_{q_1,\boldsymbol{p}}|^2\, \mathrm{d}\boldsymbol{x} - 2\,\mathrm{Re}\Big(\int_{B_R(0)} q_2\, \mathbf{curl}\, \boldsymbol{H}^i_{\boldsymbol{p}} \cdot \overline{\mathbf{curl}\, \boldsymbol{H}^s_{q_1,\boldsymbol{p}}}\, \mathrm{d}\boldsymbol{x} \Big) \\
&\quad + \frac{\mathrm{i}k}{8\pi^2} \int_{S^2} F_{q_1}\boldsymbol{p} \cdot \overline{F_{q_2}\boldsymbol{p}}\, \mathrm{d}s\,.
\end{aligned}$$

Furthermore,

$$\begin{aligned}
&\int_{B_R(0)} \big(\varepsilon_{r,2}^{-1} |\,\mathbf{curl}(\boldsymbol{H}^s_{q_2,\boldsymbol{p}} - \boldsymbol{H}^s_{q_1,\boldsymbol{p}})|^2 - k^2 |\boldsymbol{H}^s_{q_2,\boldsymbol{p}} - \boldsymbol{H}^s_{q_1,\boldsymbol{p}}|^2\big)\, \mathrm{d}\boldsymbol{x} \\
&\quad + \int_{\partial B_R(0)} \overline{(\boldsymbol{H}^s_{q_2,\boldsymbol{p}} - \boldsymbol{H}^s_{q_1,\boldsymbol{p}})} \cdot (\boldsymbol{\nu} \times \mathbf{curl}(\boldsymbol{H}^s_{q_2,\boldsymbol{p}} - \boldsymbol{H}^s_{q_1,\boldsymbol{p}}))\, \mathrm{d}s
\end{aligned}$$

$$
\begin{aligned}
&= \int_{B_R(0)} q_2 \operatorname{\mathbf{curl}} \boldsymbol{H}^i_{\boldsymbol{p}} \cdot \overline{\operatorname{\mathbf{curl}} \boldsymbol{H}^s_{q_2,\boldsymbol{p}}} \,\mathrm{d}\boldsymbol{x} + 2\,\mathrm{Re}\Big(\int_{B_R(0)} (q_1 - q_2) \operatorname{\mathbf{curl}} \boldsymbol{H}^i_{\boldsymbol{p}} \cdot \overline{\operatorname{\mathbf{curl}} \boldsymbol{H}^s_{q_1,\boldsymbol{p}}} \,\mathrm{d}\boldsymbol{x}\Big) \\
&\quad - \int_{B_R(0)} q_1 \overline{\operatorname{\mathbf{curl}} \boldsymbol{H}^i_{\boldsymbol{p}}} \cdot \operatorname{\mathbf{curl}} \boldsymbol{H}^s_{q_1,\boldsymbol{p}} \,\mathrm{d}\boldsymbol{x} + \int_{B_R(0)} (q_1 - q_2) |\operatorname{\mathbf{curl}} \boldsymbol{H}^s_{q_1,\boldsymbol{p}}|^2 \,\mathrm{d}\boldsymbol{x} \\
&\quad + \frac{\mathrm{i}k}{8\pi^2} \int_{S^2} F_{q_1} \boldsymbol{p} \cdot \overline{F_{q_2} \boldsymbol{p}} \,\mathrm{d}s \\
&= \int_{B_R(0)} q_2 \operatorname{\mathbf{curl}} \boldsymbol{H}^i_{\boldsymbol{p}} \cdot \overline{\operatorname{\mathbf{curl}} \boldsymbol{H}_{q_2,\boldsymbol{p}}} \,\mathrm{d}\boldsymbol{x} - \int_{B_R(0)} q_1 \overline{\operatorname{\mathbf{curl}} \boldsymbol{H}^i_{\boldsymbol{p}}} \cdot \operatorname{\mathbf{curl}} \boldsymbol{H}_{q_1,\boldsymbol{p}} \,\mathrm{d}\boldsymbol{x} \\
&\quad + \int_{B_R(0)} (q_1 - q_2) |\operatorname{\mathbf{curl}} \boldsymbol{H}_{q_1,\boldsymbol{p}}|^2 \,\mathrm{d}\boldsymbol{x} + \frac{\mathrm{i}k}{8\pi^2} \int_{S^2} F_{q_1} \boldsymbol{p} \cdot \overline{F_{q_2} \boldsymbol{p}} \,\mathrm{d}s\,.
\end{aligned}
$$

Finally, we use the identity (3.24) to obtain

$$
\begin{aligned}
&\int_{B_R(0)} \big(\varepsilon_{r,2}^{-1} |\operatorname{\mathbf{curl}}(\boldsymbol{H}^s_{q_2,\boldsymbol{p}} - \boldsymbol{H}^s_{q_1,\boldsymbol{p}})|^2 - k^2 |\boldsymbol{H}^s_{q_2,\boldsymbol{p}} - \boldsymbol{H}^s_{q_1,\boldsymbol{p}}|^2\big) \,\mathrm{d}\boldsymbol{x} \\
&\quad + \int_{\partial B_R(0)} \overline{(\boldsymbol{H}^s_{q_2,\boldsymbol{p}} - \boldsymbol{H}^s_{q_1,\boldsymbol{p}})} \cdot \big(\boldsymbol{\nu} \times \operatorname{\mathbf{curl}}(\boldsymbol{H}^s_{q_2,\boldsymbol{p}} - \boldsymbol{H}^s_{q_1,\boldsymbol{p}})\big) \,\mathrm{d}s \\
&= \int_{S^2} \big(\boldsymbol{p} \cdot \overline{F_{q_2} \boldsymbol{p}} - \overline{\boldsymbol{p}} \cdot F_{q_1} \boldsymbol{p}\big) \,\mathrm{d}s + \int_{B_R(0)} (q_1 - q_2) |\operatorname{\mathbf{curl}} \boldsymbol{H}_{q_1,\boldsymbol{p}}|^2 \,\mathrm{d}\boldsymbol{x} \\
&\quad + \frac{\mathrm{i}k}{8\pi^2} \int_{S^2} F_{q_1} \boldsymbol{p} \cdot \overline{F_{q_2} \boldsymbol{p}} \,\mathrm{d}s\,.
\end{aligned}
$$

□

Next, we show that the right-hand side of (3.34) is nonnegative if the density $\boldsymbol{p} \in L^2_t(S^2, \mathbb{C}^3)$ belongs to the complement of a certain finite-dimensional subspace $V \subseteq L^2_t(S^2, \mathbb{C}^3)$. We recall the definition (3.17) of the exterior Calderon operator and define the space

$$
\begin{aligned}
\mathcal{X} := \Big\{ \boldsymbol{v} \in H(\operatorname{\mathbf{curl}}; B_R(0)) \;\Big|\; &\operatorname{div} \boldsymbol{v} = 0 \text{ in } B_R(0) \\
&\text{and } \boldsymbol{\nu} \cdot \boldsymbol{v}|_{\partial B_R(0)} = k^{-2} \operatorname{Curl}_{\partial B_R(0)}\big(\Lambda(\boldsymbol{\nu} \times \boldsymbol{v}|_{\partial B_R(0)})\big) \Big\}
\end{aligned}
$$

equipped with the inner product $\langle \cdot, \cdot \rangle_{\mathcal{X}} := \langle \cdot, \cdot \rangle_{H(\operatorname{\mathbf{curl}}; B_R(0))}$. Then, $(\mathcal{X}, \|\cdot\|_{\mathcal{X}})$ is a Hilbert space (see, e.g., [Mon03, Lem. 10.3]) and the embedding operator $\mathcal{J} : \mathcal{X} \hookrightarrow L^2(B_R(0), \mathbb{C}^3)$ is compact (see, e.g., [Mon03, Lem. 10.4]). At this point, one has to remember that the Calderon operator introduced in (3.17) possesses an additional $\times\boldsymbol{\nu}$ when compared to the Calderon operator in [Mon03].

From (3.27) it follows for $j \in \{1, 2\}$ that

$$
\boldsymbol{H}^s_{q_j,\boldsymbol{p}} = -k^{-2}\Big(\operatorname{\mathbf{curl}}(q_j \operatorname{\mathbf{curl}} \boldsymbol{H}^i_{\boldsymbol{p}}) - \operatorname{\mathbf{curl}}(\varepsilon_{r,j}^{-1} \operatorname{\mathbf{curl}} \boldsymbol{H}^s_{q_j,\boldsymbol{p}})\Big) \qquad \text{in } \mathbb{R}^3\,.
$$

Thus, utilizing (B.2) we see that $\operatorname{div}(\boldsymbol{H}^s_{q_2,\boldsymbol{p}} - \boldsymbol{H}^s_{q_1,\boldsymbol{p}}) = 0$ in $\mathbb{R}^3$. Since it is $\varepsilon_{r,j} \equiv 1$ on the boundary $\partial B_R(0)$, using (B.5) we obtain from (3.11b) that

$$
\begin{aligned}
\boldsymbol{\nu} \cdot (\boldsymbol{H}^s_{q_2,\boldsymbol{p}} - \boldsymbol{H}^s_{q_1,\boldsymbol{p}})\big|_{\partial B_R(0)} &= k^{-2} \boldsymbol{\nu} \cdot \operatorname{\mathbf{curl}} \operatorname{\mathbf{curl}} (\boldsymbol{H}^s_{q_2,\boldsymbol{p}} - \boldsymbol{H}^s_{q_1,\boldsymbol{p}})\big|_{\partial B_R(0)} \\
&= k^{-2} \operatorname{Curl}_{\partial B_R(0)}\big((\boldsymbol{\nu} \times \operatorname{\mathbf{curl}}(\boldsymbol{H}^s_{q_2,\boldsymbol{p}} - \boldsymbol{H}^s_{q_1,\boldsymbol{p}})\big|_{\partial B_R(0)}) \times \boldsymbol{\nu}\big) \\
&= k^{-2} \operatorname{Curl}_{\partial B_R(0)}\big(\Lambda(\boldsymbol{\nu} \times (\boldsymbol{H}^s_{q_2,\boldsymbol{p}} - \boldsymbol{H}^s_{q_1,\boldsymbol{p}})\big|_{\partial B_R(0)})\big)\,.
\end{aligned}
$$

Altogether, we find that $\boldsymbol{H}^s_{q_2,\boldsymbol{p}} - \boldsymbol{H}^s_{q_1,\boldsymbol{p}} \in \mathcal{X}$.

Let $D \subset\subset B_R(0)$ open and Lipschitz bounded, and let $q \in \mathcal{Y}_D$. We define the sesquilinear form $A : \mathcal{X} \times \mathcal{X} \to \mathbb{C}$ by

$$A(\boldsymbol{u}, \boldsymbol{v}) := \int_{B_R(0)} \varepsilon_r^{-1} (\mathbf{curl}\, \boldsymbol{u} \cdot \overline{\mathbf{curl}\, \boldsymbol{v}} + \boldsymbol{u} \cdot \overline{\boldsymbol{v}}) \, \mathrm{d}\boldsymbol{x} \qquad \text{for all } \boldsymbol{u}, \boldsymbol{v} \in \mathcal{X}\,.$$

Applying the Cauchy-Schwarz inequality gives

$$\begin{aligned} |A(\boldsymbol{u}, \boldsymbol{v})| &\leq \|\varepsilon_r^{-1}\|_{L^\infty(\mathbb{R}^3)} \Big| \int_{B_R(0)} (\mathbf{curl}\, \boldsymbol{u} \cdot \overline{\mathbf{curl}\, \boldsymbol{v}} + \boldsymbol{u} \cdot \overline{\boldsymbol{v}}) \, \mathrm{d}\boldsymbol{x} \Big| \\ &= \|\varepsilon_r^{-1}\|_{L^\infty(\mathbb{R}^3)} |\langle \boldsymbol{u}, \boldsymbol{v} \rangle_{\mathcal{X}}| \leq \|\varepsilon_r^{-1}\|_{L^\infty(\mathbb{R}^3)} \|\boldsymbol{u}\|_{\mathcal{X}} \|\boldsymbol{v}\|_{\mathcal{X}}\,, \end{aligned}$$

and we have

$$\operatorname{Re} A(\boldsymbol{v}, \boldsymbol{v}) = \int_{B_R(0)} (1 - q)(|\,\mathbf{curl}\, \boldsymbol{v}|^2 + |\boldsymbol{v}|^2) \, \mathrm{d}\boldsymbol{x} \geq \operatorname{ess\,inf}(1 - q) \|\boldsymbol{v}\|^2_{\mathcal{X}}$$

for all $\boldsymbol{u}, \boldsymbol{v} \in \mathcal{X}$. Recalling the definition (3.6) of $\mathcal{Y}_D$, we can employ the Lax-Milgram lemma (see, e.g., [Lax02, p. 57]) to get the existence of a bounded linear self-adjoint operator $I_q : \mathcal{X} \to \mathcal{X}$ with bounded inverse that satisfies

$$\langle I_q \boldsymbol{u}, \boldsymbol{v} \rangle_{\mathcal{X}} = A(\boldsymbol{u}, \boldsymbol{v}) = \int_{B_R(0)} \varepsilon_r^{-1} (\mathbf{curl}\, \boldsymbol{u} \cdot \overline{\mathbf{curl}\, \boldsymbol{v}} + \boldsymbol{u} \cdot \overline{\boldsymbol{v}}) \, \mathrm{d}\boldsymbol{x} \qquad \text{for all } \boldsymbol{u}, \boldsymbol{v} \in \mathcal{X}\,.$$

Furthermore, let $K : \mathcal{X} \to \mathcal{X}$ and $K_q : \mathcal{X} \to \mathcal{X}$ be given by

$$K\boldsymbol{v} := \mathcal{J}^* \mathcal{J} \boldsymbol{v} \qquad \text{and} \qquad K_q \boldsymbol{v} := \mathcal{J}^* (\varepsilon_r^{-1} \mathcal{J} \boldsymbol{v})\,,$$

respectively, where $\mathcal{J} : \mathcal{X} \hookrightarrow L^2(B_R(0), \mathbb{C}^3)$ is the compact embedding operator. Then, K and K_q are compact self-adjoint linear operators, and for any $\boldsymbol{v} \in \mathcal{X}$,

$$\big\langle (I_q - K_q - k^2 K) \boldsymbol{v}, \boldsymbol{v} \big\rangle_{\mathcal{X}} = \int_{B_R(0)} (\varepsilon_r^{-1} |\,\mathbf{curl}\, \boldsymbol{v}|^2 - k^2 |\boldsymbol{v}|^2) \, \mathrm{d}\boldsymbol{x}\,. \tag{3.35}$$

For $0 < \varepsilon < R$ we denote by $N_\varepsilon : \mathcal{X} \to H^{-1/2}(\mathrm{Curl}; \partial B_R(0))$ the linear operator that maps $\boldsymbol{v} \in \mathcal{X}$ to the projection on the tangent plane $(\boldsymbol{\nu} \times \mathbf{curl}\, \boldsymbol{v}_\varepsilon|_{\partial B_R(0)}) \times \boldsymbol{\nu}$, where $\boldsymbol{v}_\varepsilon$ is the unique radiating solution to the exterior boundary value problem

$$\mathbf{curl}\,\mathbf{curl}\, \boldsymbol{v}_\varepsilon - k^2 \boldsymbol{v}_\varepsilon = 0 \quad \text{in } \mathbb{R}^3 \setminus \overline{B_{R-\varepsilon}(0)}\,, \qquad \boldsymbol{\nu} \times \boldsymbol{v}_\varepsilon = \boldsymbol{\nu} \times \boldsymbol{v} \quad \text{on } \partial B_{R-\varepsilon}(0)\,. \tag{3.36}$$

Since Remark 3.1 implies that $\boldsymbol{v}_\varepsilon$ is smooth away from the boundary $\partial B_{R-\varepsilon}(0)$, this operator is compact. Given any $\boldsymbol{v} \in \mathcal{X}$ that can be extended to a radiating solution to Maxwell's equations

$$\mathbf{curl}\,\mathbf{curl}\, \boldsymbol{v} - k^2 \boldsymbol{v} = 0 \quad \text{in } \mathbb{R}^3 \setminus \overline{B_{R-\varepsilon}(0)}\,,$$

we find that

$$N_\varepsilon \boldsymbol{v} = (\boldsymbol{\nu} \times \mathbf{curl}\, \boldsymbol{v}|_{\partial B_R(0)}) \times \boldsymbol{\nu} \qquad \text{and} \qquad \Lambda^{-1} N_\varepsilon \boldsymbol{v} = \boldsymbol{\nu} \times \boldsymbol{v}|_{\partial B_R(0)}\,,$$

since solutions to the exterior boundary value problem (3.36) are unique. Accordingly,

$$\begin{aligned}\langle N_\varepsilon^* \Lambda^{-1} N_\varepsilon \boldsymbol{v}, \boldsymbol{v} \rangle_{\mathcal{X}} &= \int_{\partial B_R(0)} \Lambda^{-1} N_\varepsilon \boldsymbol{v} \cdot N_\varepsilon \boldsymbol{v} \, \mathrm{d}s \\ &= \int_{\partial B_R(0)} (\boldsymbol{\nu} \times \boldsymbol{v}) \cdot ((\boldsymbol{\nu} \times \overline{\mathbf{curl}\, \boldsymbol{v}}) \times \boldsymbol{\nu}) \, \mathrm{d}s \\ &= -\int_{\partial B_R(0)} (\boldsymbol{\nu} \times \overline{\mathbf{curl}\, \boldsymbol{v}}) \cdot \boldsymbol{v} \, \mathrm{d}s \,, \end{aligned} \tag{3.37}$$

and in particular, this holds for $\boldsymbol{v} = \boldsymbol{H}^s_{q_2,\boldsymbol{p}} - \boldsymbol{H}^s_{q_1,\boldsymbol{p}}$ if $D_1, D_2 \subset\subset B_R(0)$.

We summarize our previous considerations in the next lemma.

Lemma 3.13. *Let $D_1, D_2 \subset\subset B_R(0)$ be open and Lipschitz bounded, and let $q_1 \in \mathcal{Y}_{D_1}$ and $q_2 \in \mathcal{Y}_{D_2}$. Then, there exists a finite-dimensional subspace $V \subseteq L^2_t(S^2, \mathbb{C}^3)$ such that*

$$\begin{aligned}&\int_{B_R(0)} \Big(\varepsilon_{r,2}^{-1} |\, \mathbf{curl}(\boldsymbol{H}^s_{q_2,\boldsymbol{p}} - \boldsymbol{H}^s_{q_1,\boldsymbol{p}})|^2 - k^2 |\boldsymbol{H}^s_{q_2,\boldsymbol{p}} - \boldsymbol{H}^s_{q_1,\boldsymbol{p}}|^2 \Big) \, \mathrm{d}\boldsymbol{x} \\ &+ \mathrm{Re}\Big(\int_{\partial B_R(0)} \overline{(\boldsymbol{H}^s_{q_2,\boldsymbol{p}} - \boldsymbol{H}^s_{q_1,\boldsymbol{p}})} \cdot (\boldsymbol{\nu} \times \mathbf{curl}(\boldsymbol{H}^s_{q_2,\boldsymbol{p}} - \boldsymbol{H}^s_{q_1,\boldsymbol{p}})) \times \boldsymbol{\nu} \, \mathrm{d}s \Big) \geq 0 \qquad \text{for all } \boldsymbol{p} \in V^\perp \,. \end{aligned}$$

Proof. Let $q_1 \in \mathcal{Y}_{D_1}$ and $q_2 \in \mathcal{Y}_{D_2}$ for some $D_1, D_2 \subset\subset B_R(0)$ that are open and Lipschitz bounded, and let $\varepsilon > 0$ be sufficiently small, so that $\overline{D_1 \cup D_2} \subset B_{R-\varepsilon}(0)$. Then, combining (3.35) and (3.37) we see that

$$\begin{aligned}&\int_{B_R(0)} \Big(\varepsilon_{r,2}^{-1} |\, \mathbf{curl}(\boldsymbol{H}^s_{q_2,\boldsymbol{p}} - \boldsymbol{H}^s_{q_1,\boldsymbol{p}})|^2 - k^2 |\boldsymbol{H}^s_{q_2,\boldsymbol{p}} - \boldsymbol{H}^s_{q_1,\boldsymbol{p}}|^2 \Big) \, \mathrm{d}\boldsymbol{x} \\ &\quad + \mathrm{Re}\Big(\int_{\partial B_R(0)} \overline{(\boldsymbol{H}^s_{q_2,\boldsymbol{p}} - \boldsymbol{H}^s_{q_1,\boldsymbol{p}})} \cdot (\boldsymbol{\nu} \times \mathbf{curl}(\boldsymbol{H}^s_{q_2,\boldsymbol{p}} - \boldsymbol{H}^s_{q_1,\boldsymbol{p}}) \, \mathrm{d}s \Big) \\ &= \big\langle (I_{q_2} - K_{q_2} - k^2 K - \mathrm{Re}(N_\varepsilon^* \Lambda^{-1} N_\varepsilon))(A_2 - A_1)\boldsymbol{p}, (A_2 - A_1)\boldsymbol{p} \big\rangle_{\mathcal{X}} \,, \end{aligned}$$

where, for $j = 1, 2$, we denote by $A_j : L^2_t(S^2, \mathbb{C}^3) \to \mathcal{X}$ the bounded linear operator that maps densities $\boldsymbol{p} \in L^2_t(S^2, \mathbb{C}^3)$ to the restriction of the corresponding scattered magnetic field $\boldsymbol{H}^s_{q_j,\boldsymbol{p}}$ to $B_R(0)$.

Furthermore, we denote by $W \subseteq \mathcal{X}$ the sum of eigenspaces of the compact self-adjoint operator $K_{q_2} + k^2 K + \mathrm{Re}(N_\varepsilon^* \Lambda^{-1} N_\varepsilon)$ associated to eigenvalues larger than

$$c_{\min} := \operatorname*{ess\,inf}_{\boldsymbol{x} \in B_R(0)} \varepsilon_{r,2}^{-1}(\boldsymbol{x}) > 0 \,.$$

From the spectral theorem for compact self-adjoint operators (see Remark 2.1) it follows that the subspace W is finite dimensional. Moreover, using the min-max theorem (see, e.g., [Lax02, p. 318]) we find for all $\boldsymbol{w} \in W^\perp$ that

$$\big\langle (I_{q_2} - K_{q_2} - k^2 K - \mathrm{Re}(N_\varepsilon^* \Lambda^{-1} N_\varepsilon))\boldsymbol{w}, \boldsymbol{w} \big\rangle_{\mathcal{X}} \geq \int_{B_R(0)} (\varepsilon_{r,2}^{-1} - c_{\min})(|\, \mathbf{curl}\, \boldsymbol{w}|^2 + |\boldsymbol{w}|^2) \, \mathrm{d}\boldsymbol{x} \geq 0$$

because $q_2 = 1 - \varepsilon_{r,2}^{-1} \in \mathcal{Y}_{D_2}$. Besides, we observe that, for any $\boldsymbol{p} \in L_t^2(S^2, \mathbb{C}^3)$,

$$(A_2 - A_1)\boldsymbol{p} \in W^\perp \qquad \text{if and only if} \qquad \boldsymbol{p} \in \left((A_2 - A_1)^* W\right)^\perp .$$

Since $\dim((A_2 - A_1)^* W) \leq \dim(W) < \infty$, choosing $V := (A_2 - A_1)^* W \subseteq L_t^2(S^2, \mathbb{C}^3)$ ends the proof. □

Proof of Theorem 3.8. We take the real part of (3.34) and use (3.33). Then, Lemma 3.13 yields the result. □

An immediate consequence of Theorem 3.8 and Corollary 3.10 are the following properties concerning the number of positive or negative eigenvalues of the far field operator F_q.

Corollary 3.14. *Let $D \subseteq \mathbb{R}^3$ be open and Lipschitz bounded, and let $q \in \mathcal{Y}_D$.*

(a) If $-\infty < q \leq q_{\max} < 0$ for some constant $q_{\max} \in \mathbb{R}$, then $\operatorname{Re}(F_q) \leq_{\text{fin}} 0$.

(b) If $0 < q_{\min} \leq q < 1$ for some constant $q_{\min} \in \mathbb{R}$, then $\operatorname{Re}(F_q) \geq_{\text{fin}} 0$.

Proof. (a) We set $q_1 = 0$ and $q_2 = q$ in Corollary 3.10 and obtain the existence of a finite-dimensional subspace $V \subseteq L_t^2(S^2, \mathbb{C}^3)$ such that

$$\operatorname{Re}\Big(\int_{S^2} \boldsymbol{p} \cdot \overline{F_q \boldsymbol{p}} \, \mathrm{d}s\Big) \leq \int_D q \, |\operatorname{\mathbf{curl}} \boldsymbol{H}_{q,\boldsymbol{p}}|^2 \, \mathrm{d}\boldsymbol{x} \leq q_{\max} \int_D |\operatorname{\mathbf{curl}} \boldsymbol{H}_{q,\boldsymbol{p}}|^2 \, \mathrm{d}\boldsymbol{x} \leq 0$$

for all $\boldsymbol{p} \in V^\perp$. Thus, the assertion follows from Lemma 2.2.

(b) We set $q_1 = 0$ and $q_2 = q$ in Theorem 3.8 and deduce that there exists a finite-dimensional subspace $V \subseteq L_t^2(S^2, \mathbb{C}^3)$ such that

$$\operatorname{Re}\Big(\int_{S^2} \boldsymbol{p} \cdot \overline{F_q \boldsymbol{p}} \, \mathrm{d}s\Big) \geq \int_D q \, |\operatorname{\mathbf{curl}} \boldsymbol{H}^i_{\boldsymbol{p}}|^2 \, \mathrm{d}\boldsymbol{x} \geq q_{\min} \int_D |\operatorname{\mathbf{curl}} \boldsymbol{H}^i_{\boldsymbol{p}}|^2 \, \mathrm{d}\boldsymbol{x} \geq 0$$

for all $\boldsymbol{p} \in V^\perp$. Applying Lemma 2.2 yields the assertion. □

3.4. Sign-Definite Scattering Objects

We aim to establish criteria to determine the shape and position of a scatterer D with permittivity contrast q in terms of the magnetic far field operator F_q. In this section, we focus on scatterers with either strictly negative or strictly positive contrast on D. The general case will be treated in Section 3.5.2. We present a rigorous shape characterization result for sign-definite scattering objects in Subsection 3.4.2 below. To this end, we utilize the already derived monotonicity relation for the far field operator on the one hand, and we make use of localized vector wave functions that we introduce in the following subsection on the other.

3.4.1. Localized Vector Wave Functions

We show the existence of *localized vector wave functions*, which are solutions to the scattering problem (3.11) that have arbitrarily large energy in some prescribed region and arbitrarily small energy in another prescribed region. Recalling the localized wave functions introduced in Subsection 2.3.2 when studying the acoustic obstacle scattering problem, these can be interpreted as the analog for the electromagnetic medium scattering problem. In [HLL18], the authors established related results for solutions to Maxwell's equations on bounded domains. We extend this concept to unbounded domains.

Theorem 3.15 (Localized Vector Wave Functions)**.** *Suppose that $D \subseteq \mathbb{R}^3$ is open and Lipschitz bounded, let $q \in \mathcal{Y}_D$, and let $B, \Omega \subseteq \mathbb{R}^3$ be open and bounded such that $\mathbb{R}^3 \setminus \overline{\Omega}$ is connected.*

If $B \not\subseteq \Omega$, then for any finite-dimensional subspace $V \subseteq L_t^2(S^2, \mathbb{C}^3)$ there exists a sequence $(\boldsymbol{p}_m)_{m\in\mathbb{N}} \subseteq V^\perp$ such that

$$\int_B |\operatorname{\mathbf{curl}} \boldsymbol{H}_{q,\boldsymbol{p}_m}|^2 \,\mathrm{d}\boldsymbol{x} \to \infty \quad \text{and} \quad \int_\Omega |\operatorname{\mathbf{curl}} \boldsymbol{H}_{q,\boldsymbol{p}_m}|^2 \,\mathrm{d}\boldsymbol{x} \to 0 \quad \text{as } m \to \infty\,, \tag{3.38}$$

where $\boldsymbol{H}_{q,\boldsymbol{p}_m} \in H_{\mathrm{loc}}(\mathbf{curl}; \mathbb{R}^3)$ is given by (3.21a) *with $\boldsymbol{p} = \boldsymbol{p}_m$.*

When establishing the localized wave functions in Subsection 2.3.2, Lemma 2.21 served as an important tool in the proof. In order to be able to apply this lemma in the context of this chapter, we need to identify appropriate operators in a first step and investigate the ranges of their adjoints afterward. Therefore, we begin with defining the operator $L_{q,\Omega}$ that maps $\boldsymbol{p} \in L_t^2(S^2, \mathbb{C}^3)$ to the restriction to Ω of the solution $\boldsymbol{E}_{q,\boldsymbol{p}}$ to the scattering problem (3.10) and computing its adjoint.

Lemma 3.16. *Suppose that $D \subseteq \mathbb{R}^3$ is open and Lipschitz bounded, let $q \in \mathcal{Y}_D$, and assume that $\Omega \subseteq \mathbb{R}^3$ is open and bounded. We define*

$$L_{q,\Omega} : L_t^2(S^2, \mathbb{C}^3) \to L^2(\Omega, \mathbb{C}^3)\,, \quad L_{q,\Omega}\,\boldsymbol{p} := -\frac{1}{\mathrm{i}\omega\varepsilon} \operatorname{\mathbf{curl}} \boldsymbol{H}_{q,\boldsymbol{p}}|_\Omega = \boldsymbol{E}_{q,\boldsymbol{p}}|_\Omega\,. \tag{3.39}$$

Then, $L_{q,\Omega}$ is a compact linear operator and its adjoint is given by

$$L_{q,\Omega}^* : L^2(\Omega, \mathbb{C}^3) \to L_t^2(S^2, \mathbb{C}^3)\,, \quad L_{q,\Omega}^* \boldsymbol{f} := \sqrt{\frac{\mu_0}{\varepsilon_0}} \mathcal{S}_q^*(\boldsymbol{\nu} \times \boldsymbol{e}^\infty)\,,$$

where $\boldsymbol{e}^\infty \in L_t^2(S^2, \mathbb{C}^3)$ is the electric far field pattern of the radiating solution $\boldsymbol{e} \in H_{\mathrm{loc}}(\mathbf{curl}; \mathbb{R}^3)$ to

$$\operatorname{\mathbf{curl}} \operatorname{\mathbf{curl}} \boldsymbol{e} - k^2 \varepsilon_r \boldsymbol{e} = \boldsymbol{f} \qquad \text{in } \mathbb{R}^3\,. \tag{3.40}$$

Proof. The integral representation (3.21a) shows that $L_{q,\Omega}$ is an integral operator with square-integrable kernel and thus a Hilbert-Schmidt operator (see, e.g., [DS63, p. 1009]). Since these operators are known to be compact (see, e.g., [DS63, p. 1012]), this implies the compactness of $L_{q,\Omega}$. The existence of a unique radiating solution $\boldsymbol{e} \in H_{\mathrm{loc}}(\mathbf{curl}; \mathbb{R}^3)$ to (3.40) follows from Remark 3.6.

Let $R > 0$ be sufficiently large such that $\overline{D \cup \Omega} \subseteq B_R(0)$. Utilizing the complex conjugate of

the variational formulation of (3.40) with test function $\overline{\boldsymbol{\psi}} \in H(\mathbf{curl}; B_R(0))$ gives

$$\int_{B_R(0)} (\overline{\mathbf{curl}\, \boldsymbol{e}} \cdot \mathbf{curl}\, \boldsymbol{\psi} - k^2 \varepsilon_r \overline{\boldsymbol{e}} \cdot \boldsymbol{\psi}) \, \mathrm{d}\boldsymbol{x} = \int_{B_R(0)} \overline{\boldsymbol{f}} \cdot \boldsymbol{\psi} \, \mathrm{d}\boldsymbol{x} + \int_{\partial B_R(0)} (\boldsymbol{\nu} \times \boldsymbol{\psi}) \cdot \overline{\mathbf{curl}\, \boldsymbol{e}} \, \mathrm{d}s \,. \quad (3.41)$$

Combining (3.39) with (3.41), using the variational formulation of (3.10b) we obtain that, for any $\boldsymbol{f} \in L^2(\Omega, \mathbb{C}^3)$ and $\boldsymbol{p} \in L_t^2(S^2, \mathbb{C}^3)$,

$$\begin{aligned}
&\int_\Omega (L_{q,\Omega} \boldsymbol{p}) \cdot \overline{\boldsymbol{f}} \, \mathrm{d}\boldsymbol{x} = \int_{B_R(0)} \boldsymbol{E}_{q,\boldsymbol{p}} \cdot \overline{\boldsymbol{f}} \, \mathrm{d}\boldsymbol{x} \\
&= \int_{B_R(0)} (\mathbf{curl}\, \boldsymbol{E}_{q,\boldsymbol{p}} \cdot \overline{\mathbf{curl}\, \boldsymbol{e}} - k^2 \varepsilon_r \boldsymbol{E}_{q,\boldsymbol{p}} \cdot \overline{\boldsymbol{e}}) \, \mathrm{d}\boldsymbol{x} - \int_{\partial B_R(0)} (\boldsymbol{\nu} \times \boldsymbol{E}_{q,\boldsymbol{p}}) \cdot \overline{\mathbf{curl}\, \boldsymbol{e}} \, \mathrm{d}s \\
&= \int_{\partial B_R(0)} ((\boldsymbol{\nu} \times \overline{\boldsymbol{e}}) \cdot \mathbf{curl}\, \boldsymbol{E}_{\boldsymbol{p}}^i - (\boldsymbol{\nu} \times \boldsymbol{E}_{\boldsymbol{p}}^i) \cdot \overline{\mathbf{curl}\, \boldsymbol{e}}) \, \mathrm{d}s \\
&\quad + \int_{\partial B_R(0)} ((\boldsymbol{\nu} \times \overline{\boldsymbol{e}}) \cdot \mathbf{curl}\, \boldsymbol{E}_{q,\boldsymbol{p}}^s - (\boldsymbol{\nu} \times \boldsymbol{E}_{q,\boldsymbol{p}}^s) \cdot \overline{\mathbf{curl}\, \boldsymbol{e}}) \, \mathrm{d}s \,. \qquad (3.42)
\end{aligned}$$

We discuss the two integrals on the right-hand side of (3.42) separately. First, we calculate the curl of $\boldsymbol{E}_{\boldsymbol{p}}^i$, given by (3.20). Using (B.3) together with the fact that $\boldsymbol{p}$ is a tangential vector field, it follows that

$$\mathbf{curl}\, \boldsymbol{E}_{\boldsymbol{p}}^i(\boldsymbol{x}) = -\sqrt{\frac{\mu_0}{\varepsilon_0}} \int_{S^2} (\nabla e^{\mathrm{i}k\boldsymbol{\theta}\cdot\boldsymbol{x}} \times (\boldsymbol{\theta} \times \boldsymbol{p}(\boldsymbol{\theta})) \, \mathrm{d}s(\boldsymbol{\theta}) = \mathrm{i}\omega\mu_0 \int_{S^2} \boldsymbol{p}(\boldsymbol{\theta}) e^{\mathrm{i}k\boldsymbol{x}\cdot\boldsymbol{\theta}} \, \mathrm{d}s(\boldsymbol{\theta}) \,, \quad (3.43)$$

for $\boldsymbol{x} \in \mathbb{R}^3$. Inserting (3.43) we find for the first integral that

$$\begin{aligned}
&\int_{\partial B_R(0)} ((\boldsymbol{\nu} \times \overline{\boldsymbol{e}}) \cdot \mathbf{curl}\, \boldsymbol{E}_{\boldsymbol{p}}^i - (\boldsymbol{\nu} \times \boldsymbol{E}_{\boldsymbol{p}}^i) \cdot \overline{\mathbf{curl}\, \boldsymbol{e}}) \, \mathrm{d}s \\
&= \int_{\partial B_R(0)} \Big((\boldsymbol{\nu}(\boldsymbol{x}) \times \overline{\boldsymbol{e}(\boldsymbol{x})}) \cdot \Big(\mathrm{i}\omega\mu_0 \int_{S^2} \boldsymbol{p}(\boldsymbol{\theta}) e^{\mathrm{i}k\boldsymbol{\theta}\cdot\boldsymbol{x}} \, \mathrm{d}s(\boldsymbol{\theta}) \Big) \\
&\qquad\qquad - \Big(\sqrt{\frac{\mu_0}{\varepsilon_0}} \int_{S^2} (\boldsymbol{\theta} \times \boldsymbol{p}(\boldsymbol{\theta})) e^{\mathrm{i}k\boldsymbol{\theta}\cdot\boldsymbol{x}} \, \mathrm{d}s(\boldsymbol{\theta}) \Big) \cdot (\boldsymbol{\nu}(\boldsymbol{x}) \times \overline{\mathbf{curl}\, \boldsymbol{e}(\boldsymbol{x})}) \Big) \, \mathrm{d}s(\boldsymbol{x}) \\
&= \int_{S^2} \boldsymbol{p}(\boldsymbol{\theta}) \cdot \int_{\partial B_R(0)} \Big(\mathrm{i}\omega\mu_0 (\boldsymbol{\nu}(\boldsymbol{x}) \times \overline{\boldsymbol{e}(\boldsymbol{x})}) - \sqrt{\frac{\mu_0}{\varepsilon_0}} (\boldsymbol{\nu}(\boldsymbol{x}) \times \overline{\mathbf{curl}\, \boldsymbol{e}(\boldsymbol{x})}) \times \boldsymbol{\theta} \Big) e^{\mathrm{i}k\boldsymbol{\theta}\cdot\boldsymbol{x}} \, \mathrm{d}s(\boldsymbol{x}) \, \mathrm{d}s(\boldsymbol{\theta}) \,.
\end{aligned}$$

On the other hand, the representation formula for the far field pattern $\boldsymbol{e}^\infty$ of $\boldsymbol{e}$ analogous to (3.15) gives

$$\begin{aligned}
\sqrt{\frac{\mu_0}{\varepsilon_0}} \, \boldsymbol{\theta} \times \overline{\boldsymbol{e}^\infty(\boldsymbol{\theta})} = \int_{\partial B_R(0)} \Big(\Big(\boldsymbol{\theta} \times \Big(\mathrm{i}\omega\mu_0 (\boldsymbol{\nu}(\boldsymbol{x}) \times \overline{\boldsymbol{e}(\boldsymbol{x})}) \Big) \Big) \times \boldsymbol{\theta} \\
- \sqrt{\frac{\mu_0}{\varepsilon_0}} (\boldsymbol{\nu}(\boldsymbol{x}) \times \overline{\mathbf{curl}\, \boldsymbol{e}(\boldsymbol{x})}) \times \boldsymbol{\theta} \Big) e^{\mathrm{i}k\boldsymbol{\theta}\cdot\boldsymbol{x}} \, \mathrm{d}s(\boldsymbol{x})
\end{aligned}$$

for $\boldsymbol{\theta} \in S^2$, and thus

$$\int_{\partial B_R(0)} \Big((\boldsymbol{\nu} \times \overline{\boldsymbol{e}}) \cdot \mathbf{curl}\, \boldsymbol{E}_{\boldsymbol{p}}^i - (\boldsymbol{\nu} \times \boldsymbol{E}_{\boldsymbol{p}}^i) \cdot \overline{\mathbf{curl}\, \boldsymbol{e}} \Big) \, \mathrm{d}s = \sqrt{\frac{\mu_0}{\varepsilon_0}} \int_{S^2} \boldsymbol{p}(\boldsymbol{\theta}) \cdot (\boldsymbol{\theta} \times \overline{\boldsymbol{e}^\infty(\boldsymbol{\theta})}) \, \mathrm{d}s(\boldsymbol{\theta}) \,, \quad (3.44)$$

since $\boldsymbol{p}(\boldsymbol{\theta}) \cdot \boldsymbol{\theta} = 0$.

Next, we consider the second integral on the right-hand side of (3.42). We insert (3.21b) and apply the radiation condition (3.10d) as well as the far field expansion (3.14). This gives, as $R \to \infty$,

$$\begin{aligned}
&\int_{\partial B_R(0)} \big((\boldsymbol{\nu} \times \overline{\boldsymbol{e}}) \cdot \mathbf{curl}\, \boldsymbol{E}^s_{q,\boldsymbol{p}} - (\boldsymbol{\nu} \times \boldsymbol{E}^s_{q,\boldsymbol{p}}) \cdot \overline{\mathbf{curl}\, \boldsymbol{e}}\big)\, \mathrm{d}s \\
&= \int_{S^2} \int_{\partial B_R(0)} \Big(-\Big(\frac{\boldsymbol{x}}{|\boldsymbol{x}|} \times \mathbf{curl}\, \boldsymbol{E}^s_q(\boldsymbol{x};\boldsymbol{\theta}) \boldsymbol{p}(\boldsymbol{\theta}) \Big) \cdot \overline{\boldsymbol{e}(\boldsymbol{x})} \\
&\qquad\qquad + (\boldsymbol{E}^s_q(\boldsymbol{x};\boldsymbol{\theta}) \boldsymbol{p}(\boldsymbol{\theta})) \cdot \Big(\frac{\boldsymbol{x}}{|\boldsymbol{x}|} \times \overline{\mathbf{curl}\, \boldsymbol{e}(\boldsymbol{x})} \Big) \Big)\, \mathrm{d}s(\boldsymbol{x})\, \mathrm{d}s(\boldsymbol{\theta}) \\
&= 2\mathrm{i}k \int_{S^2} \int_{\partial B_R(0)} (\boldsymbol{E}^s_q(\boldsymbol{x};\boldsymbol{\theta}) \boldsymbol{p}(\boldsymbol{\theta})) \cdot \overline{\boldsymbol{e}(\boldsymbol{x})}\, \mathrm{d}s(\boldsymbol{x})\, \mathrm{d}s(\boldsymbol{\theta}) + o(1) \\
&= \frac{\mathrm{i}k}{8\pi^2} \int_{S^2} \int_{S^2} (\boldsymbol{E}^\infty_q(\widehat{\boldsymbol{x}};\boldsymbol{\theta}) \boldsymbol{p}(\boldsymbol{\theta})) \cdot \overline{\boldsymbol{e}^\infty(\widehat{\boldsymbol{x}})}\, \mathrm{d}s(\widehat{\boldsymbol{x}})\, \mathrm{d}s(\boldsymbol{\theta}) + o(1)\,.
\end{aligned}$$

Recalling from Lemma 3.2 that $\boldsymbol{E}^\infty_q(\widehat{\boldsymbol{x}}) = -\sqrt{\frac{\mu_0}{\varepsilon_0}}\, \widehat{\boldsymbol{x}} \times \boldsymbol{H}^\infty_q(\widehat{\boldsymbol{x}})$ for all $\widehat{\boldsymbol{x}} \in S^2$, we obtain

$$\int_{S^2} \int_{S^2} (\boldsymbol{E}^\infty_q(\widehat{\boldsymbol{x}};\boldsymbol{\theta}) \boldsymbol{p}(\boldsymbol{\theta})) \cdot \overline{\boldsymbol{e}^\infty(\widehat{\boldsymbol{x}})}\, \mathrm{d}s(\widehat{\boldsymbol{x}})\, \mathrm{d}s(\boldsymbol{\theta}) = \sqrt{\frac{\mu_0}{\varepsilon_0}} \int_{S^2} (F_q \boldsymbol{p})(\widehat{\boldsymbol{x}}) \cdot (\widehat{\boldsymbol{x}} \times \overline{\boldsymbol{e}^\infty(\widehat{\boldsymbol{x}})})\, \mathrm{d}s(\widehat{\boldsymbol{x}})\,,$$

and the second integral on the right-hand side of (3.42) becomes

$$\begin{aligned}
&\int_{\partial B_R(0)} \big((\boldsymbol{\nu} \times \overline{\boldsymbol{e}}) \cdot \mathbf{curl}\, \boldsymbol{E}^s_{q,\boldsymbol{p}} - (\boldsymbol{\nu} \times \boldsymbol{E}^s_{q,\boldsymbol{p}}) \cdot \overline{\mathbf{curl}\, \boldsymbol{e}}\big)\, \mathrm{d}s \\
&= \sqrt{\frac{\mu_0}{\varepsilon_0}} \frac{\mathrm{i}k}{8\pi^2} \int_{S^2} \boldsymbol{p}(\widehat{\boldsymbol{x}}) \cdot \overline{F^*_q(\widehat{\boldsymbol{x}} \times \boldsymbol{e}^\infty(\widehat{\boldsymbol{x}}))}\, \mathrm{d}s(\widehat{\boldsymbol{x}}) + o(1)\,. \qquad (3.45)
\end{aligned}$$

Connecting (3.42), (3.44), (3.45) and recalling the definition (3.19) of the scattering operator $\mathcal{S}_q$, we finally obtain that

$$\int_\Omega (L_{q,\Omega} \boldsymbol{p}) \cdot \overline{\boldsymbol{f}}\, \mathrm{d}\boldsymbol{x} = \sqrt{\frac{\mu_0}{\varepsilon_0}} \int_{S^2} \boldsymbol{p}(\widehat{\boldsymbol{x}}) \cdot \overline{\mathcal{S}^*_q(\widehat{\boldsymbol{x}} \times \boldsymbol{e}^\infty(\widehat{\boldsymbol{x}}))}\, \mathrm{d}s(\widehat{\boldsymbol{x}})\,. \qquad \square$$

Proceeding further, we have a closer look at the ranges of the adjoint operators of $L_{q,B}$ and $L_{q,\Omega}$ corresponding to two non-intersecting subsets $B, \Omega \subseteq \mathbb{R}^3$.

Lemma 3.17. *Suppose that $D \subseteq \mathbb{R}^3$ is open and Lipschitz bounded, and let $q \in \mathcal{Y}_D$. Let $B, \Omega \subseteq \mathbb{R}^3$ be open and bounded such that $\mathbb{R}^3 \setminus (\overline{B \cup \Omega})$ is connected and $\overline{B \cap \Omega} = \emptyset$. Then,*

$$\mathcal{R}(L^*_{q,B}) \cap \mathcal{R}(L^*_{q,\Omega}) = \{0\}\,,$$

and $\mathcal{R}(L^*_{q,B}), \mathcal{R}(L^*_{q,\Omega}) \subseteq L^2_t(S^2, \mathbb{C}^3)$ are both dense.

Proof. We assume that $\boldsymbol{\phi} \in \mathcal{R}(L^*_{q,B}) \cap \mathcal{R}(L^*_{q,\Omega})$. Then, we know from Lemma 3.16 that there exist sources $\boldsymbol{f}_B \in L^2(B, \mathbb{C}^3)$ and $\boldsymbol{f}_\Omega \in L^2(\Omega, \mathbb{C}^3)$ such that

$$\boldsymbol{\phi} = \sqrt{\frac{\mu_0}{\varepsilon_0}} \mathcal{S}^*_q(\boldsymbol{\nu} \times \boldsymbol{e}^\infty_B) = \sqrt{\frac{\mu_0}{\varepsilon_0}} \mathcal{S}^*_q(\boldsymbol{\nu} \times \boldsymbol{e}^\infty_\Omega)\,, \qquad (3.46)$$

where $\boldsymbol{e}_B, \boldsymbol{e}_\Omega \in H_{\mathrm{loc}}(\mathbf{curl}; \mathbb{R}^3)$ are radiating solutions to

$$\mathbf{curl}\,\mathbf{curl}\,\boldsymbol{e}_B - k^2\varepsilon_r \boldsymbol{e}_B = \boldsymbol{f}_B \quad \text{and} \quad \mathbf{curl}\,\mathbf{curl}\,\boldsymbol{e}_\Omega - k^2\varepsilon_r \boldsymbol{e}_\Omega = \boldsymbol{f}_\Omega \qquad \text{in } \mathbb{R}^3\,.$$

Since $\mathcal{S}_q$ is unitary, from (3.46) it follows that $\boldsymbol{e}_B^\infty = \boldsymbol{e}_\Omega^\infty$. Thus, Rellich's lemma 3.3 and the unique continuation principle in Theorem 3.4 imply that $\boldsymbol{e}_B = \boldsymbol{e}_\Omega$ in $\mathbb{R}^3 \setminus (\overline{B \cup \Omega})$. We may define $\boldsymbol{e} \in H_{\mathrm{loc}}(\mathbf{curl}; \mathbb{R}^3)$ by

$$\boldsymbol{e} := \begin{cases} \boldsymbol{e}_B = \boldsymbol{e}_\Omega & \text{in } \mathbb{R}^3 \setminus (\overline{B \cup \Omega})\,, \\ \boldsymbol{e}_B & \text{in } \Omega\,, \\ \boldsymbol{e}_\Omega & \text{in } B\,. \end{cases}$$

Then, $\boldsymbol{e}$ is a radiating solution to

$$\mathbf{curl}\,\mathbf{curl}\,\boldsymbol{e} - k^2\varepsilon_r \boldsymbol{e} = 0 \qquad \text{in } \mathbb{R}^3\,.$$

The uniqueness result [BCTX12, Thm. 2] shows that $\boldsymbol{e}$ must vanish identically in $\mathbb{R}^3$. In particular $\boldsymbol{e}^\infty = 0$, and thus $\boldsymbol{\phi} = 0$.

To show that $\mathcal{R}(L_{q,B}^*) \subseteq L_t^2(S^2, \mathbb{C}^3)$ is dense, it suffices to prove the injectivity of the operator $L_{q,B}$, because $\overline{\mathcal{R}(L_{q,B}^*)} = \mathcal{N}(L_{q,B})^\perp$ (see, e.g., [Mon03, Thm. 2.15]). Suppose that $L_{q,B}\boldsymbol{p} = \boldsymbol{E}_{q,\boldsymbol{p}}|_B = 0$. Then, the unique continuation principle in Theorem 3.4 implies that $\boldsymbol{E}_{q,\boldsymbol{p}} = 0$ in $\mathbb{R}^3$. In particular, $\boldsymbol{E}_{\boldsymbol{p}}^i = \boldsymbol{E}_{q,\boldsymbol{p}}^s$ is an entire radiating solution to Maxwell's equations (3.10a), and therefore, $\boldsymbol{E}_{\boldsymbol{p}}^i = \boldsymbol{H}_{\boldsymbol{p}}^i = 0$ in $\mathbb{R}^3$ by Lemma 3.7. Thus, [CK19, Thm. 3.27] gives $\boldsymbol{p} = 0$. The denseness of $\mathcal{R}(L_{q,\Omega}^*) \subseteq L_t^2(S^2, \mathbb{C}^3)$ follows analogously. □

Now, everything is prepared to show Theorem 3.38 using Lemma 2.21.

Proof of Theorem 3.38. Let $D \subseteq \mathbb{R}^3$ be open and Lipschitz bounded, let $q \in \mathcal{Y}_D$, and let $B, \Omega \subseteq \mathbb{R}^3$ be open and bounded such that $\mathbb{R}^3 \setminus \overline{\Omega}$ is connected. Suppose that $B \not\subseteq \Omega$, and let $V \subseteq L_t^2(S^2, \mathbb{C}^3)$ be a finite-dimensional subspace. Without loss of generality, we assume that $\overline{B \cap \Omega} = \emptyset$ and that $\mathbb{R}^3 \setminus (\overline{B \cup \Omega})$ is connected (otherwise we replace B with a sufficiently small ball $\widetilde{B} \subseteq B \setminus \Omega_\rho$, where Ω_ρ denotes a sufficiently small neighborhood of Ω). We introduce the orthogonal projection $P_V : L_t^2(S^2, \mathbb{C}^3) \to L_t^2(S^2, \mathbb{C}^3)$ onto V.

From Lemma 3.17 we know that $\mathcal{R}(L_{q,B}^*) \subseteq L_t^2(S^2, \mathbb{C}^3)$ is dense, and therefore, $\mathcal{R}(L_{q,B}^*)$ is infinite dimensional. Together with the fact that $\mathcal{R}(L_{q,B}^*) \cap \mathcal{R}(L_{q,\Omega}^*) = \{0\}$, the dimensionality argument from Lemma 2.23 shows that

$$\mathcal{R}(L_{q,B}^*) \not\subseteq \mathcal{R}(L_{q,\Omega}^*) + V = \mathcal{R}\Big(\begin{bmatrix} L_{q,\Omega}^* & P_V \end{bmatrix}\Big) = \mathcal{R}\Bigg(\begin{bmatrix} L_{q,\Omega} \\ P_V \end{bmatrix}^*\Bigg)\,,$$

where we used that $P_V^* = P_V$. From Lemma 2.21, it follows that there does not exist a constant $C > 0$ such that

$$\|L_{q,B}\boldsymbol{p}\|_{L^2(B,\mathbb{C}^3)}^2 \leq C^2 \left\| \begin{bmatrix} L_{q,\Omega} \\ P_V \end{bmatrix} \boldsymbol{p} \right\|_{L^2(\Omega,\mathbb{C}^3) \times L_t^2(S^2,\mathbb{C}^3)}^2 = C^2 \big(\|L_{q,\Omega}\boldsymbol{p}\|_{L^2(\Omega,\mathbb{C}^3)}^2 + \|P_V \boldsymbol{p}\|_{L_t^2(S^2,\mathbb{C}^3)}^2 \big) \quad (3.47)$$

holds for all $\boldsymbol{p} \in L_t^2(S^2, \mathbb{C}^3)$. At this point, we remind the reader of the notation (2.6). From estimate (3.47), we deduce that one can find a sequence $(\widetilde{\boldsymbol{p}}_m)_{m\in\mathbb{N}} \subseteq L_t^2(S^2, \mathbb{C}^3)$ such that

$$\|L_{q,B}\widetilde{\boldsymbol{p}}_m\|^2_{L^2(B,\mathbb{C}^3)} \to \infty \qquad \text{and} \qquad \|L_{q,\Omega}\widetilde{\boldsymbol{p}}_m\|^2_{L^2(\Omega,\mathbb{C}^3)} + \|P_V\widetilde{\boldsymbol{p}}_m\|^2_{L_t^2(S^2,\mathbb{C}^3)} \to 0$$

as $m \to \infty$. Setting $\boldsymbol{p}_m := \widetilde{\boldsymbol{p}}_m - P_V\widetilde{\boldsymbol{p}}_m \in V^\perp$ for all $m \in \mathbb{N}$ yields

$$\begin{aligned}
\|L_{q,B}\boldsymbol{p}_m\|_{L^2(B,\mathbb{C}^3)} &\geq \big|\|L_{q,B}\widetilde{\boldsymbol{p}}_m\|_{L^2(B,\mathbb{C}^3)} - \|L_{q,B}P_V\widetilde{\boldsymbol{p}}_m\|_{L^2(B,\mathbb{C}^3)}\big| \\
&\geq \|L_{q,B}\widetilde{\boldsymbol{p}}_m\|_{L^2(B,\mathbb{C}^3)} - \|L_{q,B}\|\|P_V\widetilde{\boldsymbol{p}}_m\|_{L_t^2(S^2,\mathbb{C}^3)} \to \infty\,, \\
\|L_{q,\Omega}\boldsymbol{p}_m\|_{L^2(\Omega,\mathbb{C}^3)} &\leq \|L_{q,\Omega}\widetilde{\boldsymbol{p}}_m\|_{L^2(\Omega,\mathbb{C}^3)} + \|L_{q,\Omega}\|\|P_V\widetilde{\boldsymbol{p}}_m\|_{L_t^2(S^2,\mathbb{C}^3)} \to 0
\end{aligned}$$

as $m \to \infty$. From Lemma 3.16, we recall the definitions $L_{q,B}\boldsymbol{p}_m = -\frac{1}{\mathrm{i}\omega\varepsilon}\,\mathbf{curl}\,\boldsymbol{H}_{q,\boldsymbol{p}_m}|_B$ and $L_{q,\Omega}\boldsymbol{p}_m = -\frac{1}{\mathrm{i}\omega\varepsilon}\,\mathbf{curl}\,\boldsymbol{H}_{q,\boldsymbol{p}_m}|_\Omega$ and get

$$\begin{aligned}
\int_B |L_{q,B}\boldsymbol{p}_m|^2 \,\mathrm{d}\boldsymbol{x} &= \int_B \frac{1}{\omega^2\varepsilon^2}|\,\mathbf{curl}\,\boldsymbol{H}_{q,\boldsymbol{p}_m}|^2 \,\mathrm{d}\boldsymbol{x} \leq \frac{1}{\omega^2}\Big\|\frac{1}{\varepsilon^2}\Big\|_{L^\infty(\mathbb{R}^3)}\int_B |\,\mathbf{curl}\,\boldsymbol{H}_{q,\boldsymbol{p}_m}|^2 \,\mathrm{d}\boldsymbol{x}\,, \\
\int_\Omega |L_{q,\Omega}\boldsymbol{p}_m|^2 \,\mathrm{d}\boldsymbol{x} &= \int_\Omega \frac{1}{\omega^2\varepsilon^2}|\,\mathbf{curl}\,\boldsymbol{H}_{q,\boldsymbol{p}_m}|^2 \,\mathrm{d}\boldsymbol{x} \geq \frac{1}{\omega^2}\operatorname{ess\,inf}\frac{1}{\varepsilon^2}\int_\Omega |\,\mathbf{curl}\,\boldsymbol{H}_{q,\boldsymbol{p}_m}|^2 \,\mathrm{d}\boldsymbol{x}\,.
\end{aligned}$$

This ends the proof. □

Theorem 3.18. *Suppose that $D_1, D_2 \subseteq \mathbb{R}^3$ are open and Lipschitz bounded, let $q_1 \in \mathcal{Y}_{D_1}$ and $q_2 \in \mathcal{Y}_{D_2}$, and assume that $\Omega \subseteq \mathbb{R}^3$ is open and bounded. If $q_1(\boldsymbol{x}) = q_2(\boldsymbol{x})$ for almost every $\boldsymbol{x} \in \mathbb{R}^3 \setminus \overline{\Omega}$, then there exist constants $c, C > 0$ such that*

$$c\int_\Omega |\,\mathbf{curl}\,\boldsymbol{H}_{q_1,\boldsymbol{p}}|^2 \,\mathrm{d}\boldsymbol{x} \leq \int_\Omega |\,\mathbf{curl}\,\boldsymbol{H}_{q_2,\boldsymbol{p}}|^2 \,\mathrm{d}\boldsymbol{x} \leq C\int_\Omega |\,\mathbf{curl}\,\boldsymbol{H}_{q_1,\boldsymbol{p}}|^2 \,\mathrm{d}\boldsymbol{x} \tag{3.48}$$

for all $\boldsymbol{p} \in L_t^2(S^2, \mathbb{C}^3)$.

Proof. Lemma 3.16 shows that, for any $\boldsymbol{f} \in L^2(\Omega, \mathbb{C}^3)$,

$$L^*_{q_1,\Omega}\boldsymbol{f} = \sqrt{\frac{\mu_0}{\varepsilon_0}}\mathcal{S}^*_{q_1}(\boldsymbol{\nu}\times\boldsymbol{e}_1^\infty) \qquad \text{and} \qquad L^*_{q_2,\Omega}\boldsymbol{f} = \sqrt{\frac{\mu_0}{\varepsilon_0}}\mathcal{S}^*_{q_2}(\boldsymbol{\nu}\times\boldsymbol{e}_2^\infty)\,, \tag{3.49}$$

where $\boldsymbol{e}_j^\infty$, $j = 1, 2$, are the far field patterns of radiating solutions to

$$\mathbf{curl}\,\mathbf{curl}\,\boldsymbol{e}_j - k^2\varepsilon_{r,j}\boldsymbol{e}_j = \boldsymbol{f} \qquad \text{in } \mathbb{R}^3\,.$$

Moreover, we observe that

$$\begin{aligned}
\mathbf{curl}\,\mathbf{curl}\,\boldsymbol{e}_1 - k^2\varepsilon_{r,2}\boldsymbol{e}_1 &= \boldsymbol{f} - k^2(\varepsilon_{r,2} - \varepsilon_{r,1})\boldsymbol{e}_1 \qquad \text{in } \mathbb{R}^3\,, \\
\mathbf{curl}\,\mathbf{curl}\,\boldsymbol{e}_2 - k^2\varepsilon_{r,1}\boldsymbol{e}_2 &= \boldsymbol{f} - k^2(\varepsilon_{r,1} - \varepsilon_{r,2})\boldsymbol{e}_2 \qquad \text{in } \mathbb{R}^3\,.
\end{aligned}$$

Since by assumption $\varepsilon_{r,1} - \varepsilon_{r,2}$ vanishes almost everywhere outside of Ω, this implies that

$$\sqrt{\frac{\mu_0}{\varepsilon_0}}\mathcal{S}^*_{q_2}(\boldsymbol{\nu}\times\boldsymbol{e}_1^\infty) = L^*_{q_2,\Omega}(\boldsymbol{f} - k^2(\varepsilon_{r,2} - \varepsilon_{r,1})\boldsymbol{e}_1)\,, \tag{3.50a}$$

$$\sqrt{\frac{\mu_0}{\varepsilon_0}}\mathcal{S}_{q_1}^*(\boldsymbol{\nu}\times\boldsymbol{e}_2^\infty) \;=\; L_{q_1,\Omega}^*(\boldsymbol{f}-k^2(\varepsilon_{r,1}-\varepsilon_{r,2})\boldsymbol{e}_2)\,. \tag{3.50b}$$

Let $\boldsymbol{\phi}\in\mathcal{R}(\mathcal{S}_{q_1}L_{q_1,\Omega}^*)$. Since $\mathcal{S}_{q_1}$ and $\mathcal{S}_{q_2}$ are unitary, (3.49) and (3.50) imply that

$$\boldsymbol{\phi} \;=\; \mathcal{S}_{q_1}L_{q_1,\Omega}^*\boldsymbol{f} \;=\; \sqrt{\frac{\mu_0}{\varepsilon_0}}(\boldsymbol{\nu}\times\boldsymbol{e}_1^\infty) \;=\; \mathcal{S}_{q_2}L_{q_2,\Omega}^*(\boldsymbol{f}-k^2(\varepsilon_{r,2}-\varepsilon_{r,1})\boldsymbol{e}_1)\,,$$

i.e., $\mathcal{R}(\mathcal{S}_{q_1}L_{q_1,\Omega}^*)\subseteq\mathcal{R}(\mathcal{S}_{q_2}L_{q_2,\Omega}^*)$. Analogously, we obtain $\mathcal{R}(\mathcal{S}_{q_1}L_{q_1,\Omega}^*)\supseteq\mathcal{R}(\mathcal{S}_{q_2}L_{q_2,\Omega}^*)$ and therefore $\mathcal{R}(\mathcal{S}_{q_1}L_{q_1,\Omega}^*)=\mathcal{R}(\mathcal{S}_{q_2}L_{q_2,\Omega}^*)$. It remains to show that $\mathcal{R}(\mathcal{S}_{q_j}L_{q_j,\Omega}^*)=\mathcal{R}(L_{q_j,\Omega}^*)$ for $j=1,2$. Then, it follows from Lemma 2.21 that there exist constants $C_1,C_2>0$ such that

$$C_1\|L_{q_1,\Omega}\boldsymbol{p}\|_{L^2(\Omega,\mathbb{C}^3)}^2 \;\le\; \|L_{q_2,\Omega}\boldsymbol{p}\|_{L^2(\Omega,\mathbb{C}^3)}^2 \;\le\; C_2\|L_{q_1,\Omega}\boldsymbol{p}\|_{L^2(\Omega,\mathbb{C}^3)}^2 \qquad \text{for all } \boldsymbol{p}\in L_t^2(S^2,\mathbb{C}^3)\,.$$

Inserting definition (3.39), the estimate on the left-hand side yields

$$\begin{aligned}&\frac{C_1}{\omega^2}\operatorname{ess\,inf}\frac{1}{\varepsilon_1^2}\int_\Omega|\operatorname{\mathbf{curl}}\boldsymbol{H}_{q_1,\boldsymbol{p}}|^2\,\mathrm{d}\boldsymbol{x} \;\le\; C_1\int_\Omega\frac{1}{\omega^2\varepsilon_1^2}|\operatorname{\mathbf{curl}}\boldsymbol{H}_{q_1,\boldsymbol{p}}|^2\,\mathrm{d}\boldsymbol{x}\\ &\le\int_\Omega\frac{1}{\omega^2\varepsilon_2^2}|\operatorname{\mathbf{curl}}\boldsymbol{H}_{q_2,\boldsymbol{p}}|^2\,\mathrm{d}\boldsymbol{x} \;\le\; \frac{1}{\omega^2}\Big\|\frac{1}{\varepsilon_2^2}\Big\|_{L^\infty(\mathbb{R}^3)}\int_\Omega|\operatorname{\mathbf{curl}}\boldsymbol{H}_{q_2,\boldsymbol{p}}|^2\,\mathrm{d}\boldsymbol{x}\,.\end{aligned}$$

Thus, the left-hand side of (3.48) is satisfied with $c:=C_1\big(\operatorname{ess\,inf}\varepsilon_1^{-2}\big)\|\varepsilon_2^2\|_{L^\infty(\mathbb{R}^3)}$. Analogously, one gets the estimate on the right-hand side of (3.48).

Using (3.19) we find that for any $\boldsymbol{f}\in L^2(\Omega,\mathbb{C}^3)$,

$$\mathcal{S}_{q_j}L_{q_j,\Omega}^*\boldsymbol{f} \;=\; L_{q_j,\Omega}^*\boldsymbol{f}+\frac{\mathrm{i}k}{8\pi^2}F_{q_j}L_{q_j,\Omega}^*\boldsymbol{f}\,. \tag{3.51}$$

The definition of the far field operator F_{q_j} in (3.18) together with our notation from (3.21c) shows that $F_{q_j}L_{q_j,\Omega}^*\boldsymbol{f}=\boldsymbol{H}_{q_j,\boldsymbol{p}_{j,\boldsymbol{f}}}^\infty$ with $\boldsymbol{p}_{j,\boldsymbol{f}}:=L_{q_j,\Omega}^*\boldsymbol{f}$. Since (3.10) implies that the corresponding scattered electric field $\boldsymbol{E}_{q_j,\boldsymbol{p}_{j,\boldsymbol{f}}}^s$ is a radiating solution to

$$\operatorname{\mathbf{curl}}\operatorname{\mathbf{curl}}\boldsymbol{E}_{q_j,\boldsymbol{p}_{j,\boldsymbol{f}}}^s-k^2\varepsilon_{r,j}\boldsymbol{E}_{q_j,\boldsymbol{p}_{j,\boldsymbol{f}}}^s \;=\; -k^2(1-\varepsilon_{r,j})\boldsymbol{E}_{\boldsymbol{p}_{j,\boldsymbol{f}}}^i \qquad \text{in } \mathbb{R}^3\,,$$

we find using Lemmas 3.2 and 3.16 that

$$\boldsymbol{H}_{q_j,\boldsymbol{p}_{j,\boldsymbol{f}}}^\infty \;=\; \sqrt{\frac{\varepsilon_0}{\mu_0}}\,\boldsymbol{\nu}\times\boldsymbol{E}_{q_j,\boldsymbol{p}_{j,\boldsymbol{f}}}^\infty \;=\; \frac{\varepsilon_0}{\mu_0}\mathcal{S}_{q_j}L_{q_j,\Omega}^*(-k^2(1-\varepsilon_{r,j})\boldsymbol{E}_{\boldsymbol{p}_{j,\boldsymbol{f}}}^i)\,.$$

Substituting this into (3.51) and rearranging terms shows that, for any $\boldsymbol{f}\in L^2(\Omega,\mathbb{C}^3)$,

$$L_{q_j,\Omega}^*\boldsymbol{f} \;=\; \mathcal{S}_{q_j}L_{q_j,\Omega}^*\Big(\boldsymbol{f}+\frac{\mathrm{i}k}{8\pi^2}\omega^2\varepsilon_0^2(1-\varepsilon_{r,j})\boldsymbol{E}_{\boldsymbol{p}_{j,\boldsymbol{f}}}^i\Big)\,,$$

i.e., $\mathcal{R}(L_{q_j,\Omega}^*)\subseteq\mathcal{R}(\mathcal{S}_{q_j}L_{q_j,\Omega}^*)$ for $j=1,2$.

Similarly, using (3.49) we have that, for any $\boldsymbol{f}\in L^2(\Omega,\mathbb{C}^3)$,

$$\mathcal{S}_{q_j}L_{q_j,\Omega}^*\boldsymbol{f} \;=\; \sqrt{\frac{\mu_0}{\varepsilon_0}}\,\mathcal{S}_{q_j}^*\big(\mathcal{S}_{q_j}(\boldsymbol{\nu}\times\boldsymbol{e}_j^\infty)\big) \;=\; \sqrt{\frac{\mu_0}{\varepsilon_0}}\,\mathcal{S}_{q_j}^*\Big((\boldsymbol{\nu}\times\boldsymbol{e}_j^\infty)+\frac{\mathrm{i}k}{8\pi^2}F_{q_j}(\boldsymbol{\nu}\times\boldsymbol{e}_j^\infty)\Big)\,. \tag{3.52}$$

Writing $\boldsymbol{p}_{j,\boldsymbol{f}} := \boldsymbol{\nu} \times \boldsymbol{e}_j^\infty$ we obtain as before that

$$F_{q_j}(\boldsymbol{\nu} \times \boldsymbol{e}_j^\infty) \;=\; \boldsymbol{H}^\infty_{q_j,\boldsymbol{p}_{j,\boldsymbol{f}}} \;=\; \frac{\varepsilon_0}{\mu_0} \mathcal{S}_{q_j} L^*_{q_j,\Omega}(-k^2(1-\varepsilon_{r,j}) \boldsymbol{E}^i_{\boldsymbol{p}_{j,\boldsymbol{f}}}) \,.$$

Accordingly, substituting this into (3.52) and applying (3.49) we find that, for any $\boldsymbol{f} \in L^2(\Omega, \mathbb{C}^3)$,

$$\mathcal{S}_{q_j} L^*_{q_j,\Omega} \boldsymbol{f} \;=\; L^*_{q_j,\Omega}\Big(\boldsymbol{f} - \sqrt{\frac{\mu_0}{\varepsilon_0}} \frac{\mathrm{i}k}{8\pi^2} \omega^2 \varepsilon_0^2 (1-\varepsilon_{r,j})\, \boldsymbol{E}^i_{\boldsymbol{p}_{j,\boldsymbol{f}}}\Big) \,,$$

i.e., $\mathcal{R}(\mathcal{S}_{q_j} L^*_{q_j,\Omega}) \subseteq \mathcal{R}(L^*_{q_j,\Omega})$ for $j = 1, 2$. □

Our first application of Theorem 3.15 is the following simple uniqueness result for the inverse scattering problem. This should be compared to (3.23) in Theorem 3.8.

Theorem 3.19. *Suppose that $D_1, D_2 \subseteq \mathbb{R}^3$ are open and Lipschitz bounded, let $q_1 \in \mathcal{Y}_{D_1}$ and $q_2 \in \mathcal{Y}_{D_2}$. If $O \subseteq \mathbb{R}^3$ is an unbounded domain such that*

$$q_1 \;\leq\; q_2 \qquad \text{almost everywhere in } O \,, \tag{3.53}$$

and if $B \subseteq O$ is open with

$$q_1 \;\leq\; q_2 - c \qquad \text{almost everywhere in } B \text{ for some } c > 0 \,, \tag{3.54}$$

then

$$\mathrm{Re}(\mathcal{S}^*_{q_1} F_{q_1}) \not\geq_{\mathrm{fin}} \mathrm{Re}(\mathcal{S}^*_{q_1} F_{q_2}) \,.$$

In particular, $F_{q_1} \neq F_{q_2}$.

Proof. Suppose that there is a finite-dimensional subspace $V_1 \subseteq L^2_t(S^2, \mathbb{C}^3)$ such that

$$\mathrm{Re}\Big(\int_{S^2} \boldsymbol{p} \cdot \overline{\mathcal{S}^*_{q_1}(F_{q_2} - F_{q_1})\boldsymbol{p}}\, \mathrm{d}s\Big) \;\leq\; 0 \qquad \text{for all } \boldsymbol{p} \in V_1^\perp \,.$$

Then, Theorem 3.8 shows that there exists another finite-dimensional subspace $V_2 \subseteq L^2_t(S^2, \mathbb{C}^3)$ such that

$$\mathrm{Re}\Big(\int_{S^2} \boldsymbol{p} \cdot \overline{\mathcal{S}^*_{q_1}(F_{q_2} - F_{q_1})\boldsymbol{p}}\, \mathrm{d}s\Big) \;\geq\; \int_{\mathbb{R}^3} (q_2 - q_1)\, |\operatorname{\mathbf{curl}} \boldsymbol{H}_{q_1,\boldsymbol{p}}|^2 \,\mathrm{d}\boldsymbol{x} \qquad \text{for all } \boldsymbol{p} \in V_2^\perp \,.$$

Defining the finite-dimensional subspace $V := V_1 + V_2$, we obtain that $V^\perp \neq \{0\}$. Thus, using assumptions (3.53) and (3.54) we find that, for any $\boldsymbol{p} \in V^\perp$,

$$\begin{aligned}
0 \;&\geq\; \mathrm{Re}\Big(\int_{S^2} \boldsymbol{p} \cdot \overline{\mathcal{S}^*_{q_1}(F_{q_2} - F_{q_1})\boldsymbol{p}}\, \mathrm{d}s\Big) \;\geq\; \int_{\mathbb{R}^3} (q_2 - q_1)\, |\operatorname{\mathbf{curl}} \boldsymbol{H}_{q_1,\boldsymbol{p}}|^2 \,\mathrm{d}\boldsymbol{x} \\
&=\; \int_O (q_2 - q_1)\, |\operatorname{\mathbf{curl}} \boldsymbol{H}_{q_1,\boldsymbol{p}}|^2 \,\mathrm{d}\boldsymbol{x} + \int_{\mathbb{R}^3 \setminus \overline{O}} (q_2 - q_1)\, |\operatorname{\mathbf{curl}} \boldsymbol{H}_{q_1,\boldsymbol{p}}|^2 \,\mathrm{d}\boldsymbol{x} \\
&\geq\; c \int_B |\operatorname{\mathbf{curl}} \boldsymbol{H}_{q_1,\boldsymbol{p}}|^2 \,\mathrm{d}\boldsymbol{x} - (\|q_1\|_{L^\infty(\mathbb{R}^3)} + \|q_2\|_{L^\infty(\mathbb{R}^3)}) \int_{\mathbb{R}^3 \setminus \overline{O}} |\operatorname{\mathbf{curl}} \boldsymbol{H}_{q_1,\boldsymbol{p}}|^2 \,\mathrm{d}\boldsymbol{x} \,.
\end{aligned}$$

However, this contradicts Theorem 3.15 with $D = D_1$, $q = q_1$ and $\Omega = \mathbb{R}^3 \setminus \overline{O}$ implying $B \not\subseteq \Omega$,

which guarantees the existence of a sequence $(\boldsymbol{p}_m)_{m\in\mathbb{N}} \subseteq V^\perp$ with

$$\int_B |\operatorname{\mathbf{curl}} \boldsymbol{H}_{q_1,\boldsymbol{p}_m}|^2 \,\mathrm{d}\boldsymbol{x} \to \infty \quad \text{and} \quad \int_{\mathbb{R}^3\setminus\overline{O}} |\operatorname{\mathbf{curl}} \boldsymbol{H}_{q_1,\boldsymbol{p}_m}|^2 \,\mathrm{d}\boldsymbol{x} \to 0 \quad \text{as } m \to \infty\,.$$

Thus, applying Lemma 2.2 yields $\operatorname{Re}(\mathcal{S}_{q_1}^*(F_{q_2} - F_{q_1})) \not\leq_{\text{fin}} 0$. □

3.4.2. Monotonicity-Based Shape Reconstruction

As for the inverse acoustic obstacle scattering problem, we introduce certain probing domains and derive criteria to determine whether these domains are contained inside the scatterer D or not. Let $B \subseteq \mathbb{R}^3$ be open and bounded. The *magnetic Herglotz operator* $H_B : L_t^2(S^2,\mathbb{C}^3) \to L^2(B,\mathbb{C}^3)$ is defined by

$$(H_B\boldsymbol{p})(\boldsymbol{y}) := \int_{S^2} \operatorname{\mathbf{curl}}_{\boldsymbol{y}}(e^{\mathrm{i}k\boldsymbol{y}\cdot\boldsymbol{\theta}}\boldsymbol{p}(\boldsymbol{\theta}))\,\mathrm{d}s(\boldsymbol{\theta}) = \mathrm{i}k\int_{S^2} e^{\mathrm{i}k\boldsymbol{y}\cdot\boldsymbol{\theta}}\,(\boldsymbol{\theta}\times\boldsymbol{p}(\boldsymbol{\theta}))\,\mathrm{d}s(\boldsymbol{\theta})\,, \qquad \boldsymbol{y}\in B\,.$$

This is an integral operator with smooth kernel, which implies compactness (see, e.g., [Kre14, Thm. 2.28]). The adjoint operator $H_B^* : L^2(B,\mathbb{C}^3) \to L_t^2(S^2,\mathbb{C}^3)$ satisfies

$$(H_B^*\boldsymbol{f})(\widehat{\boldsymbol{x}}) = \mathrm{i}k\,\widehat{\boldsymbol{x}}\times\int_B e^{-\mathrm{i}k\boldsymbol{y}\cdot\widehat{\boldsymbol{x}}}\boldsymbol{f}(\boldsymbol{y})\,\mathrm{d}\boldsymbol{y}\,, \qquad \widehat{\boldsymbol{x}}\in S^2\,.$$

Again, we call the operator $H_B^*H_B : L_t^2(S^2,\mathbb{C}^3) \to L_t^2(S^2,\mathbb{C}^3)$ *probing operator*, and we calculate

$$(H_B^*H_B\boldsymbol{p})(\widehat{\boldsymbol{x}}) = -k^2\,\widehat{\boldsymbol{x}}\times\Big(\int_{S^2}\Big(\int_B e^{\mathrm{i}k\boldsymbol{y}\cdot(\boldsymbol{\theta}-\widehat{\boldsymbol{x}})}\,\mathrm{d}\boldsymbol{y}\Big)(\boldsymbol{\theta}\times\boldsymbol{p}(\boldsymbol{\theta}))\,\mathrm{d}s(\boldsymbol{\theta})\Big)\,, \qquad \widehat{\boldsymbol{x}}\in S^2\,. \tag{3.55}$$

This operator is self-adjoint and positive semi-definite. Moreover, it is compact, and for all $\boldsymbol{p}\in L_t^2(S^2,\mathbb{C}^3)$ we have that

$$\begin{aligned}
&\int_{S^2}\boldsymbol{p}\cdot\overline{H_B^*H_B\boldsymbol{p}}\,\mathrm{d}s\\
&= k^2\int_{S^2}\Big(\int_B\Big(\int_{S^2} e^{\mathrm{i}k\boldsymbol{y}\cdot(\widehat{\boldsymbol{x}}-\boldsymbol{\theta})}\boldsymbol{p}(\widehat{\boldsymbol{x}})\cdot(\overline{(\boldsymbol{\theta}\times\boldsymbol{p}(\boldsymbol{\theta}))}\times\widehat{\boldsymbol{x}})\,\mathrm{d}s(\boldsymbol{\theta})\Big)\,\mathrm{d}\boldsymbol{y}\Big)\,\mathrm{d}s(\widehat{\boldsymbol{x}})\\
&= \int_B\Big(\mathrm{i}k\int_{S^2} e^{\mathrm{i}k\boldsymbol{y}\cdot\widehat{\boldsymbol{x}}}\,(\widehat{\boldsymbol{x}}\times\boldsymbol{p}(\widehat{\boldsymbol{x}}))\,\mathrm{d}s(\widehat{\boldsymbol{x}})\Big)\cdot\overline{\Big(\mathrm{i}k\int_{S^2} e^{\mathrm{i}k\boldsymbol{y}\cdot\boldsymbol{\theta}}\,(\boldsymbol{\theta}\times\boldsymbol{p}(\boldsymbol{\theta}))\,\mathrm{d}s(\boldsymbol{\theta})\Big)}\,\mathrm{d}\boldsymbol{y}\\
&= \int_B |\operatorname{\mathbf{curl}}\boldsymbol{H}_{\boldsymbol{p}}^i|^2\,\mathrm{d}\boldsymbol{x}\,,
\end{aligned} \tag{3.56}$$

where $\boldsymbol{H}_{\boldsymbol{p}}^i$ is the incident magnetic field from (3.20). This should be compared to the corresponding expression for the magnetic far field operator in (3.24).

We already know from Corollary 3.14 that the operator F_q is negative definite up to some finite-dimensional subspace if the contrast function is strictly negative on D. In the next theorem, we show that this remains true even if we add multiple of the positive semi-definite probing operator $H_B^*H_B$ as long as the probing domain B is contained inside the scatterer D, at least when the factor in front of the probing operator is not too large. In contrast, if B is not contained within D, we show that the contrary holds.

Theorem 3.20 (Shape Characterization for Strictly Negative Contrast Functions)**.** *Let $D \subseteq \mathbb{R}^3$ be open and Lipschitz bounded such that $\mathbb{R}^3 \setminus \overline{D}$ is connected, and let $q \in \mathcal{Y}_D$. Suppose that $-\infty < q_{\min} \leq q \leq q_{\max} < 0$ for some constants $q_{\min}, q_{\max} \in \mathbb{R}$, and let $B \subseteq B_R(0)$ be open and bounded.*

(a) If $B \subseteq D$, then there exists a constant $C > 0$ such that

$$\alpha H_B^* H_B \geq_{\text{fin}} \operatorname{Re}(F_q) \qquad \text{for all } \alpha \geq C q_{\max}\,.$$

(b) If $B \not\subseteq D$, then

$$\alpha H_B^* H_B \not\geq_{\text{fin}} \operatorname{Re}(F_q) \qquad \text{for any } \alpha < 0\,.$$

Proof. Suppose that $B \subseteq D$. Applying Corollary 3.10 with $q_1 = 0$ and $q_2 = q$ we obtain a finite-dimensional subspace $V \subseteq L_t^2(S^2, \mathbb{C}^3)$ such that

$$\operatorname{Re}\Big(\int_{S^2} \boldsymbol{p} \cdot \overline{F_q \boldsymbol{p}}\, \mathrm{d}s\Big) \leq \int_D q\, |\operatorname{\mathbf{curl}} \boldsymbol{H}_{q,\boldsymbol{p}}|^2\, \mathrm{d}\boldsymbol{x} \leq q_{\max} \int_D |\operatorname{\mathbf{curl}} \boldsymbol{H}_{q,\boldsymbol{p}}|^2\, \mathrm{d}\boldsymbol{x} \qquad \text{for all } p \in V^\perp\,.$$

Furthermore, Theorem 3.18 with $q_1 = 0$, $q_2 = q$ and $\Omega = D$ shows that there exists a constant $C > 0$ such that

$$\int_D |\operatorname{\mathbf{curl}} \boldsymbol{H}_{q,\boldsymbol{p}}|^2\, \mathrm{d}\boldsymbol{x} \leq C \int_D |\operatorname{\mathbf{curl}} \boldsymbol{H}_{\boldsymbol{p}}^i|^2\, \mathrm{d}\boldsymbol{x} \qquad \text{for all } \boldsymbol{p} \in L_t^2(S^2, \mathbb{C}^3)\,.$$

Together, this gives

$$\operatorname{Re}\Big(\int_{S^2} \boldsymbol{p} \cdot \overline{F_q \boldsymbol{p}}\, \mathrm{d}s\Big) \leq C q_{\max} \int_D |\operatorname{\mathbf{curl}} \boldsymbol{H}_{\boldsymbol{p}}^i|^2\, \mathrm{d}\boldsymbol{x} \leq C q_{\max} \int_B |\operatorname{\mathbf{curl}} \boldsymbol{H}_{\boldsymbol{p}}^i|^2\, \mathrm{d}\boldsymbol{x}$$

for all $\boldsymbol{p} \in V^\perp$, since $q_{\max}$ is negative and $B \subseteq D$. In particular, using (3.56) we find that

$$\operatorname{Re}(F_q) \leq_{\text{fin}} \alpha H_B^* H_B \qquad \text{for all } \alpha \geq C q_{\max}\,,$$

and part (a) follows with Lemma 2.2.

For part (b), we assume that $B \not\subseteq D$, and that there exists $\alpha < 0$ with $\alpha H_B^* H_B \geq_{\text{fin}} \operatorname{Re}(F_q)$. This means that there exists a finite-dimensional subspace $V_1 \subseteq L_t^2(S^2, \mathbb{C}^3)$ such that

$$\alpha \int_{S^2} \boldsymbol{p} \cdot \overline{H_B^* H_B \boldsymbol{p}}\, \mathrm{d}s \geq \operatorname{Re}\Big(\int_{S^2} \boldsymbol{p} \cdot \overline{F_q \boldsymbol{p}}\, \mathrm{d}s\Big) \qquad \text{for all } \boldsymbol{p} \in V_1^\perp\,. \tag{3.57}$$

On the other hand, Theorem 3.8 with $q_1 = 0$ and $q_2 = q$ gives a finite-dimensional subspace $V_2 \subseteq L_t^2(S^2, \mathbb{C}^3)$ such that

$$\operatorname{Re}\Big(\int_{S^2} \boldsymbol{p} \cdot \overline{F_q \boldsymbol{p}}\, \mathrm{d}s\Big) \geq \int_D q\, |\operatorname{\mathbf{curl}} \boldsymbol{H}_{\boldsymbol{p}}^i|^2\, \mathrm{d}\boldsymbol{x} \geq q_{\min} \int_D |\operatorname{\mathbf{curl}} \boldsymbol{H}_{\boldsymbol{p}}^i|^2\, \mathrm{d}\boldsymbol{x} \qquad \text{for all } \boldsymbol{p} \in V_2^\perp\,. \tag{3.58}$$

Let $V := V_1 + V_2$. Then, V is finite-dimensional as well and $V^\perp \neq \{0\}$. Combining (3.57) and (3.58) with (3.56) we deduce that

$$\alpha \int_B |\operatorname{\mathbf{curl}} \boldsymbol{H}_{\boldsymbol{p}}^i|^2\, \mathrm{d}\boldsymbol{x} \geq q_{\min} \int_D |\operatorname{\mathbf{curl}} \boldsymbol{H}_{\boldsymbol{p}}^i|^2\, \mathrm{d}\boldsymbol{x} \qquad \text{for all } \boldsymbol{p} \in V^\perp\,.$$

Applying Theorem 3.15 with $q = 0$ and $\Omega = D$ guarantees the existence of a sequence $(\boldsymbol{p}_m)_{m\in\mathbb{N}} \subseteq V^\perp$ satisfying

$$\int_B |\operatorname{\mathbf{curl}} \boldsymbol{H}^i_{\boldsymbol{p}_m}|^2 \,\mathrm{d}\boldsymbol{x} \to \infty \quad \text{and} \quad \int_D |\operatorname{\mathbf{curl}} \boldsymbol{H}^i_{\boldsymbol{p}_m}|^2 \,\mathrm{d}\boldsymbol{x} \to 0 \quad \text{as } m \to \infty\,.$$

Since $\alpha < 0$, this yields a contradiction. □

The next result is analogous to Theorem 3.20, but with contrast functions that are strictly positive on D.

Theorem 3.21 (Shape Characterization for Strictly Positive Contrast Functions)**.** *Let $D \subseteq \mathbb{R}^3$ be open and Lipschitz bounded such that $\mathbb{R}^3 \setminus \overline{D}$ is connected, and let $q \in \mathcal{Y}_D$. Suppose that $0 < q_{\min} \le q \le q_{\max} < 1$ for some constants $q_{\min}, q_{\max} \in \mathbb{R}$, and let $B \subseteq \mathbb{R}^3$ be open and bounded.*

(a) If $B \subseteq D$, then

$$\alpha H_B^* H_B \le_{\text{fin}} \operatorname{Re}(F_q) \qquad \text{for all } \alpha \le q_{\min}\,.$$

(b) If $B \not\subseteq D$, then

$$\alpha H_B^* H_B \not\le_{\text{fin}} \operatorname{Re}(F_q) \qquad \text{for any } \alpha > 0\,.$$

Proof. Let $B \subseteq D$ and $\alpha \le q_{\min}$. Theorem 3.8 with $q_1 = 0$ and $q_2 = q$ guarantees the existence of a finite-dimensional subspace $V \subseteq L^2_t(S^2, \mathbb{C}^3)$ such that

$$\operatorname{Re}\Big(\int_{S^2} \boldsymbol{p} \cdot \overline{F_q \boldsymbol{p}} \,\mathrm{d}s\Big) \ge \int_D q\, |\operatorname{\mathbf{curl}} \boldsymbol{H}^i_{\boldsymbol{p}}|^2 \,\mathrm{d}\boldsymbol{x} \ge q_{\min} \int_D |\operatorname{\mathbf{curl}} \boldsymbol{H}^i_{\boldsymbol{p}}|^2 \,\mathrm{d}\boldsymbol{x} \qquad \text{for all } \boldsymbol{p} \in V^\perp\,.$$

Since $B \subseteq D$ and $q_{\min} \ge \alpha$, (3.56) yields

$$\operatorname{Re}\Big(\int_{S^2} \boldsymbol{p} \cdot \overline{F_q \boldsymbol{p}} \,\mathrm{d}s\Big) \ge \alpha \int_B |\operatorname{\mathbf{curl}} \boldsymbol{H}^i_{\boldsymbol{p}}|^2 \,\mathrm{d}\boldsymbol{x} = \alpha \int_{S^2} \boldsymbol{p} \cdot \overline{H_B^* H_B \boldsymbol{p}} \,\mathrm{d}s \qquad \text{for all } \boldsymbol{p} \in V^\perp\,.$$

Now, applying Lemma 2.2 shows part (a).

Next, we assume that $B \not\subseteq D$ and that there exists $\alpha > 0$ with $\alpha H_B^* H_B \le_{\text{fin}} \operatorname{Re}(F_q)$. The latter implies the existence of a finite-dimensional subspace $V_1 \subseteq L^2_t(S^2, \mathbb{C}^3)$ such that

$$\alpha \int_{S^2} \boldsymbol{p} \cdot \overline{H_B^* H_B \boldsymbol{p}} \,\mathrm{d}s \le \operatorname{Re}\Big(\int_{S^2} \boldsymbol{p} \cdot \overline{F_q \boldsymbol{p}} \,\mathrm{d}s\Big) \qquad \text{for all } \boldsymbol{p} \in V_1^\perp. \tag{3.59}$$

Moreover, Corollary 3.10 with $q_1 = 0$ and $q_2 = q$ shows that there is a finite-dimensional subspace $V_2 \subseteq L^2_t(S^2, \mathbb{C}^3)$ such that

$$\operatorname{Re}\Big(\int_{S^2} \boldsymbol{p} \cdot \overline{F_q \boldsymbol{p}} \,\mathrm{d}s\Big) \le \int_D q\, |\operatorname{\mathbf{curl}} \boldsymbol{H}_{q,\boldsymbol{p}}|^2 \,\mathrm{d}\boldsymbol{x} \le q_{\max} \int_D |\operatorname{\mathbf{curl}} \boldsymbol{H}_{q,\boldsymbol{p}}|^2 \,\mathrm{d}\boldsymbol{x} \qquad \text{for all } \boldsymbol{p} \in V_2^\perp. \tag{3.60}$$

We set $V := V_1 + V_2$. Then, V is finite dimensional and $V^\perp \ne \{0\}$. Combining (3.59) and (3.60) with (3.56) we obtain that

$$\alpha \int_B |\operatorname{\mathbf{curl}} \boldsymbol{H}^i_{\boldsymbol{p}}|^2 \,\mathrm{d}\boldsymbol{x} \le q_{\max} \int_D |\operatorname{\mathbf{curl}} \boldsymbol{H}_{q,\boldsymbol{p}}|^2 \,\mathrm{d}\boldsymbol{x} \qquad \text{for all } \boldsymbol{p} \in V^\perp\,.$$

To further estimate the right-hand side we use Theorem 3.18 with $q_1 = 0$, $q_2 = q$ and $\Omega = D$, and we find that

$$\alpha \int_B |\operatorname{\mathbf{curl}} \boldsymbol{H}^i_{\boldsymbol{p}}|^2 \,\mathrm{d}\boldsymbol{x} \leq C q_{\max} \int_D |\operatorname{\mathbf{curl}} \boldsymbol{H}^i_{\boldsymbol{p}}|^2 \,\mathrm{d}\boldsymbol{x} \qquad \text{for all } \boldsymbol{p} \in V^\perp$$

with some $C > 0$. However, this contradicts Theorem 3.15 with $q = 0$ and $\Omega = D$, which implies the existence of a sequence $(\boldsymbol{p}_m)_{m\in\mathbb{N}} \subseteq V^\perp$ such that

$$\int_B |\operatorname{\mathbf{curl}} \boldsymbol{H}^i_{\boldsymbol{p}_m}|^2 \,\mathrm{d}\boldsymbol{x} \to \infty \qquad \text{and} \qquad \int_D |\operatorname{\mathbf{curl}} \boldsymbol{H}^i_{\boldsymbol{p}_m}|^2 \,\mathrm{d}\boldsymbol{x} \to 0 \qquad \text{as } m \to \infty\,. \qquad \square$$

3.5. Indefinite Scattering Objects

In this section, we allow for indefinite scattering objects, i.e., for the general case when the contrast function q is neither strictly negative nor strictly positive on D. We establish a shape characterization result similar to Theorems 3.20 and 3.21 in Subsection 3.5.2 and comment on the special case when the scattering object can be separated into a part with strictly negative and a part with strictly positive contrast. As in the previous subsection, in our proofs, we make use of the monotonicity relation from Section 3.3. In addition, we exploit the existence of simultaneously localized vector wave functions extending the already established localized vector wave functions.

3.5.1. Simultaneously Localized Vector Wave Functions

To justify the shape characterization for indefinite scattering objects, we require a refined version of Theorem 3.15, where we showed the existence of localized vector wave functions. In Theorem 3.22, we not only control the energy of the total field $\boldsymbol{H}_{q,\boldsymbol{p}}$, as was done in Theorem 3.15, but also the energy of the incident field $\boldsymbol{H}^i_{\boldsymbol{p}}$. In Subsection 3.5.1, we established analogous theorems for the Helmholtz obstacle scattering problem. Furthermore, similar results have been presented for the Schrödinger equation in [HL20] and for the Helmholtz medium scattering problem in [GH21].

Theorem 3.22 (Simultaneously Localized Vector Wave Functions)**.** *Let $D \subseteq \mathbb{R}^3$ be open and Lipschitz bounded, and let $q \in \mathcal{Y}_D$ with $q|_D \in C^1(\overline{D})$. Let $E, M \subseteq \mathbb{R}^3$ be open and Lipschitz bounded such that $\operatorname{supp}(q) \subseteq \overline{E \cup M}$, $\mathbb{R}^3 \setminus \overline{M}$ is connected, and $E \cap M = \emptyset$ (see Figure 3.1 for an exemplary visualization of the geometry).*

Then, for any finite-dimensional subspace $V \subseteq L^2_t(S^2, \mathbb{C}^3)$ there exists a sequence $(\boldsymbol{p}_m)_{m\in\mathbb{N}} \subseteq V^\perp$ such that

$$\int_E |\operatorname{\mathbf{curl}} \boldsymbol{H}_{q,\boldsymbol{p}_m}|^2 \,\mathrm{d}\boldsymbol{x} \to \infty \qquad \textit{and} \qquad \int_M (|\operatorname{\mathbf{curl}} \boldsymbol{H}_{q,\boldsymbol{p}_m}|^2 + |\operatorname{\mathbf{curl}} \boldsymbol{H}^i_{\boldsymbol{p}_m}|^2) \,\mathrm{d}\boldsymbol{x} \to 0$$

as $m \to \infty$, where $\boldsymbol{H}^i_{\boldsymbol{p}_m}, \boldsymbol{H}_{q,\boldsymbol{p}_m} \in H_{\mathrm{loc}}(\mathbf{curl}; \mathbb{R}^3)$ are given by (3.20) *and* (3.21a) *with $\boldsymbol{p} = \boldsymbol{p}_m$.*

The proof of Theorem 3.22 relies on the following three lemmas. Lemma 3.23 extends the result of Lemma 3.16. The goal is to allow for more general arguments for the adjoint $L^*_{q,\Omega}$.

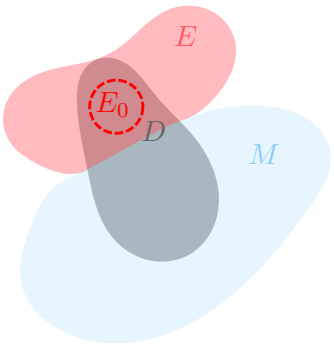

FIGURE 3.1. Visualization of an exemplary geometry from Theorem 3.22 and Lemma 3.25.

Lemma 3.23. *Suppose that $D \subseteq \mathbb{R}^3$ is open and Lipschitz bounded, let $q \in \mathcal{Y}_D$, and assume that $\Omega \subseteq \mathbb{R}^3$ is open and bounded. We define*

$$L_{q,\Omega} : L_t^2(S^2, \mathbb{C}^3) \to H(\mathbf{curl}; \Omega), \quad L_{q,\Omega}\, \boldsymbol{p} := -\frac{1}{\mathrm{i}\omega\varepsilon}\, \mathbf{curl}\, \boldsymbol{H}_{q,\boldsymbol{p}}|_\Omega = \boldsymbol{E}_{q,\boldsymbol{p}}|_\Omega . \tag{3.61}$$

Then, $L_{q,\Omega}$ is a bounded linear operator and its adjoint is given by

$$L_{q,\Omega}^* : H(\mathbf{curl}; \Omega)^* \to L_t^2(S^2, \mathbb{C}^3), \quad L_{q,\Omega}^* \boldsymbol{f} := \sqrt{\frac{\mu_0}{\varepsilon_0}}\, \mathcal{S}_q^*(\boldsymbol{\nu} \times \boldsymbol{e}^\infty), \tag{3.62}$$

where $\boldsymbol{e}^\infty \in L_t^2(S^2, \mathbb{C}^3)$ is the far field pattern of the radiating solution $\boldsymbol{e} \in H_{\mathrm{loc}}(\mathbf{curl}; \mathbb{R}^3)$ to

$$\mathbf{curl}\, \mathbf{curl}\, \boldsymbol{e} - k^2 \varepsilon_r \boldsymbol{e} = \boldsymbol{f} \qquad \text{in } \mathbb{R}^3 . \tag{3.63}$$

Proof. The well-posedness of the scattering problem (3.5)–(3.9) and the integral representation (3.21a) show that $L_{q,\Omega}$ is a bounded linear operator. Besides, the existence of a unique radiating solution $\boldsymbol{e} \in H_{\mathrm{loc}}(\mathbf{curl}; \mathbb{R}^3)$ to (3.63) follows from Remark 3.6.

Let $R > 0$ be sufficiently large such that $\overline{D \cup \Omega} \subseteq B_R(0)$. Replacing (3.41) by

$$\int_{B_R(0)} \left(\overline{\mathbf{curl}\, \boldsymbol{e}} \cdot \mathbf{curl}\, \boldsymbol{\psi} - k^2 \varepsilon_r \overline{\boldsymbol{e}} \cdot \boldsymbol{\psi} \right) \mathrm{d}\boldsymbol{x} = \langle \overline{\boldsymbol{f}}, \boldsymbol{\psi} \rangle_* + \int_{\partial B_R(0)} (\boldsymbol{\nu} \times \boldsymbol{\psi}) \cdot \overline{\mathbf{curl}\, \boldsymbol{e}}\, \mathrm{d}s$$

for any $\boldsymbol{\psi} \in H(\mathbf{curl}; B_R(0))$ we find as in (3.42) that, for any $\boldsymbol{f} \in H(\mathbf{curl}; \Omega)^*$ and $\boldsymbol{p} \in L_t^2(S^2, \mathbb{C}^3)$,

$$\begin{aligned}
\langle \overline{\boldsymbol{f}}, L_{q,\Omega} \boldsymbol{p} \rangle_* &= \langle \overline{\boldsymbol{f}}, \boldsymbol{E}_{q,\boldsymbol{p}} \rangle_* \\
&= \int_{B_R(0)} \left(\mathbf{curl}\, \boldsymbol{E}_{q,\boldsymbol{p}} \cdot \overline{\mathbf{curl}\, \boldsymbol{e}} - k^2 \varepsilon_r \boldsymbol{E}_{q,\boldsymbol{p}} \cdot \overline{\boldsymbol{e}} \right) \mathrm{d}\boldsymbol{x} - \int_{\partial B_R(0)} (\boldsymbol{\nu} \times \boldsymbol{E}_{q,\boldsymbol{p}}) \cdot \overline{\mathbf{curl}\, \boldsymbol{e}}\, \mathrm{d}s \\
&= \int_{\partial B_R(0)} \left((\boldsymbol{\nu} \times \overline{\boldsymbol{e}}) \cdot \mathbf{curl}\, \boldsymbol{E}_{\boldsymbol{p}}^i - (\boldsymbol{\nu} \times \boldsymbol{E}_{\boldsymbol{p}}^i) \cdot \overline{\mathbf{curl}\, \boldsymbol{e}} \right) \mathrm{d}s \\
&\quad + \int_{\partial B_R(0)} \left((\boldsymbol{\nu} \times \overline{\boldsymbol{e}}) \cdot \mathbf{curl}\, \boldsymbol{E}_{q,\boldsymbol{p}}^s - (\boldsymbol{\nu} \times \boldsymbol{E}_{q,\boldsymbol{p}}^s) \cdot \overline{\mathbf{curl}\, \boldsymbol{e}} \right) \mathrm{d}s .
\end{aligned}$$

Therewith, we can proceed exactly as in the proof of Lemma 3.16 to show (3.62). □

Lemma 3.24. *Let $D \subseteq \mathbb{R}^3$ be open and Lipschitz bounded, let $q \in \mathcal{Y}_D$, and assume that $E, E_0 \subseteq \mathbb{R}^3$ are open and bounded with $E_0 \subset\subset E$. Then, there exists a constant $C > 0$ such that*

$$\|L_{q,E_0}\boldsymbol{p}\|_{H(\mathbf{curl};E_0)} \leq C\|L_{q,E}\boldsymbol{p}\|_{L^2(E,\mathbb{C}^3)} \qquad \text{for all } \boldsymbol{p} \in L^2_t(S^2,\mathbb{C}^3)\,.$$

Proof. From definition (3.61), we have that $L_{q,E_0}\boldsymbol{p} = \boldsymbol{E}_{q,\boldsymbol{p}}|_{E_0}$ and $L_{q,E}\boldsymbol{p} = \boldsymbol{E}_{q,\boldsymbol{p}}|_E$, where $\boldsymbol{E}_{q,\boldsymbol{p}}$ satisfies

$$\int_{\mathbb{R}^3} (\mathbf{curl}\,\boldsymbol{E}_{q,\boldsymbol{p}} \cdot \mathbf{curl}\,\boldsymbol{\psi} - k^2\varepsilon_r \boldsymbol{E}_{q,\boldsymbol{p}} \cdot \boldsymbol{\psi})\,\mathrm{d}\boldsymbol{x} = 0 \qquad \text{for all } \boldsymbol{\psi} \in H_0(\mathbf{curl};\mathbb{R}^3)\,. \tag{3.64}$$

Let $\eta \in C^\infty(\mathbb{R}^3)$ be a smooth cutoff function with $\eta \equiv 1$ in E_0 and $\eta \equiv 0$ in $\mathbb{R}^3 \setminus \overline{E}$. We set $\boldsymbol{\psi} := \eta^2\overline{\boldsymbol{E}_{q,\boldsymbol{p}}}$ and use it as a test function in (3.64). Utilizing (B.3), this yields

$$\begin{aligned} 0 &= \int_{\mathbb{R}^3} (\mathbf{curl}\,\boldsymbol{E}_{q,\boldsymbol{p}} \cdot \mathbf{curl}(\eta^2\overline{\boldsymbol{E}_{q,\boldsymbol{p}}}) - k^2\varepsilon_r \boldsymbol{E}_{q,\boldsymbol{p}} \cdot (\eta^2\overline{\boldsymbol{E}_{q,\boldsymbol{p}}}))\,\mathrm{d}\boldsymbol{x} \\ &= \int_{\mathbb{R}^3} (\mathbf{curl}\,\boldsymbol{E}_{q,\boldsymbol{p}} \cdot (2\eta\nabla\eta \times \overline{\boldsymbol{E}_{q,\boldsymbol{p}}} + \eta^2\,\mathbf{curl}\,\overline{\boldsymbol{E}_{q,\boldsymbol{p}}}) - k^2\eta^2\varepsilon_r \boldsymbol{E}_{q,\boldsymbol{p}} \cdot \overline{\boldsymbol{E}_{q,\boldsymbol{p}}})\,\mathrm{d}\boldsymbol{x}\,. \end{aligned}$$

Since $\eta \equiv 0$ in $\mathbb{R}^3 \setminus \overline{E}$, we obtain

$$\int_{\mathbb{R}^3} \eta^2 |\,\mathbf{curl}\,\boldsymbol{E}_{q,\boldsymbol{p}}|^2\,\mathrm{d}\boldsymbol{x} = 2\int_E \eta\,\mathbf{curl}\,\boldsymbol{E}_{q,\boldsymbol{p}} \cdot (\overline{\boldsymbol{E}_{q,\boldsymbol{p}}} \times \nabla\eta)\,\mathrm{d}\boldsymbol{x} + k^2\int_E \varepsilon_r\eta^2|\boldsymbol{E}_{q,\boldsymbol{p}}|^2\,\mathrm{d}\boldsymbol{x}\,. \tag{3.65}$$

Utilizing the Cauchy-Schwarz inequality and the arithmetic-geometric mean inequality, we estimate

$$\begin{aligned} 2\int_E \eta\,\mathbf{curl}\,\boldsymbol{E}_{q,\boldsymbol{p}} \cdot (\overline{\boldsymbol{E}_{q,\boldsymbol{p}}} \times \nabla\eta)\,\mathrm{d}\boldsymbol{x} &\leq 2\|\eta\,\mathbf{curl}\,\boldsymbol{E}_{q,\boldsymbol{p}}\|_{L^2(E,\mathbb{C}^3)}\|\boldsymbol{E}_{q,\boldsymbol{p}} \times \nabla\eta\|_{L^2(E,\mathbb{C}^3)} \\ &\leq \delta\|\eta\,\mathbf{curl}\,\boldsymbol{E}_{q,\boldsymbol{p}}\|^2_{L^2(E,\mathbb{C}^3)} + \frac{1}{\delta}\|\boldsymbol{E}_{q,\boldsymbol{p}} \times \nabla\eta\|^2_{L^2(E,\mathbb{C}^3)} \end{aligned}$$

for any $\delta > 0$. Plugging this into (3.65) yields

$$\begin{aligned} &\int_{\mathbb{R}^3} \eta^2 |\,\mathbf{curl}\,\boldsymbol{E}_{q,\boldsymbol{p}}|^2\,\mathrm{d}\boldsymbol{x} \\ &\leq \delta\int_E \eta^2 |\,\mathbf{curl}\,\boldsymbol{E}_{q,\boldsymbol{p}}|^2\,\mathrm{d}\boldsymbol{x} + \frac{1}{\delta}\int_E |\boldsymbol{E}_{q,\boldsymbol{p}}|^2|\nabla\eta|^2\,\mathrm{d}\boldsymbol{x} + k^2\|\varepsilon_r\|_{L^\infty(\mathbb{R}^3)}\int_E |\boldsymbol{E}_{q,\boldsymbol{p}}|^2\,\mathrm{d}\boldsymbol{x} \\ &\leq \delta\int_{\mathbb{R}^3} \eta^2 |\,\mathbf{curl}\,\boldsymbol{E}_{q,\boldsymbol{p}}|^2\,\mathrm{d}\boldsymbol{x} + \frac{c_1}{\delta}\int_E |\boldsymbol{E}_{q,\boldsymbol{p}}|^2\,\mathrm{d}\boldsymbol{x} + k^2\|\varepsilon_r\|_{L^\infty(\mathbb{R}^3)}\int_E |\boldsymbol{E}_{q,\boldsymbol{p}}|^2\,\mathrm{d}\boldsymbol{x}\,, \end{aligned}$$

where $c_1 > 0$ is a constant. As $\eta \equiv 1$ in E_0, this implies that

$$\begin{aligned} (1-\delta)\int_{E_0} |\,\mathbf{curl}\,\boldsymbol{E}_{q,\boldsymbol{p}}|^2\,\mathrm{d}\boldsymbol{x} = (1-\delta)\int_{E_0} \eta^2 |\,\mathbf{curl}\,\boldsymbol{E}_{q,\boldsymbol{p}}|^2\,\mathrm{d}\boldsymbol{x} &\leq (1-\delta)\int_{\mathbb{R}^3} \eta^2 |\,\mathbf{curl}\,\boldsymbol{E}_{q,\boldsymbol{p}}|^2\,\mathrm{d}\boldsymbol{x} \\ &\leq \Big(\frac{c_1}{\delta} + k^2\|\varepsilon_r\|_{L^\infty(\mathbb{R}^3)}\Big)\int_E |\boldsymbol{E}_{q,\boldsymbol{p}}|^2\,\mathrm{d}\boldsymbol{x}\,. \end{aligned}$$

We choose $\delta = 1/2$ and find that

$$\frac{1}{2}\int_{E_0} |\operatorname{\mathbf{curl}} \boldsymbol{E}_{q,\boldsymbol{p}}|^2 \,\mathrm{d}\boldsymbol{x} \leq (2c_1 + k^2\|\varepsilon_r\|_{L^\infty(\mathbb{R}^3)}) \int_E |\boldsymbol{E}_{q,\boldsymbol{p}}|^2 \,\mathrm{d}\boldsymbol{x}\,,$$

and thus,

$$\|\operatorname{\mathbf{curl}} \boldsymbol{E}_{q,\boldsymbol{p}}\|^2_{L^2(E_0,\mathbb{C}^3)} \leq c_2 \|\boldsymbol{E}_{q,\boldsymbol{p}}\|^2_{L^2(E,\mathbb{C}^3)}$$

for some constant $c_2 > 0$. Since $E_0 \subset\subset E$, we arrive at

$$\|\boldsymbol{E}_{q,\boldsymbol{p}}\|^2_{H(\mathbf{curl};E_0)} = \|\operatorname{\mathbf{curl}} \boldsymbol{E}_{q,\boldsymbol{p}}\|^2_{L^2(E_0,\mathbb{C}^3)} + \|\boldsymbol{E}_{q,\boldsymbol{p}}\|^2_{L^2(E_0,\mathbb{C}^3)} \leq (c_2+1)\|\boldsymbol{E}_{q,\boldsymbol{p}}\|^2_{L^2(E,\mathbb{C}^3)}\,.$$

Finally, the assertion follows by setting $C := \sqrt{c_2+1}$. □

Lemma 3.25. *Let $D \subseteq \mathbb{R}^3$ be open and Lipschitz bounded, and let $q \in \mathcal{Y}_D$ with $q|_D \in C^1(\overline{D})$. Let $E, M \subseteq \mathbb{R}^3$ be open and Lipschitz bounded such that $\operatorname{supp}(q) \subseteq \overline{E \cup M}$, $\mathbb{R}^3 \setminus \overline{M}$ is connected, and $E \cap M = \emptyset$. Assume furthermore that $E_0 \subseteq \mathbb{R}^3$ is a sufficiently small ball such that $E_0 \subset\subset E$ (see Figure 3.1 for an exemplary visualization of the geometry). Then,*

$$\mathcal{R}(L^*_{q,E_0}) \not\subseteq \mathcal{R}\Big(\begin{bmatrix} L^*_{q,M} & L^*_{0,M}\end{bmatrix}\Big)\,,$$

and there exists an infinite-dimensional subspace $Z \subseteq \mathcal{R}(L^*_{q,E_0})$ such that

$$Z \cap \mathcal{R}\Big(\begin{bmatrix} L^*_{q,M} & L^*_{0,M}\end{bmatrix}\Big) = \{0\}\,.$$

Proof. Let $\boldsymbol{h} \in \mathcal{R}(L^*_{q,E_0}) \cap \mathcal{R}([L^*_{q,M}\ L^*_{0,M}])$. Lemma 3.23 shows that there are $\boldsymbol{f}_{q,E_0} \in H(\mathbf{curl}; E_0)^*$ and $\boldsymbol{f}_{q,M}, \boldsymbol{f}_{0,M} \in H(\mathbf{curl}; M)^*$ such that the far field patterns $\boldsymbol{e}^\infty_{q,E_0}, \boldsymbol{e}^\infty_{q,M}, \boldsymbol{e}^\infty_{0,M}$ of the radiating solutions $\boldsymbol{e}_{q,E_0}, \boldsymbol{e}_{q,M}, \boldsymbol{e}_{0,M} \in H_{\mathrm{loc}}(\mathbf{curl}; \mathbb{R}^3)$ to

$$\begin{aligned}
\operatorname{\mathbf{curl}}\operatorname{\mathbf{curl}} \boldsymbol{e}_{q,E_0} - k^2\varepsilon_r \boldsymbol{e}_{q,E_0} &= \boldsymbol{f}_{q,E_0} && \text{in } \mathbb{R}^3\,,\\
\operatorname{\mathbf{curl}}\operatorname{\mathbf{curl}} \boldsymbol{e}_{q,M} - k^2\varepsilon_r \boldsymbol{e}_{q,M} &= \boldsymbol{f}_{q,M} && \text{in } \mathbb{R}^3\,,\\
\operatorname{\mathbf{curl}}\operatorname{\mathbf{curl}} \boldsymbol{e}_{0,M} - k^2 \boldsymbol{e}_{0,M} &= \boldsymbol{f}_{0,M} && \text{in } \mathbb{R}^3
\end{aligned}$$

satisfy

$$\sqrt{\frac{\varepsilon_0}{\mu_0}}\boldsymbol{h} = \mathcal{S}^*_q(\boldsymbol{\nu} \times \boldsymbol{e}^\infty_{q,E_0}) = \mathcal{S}^*_q(\boldsymbol{\nu} \times \boldsymbol{e}^\infty_{q,M}) + \boldsymbol{\nu} \times \boldsymbol{e}^\infty_{0,M}\,.$$

Here, we used that $\mathcal{S}_0$ is the identity operator. Recalling the definition of the scattering operator in (3.19) and utilizing its unitarity, we find that

$$\begin{aligned}
0 &= \boldsymbol{\nu} \times \boldsymbol{e}^\infty_{q,E_0} - \boldsymbol{\nu} \times \boldsymbol{e}^\infty_{q,M} - \mathcal{S}_q(\boldsymbol{\nu} \times \boldsymbol{e}^\infty_{0,M})\\
&= \boldsymbol{\nu} \times \boldsymbol{e}^\infty_{q,E_0} - \boldsymbol{\nu} \times \boldsymbol{e}^\infty_{q,M} - \boldsymbol{\nu} \times \boldsymbol{e}^\infty_{0,M} - \frac{\mathrm{i}k}{8\pi^2} F_q \boldsymbol{e}^\infty_{0,M}\,.
\end{aligned}$$

The definition of the far field operator in (3.18) together with our notation from (3.21c) and

Lemma 3.2 imply that

$$\frac{\mathrm{i}k}{8\pi^2} F_q \boldsymbol{e}^\infty_{0,M} \;=\; \frac{\mathrm{i}k}{8\pi^2} \boldsymbol{H}^\infty_{q,\boldsymbol{e}^\infty_{0,M}} \;=\; \sqrt{\frac{\varepsilon_0}{\mu_0}} \frac{\mathrm{i}k}{8\pi^2} \boldsymbol{\nu} \times \boldsymbol{E}^\infty_{q,\boldsymbol{e}^\infty_{0,M}} \;=\; \boldsymbol{\nu} \times \boldsymbol{E}^\infty_{q,\boldsymbol{p}}\,,$$

where $\boldsymbol{p} = \sqrt{\frac{\varepsilon_0}{\mu_0}} \frac{\mathrm{i}k}{8\pi^2} \boldsymbol{e}^\infty_{0,M}$. Consequently, $\boldsymbol{E}^\infty_{q,\boldsymbol{p}}$ is the far field pattern of the radiating solution $\boldsymbol{E}^s_{q,\boldsymbol{p}} \in H_{\mathrm{loc}}(\mathbf{curl}; \mathbb{R}^3)$ to

$$\mathbf{curl}\,\mathbf{curl}\, \boldsymbol{E}^s_{q,\boldsymbol{p}} - k^2 \varepsilon_r \boldsymbol{E}^s_{q,\boldsymbol{p}} \;=\; -k^2(1-\varepsilon_r)\boldsymbol{E}^i_{\boldsymbol{p}} \qquad \text{in } \mathbb{R}^3\,.$$

Accordingly,

$$0 \;=\; \boldsymbol{\nu} \times \boldsymbol{e}^\infty_{q,E_0} - (\boldsymbol{\nu} \times \boldsymbol{e}^\infty_{q,M} + \boldsymbol{\nu} \times \boldsymbol{e}^\infty_{0,M} + \boldsymbol{\nu} \times \boldsymbol{E}^\infty_{q,\boldsymbol{p}})\,.$$

Since $q \in \mathcal{Y}_D$ and $\mathbb{R}^3 \setminus (\overline{E_0 \cup M})$ is connected, Rellich's lemma 3.3 and the unique continuation principle in Theorem 3.4 guarantee that

$$\boldsymbol{e}_{q,E_0} - (\boldsymbol{e}_{q,M} + \boldsymbol{e}_{0,M} + \boldsymbol{E}^s_{q,\boldsymbol{p}}) \;=\; 0 \qquad \text{in } \mathbb{R}^3 \setminus (\overline{E_0 \cup M})\,. \tag{3.66}$$

Let $\Gamma := \partial E_0$. As E_0 is a ball, its boundary Γ is smooth. Next, we discuss the regularity of the traces of $\boldsymbol{\nu} \times \boldsymbol{e}_{q,E_0}|_\Gamma = \boldsymbol{\nu} \times (\boldsymbol{e}_{q,M} + \boldsymbol{e}_{0,M} + \boldsymbol{E}^s_{q,\boldsymbol{p}})|_\Gamma$ at Γ. By construction, we may assume that Γ is bounded away from $\overline{M}$. Since $\operatorname{supp}(\boldsymbol{f}_{q,M} + \boldsymbol{f}_{0,M}) \subseteq \overline{M}$, regularity results for time-harmonic Maxwell's equations from [Web81] show that any point $\boldsymbol{x} \in \Gamma$ possesses an open neighborhood $U \subseteq \mathbb{R}^3$ such that $(\boldsymbol{e}_{q,M} + \boldsymbol{e}_{0,M} + \boldsymbol{E}_{q,\boldsymbol{p}})|_{E_0 \cap U} \in H^2(E_0 \cap U, \mathbb{C}^3)$ and $(\boldsymbol{e}_{q,M} + \boldsymbol{e}_{0,M} + \boldsymbol{E}_{q,\boldsymbol{p}})|_{U \setminus \overline{E_0}} \in H^2(U \setminus \overline{E_0}, \mathbb{C}^3)$. Thus, applying the trace operator on $H^2(U \setminus \overline{E_0}, \mathbb{C}^3)$ and taking the cross product with $\boldsymbol{\nu} \in C^\infty(\Gamma, \mathbb{R}^3)$, we find that

$$\boldsymbol{\nu} \times (\boldsymbol{e}_{q,M} + \boldsymbol{e}_{0,M} + \boldsymbol{E}_{q,\boldsymbol{p}})|_\Gamma \in H^{3/2}_t(\Gamma \cap U, \mathbb{C}^3)$$

(see, e.g., [Gri11, p. 21]). Since $\boldsymbol{x} \in \Gamma$ is arbitrary and $\boldsymbol{E}^i_{\boldsymbol{p}} = \boldsymbol{E}_{q,\boldsymbol{p}} - \boldsymbol{E}^s_{q,\boldsymbol{p}}$ is smooth throughout $\mathbb{R}^3$ by Remark 3.1, this implies that $\boldsymbol{\nu} \times (\boldsymbol{e}_{q,M} + \boldsymbol{e}_{0,M} + \boldsymbol{E}^s_{q,\boldsymbol{p}})|_\Gamma \in H^{3/2}_t(\Gamma, \mathbb{C}^3)$. Inserting identity (3.66) we find that

$$\boldsymbol{\nu} \times \boldsymbol{e}_{q,E_0}|_\Gamma \;=\; \boldsymbol{\nu} \times (\boldsymbol{e}_{q,M} + \boldsymbol{e}_{0,M} + \boldsymbol{E}^s_{q,\boldsymbol{p}})|_\Gamma \;\in\; H^{3/2}_t(\Gamma, \mathbb{C}^3)\,.$$

To prove the lemma, we will construct a sufficiently large class of sources $\boldsymbol{f} \in H(\mathbf{curl}; E_0)^*$ such that $L^*_{q,E_0}\boldsymbol{f} \notin \mathcal{R}([L^*_{q,M} \quad L^*_{0,M}])$. Let $\boldsymbol{g} \in H^{-1/2}(\mathrm{Div}; \Gamma)$. Moreover, let $\boldsymbol{U}^+ \in H_{\mathrm{loc}}(\mathbf{curl}; \mathbb{R}^3 \setminus \overline{E_0})$ be the unique radiating solution to the exterior boundary problem

$$\mathbf{curl}\,\mathbf{curl}\, \boldsymbol{U}^+ - k^2 \varepsilon_r \boldsymbol{U}^+ \;=\; 0 \quad \text{in } \mathbb{R}^3 \setminus \overline{E_0}\,, \qquad \boldsymbol{\nu} \times \boldsymbol{U}^+ \;=\; \boldsymbol{g} \quad \text{on } \Gamma \tag{3.67}$$

(see, e.g., [KH15, Thm. 5.64]). Similarly, we define $\boldsymbol{U}^- \in H(\mathbf{curl}; E_0)$ as the unique solution to the interior boundary value problem

$$\mathbf{curl}\,\mathbf{curl}\, \boldsymbol{U}^- - k^2(\varepsilon_r + \mathrm{i})\boldsymbol{U}^- \;=\; 0 \quad \text{in } E_0\,, \qquad \boldsymbol{\nu} \times \boldsymbol{U}^- \;=\; \boldsymbol{g} \quad \text{on } \Gamma \tag{3.68}$$

(see, e.g., [KH15, Thm. 4.41]). Here, we added i to ε_r in order to avoid interior eigenvalues.

Therewith, we define $\boldsymbol{U} \in L^2_{\mathrm{loc}}(\mathbb{R}^3, \mathbb{C}^3) \subseteq H(\mathbf{curl}; \mathbb{R}^3)$ by

$$\boldsymbol{U} := \begin{cases} \boldsymbol{U}^- & \text{in } E_0\,, \\ \boldsymbol{U}^+ & \text{in } \mathbb{R}^3 \setminus \overline{E_0}\,, \end{cases}$$

and $\boldsymbol{f} \in H(\mathbf{curl}; E_0)^*$ by

$$\boldsymbol{f} := \mathrm{i}k^2 \boldsymbol{U}^- + \pi_t^*(\boldsymbol{\nu} \times \mathbf{curl}\, \boldsymbol{U}^+|_\Gamma - \boldsymbol{\nu} \times \mathbf{curl}\, \boldsymbol{U}^-|_\Gamma)\,,$$

where $\pi_t^* : H^{-1/2}(\mathrm{Div}; \Gamma) \to H(\mathbf{curl}; E_0)^*$ denotes the adjoint of the interior tangential trace operator π_t from (3.3). As $\boldsymbol{\nu} \times \boldsymbol{U}^+ = \boldsymbol{\nu} \times \boldsymbol{U}^-$ on the boundary Γ, we have $\boldsymbol{U} \in H_{\mathrm{loc}}(\mathbf{curl}; \mathbb{R}^3)$ (see, e.g., [Mon03, Lem. 5.3]). Utilizing the variational formulations of (3.67)–(3.68) we calculate, for all $\boldsymbol{\psi} \in H_0(\mathbf{curl}; \mathbb{R}^3)$,

$$\begin{aligned}
&\int_{\mathbb{R}^3} (\mathbf{curl}\, \boldsymbol{U} \cdot \mathbf{curl}\, \boldsymbol{\psi} - k^2 \varepsilon_r \boldsymbol{U} \cdot \boldsymbol{\psi})\, \mathrm{d}\boldsymbol{x} \\
&= \int_{\mathbb{R}^3 \setminus \overline{E_0}} (\mathbf{curl}\, \boldsymbol{U}^+ \cdot \mathbf{curl}\, \boldsymbol{\psi} - k^2 \varepsilon_r \boldsymbol{U}^+ \cdot \boldsymbol{\psi})\, \mathrm{d}\boldsymbol{x} + \int_{E_0} (\mathbf{curl}\, \boldsymbol{U}^- \cdot \mathbf{curl}\, \boldsymbol{\psi} - k^2 \varepsilon_r \boldsymbol{U}^- \cdot \boldsymbol{\psi})\, \mathrm{d}\boldsymbol{x} \\
&= \int_\Gamma (\boldsymbol{\nu} \times \mathbf{curl}\, \boldsymbol{U}^+) \cdot \pi_t(\boldsymbol{\psi})\, \mathrm{d}s - \int_\Gamma (\boldsymbol{\nu} \times \mathbf{curl}\, \boldsymbol{U}^-) \cdot \pi_t(\boldsymbol{\psi})\, \mathrm{d}s + \int_{E_0} \mathrm{i}k^2 \boldsymbol{U}^- \cdot \boldsymbol{\psi}\, \mathrm{d}\boldsymbol{x} \\
&= \int_{E_0} \Big(\mathrm{i}k^2 \boldsymbol{U}^- + \pi_t^*(\boldsymbol{\nu} \times \mathbf{curl}\, \boldsymbol{U}^+|_\Gamma - \boldsymbol{\nu} \times \mathbf{curl}\, \boldsymbol{U}^-|_\Gamma) \Big) \cdot \boldsymbol{\psi}\, \mathrm{d}\boldsymbol{x}\,.
\end{aligned}$$

This shows that

$$\mathbf{curl}\, \mathbf{curl}\, \boldsymbol{U} - k^2 \varepsilon_r \boldsymbol{U} \;=\; \boldsymbol{f} \quad \text{in } \mathbb{R}^3\,.$$

Accordingly, $L^*_{q,E_0} \boldsymbol{f} = \sqrt{\frac{\mu_0}{\varepsilon_0}}\, \mathcal{S}_q^*(\boldsymbol{\nu} \times \boldsymbol{U}^\infty)$, where $\boldsymbol{U}^\infty \in L^2_t(S^2, \mathbb{C}^3)$ coincides with the far field of the radiating solution $\boldsymbol{U}^+$ to the exterior boundary value problem (3.67). If $\boldsymbol{g} \notin H^{3/2}_t(\Gamma, \mathbb{C}^3)$, then $L^*_{q,E_0} \boldsymbol{f} \notin \mathcal{R}([L^*_{q,M}\ L^*_{0,M}])$. Otherwise the first part of the proof (with $\boldsymbol{f}$ and $\boldsymbol{U}$ playing the roles of $\boldsymbol{f}_{q,E_0}$ and $\boldsymbol{e}_{q,E_0}$) would imply that $\boldsymbol{g} = \boldsymbol{\nu} \times \boldsymbol{U}|_\Gamma \in H^{3/2}_t(\Gamma, \mathbb{C}^3)$, which is a contradiction.

Now, let $\boldsymbol{X} \subseteq H^{-1/2}(\mathrm{Div}; \Gamma)$ be the infinite-dimensional subspace that we constructed in Lemma A.2. Then, it holds $\boldsymbol{X} \cap H^{3/2}_t(\Gamma, \mathbb{C}^3) = \{0\}$. We define $G_{E_0} : H^{-1/2}(\mathrm{Div}; \Gamma) \to L^2_t(S^2, \mathbb{C}^3)$ as the operator that maps $\boldsymbol{g} \in H^{-1/2}(\mathrm{Div}; \Gamma)$ to $\boldsymbol{\nu} \times \boldsymbol{U}^\infty$, where $\boldsymbol{U}^\infty$ is the far field pattern of the radiating solution $\boldsymbol{U}^+$ of the exterior boundary value problem (3.67). Eventually, Rellich's lemma 3.3 and the unique continuation principle in Theorem 3.4 show that G_{E_0} is one-to-one, and thus

$$Z := \sqrt{\frac{\mu_0}{\varepsilon_0}}\, \mathcal{S}_q^* G_{E_0}(\boldsymbol{X}) \subseteq L^2_t(S^2, \mathbb{C}^3)$$

is an infinite-dimensional subspace as well. Furthermore, we have just shown that

$$Z \subseteq \mathcal{R}(L^*_{q,E_0}) \qquad \text{and} \qquad Z \cap \mathcal{R}\Big(\begin{bmatrix} L^*_{q,M} & L^*_{0,M} \end{bmatrix}\Big) \;=\; \{0\}\,. \qquad \square$$

At this point, we give the proof of Theorem 3.22.

Proof of Theorem 3.22. Let $V \subseteq L^2_t(S^2, \mathbb{C}^3)$ be a finite-dimensional subspace. We denote by $P_V : L^2_t(S^2, \mathbb{C}^3) \to L^2_t(S^2, \mathbb{C}^3)$ the orthogonal projection on V. Assume that $E_0 \subseteq \mathbb{R}^3$ is a

sufficiently small ball such that $E_0 \subset\subset E$. Combining Lemma 3.25 with the dimensionality argument from Lemma 2.23 shows that

$$Z \not\subseteq \mathcal{R}\Big(\begin{bmatrix} L_{q,M}^* & L_{0,M}^* \end{bmatrix}\Big) + V = \mathcal{R}\Big(\begin{bmatrix} L_{q,M}^* & L_{0,M}^* & P_V \end{bmatrix}\Big),$$

where $Z \subseteq \mathcal{R}(L_{q,E_0}^*)$ denotes the infinite-dimensional subspace in Lemma 3.25. Thus,

$$\mathcal{R}(L_{q,E_0}^*) \not\subseteq \mathcal{R}\Big(\begin{bmatrix} L_{q,M}^* & L_{0,M}^* & P_V \end{bmatrix}\Big),$$

and accordingly, Lemma 2.21 implies that there is no constant $C > 0$ such that

$$\begin{aligned} \|L_{q,E_0}\boldsymbol{p}\|_{H(\mathbf{curl};E_0)}^2 &\leq C^2 \left\| \begin{bmatrix} L_{q,M} \\ L_{0,M} \\ P_V \end{bmatrix} \boldsymbol{p} \right\|_{H(\mathbf{curl};M)\times H(\mathbf{curl};M)\times L_t^2(S^2,\mathbb{C}^3)}^2 \\ &= C^2\big(\|L_{q,M}\boldsymbol{p}\|_{H(\mathbf{curl};M)}^2 + \|L_{0,M}\boldsymbol{p}\|_{H(\mathbf{curl};M)}^2 + \|P_V\boldsymbol{p}\|_{L_t^2(S^2,\mathbb{C}^3)}^2\big) \end{aligned}$$

for all $\boldsymbol{p} \in L_t^2(S^2,\mathbb{C}^3)$. Hence, there exists a sequence $(\widetilde{\boldsymbol{p}}_m)_{m\in\mathbb{N}} \subseteq L_t^2(S^2,\mathbb{C}^3)$ such that

$$\|L_{q,E_0}\widetilde{\boldsymbol{p}}_m\|_{H(\mathbf{curl};E_0)}^2 \to \infty$$

and

$$\|L_{q,M}\widetilde{\boldsymbol{p}}_m\|_{H(\mathbf{curl};M)}^2 + \|L_{0,M}\widetilde{\boldsymbol{p}}_m\|_{H(\mathbf{curl};M)}^2 + \|P_V\widetilde{\boldsymbol{p}}_m\|_{L_t^2(S^2,\mathbb{C}^3)}^2 \to 0$$

as $m \to \infty$. From Lemma 3.24, it follows that

$$\|L_{q,E}\widetilde{\boldsymbol{p}}_m\|_{L^2(E,\mathbb{C}^3)}^2 \to \infty,$$

and the definition (3.1) of the inner product in $H(\mathbf{curl};M)$ implies that

$$\|L_{q,M}\widetilde{\boldsymbol{p}}_m\|_{L^2(M,\mathbb{C}^3)}^2 + \|L_{0,M}\widetilde{\boldsymbol{p}}_m\|_{L^2(M,\mathbb{C}^3)}^2 + \|P_V\widetilde{\boldsymbol{p}}_m\|_{L_t^2(S^2,\mathbb{C}^3)}^2 \to 0$$

as $m \to \infty$. Setting $\boldsymbol{p}_m := \widetilde{\boldsymbol{p}}_m - P_V\widetilde{\boldsymbol{p}}_m \in V^\perp \subseteq L_t^2(S^2,\mathbb{C}^3)$ for any $m \in \mathbb{N}$, we finally obtain

$$\begin{aligned} \|L_{q,E}\boldsymbol{p}_m\|_{L^2(E,\mathbb{C}^3)} &\geq \big|\|L_{q,E}\widetilde{\boldsymbol{p}}_m\|_{L^2(E,\mathbb{C}^3))} - \|L_{q,E}P_V\widetilde{\boldsymbol{p}}_m\|_{L^2(E,\mathbb{C}^3)}\big| \\ &\geq \|L_{q,E}\widetilde{\boldsymbol{p}}_m\|_{L^2(E,\mathbb{C}^3)} - \|L_{q,E}\|\|P_V\widetilde{\boldsymbol{p}}_m\|_{L_t^2(S^2,\mathbb{C}^3)} \to \infty, \\ \|L_{q,M}\boldsymbol{p}_m\|_{L^2(M,\mathbb{C}^3)} + \|L_{0,M}\boldsymbol{p}_m\|_{L^2(M,\mathbb{C}^3)} &\leq \|L_{q,M}\widetilde{\boldsymbol{p}}_m\|_{L^2(M,\mathbb{C}^3)} + \|L_{0,M}\widetilde{\boldsymbol{p}}_m\|_{L^2(M,\mathbb{C}^3)} \\ &\quad + (\|L_{q,M}\| + \|L_{0,M}\|)\|P_V\widetilde{\boldsymbol{p}}_m\|_{L_t^2(S^2,\mathbb{C}^3)} \to 0 \end{aligned}$$

as $m \to \infty$. Recalling that $L_{q,E}\boldsymbol{p}_m = -\frac{1}{\mathrm{i}\omega\varepsilon}\,\mathbf{curl}\,\boldsymbol{H}_{q,\boldsymbol{p}_m}|_E$, $L_{q,M}\boldsymbol{p}_m = -\frac{1}{\mathrm{i}\omega\varepsilon}\,\mathbf{curl}\,\boldsymbol{H}_{q,\boldsymbol{p}_m}|_M$ and $L_{0,M}\boldsymbol{p}_m = -\frac{1}{\mathrm{i}\omega\varepsilon_0}\,\mathbf{curl}\,\boldsymbol{H}^i_{\boldsymbol{p}_m}|_M$, it follows that

$$\int_E |L_{q,E}\boldsymbol{p}_m|^2 \,\mathrm{d}\boldsymbol{x} = \int_E \frac{1}{\omega^2\varepsilon^2}|\,\mathbf{curl}\,\boldsymbol{H}_{q,\boldsymbol{p}_m}|^2 \,\mathrm{d}\boldsymbol{x} \leq \frac{1}{\omega^2}\Big\|\frac{1}{\varepsilon^2}\Big\|_{L^\infty(\mathbb{R}^3)} \int_E |\,\mathbf{curl}\,\boldsymbol{H}_{q,\boldsymbol{p}_m}|^2 \,\mathrm{d}\boldsymbol{x}$$

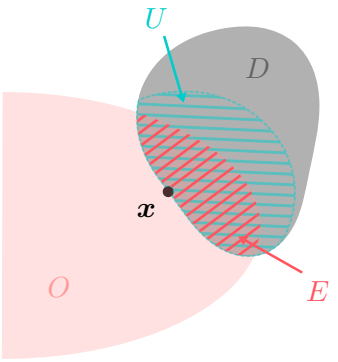

FIGURE 3.2. Visualization of an exemplary geometry from Theorem 3.26.

and

$$\int_M (|L_{q,m}\boldsymbol{p}_m|^2 + |L_{0,m}\boldsymbol{p}_m|^2)\,\mathrm{d}\boldsymbol{x} = \int_M \frac{1}{\omega^2\varepsilon^2}|\operatorname{\mathbf{curl}} \boldsymbol{H}_{q,\boldsymbol{p}_m}|^2\,\mathrm{d}\boldsymbol{x} + \int_M \frac{1}{\omega^2\varepsilon_0^2}|\operatorname{\mathbf{curl}} \boldsymbol{H}^i_{\boldsymbol{p}_m}|^2\,\mathrm{d}\boldsymbol{x}$$
$$\geq \frac{1}{\omega^2}\min\{\operatorname{ess\,inf}\frac{1}{\varepsilon^2}, \frac{1}{\varepsilon_0^2}\}\int_M (|\operatorname{\mathbf{curl}} \boldsymbol{H}_{q,\boldsymbol{p}_m}|^2 + |\operatorname{\mathbf{curl}} \boldsymbol{H}^i_{\boldsymbol{p}_m}|^2)\,\mathrm{d}\boldsymbol{x}\,.$$

This ends the proof. □

3.5.2. MONOTONICITY-BASED SHAPE RECONSTRUCTION

In this subsection, we develop a rigorous shape characterization for indefinite scattering objects in terms of the far field operator F_q and the probing operator $H_B^* H_B$ corresponding to a probing domain B. While the criteria that we presented in Theorems 3.20 and 3.21 determine whether the probing domain B is contained inside the scattering object D or not, the criterion in Theorem 3.26 characterizes whether a certain probing domain B contains the scatterer D or not.

Theorem 3.26 (Shape Characterization for Indefinite Contrast Functions)**.** *Let $D \subseteq \mathbb{R}^3$ be open and Lipschitz bounded and $\mathbb{R}^3 \setminus \overline{D}$ be connected. Let $q \in \mathcal{Y}_D$ with $q|_D \in C^1(\overline{D})$, and suppose that $-\infty < q_{\min} \leq q \leq q_{\max} < 1$ on D for some constants $q_{\min}, q_{\max} \in \mathbb{R}$. Furthermore, we assume that for any point $\boldsymbol{x} \in \partial D$ on the boundary of D, and for any neighborhood $U \subseteq \overline{D}$ of $\boldsymbol{x}$ in $\overline{D}$, there exists a connected unbounded domain $O \subseteq \mathbb{R}^3$ with $\emptyset \neq E := O \cap D \subseteq U$ such that*

$$q|_E \leq q_{\max,E} < 0 \qquad \text{or} \qquad q|_E \geq q_{\min,E} > 0 \tag{3.69}$$

for some constants $q_{\min,E}, q_{\max,E} \in \mathbb{R}$ (see Figure 3.2 for an exemplary visualization of the geometry).

Let $B \subseteq \mathbb{R}^3$ be open such that $\mathbb{R}^3 \setminus \overline{B}$ is connected, and let $H_B^* H_B$ denote the corresponding probing operator from (3.55)*.*

(a) If $D \subseteq B$, then there exists a constant $C > 0$ such that

$$\alpha H_B^* H_B \leq_{\text{fin}} \operatorname{Re}(F_q) \leq_{\text{fin}} \beta H_B^* H_B \tag{3.70}$$

for all $\alpha \leq \min\{0, q_{\min}\}$, $\beta \geq \max\{0, Cq_{\max}\}$

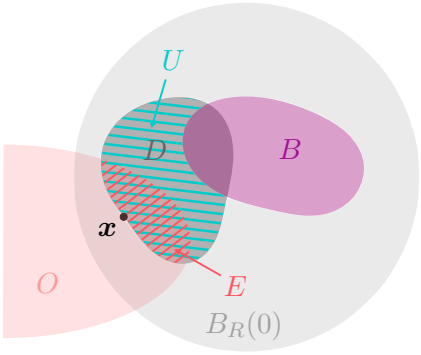

Figure 3.3. Visualization of an exemplary geometry from the proof of Theorem 3.26 (b).

(b) If $D \not\subseteq B$, then

$$\alpha H_B^* H_B \not\leq_{\text{fin}} \operatorname{Re}(F_q) \quad \textit{for any } \alpha \in \mathbb{R} \tag{3.71a}$$

or

$$\operatorname{Re}(F_q) \not\leq_{\text{fin}} \beta H_B^* H_B \quad \textit{for any } \beta \in \mathbb{R}\,. \tag{3.71b}$$

Proof. Let $D \subseteq B$. Using Corollary 3.10 with $q_1 = 0$ and $q_2 = q$ we find that there is a finite-dimensional subspace $V_1 \subseteq L_t^2(S^2, \mathbb{C}^3)$ such that, for all $\boldsymbol{p} \in V_1^\perp$,

$$\operatorname{Re}\Big(\int_{S^2} \boldsymbol{p} \cdot \overline{F_q \boldsymbol{p}}\, \mathrm{d}s\Big) \leq \int_D q |\operatorname{\mathbf{curl}} \boldsymbol{H}_{q,\boldsymbol{p}}|^2 \,\mathrm{d}\boldsymbol{x} \leq q_{\max} \int_D |\operatorname{\mathbf{curl}} \boldsymbol{H}_{q,\boldsymbol{p}}|^2 \,\mathrm{d}\boldsymbol{x}\,.$$

To further estimate we apply Theorem 3.18 with $q_1 = 0$, $q_2 = q$ and $\Omega = D$, and we obtain that there exists a constant $C > 0$ such that

$$\operatorname{Re}\Big(\int_{S^2} \boldsymbol{p} \cdot \overline{F_q \boldsymbol{p}}\, \mathrm{d}s\Big) \leq C q_{\max} \int_D |\operatorname{\mathbf{curl}} \boldsymbol{H}_{\boldsymbol{p}}^i|^2 \,\mathrm{d}\boldsymbol{x} \leq \beta \int_B |\operatorname{\mathbf{curl}} \boldsymbol{H}_{\boldsymbol{p}}^i|^2 \,\mathrm{d}\boldsymbol{x}$$

for all $\boldsymbol{p} \in V_1^\perp$ and any $\beta \geq \max\{0, C q_{\max}\}$.

On the other hand, Theorem 3.8 with $q_1 = 0$ and $q_2 = q$ gives a finite-dimensional subspace $V_2 \subseteq L_t^2(S^2, \mathbb{C}^3)$ such that, for all $\boldsymbol{p} \in V_2^\perp$ and any $\alpha \leq \min\{0, q_{\min}\}$,

$$\operatorname{Re}\Big(\int_{S^2} \boldsymbol{p} \cdot \overline{F_q \boldsymbol{p}}\, \mathrm{d}s\Big) \geq \int_D q |\operatorname{\mathbf{curl}} \boldsymbol{H}_{\boldsymbol{p}}^i|^2 \,\mathrm{d}\boldsymbol{x} \geq q_{\min} \int_D |\operatorname{\mathbf{curl}} \boldsymbol{H}_{\boldsymbol{p}}^i|^2 \,\mathrm{d}\boldsymbol{x} \geq \alpha \int_B |\operatorname{\mathbf{curl}} \boldsymbol{H}_{\boldsymbol{p}}^i|^2 \,\mathrm{d}\boldsymbol{x}\,.$$

Thus, we utilize Lemma 2.2 and part (a) is proven.

Part (b) is shown by contradiction. Let $D \not\subseteq B$, then $U := D \setminus B$ is not empty. By assumption there exists a point $\boldsymbol{x} \in \overline{U} \cap \partial D$ and a connected unbounded open neighborhood $O \subseteq \mathbb{R}^3$ of $\boldsymbol{x}$ with $O \cap D \subseteq U$ and $O \cap B = \emptyset$, such that (3.69) is satisfied with $E := O \cap D$. Let $R > 0$ be large enough such that $B, D \subseteq B_R(0)$. Without loss of generality, we suppose that $O \cap B_R(0)$, and $B_R(0) \setminus \overline{O}$ are connected. An example of how the geometry could look like is depicted in Figure 3.3.

If $q|_E \leq q_{\max,E} < 0$, we assume that $\alpha H_B^* H_B \leq_{\text{fin}} \operatorname{Re}(F_q)$ for some $\alpha \in \mathbb{R}$. Then, we apply Corollary 3.10 with $q_1 = 0$ and $q_2 = q$ and recall (3.56). This shows that there exists a finite-dimensional subspace $V_3 \subseteq L_t^2(S^2, \mathbb{C}^3)$ such that, for any $\boldsymbol{p} \in V_3^\perp$,

$$\begin{aligned}
0 &\leq \int_{S^2} \boldsymbol{p} \cdot \overline{(\operatorname{Re}(F_q)\boldsymbol{p} - \alpha H_B^* H_B \boldsymbol{p})}\, \mathrm{d}s \leq \int_{B_R(0)} (q|\operatorname{\mathbf{curl}} \boldsymbol{H}_{q,\boldsymbol{p}}|^2 - \alpha\chi_B |\operatorname{\mathbf{curl}} \boldsymbol{H}_{\boldsymbol{p}}^i|^2)\, \mathrm{d}\boldsymbol{x} \\
&= \int_{B_R(0)\setminus\overline{O}} (q|\operatorname{\mathbf{curl}} \boldsymbol{H}_{q,\boldsymbol{p}}|^2 - \alpha\chi_B |\operatorname{\mathbf{curl}} \boldsymbol{H}_{\boldsymbol{p}}^i|^2)\, \mathrm{d}\boldsymbol{x} \\
&\quad + \int_{B_R(0)\cap O} (q|\operatorname{\mathbf{curl}} \boldsymbol{H}_{q,\boldsymbol{p}}|^2 - \alpha\chi_B |\operatorname{\mathbf{curl}} \boldsymbol{H}_{\boldsymbol{p}}^i|^2)\, \mathrm{d}\boldsymbol{x} \\
&\leq q_{\max} \int_{B_R(0)\setminus\overline{O}} |\operatorname{\mathbf{curl}} \boldsymbol{H}_{q,\boldsymbol{p}}|^2\, \mathrm{d}\boldsymbol{x} + |\alpha| \int_{B_R(0)\setminus\overline{O}} |\operatorname{\mathbf{curl}} \boldsymbol{H}_{\boldsymbol{p}}^i|^2\, \mathrm{d}\boldsymbol{x} + q_{\max,E} \int_E |\operatorname{\mathbf{curl}} \boldsymbol{H}_{q,\boldsymbol{p}}|^2\, \mathrm{d}\boldsymbol{x}\,.
\end{aligned}$$

Let $M := B_R(0) \setminus \overline{O}$. Using Theorem 3.22 we obtain a sequence $(\boldsymbol{p}_m)_{m\in\mathbb{N}} \subseteq V_3^\perp$ such that

$$\int_E |\operatorname{\mathbf{curl}} \boldsymbol{H}_{q,\boldsymbol{p}_m}|^2\, \mathrm{d}\boldsymbol{x} \to \infty \qquad \text{and} \qquad \int_{B_R(0)\setminus\overline{O}} (|\operatorname{\mathbf{curl}} \boldsymbol{H}_{q,\boldsymbol{p}_m}|^2 + |\operatorname{\mathbf{curl}} \boldsymbol{H}_{\boldsymbol{p}_m}^i|^2)\, \mathrm{d}\boldsymbol{x} \to 0$$

as $m \to \infty$. However, since $q_{\max,E} < 0$ this gives a contradiction. Therefore, $\alpha H_B^* H_B \not\leq_{\text{fin}} \operatorname{Re}(F_q)$ for all $\alpha \in \mathbb{R}$.

Now, we assume that $q|_E \geq q_{\min,E} > 0$ and that $\operatorname{Re}(F_q) \leq_{\text{fin}} \beta H_B^* H_B$ for some $\beta \in \mathbb{R}$. Theorem 3.8 with $q_1 = 0$ and $q_2 = q$ guarantees the existence of a finite-dimensional subspace $V_4 \subseteq L_t^2(S^2, \mathbb{C}^3)$ such that, for any $\boldsymbol{p} \in V_4^\perp$,

$$\begin{aligned}
0 &\geq \int_{S^2} \boldsymbol{p} \cdot \overline{(\operatorname{Re}(F_q)\boldsymbol{p} - \beta H_B^* H_B \boldsymbol{p})}\, \mathrm{d}s \geq \int_{B_R(0)} (q - \beta\chi_B) |\operatorname{\mathbf{curl}} \boldsymbol{H}_{\boldsymbol{p}}^i|^2\, \mathrm{d}\boldsymbol{x} \\
&= \int_{B_R(0)\setminus\overline{O}} (q - \beta\chi_B) |\operatorname{\mathbf{curl}} \boldsymbol{H}_{\boldsymbol{p}}^i|^2\, \mathrm{d}\boldsymbol{x} + \int_{B_R(0)\cap O} -(\beta\chi_B - q) |\operatorname{\mathbf{curl}} \boldsymbol{H}_{\boldsymbol{p}}^i|^2\, \mathrm{d}\boldsymbol{x} \\
&\geq -(|\beta| + \|q\|_{L^\infty(\mathbb{R}^3)}) \int_{B_R(0)\setminus\overline{O}} |\operatorname{\mathbf{curl}} \boldsymbol{H}_{\boldsymbol{p}}^i|^2\, \mathrm{d}\boldsymbol{x} + q_{\min,E} \int_E |\operatorname{\mathbf{curl}} \boldsymbol{H}_{\boldsymbol{p}}^i|^2\, \mathrm{d}\boldsymbol{x}\,.
\end{aligned}$$

However, this contradicts Theorem 3.15 with $B = E$, $\Omega = B_R(0) \setminus \overline{O}$ and $q = 0$, which yields a sequence $(\boldsymbol{p}_m)_{m\in\mathbb{N}} \subseteq V_4^\perp$ with

$$\int_E |\operatorname{\mathbf{curl}} \boldsymbol{H}_{\boldsymbol{p}_m}^i|^2\, \mathrm{d}\boldsymbol{x} \to \infty \qquad \text{and} \qquad \int_{B_R(0)\setminus\overline{O}} |\operatorname{\mathbf{curl}} \boldsymbol{H}_{\boldsymbol{p}_m}^i|^2\, \mathrm{d}\boldsymbol{x} \to 0 \qquad \text{as } m \to \infty\,.$$

Thus, $\operatorname{Re}(F_q) \not\leq_{\text{fin}} \beta H_B^* H_B$ for all $\beta \in \mathbb{R}$. This ends the proof of part (b). □

The following corollary is an immediate consequence of the proof of Theorem 3.26. We consider the special case of an indefinite scattering object $D = D_1 \cup D_2$ with contrast function q such that $q_1 := q|_{D_1}$ is strictly negative on D_1 while $q_2 := q|_{D_2}$ is strictly positive on D_2. The result characterizes whether a certain probing domain B contains the negative part D_1 of the scatterer or its positive part D_2 or none of them.

Corollary 3.27. *Let $D = D_1 \cup D_2 \subseteq \mathbb{R}^3$ be open and bounded such that $\overline{D_1 \cap D_2} = \emptyset$, and $\mathbb{R}^3 \setminus \overline{D}$ is connected. Let $q \in \mathcal{Y}_D$ with $q_j := q|_{D_j} \in C^1(\overline{D_j})$, $j = 1, 2$, and suppose that*

$$\begin{aligned} -\infty < q_{1,\min} \leq q_1 \leq q_{1,\max} < 0 \qquad & \text{on } D_1\,, \\ 0 < q_{2,\min} \leq q_2 \leq q_{2,\max} < 1 \qquad & \text{on } D_2 \end{aligned}$$

for some constants $q_{1,\min}, q_{1,\max}, q_{2,\min}, q_{2,\max} \in \mathbb{R}$.

Let $B \subseteq \mathbb{R}^3$ be open such that $\mathbb{R}^3 \setminus \overline{B}$ is connected.

(a) If $D_1 \subseteq B$, then

$$\mathrm{Re}(F_q) \geq_{\mathrm{fin}} \alpha H_B^* H_B \quad \text{for all } \alpha \leq q_{1,\min}\,.$$

(b) If $D_1 \not\subseteq B$, then

$$\mathrm{Re}(F_q) \not\geq_{\mathrm{fin}} \alpha H_B^* H_B \quad \text{for any } \alpha \in \mathbb{R}\,.$$

(c) If $D_2 \subseteq B$, then there exists a constant $C > 0$ such that

$$\mathrm{Re}(F_q) \leq_{\mathrm{fin}} \alpha H_B^* H_B \quad \text{for all } \alpha \geq C q_{2,\max}\,.$$

(d) If $D_2 \not\subseteq B$, then

$$\mathrm{Re}(F_q) \not\leq_{\mathrm{fin}} \alpha H_B^* H_B \quad \text{for any } \alpha \in \mathbb{R}\,.$$

At the end of the next section, we will comment on a sampling strategy that implements the criteria in Corollary 3.27 to geometrically separate positive and negative components of mixed scattering configurations. This should be compared to Subsection 2.3.3 where we established an algorithm that allows us to separate Dirichlet and Neumann obstacles when considering the inverse acoustic scattering problem. After having separated the positive and negative components, one could, for example, utilize techniques from [Gri02, GK04, Sch09] to obtain a full shape reconstruction of the unknown scatterers. A stable numerical implementation of the monotonicity-based shape characterization for the general indefinite case from Theorem 3.26 seems to require a better understanding of the dimensions of the finite-dimensional subspaces that are excluded in the monotonicity relations in (3.70)–(3.71). For comparison, in [HPS19a, HPS19b] the authors derive a monotonicity inequality that holds up to some finite-dimensional subspace when investigating an inverse coefficient problem for the Helmholtz equation. In addition, they provide bounds on the dimension of this subspace.

3.6. Numerical Examples

We discuss numerical examples for the shape characterizations developed in Subsections 3.4.2 and 3.5.2. As we have seen when we derived numerical reconstruction procedures for the inverse acoustic scattering problem in Section 2.5, the challenge here is the finite dimensionality of numerical approximations of the operators F_q and $H_B^* H_B$. As a consequence, we have to cautiously address the question of whether the linear combinations of these operators that we studied in Theorems 3.20, 3.21 and 3.26 are positive or negative definite up to some finite-dimensional

subspace. Similar to Section 2.5, we first investigate sign-definite radially symmetric scatterers in Subsection 3.6.1. Afterward, we present a sampling strategy for sign-definite scatterers in Subsection 3.6.2. Finally, we consider indefinite scattering configurations restricting ourselves to scatterers that consist of two parts, one with positive and one with negative contrast. In Subsection 3.6.3 below, we work toward a strategy that allows us to separate the positive and the negative parts from each other.

3.6.1. An Explicit Radially Symmetric Example

To get a first impression of the results from Theorems 3.21, 3.20 and 3.26, we consider the case when the scatterer D and the probing domain B are concentric balls. In this special case, it is possible to compute the eigenvalue decompositions of the far field operator F_q and the probing operator $H_B^* H_B$ in an explicit form.

Let $D = B_r(0)$ be a ball of radius $r > 0$ centered at the origin with constant electric permittivity contrast $q < 1$, i.e., the relative electric permittivity is $\varepsilon_r^{-1} = 1 - q > 0$. We derive series expansions for the incident magnetic field and for the corresponding magnetic far field pattern to obtain explicit formulas for the eigenvalue decomposition of the magnetic far field operator F_q from (3.18).

We expand a given tangential vector field $\boldsymbol{p} \in L_t^2(S^2, \mathbb{C}^3)$ into vector spherical harmonics, i.e.,

$$\boldsymbol{p}(\boldsymbol{\theta}) = \sum_{n=1}^{\infty} \sum_{m=-n}^{n} \left(a_n^m \boldsymbol{U}_n^m(\boldsymbol{\theta}) + b_n^m \boldsymbol{V}_n^m(\boldsymbol{\theta}) \right), \qquad \boldsymbol{\theta} \in S^2. \tag{3.72}$$

Therewith, we obtain from (3.20) and (C.15) that

$$\boldsymbol{H}_{\boldsymbol{p}}^i(\boldsymbol{x}) = \frac{4\pi\, \mathrm{i}^{n-1}}{k} \sum_{n=1}^{\infty} \sum_{m=-n}^{n} \left(a_n^m \operatorname{\mathbf{curl}} \boldsymbol{M}_n^m(\boldsymbol{x}) - \mathrm{i}k\, b_n^m \boldsymbol{M}_n^m(\boldsymbol{x}) \right), \qquad \boldsymbol{x} \in \mathbb{R}^3.$$

Applying separation of variables a short computation shows that the corresponding scattered magnetic field outside the support of the scatterer is given by

$$\boldsymbol{H}_{q,\boldsymbol{p}}^s(\boldsymbol{x}) = \frac{4\pi\, \mathrm{i}^{n-1}}{k} \sum_{n=1}^{\infty} \sum_{m=-n}^{n} \left(c_n^m \operatorname{\mathbf{curl}} \boldsymbol{N}_n^m(\boldsymbol{x}) - \mathrm{i}k\, d_n^m \boldsymbol{N}_n^m(\boldsymbol{x}) \right), \qquad \boldsymbol{x} \in \mathbb{R}^3 \setminus \overline{D},$$

with $c_n^m = \beta_n^m a_n^m$ and $d_n^m = \gamma_n^m b_n^m$, where

$$\begin{aligned}
\beta_n^m &:= \frac{\kappa r j_n(kr) j_n'(\kappa r) - k r j_n(\kappa r) j_n'(kr)}{k r j_n(\kappa r)(h_n^{(1)})'(kr) - \kappa r h_n^{(1)}(kr) j_n'(\kappa r)}, \\
\gamma_n^m &:= \frac{\varepsilon_r^{-1} j_n(kr)\big(j_n(\kappa r) + \kappa r j_n'(\kappa r)\big) - j_n(\kappa r)\big(j_n(kr) + k r j_n'(kr)\big)}{k r j_n(\kappa r)(h_n^{(1)})'(kr) - \kappa r \varepsilon_r^{-1} j_n'(\kappa r) h_n^{(1)}(kr) + q h_n^{(1)}(kr) j_n(\kappa r)}
\end{aligned}$$

and $\kappa := k\sqrt{\varepsilon_r}$. We use the representation (C.14) of the far field patterns of the spherical vector wave functions $\boldsymbol{N}_n^m$ and $\operatorname{\mathbf{curl}} \boldsymbol{N}_n^m$ to see that

$$\boldsymbol{H}_{q,\boldsymbol{p}}^{\infty}(\widehat{\boldsymbol{x}}) = \frac{(4\pi)^2}{\mathrm{i}k} \sum_{n=1}^{\infty} \sum_{m=-n}^{n} \left(c_n^m \boldsymbol{U}_n^m(\widehat{\boldsymbol{x}}) + d_n^m \boldsymbol{V}_n^m(\widehat{\boldsymbol{x}}) \right), \qquad \widehat{\boldsymbol{x}} \in S^2.$$

Since $F_q \boldsymbol{p} = \boldsymbol{H}^{\infty}_{q,\boldsymbol{p}}$ for all $\boldsymbol{p} \in L^2_t(S^2, \mathbb{C}^3)$, the eigenvalues and eigenvectors of the magnetic far field operator F_q are given by $(\lambda^{(j)}_{n,r}, \boldsymbol{v}^{(j)}_{m,n})$, $m = -n, \dots, n$, $n = 1, 2, \dots$, $j = s, t$, with

$$\lambda^{(s)}_{n,r} \,=\, \frac{(4\pi)^2}{\mathrm{i}k} \beta^m_n \,, \qquad \lambda^{(t)}_{n,r} \,=\, \frac{(4\pi)^2}{\mathrm{i}k} \gamma^m_n \tag{3.73a}$$

and

$$\boldsymbol{v}^{(s)}_{m,n}(\widehat{\boldsymbol{x}}) \,=\, \boldsymbol{U}^m_n(\widehat{\boldsymbol{x}}) \,, \qquad \boldsymbol{v}^{(t)}_{m,n}(\widehat{\boldsymbol{x}}) \,=\, \boldsymbol{V}^m_n(\widehat{\boldsymbol{x}}) \,, \qquad \widehat{\boldsymbol{x}} \in S^2 \,. \tag{3.73b}$$

Similarly, we consider for the test domain $B = B_R(0)$ a ball of radius $R > 0$ centered at the origin. Then, by utilizing the Funk-Hecke formula in the form (C.12) we find that the probing operator $H^*_B H_B : L^2_t(S^2, \mathbb{C}^3) \to L^2_t(S^2, \mathbb{C}^3)$ from (3.55) satisfies

$$\begin{aligned}
(H^*_B H_B \boldsymbol{p})(\widehat{\boldsymbol{x}}) \,&=\, k^2 \Big(\int_{S^2} \Big(\int_{B_R(0)} e^{\mathrm{i}k\boldsymbol{y}\cdot(\boldsymbol{\theta} - \widehat{\boldsymbol{x}})} \, \mathrm{d}\boldsymbol{y} \Big) (\boldsymbol{\theta} \times \boldsymbol{p}(\boldsymbol{\theta})) \, \mathrm{d}s(\boldsymbol{\theta}) \Big) \times \widehat{\boldsymbol{x}} \\
&=\, k^2 \Big(\int_{S^2} \Big(\int_0^R \rho^2 \Big(\int_{S^2} e^{-\mathrm{i}k\rho\widehat{\boldsymbol{y}}\cdot(\widehat{\boldsymbol{x}} - \boldsymbol{\theta})} \, \mathrm{d}s(\widehat{\boldsymbol{y}}) \Big) \, \mathrm{d}\rho \Big) (\boldsymbol{\theta} \times \boldsymbol{p}(\boldsymbol{\theta})) \, \mathrm{d}s(\boldsymbol{\theta}) \Big) \times \widehat{\boldsymbol{x}} \\
&=\, k^2 \Big(\int_{S^2} \Big(\int_0^R 4\pi\rho^2 j_0(k\rho|\widehat{\boldsymbol{x}} - \boldsymbol{\theta}|) \, \mathrm{d}\rho \Big) (\boldsymbol{\theta} \times \boldsymbol{p}(\boldsymbol{\theta})) \, \mathrm{d}s(\boldsymbol{\theta}) \Big) \times \widehat{\boldsymbol{x}} \,, \qquad \widehat{\boldsymbol{x}} \in S^2 \,.
\end{aligned} \tag{3.74}$$

We employ the vector spherical harmonics expansion (3.72), and using (C.8) we find that, for $\boldsymbol{\theta} \in S^2$,

$$\boldsymbol{\theta} \times \boldsymbol{p}(\boldsymbol{\theta}) \,=\, \sum_{n=1}^{\infty} \sum_{m=-n}^{n} \left(a^m_n \boldsymbol{\theta} \times \boldsymbol{U}^m_n(\boldsymbol{\theta}) + b^m_n \boldsymbol{\theta} \times \boldsymbol{V}^m_n(\boldsymbol{\theta}) \right) \,=\, \sum_{n=1}^{\infty} \sum_{m=-n}^{n} \left(a^m_n \boldsymbol{V}^m_n(\boldsymbol{\theta}) - b^m_n \boldsymbol{U}^m_n(\boldsymbol{\theta}) \right) .$$

Substituting this into (3.74) yields

$$\begin{aligned}
(H^*_B H_B \boldsymbol{p})(\widehat{\boldsymbol{x}}) \,&=\, 4\pi k^2 \sum_{n=1}^{\infty} \sum_{m=-n}^{n} \Big(a^m_n \int_0^R \Big(\rho^2 \int_{S^2} j_0(k\rho|\widehat{\boldsymbol{x}} - \boldsymbol{\theta}|) \boldsymbol{V}^m_n(\boldsymbol{\theta}) \, \mathrm{d}s(\boldsymbol{\theta}) \Big) \, \mathrm{d}\rho \\
&\qquad\qquad - b^m_n \int_0^R \Big(\rho^2 \int_{S^2} j_0(k\rho|\widehat{\boldsymbol{x}} - \boldsymbol{\theta}|) \boldsymbol{U}^m_n(\boldsymbol{\theta}) \, \mathrm{d}s(\boldsymbol{\theta}) \Big) \, \mathrm{d}\rho \Big) \times \widehat{\boldsymbol{x}} \\
&=\, \sum_{n=1}^{\infty} \sum_{m=-n}^{n} \Big(a^m_n \Big((4\pi k)^2 \int_0^R j^2_n(k\rho) \rho^2 \, \mathrm{d}\rho \Big) \boldsymbol{U}^m_n(\widehat{\boldsymbol{x}}) \\
&\qquad + b^m_n \Big((4\pi k)^2 \int_0^R \Big(\big(j_n(k\rho) + k\rho j'_n(k\rho) \big)^2 + n(n+1) j^2_n(k\rho) \Big) \, \mathrm{d}\rho \Big) \boldsymbol{V}^m_n(\widehat{\boldsymbol{x}}) \Big)
\end{aligned} \tag{3.75}$$

(see, e.g., [CK19, Thm. 6.29]). Accordingly, the eigenvalues and eigenvectors of the probing operator $H^*_B H_B$ are given by $(\mu^{(j)}_{n,R}, \boldsymbol{v}^{(j)}_{m,n})$, $m = -n, \dots, n$, $n = 1, 2, \dots$, $j = s, t$, with

$$\mu^{(s)}_{n,R} \,=\, \frac{(4\pi)^2}{k} \int_0^{kR} j^2_n(\rho) \rho^2 \, \mathrm{d}\rho \,, \tag{3.76a}$$

$$\mu^{(t)}_{n,R} \,=\, \frac{(4\pi)^2}{k} \int_0^{kR} \big(n(n+1) j^2_n(\rho) + (j_n(\rho) + \rho j'_n(\rho))^2 \big) \, \mathrm{d}\rho \tag{3.76b}$$

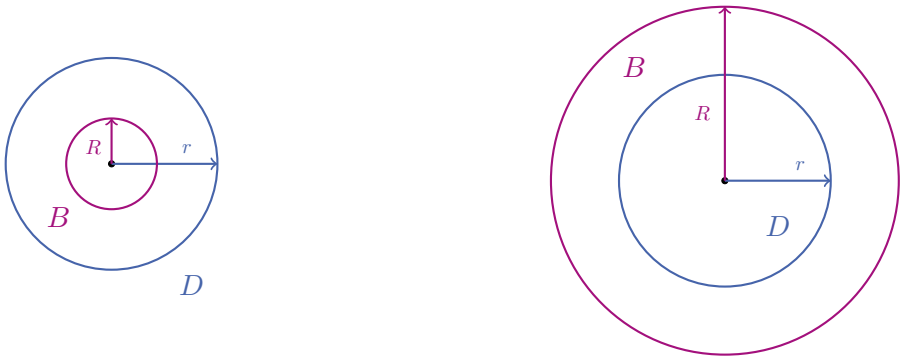

FIGURE 3.4. Visualization of the geometries of D and B for $R < r$ (left) and $R > r$ (right).

and

$$\boldsymbol{v}_{m,n}^{(s)}(\widehat{\boldsymbol{x}}) = \boldsymbol{U}_n^m(\widehat{\boldsymbol{x}}), \qquad \boldsymbol{v}_{m,n}^{(t)}(\widehat{\boldsymbol{x}}) = \boldsymbol{V}_n^m(\widehat{\boldsymbol{x}}), \qquad \widehat{\boldsymbol{x}} \in S^2. \tag{3.76c}$$

We first suppose that $-\infty < q < 0$ and thus, the shape characterizations developed in Subsections 3.4.2 and 3.5.2 yield the following.

(a) If $R < r$, then $B \subseteq D$ and $D \not\subseteq B$, respectively (see picture on the left in Figure 3.4). Thus, Theorem 3.20 (a) implies that $\operatorname{Re}(F_q) - \alpha H_B^* H_B \leq_{\text{fin}} 0$ when $\alpha \geq Cq$ with $C > 0$ as in Theorem 3.18 whereas Corollary 3.27 (b) shows that $\operatorname{Re}(F_q) - \alpha H_B^* H_B \not\geq_{\text{fin}} 0$ for any $\alpha \in \mathbb{R}$. This means that $\operatorname{Re}(F_q) - \alpha H_B^* H_B$ has only finitely many positive eigenvalues when $\alpha \geq Cq$ but infinitely many negative eigenvalues for any $\alpha \in \mathbb{R}$.

(b) If $R > r$, then $D \subseteq B$ and $B \not\subseteq D$, respectively (see picture on the right in Figure 3.4). Thus, Corollary 3.27 (a) implies that $\operatorname{Re}(F_q) - \alpha H_B^* H_B \geq_{\text{fin}} 0$ when $\alpha \leq q$ whereas Theorem 3.20 (b) shows that $\operatorname{Re}(F_q) - \alpha H_B^* H_B \not\leq_{\text{fin}} 0$ for any $\alpha < 0$. This means that $\operatorname{Re}(F_q) - \alpha H_B^* H_B$ has only finitely many negative eigenvalues when $\alpha \leq q$ but infinitely many positive eigenvalues for any $\alpha < 0$.

Now, we give a numerical example to illustrate this characterization and obtain similar results as we observed in Example 2.42 when considering a radially symmetric Dirichlet obstacle in the acoustic setting.

Example 3.28. We choose a scattering object $D = B_r(0)$ with constant contrast $q = -1/2$, i.e., $\varepsilon_r = 2/3$, and radius $r = 7$. We evaluate the eigenvalues $\operatorname{Re}(\lambda_{n,r}^{(j)})$ of the far field operator F_q, $\mu_{n,R}^{(j)}$ of the probing operator $H_B^* H_B$ and $\operatorname{Re}(\lambda_{n,r}^{(j)}) - \alpha\mu_{n,R}^{(j)}$, $j = s, t$, of the operator $\operatorname{Re}(F_q) - \alpha H_B^* H_B$ with wave number $k = 1$ for $n = 1, \ldots, 1000$. For the radii of the probing domains B, we use different values within the interval $(0, 26]$. Therefore, we employ the explicit expressions (3.73) and (3.76) of the eigenvalues. Moreover, we set the parameter $\alpha = -1/2$. In Figure 3.5, we show plots of the number of positive eigenvalues (left) and of the number of negative eigenvalues (right) $\operatorname{Re}(\lambda_{n,r}^{(j)})$ (blue, dash-dotted), $-\alpha\mu_{n,R}^{(j)}$ (purple, dashed) and $\operatorname{Re}(\lambda_{n,r}^{(j)}) - \alpha\mu_{n,R}^{(j)}$ (black, solid), $j = s, t$, within the range $n = 0, \ldots, 1000$ as a function of R.

As we would expect from Theorem 3.20 and Corollary 3.27 we observe a sharp transition in the behavior of the eigenvalues of $\operatorname{Re}(F_q) - \alpha H_B^* H_B$ at $R = r = 7$. The red dotted line in Figure 3.5

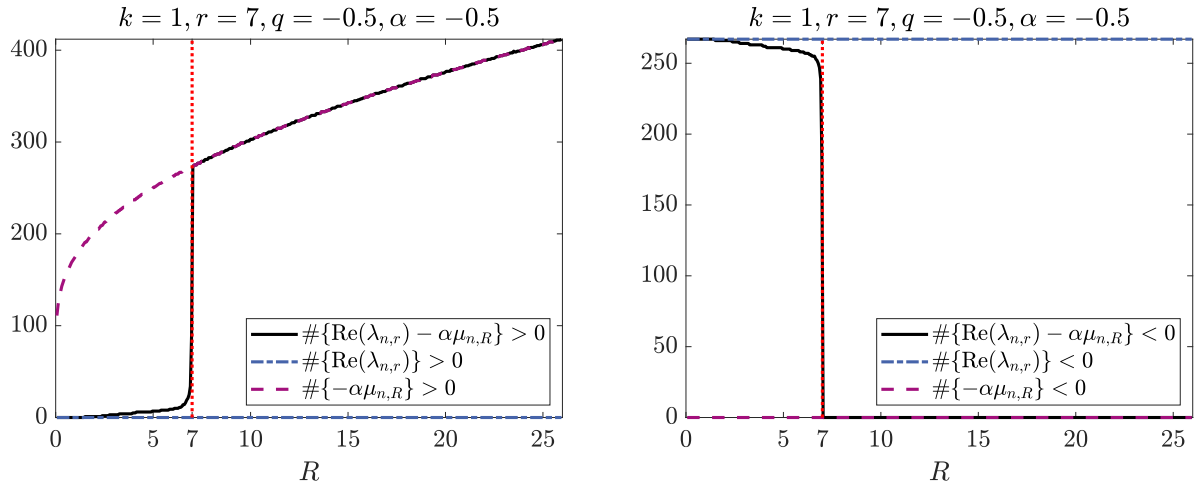

Figure 3.5. Number of positive eigenvalues (left) and number of negative eigenvalues (right) $\mathrm{Re}(\lambda_{n,r}) - \alpha\mu_{n,R}$ (black, solid) $\mathrm{Re}(\lambda_{n,r})$ (blue, dash-dotted) and $-\alpha\mu_{n,R}$ (purple, dashed) from Example 3.28 within the the range $n = 0, \ldots, 1000$ as function of R.

illustrates this point when the radii of the scatterer and the probing domain coincide. On the left-hand side of this line, the scatterer D contains the probing domain, and we notice that the contribution of the far field operator F_q dominates in the superposition $\mathrm{Re}(F_q) - \alpha H_B^* H_B$. On the right-hand side, D is contained within B, and we observe that the contribution of the operator $-\alpha H_B^* H_B$ is dominating. By visual inspection of the plots in Figure 3.5, we can easily detect the transition, i.e. the red dotted line, and therewith, we are able to estimate the radius r of the scatterer D.

Because the radius of D is independent of R, the number of positive and negative eigenvalues of F_q is constant in these plots. Corollary 3.14 (a) suggests that the number of positive eigenvalues of F_q is low, and indeed, this number is equal to zero in our example. However, one might expect the number of negative eigenvalues to be larger than 267 when computing 1000 eigenvalues. From (C.11), it follows that the sequences $(\mathrm{Re}(\lambda_{n,r}^{(j)}))_{n\in\mathbb{Z}}$, $j = s, t$, decay rapidly once the value of $|n|$ is sufficiently large. Since eigenvalues below some threshold are rounded to zero in Matlab, this explains our observation. Moreover, we know that the operator $-\alpha H_B^* H_B$ is positive semi-definite. In fact, its number of negative eigenvalues is zero in this example. Furthermore, the expansions (C.11a)–(C.11b) imply that the sequences $(\mu_{n,R}^{(j)})_{n\in\mathbb{Z}}$, $j = s, t$, also tend rapidly to zero for sufficiently large $|n|$, and the eigenvalues $\mu_n^{(j)}(R)$ are on average increasing with respect to the radius R. This is the reason for the increasing but somewhat low numbers of positive eigenvalues of $H_B^* H_B$.

Up to now, we worked with exact far field data. However, we should take into account that observed data are typically inaccurate, for example, due to measurement errors. Assuming that the far field data are known up to a perturbation of size $\delta > 0$ with respect to the spectral norm, we only consider those eigenvalues with an absolute value larger than δ (compare, e.g., [GVL13, Thm. 7.2.2]). We demonstrate the effect of neglecting small eigenvalues by repeating the previous computations but we discard those eigenvalues with an absolute value below the

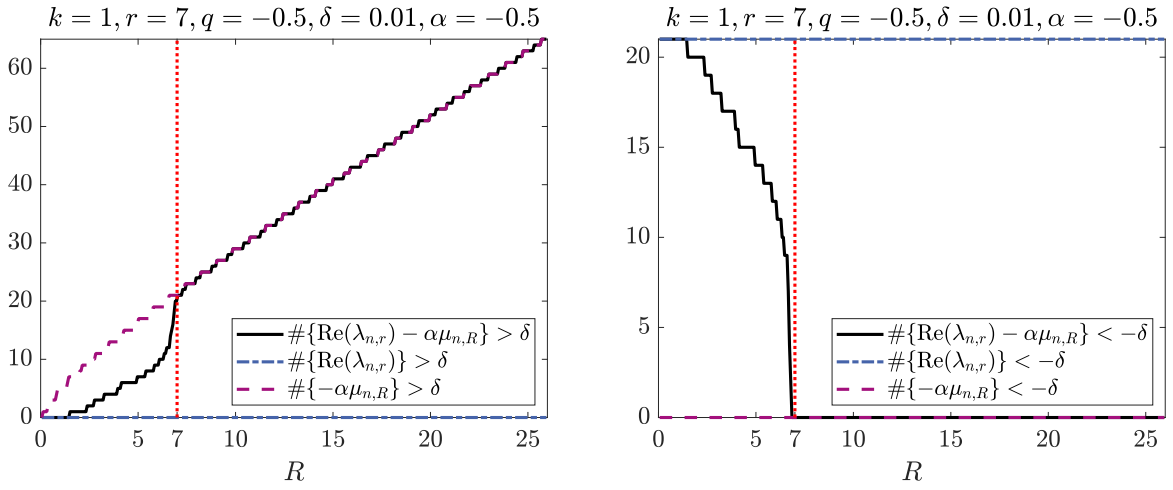

FIGURE 3.6. Same as Figure 2.7, but with $\delta = 0.01$ instead of $\delta = 0$.

threshold $\delta = 0.01$. In Figure 3.6, we show plots of the number of positive eigenvalues $\mathrm{Re}(\lambda_{n,r}^{(j)})$ (blue, dash-dotted), $-\alpha\mu_{n,R}^{(j)}$ (purple, dashed) and $\mathrm{Re}(\lambda_{n,r}^{(j)}) - \alpha\mu_{n,R}^{(j)}$ (black, solid), $j = s, t$, within the range $n = 0, \ldots, 1000$ that are larger than δ (left) and of the number of negative eigenvalues that are smaller than $-\delta$ as a function of R. However, the transition in the behavior of the eigenvalues is not as sharp as before. Since the sequences of the eigenvalues are rapidly decaying for large $|n|$, many eigenvalues remain below the threshold δ. Consequently, we observe that the numbers of counted eigenvalues are a lot lower in Figure 2.8 than in Figure 2.7. However, we get the impression that a rough estimate of the radius r would still be possible when using the threshold $\delta = 0.01$. △

For the sake of completeness, we also comment on strictly positive contrasts, i.e. $0 < q < 1$. In this case, the shape characterizations from Subsections 3.4.2 and 3.5.2 imply the following.

(a) If $R < r$, then $B \subseteq D$ and $D \not\subseteq B$, respectively. Thus, Theorem 3.21 (a) implies that $\mathrm{Re}(F_q) - \alpha H_B^* H_B$ has only finitely many negative eigenvalues when $\alpha \leq q$ whereas Corollary 3.27 (d) yields that $\mathrm{Re}(F_q) - \alpha H_B^* H_B$ has infinitely many positive eigenvalues for any $\alpha \in \mathbb{R}$.

(b) If $R > r$, then $D \subseteq B$ and $B \not\subseteq D$, respectively. Thus, Corollary 3.27 (c) implies that $\mathrm{Re}(F_q) - \alpha H_B^* H_B$ has only finitely many positive eigenvalues when $\alpha \geq Cq$ with $C > 0$ as in Theorem 3.18 whereas Theorem 3.21 (b) yields that $\mathrm{Re}(F_q) - \alpha H_B^* H_B$ has infinitely many negative eigenvalues for any $\alpha > 0$.

The following numerical example should be compared to Example 2.43 where we investigated an obstacle with Neumann boundary conditions.

Example 3.29. We consider a scattering object $D = B_r(0)$ with radius $r = 6$ and constant contrast $q = 1/2$, i.e., $\varepsilon_r = 2$. As in the previous example, we evaluate the eigenvalues $\mathrm{Re}(\lambda_{n,r}^{(j)})$, $\mu_{n,R}^{(j)}$, and $\mathrm{Re}(\lambda_{n,r}^{(j)}) - \alpha\mu_{n,R}^{(j)}$, $j = s, t$, with wave number $k = 1$ and $n = 1, \ldots, 1000$ for different values of the radius $R \in (0, 26]$ of the test domain B using (3.73) and (3.76). Besides, we set the

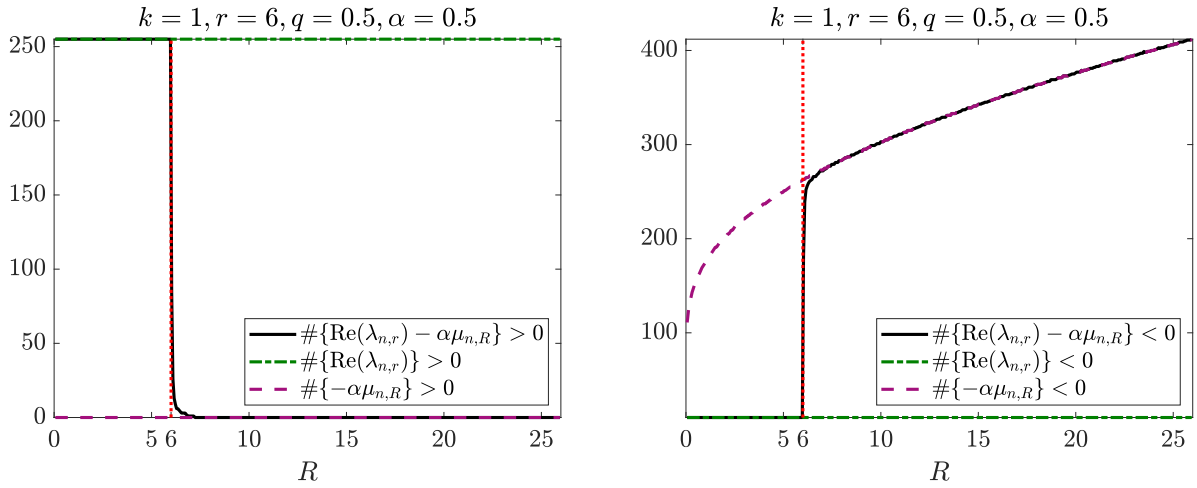

Figure 3.7. Number of positive eigenvalues (left) and number of negative eigenvalues (right) $\mathrm{Re}(\lambda_{n,r}) - \alpha\mu_{n,R}$ (black, solid), $\mathrm{Re}(\lambda_{n,r})$ (green, dash-dotted) and $-\alpha\mu_{n,R}$ (purple, dashed) from Example 3.29 within the range $n = 0, \ldots, 1000$ as function of R.

parameter $\alpha = 1/2$. In Figure 3.7, we present plots of the number of positive eigenvalues (left) and of the number of negative eigenvalues (right) $\mathrm{Re}(\lambda_{n,r}^{(j)})$ (green, dash-dotted), $-\alpha\mu_{n,R}^{(j)}$ (purple, dashed) and $\mathrm{Re}(\lambda_{n,r}^{(j)}) - \alpha\mu_{n,R}^{(j)}$ (black, solid), $j = s, t$, within the range $n = 0, \ldots, 1000$ as a function of R.

Again, we notice a sharp transition in the behavior of the eigenvalues of $\mathrm{Re}(F_q) - \alpha H_B^* H_B$ at $R = r = 6$, which could be used to estimate the value of r. In these plots, the contribution of the far field operator $\mathrm{Re}(F_q)$ dominates in the superposition $\mathrm{Re}(F_q) - \alpha H_B^* H_B$ as long as $R < r$ while the contribution of the operator $-\alpha H_B^* H_B$ dominates when $R > r$. Similar to Example 3.28, the rapid decay of the sequences $(\mathrm{Re}(\lambda_{n,r}^{(j)}))_{n\in\mathbb{Z}}$, $j = s, t$, for large $|n|$ explains the seemingly low numbers of positive eigenvalues of $\mathrm{Re}(F_q)$ in the left plot. Since the sequences $(\mu_{n,R}^{(j)})_{n\in\mathbb{Z}}$, $j = s, t$, also rapidly tend to zero once that $|n|$ is sufficiently large and they increase with respect to R, the number of negative eigenvalues of $-\alpha H_B^* H_B$ is somewhat low but increasing in the right plot. △

3.6.2. A Sampling Strategy for Sign-Definite Scatterers

After having studied radially symmetric scattering objects, we now investigate scatterers D of arbitrary shape but we restrict ourselves to the cases when the contrast function is either strictly positive or strictly negative on D. We discuss a numerical realization of the criteria established in Theorems 3.20 and 3.21. To discretize the magnetic far field operator F_q from (3.18) we use a truncated vector spherical harmonics expansion. Let $\boldsymbol{p} \in L_t^2(S^2, \mathbb{C}^3)$ as in (3.72), then applying F_q gives

$$F_q \boldsymbol{p} = \sum_{n=1}^{\infty} \sum_{m=-n}^{n} \left(a_n^m F_q \boldsymbol{U}_n^m + b_n^m F_q \boldsymbol{V}_n^m \right) \in L_t^2(S^2, \mathbb{C}^3)\,. \tag{3.77}$$

Studying the singular value decomposition of the linear operator that maps current densities supported in the ball $B_R(0)$ of radius R around the origin to their radiated far field patterns, it has been observed in [GS18] that for a large class of practically relevant source distributions the radiated far field pattern is well approximated by a vector spherical harmonics expansion of order

$$N \gtrsim kR\,. \tag{3.78}$$

This study suggests truncating the series in (3.77) at an index N that is at least slightly larger than the radius of the smallest ball around the origin that contains the scattering object. Accordingly, we use the matrix

$$\boldsymbol{F}_q \;:=\; \begin{bmatrix} \langle F_q \boldsymbol{U}_n^m, \boldsymbol{U}_{n'}^{m'} \rangle_{L_t^2(S^2,\mathbb{C}^3)} & \langle F_q \boldsymbol{V}_n^m, \boldsymbol{U}_{n'}^{m'} \rangle_{L_t^2(S^2,\mathbb{C}^3)} \\ \langle F_q \boldsymbol{U}_n^m, \boldsymbol{V}_{n'}^{m'} \rangle_{L_t^2(S^2,\mathbb{C}^3)} & \langle F_q \boldsymbol{V}_n^m, \boldsymbol{V}_{n'}^{m'} \rangle_{L_t^2(S^2,\mathbb{C}^3)} \end{bmatrix} \in \mathbb{C}^{Q\times Q} \tag{3.79}$$

with $1 \le n, n' \le N$, $-n \le m \le n$, $-n' \le m' \le n'$ and thus $Q = 2N(N+2)$ as a discrete approximation of F_q.

To discretize the *region of interest* $[-R,R]^3$ we use an equidistant grid of sampling points

$$\triangle \;:=\; \{\boldsymbol{z}_{ij\ell} = (ih, jh, \ell h) \mid -J \le i,j,\ell \le J\} \;\subseteq\; [-R,R]^3 \tag{3.80}$$

with step size $h = R/J$. For each $\boldsymbol{z}_{ij\ell} \in \triangle$ we consider a probing operator $H_{B_{ij\ell}}^* H_{B_{ij\ell}}$ as in (3.55), where the probing domain $B_{ij\ell} = B_h(\boldsymbol{z}_{ij\ell})$ is a ball of radius h centered at $\boldsymbol{z}_{ij\ell}$. This probing operator satisfies, for any $\boldsymbol{p} \in L_t^2(S^2,\mathbb{C}^3)$ and $\widehat{\boldsymbol{x}} \in S^2$,

$$\begin{aligned} (H_{B_{ij\ell}}^* H_{B_{ij\ell}} \boldsymbol{p})(\widehat{\boldsymbol{x}}) \;&=\; k^2 \Big(\int_{S^2} \Big(\int_{B_{ij\ell}} e^{\mathrm{i}k\boldsymbol{y}\cdot(\boldsymbol{\theta}-\widehat{\boldsymbol{x}})}\, \mathrm{d}\boldsymbol{y} \Big) (\boldsymbol{\theta} \times \boldsymbol{p}(\boldsymbol{\theta}))\, \mathrm{d}s(\boldsymbol{\theta}) \Big) \times \widehat{\boldsymbol{x}} \\ &=\; k^2 \Big(\int_{S^2} e^{\mathrm{i}k\boldsymbol{z}\cdot(\boldsymbol{\theta}-\widehat{\boldsymbol{x}})} \Big(\int_{B_h(0)} e^{\mathrm{i}k\boldsymbol{y}\cdot(\boldsymbol{\theta}-\widehat{\boldsymbol{x}})}\, \mathrm{d}\boldsymbol{y} \Big) (\boldsymbol{\theta} \times \boldsymbol{p}(\boldsymbol{\theta}))\, \mathrm{d}s(\boldsymbol{\theta}) \Big) \times \widehat{\boldsymbol{x}} \\ &=\; e^{-\mathrm{i}k\boldsymbol{z}\cdot\widehat{\boldsymbol{x}}} \Big(H_{B_h(0)}^* H_{B_h(0)} \big(e^{\mathrm{i}k\boldsymbol{z}\cdot(\cdot)} \boldsymbol{p} \big) \Big) (\widehat{\boldsymbol{x}})\,. \end{aligned}$$

Combining this representation with the eigenvalue expansion of $H_{B_h(0)}^* H_{B_h(0)}$ that we have derived in the previous subsection (see (3.75) and (3.76)), we find that $H_{B_{ij\ell}}^* H_{B_{ij\ell}}$ has the same eigenvalues $\mu_{n,h}^{(s)}, \mu_{n,h}^{(t)}$ as $H_{B_h(0)}^* H_{B_h(0)}$, but the corresponding eigenvectors for $H_{B_{ij\ell}}^* H_{B_{ij\ell}}$ are

$$\widetilde{\boldsymbol{v}}_{m,n}^{(s)}(\widehat{\boldsymbol{x}}) \;=\; e^{-\mathrm{i}k\boldsymbol{z}\cdot\widehat{\boldsymbol{x}}} \boldsymbol{U}_n^m(\widehat{\boldsymbol{x}}) \qquad \text{and} \qquad \widetilde{\boldsymbol{v}}_{m,n}^{(t)}(\widehat{\boldsymbol{x}}) \;=\; e^{-\mathrm{i}k\boldsymbol{z}\cdot\widehat{\boldsymbol{x}}} \boldsymbol{V}_n^m(\widehat{\boldsymbol{x}})\,, \qquad \widehat{\boldsymbol{x}} \in S^2\,.$$

Thus, we get

$$\begin{aligned} (H_{B_{ij\ell}}^* H_{B_{ij\ell}} \boldsymbol{p})(\widehat{\boldsymbol{x}}) \;=\; \sum_{n=1}^{\infty} \sum_{m=-n}^{n} \Big(&\mu_{n,h}^{(s)} \langle e^{\mathrm{i}k\boldsymbol{z}\cdot(\cdot)} \boldsymbol{p}, \boldsymbol{U}_n^m \rangle_{L_t^2(S^2,\mathbb{C}^3)} \big(e^{-\mathrm{i}k\widehat{\boldsymbol{x}}\cdot\boldsymbol{z}} \boldsymbol{U}_n^m(\widehat{\boldsymbol{x}}) \big) \\ &+ \mu_{n,h}^{(t)} \langle e^{\mathrm{i}k\boldsymbol{z}\cdot(\cdot)} \boldsymbol{p}, \boldsymbol{V}_n^m \rangle_{L_t^2(S^2,\mathbb{C}^3)} \big(e^{-\mathrm{i}k\widehat{\boldsymbol{x}}\cdot\boldsymbol{z}} \boldsymbol{V}_n^m(\widehat{\boldsymbol{x}}) \big) \Big)\,, \qquad \widehat{\boldsymbol{x}} \in S^2\,. \end{aligned}$$

Accordingly, we find for $\boldsymbol{A}_n^m \in \{\boldsymbol{U}_n^m, \boldsymbol{V}_n^m\}$ and $\boldsymbol{B}_{n'}^{m'} \in \{\boldsymbol{U}_{n'}^{m'}, \boldsymbol{V}_{n'}^{m'}\}$ with $n, n' \ge 1$, $-n \le m \le n$

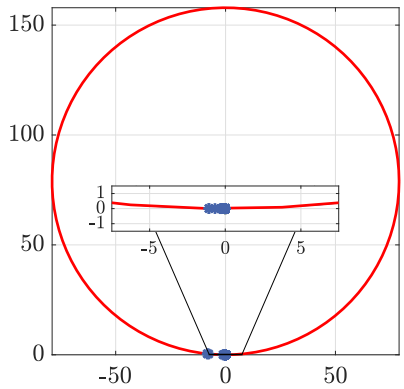

Figure 3.8. Eigenvalues of F_q (blue) from Example 3.6.2 for $k = 1$ with $N = 5$.

and $-n' \leq m' \leq n'$ that

$$\begin{aligned}\langle H^*_{B_{ij\ell}} H_{B_{ij\ell}} \boldsymbol{A}^m_n, \boldsymbol{B}^{m'}_{n'} \rangle_{L^2_t(S^2,\mathbb{C}^3)} \\ = \sum_{b=1}^{\infty} \sum_{a=-b}^{b} \Big(\mu^{(s)}_{a,h} \langle \boldsymbol{A}^m_n, e^{-\mathrm{i}k\boldsymbol{z}\cdot(\cdot)} \boldsymbol{U}^a_b \rangle_{L^2_t(S^2,\mathbb{C}^3)} \langle e^{-\mathrm{i}k\boldsymbol{z}\cdot(\cdot)} \boldsymbol{U}^a_b, \boldsymbol{B}^{m'}_{n'} \rangle_{L^2_t(S^2,\mathbb{C}^3)} \\ + \mu^{(t)}_{a,h} \langle \boldsymbol{A}^m_n, e^{-\mathrm{i}k\boldsymbol{z}\cdot(\cdot)} \boldsymbol{V}^a_b \rangle_{L^2_t(S^2,\mathbb{C}^3)} \langle e^{-\mathrm{i}k\boldsymbol{z}\cdot(\cdot)} \boldsymbol{V}^a_b, \boldsymbol{B}^{m'}_{n'} \rangle_{L^2_t(S^2,\mathbb{C}^3)} \Big) . \end{aligned} \tag{3.81}$$

Truncating the series in (3.81) and applying a quadrature rule on S^2 to evaluate the inner products (see, e.g., [AH12, Sec. 5.1]), we obtain a discrete approximation

$$\boldsymbol{T}_{B_{ij\ell}} := \begin{bmatrix} \langle H^*_{B_{ij\ell}} H_{B_{ij\ell}} \boldsymbol{U}^m_n, \boldsymbol{U}^{m'}_{n'} \rangle_{L^2_t(S^2,\mathbb{C}^3)} & \langle H^*_{B_{ij\ell}} H_{B_{ij\ell}} \boldsymbol{V}^m_n, \boldsymbol{U}^{m'}_{n'} \rangle_{L^2_t(S^2,\mathbb{C}^3)} \\ \langle H^*_{B_{ij\ell}} H_{B_{ij\ell}} \boldsymbol{U}^m_n, \boldsymbol{V}^{m'}_{n'} \rangle_{L^2_t(S^2,\mathbb{C}^3)} & \langle H^*_{B_{ij\ell}} H_{B_{ij\ell}} \boldsymbol{V}^m_n, \boldsymbol{V}^{m'}_{n'} \rangle_{L^2_t(S^2,\mathbb{C}^3)} \end{bmatrix} \in \mathbb{C}^{Q \times Q} \tag{3.82}$$

of $H^*_{B_{ij\ell}} H_{B_{ij\ell}}$ for any $-J \leq i, j, \ell \leq J$. The results from [GS18] suggest truncating the series in (3.81) at an index larger than $k|\boldsymbol{z}_{ij\ell}|$. In the following, we use the same truncation index $N \gtrsim \sqrt{3}kR$ for $\boldsymbol{F}_q$ and $H^*_{B_{ij\ell}} H_{B_{ij\ell}}$ for any $-J \leq i, j, \ell \leq J$, and thus also the same $Q = 2N(N+2)$.

First, we assume that the contrast function q is constant and strictly negative on the scattering object D. To implement the criteria from Theorem 3.20 we compute for each grid point $\boldsymbol{z}_{ij\ell} \in \triangle$ the eigenvalues $\lambda^{(ij\ell)}_1, \ldots, \lambda^{(ij\ell)}_Q \in \mathbb{R}$ of the self-adjoint matrices

$$\boldsymbol{A}^-_{B_{ij\ell}} := \mathrm{Re}(\boldsymbol{F}_q) - \alpha \boldsymbol{T}_{B_{ij\ell}} \in \mathbb{C}^{Q \times Q} , \qquad -J \leq i, j, \ell \leq J . \tag{3.83}$$

For numerical stabilization, we discard those eigenvalues whose absolute values are smaller than some threshold $\delta > 0$. This number depends on the quality of the data and should correspond to the size of the error (with respect to the spectral norm) as suggested by [GVL13, Thm. 7.2.2]). Since we do usually not exactly know this quantity, we use the magnitude of the non-unitary part of $\boldsymbol{S}_q := \boldsymbol{I}_Q + \mathrm{i}k/(8\pi^2)\boldsymbol{F}_q$ as an estimate for δ. More precisely, we take $\delta \approx \|\boldsymbol{S}^*_q \boldsymbol{S}_q - \boldsymbol{I}_Q\|_2$, because this quantity should be zero for exact data and be of the order of the data error, otherwise.

We recall the statements from Theorem 3.20. These imply that

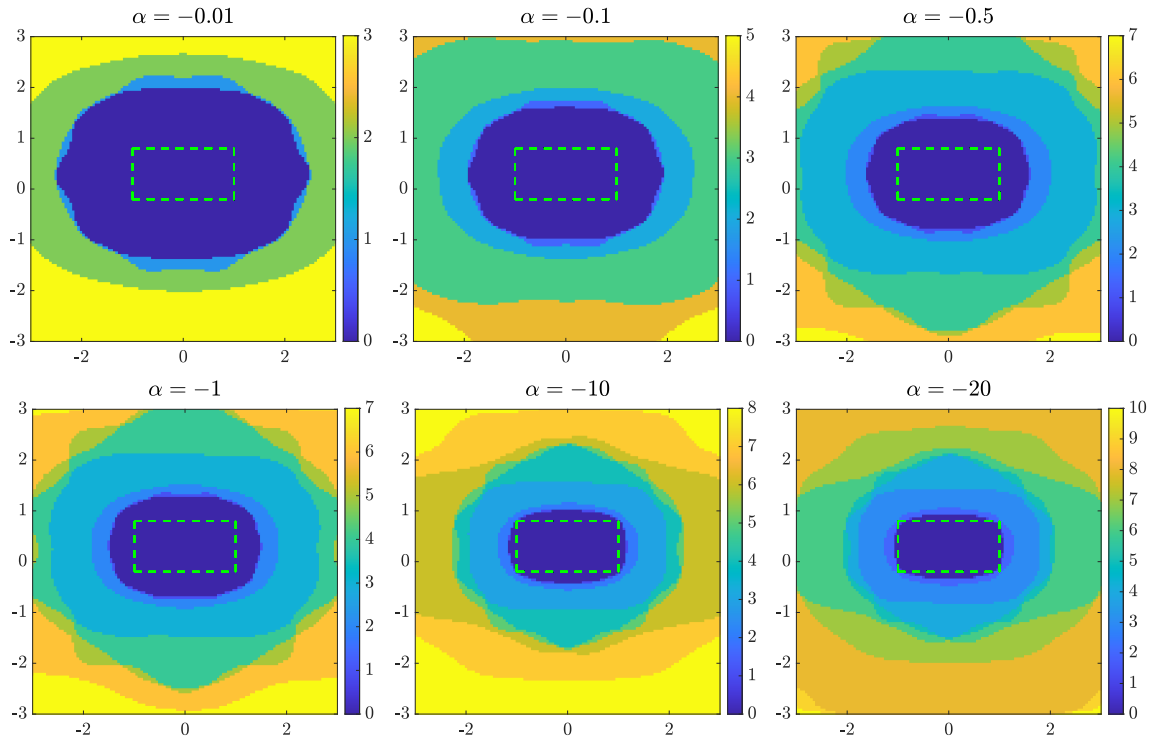

FIGURE 3.9. Visualization of the indicator function I_α^- from (3.84) for different values $\alpha \in \{-0.01, -0.1, -0.5, -1, -10, -20\}$ in the $\boldsymbol{x}_1, \boldsymbol{x}_2$-plane for $\boldsymbol{x}_3 = 0$ using simulated far field data without additional noise. The dashed lines show the exact boundaries of the cross-section of the scatterer from Example 3.6.2.

(a) if $B \subseteq D$, then $\mathrm{Re}(F_q) - \alpha H^*_{B_{ij\ell}} H_{B_{ij\ell}}$ has only finitely many positive eigenvalues for all $\alpha \geq C q_{\max}$, and

(b) if $B \not\subseteq D$, then $\mathrm{Re}(F_q) - \alpha H^*_{B_{ij\ell}} H_{B_{ij\ell}}$ has infinitely many positive eigenvalues for every $\alpha < 0$.

Together with our observations from the previous subsection, this suggests simply counting for each test ball $B_{ij\ell}$ the number of positive eigenvalues of $\boldsymbol{A}^-_{B_{ij\ell}}$, and we define the *indicator function* $I_\alpha^- : \triangle \to \mathbb{N}$,

$$I_\alpha^-(\boldsymbol{z}_{ij\ell}) := \#\{\lambda_n^{(ij\ell)} \mid \lambda_n^{(ij\ell)} > \delta\,,\ 1 \leq n \leq Q\}\,, \qquad -J \leq i,j,\ell \leq J\,. \tag{3.84}$$

Then, we expect that I_α^- is larger on sampling points $\boldsymbol{z}_{ij\ell} \in \triangle$ that are not contained inside the scattering object than on sampling points $\boldsymbol{z}_{ij\ell} \in \triangle$ that are contained inside of it. In the following example, we illustrate how the indicator function can be utilized to determine the shape and position of an unknown scattering object. We obtain similar results as achieved in Example 2.44.

Example 3.30. We consider a single scattering object D that has the shape of a cuboid as shown in Figure 3.10 (left). We use a constant contrast function $q = -1$ (i.e., the relative electric permittivity is $\varepsilon_r = 1/2$), $k = 1$ for the wave number and $N = 5$ for the truncation index in

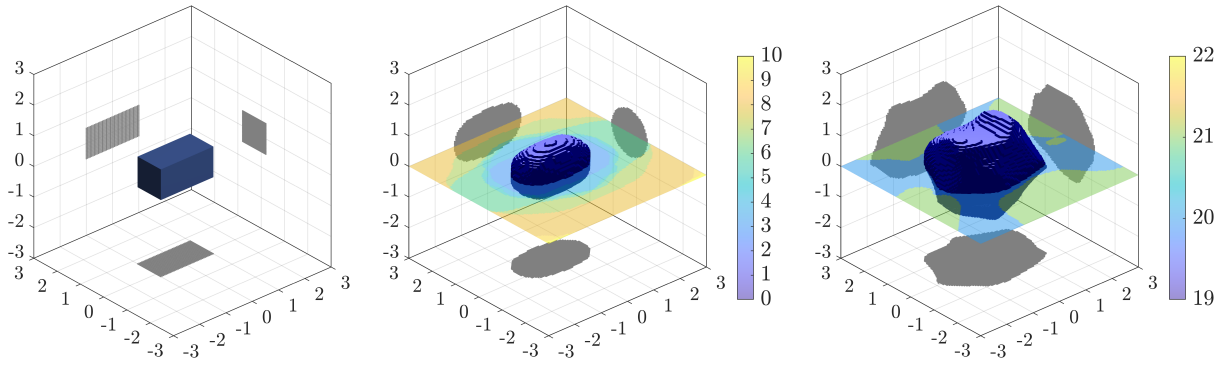

Figure 3.10. Visualization of the exact shape of the scattering object from Example 3.6.2 (left), Visualization of the isosurface $I^-_{-20} = 2$ of the indicator function from (3.84) using simulated far field data without additional noise (center) and of the isosurface $I^-_{-20} = 19$ using simulated far field data with 0.1% noise (right).

the vector spherical harmonics expansions (3.77) and (3.81) respecting condition (3.78). This means that the matrices (3.79), (3.82) and (3.83) are of the size 70×70. We simulate the far field matrix $\boldsymbol{F}_q \in \mathbb{C}^{70\times 70}$ using the C++ boundary element library Bempp [SBA+15]. Initially, we do not incorporate noise in the data and therefore use a threshold $\delta = 10^{-14}$. Thus, we only consider those eigenvalues with an absolute value larger than δ. Figure 3.8 shows a plot of the eigenvalues of $\boldsymbol{F}_q$. We clearly see that the eigenvalues lie on a circle and converge to zero. Moreover, as we would expect from Corollary 3.14, the eigenvalues converge to zero from the left side meaning their real parts are negative. In this example, the real part of $\boldsymbol{F}_q$ has indeed no positive eigenvalue.

In Figure 3.9, we show color-coded plots of the indicator function I^-_α from (3.84) in the $\boldsymbol{x}_1, \boldsymbol{x}_2$-plane for $\boldsymbol{x}_3 = 0$, i.e., we plot the number of those eigenvalues of $\boldsymbol{A}^-_{B_{ij\ell}}$ from (3.83) that are larger than δ for all grid points with a vanishing third component. The dashed lines show the exact boundaries of the cross-section of the scatterer. For the reconstructions, we use the sampling grid $\triangle$ from (3.80) with step size $h = 0.05$ in the region of interest $[-3, 3]^3$, i.e., we have 121 grid points in each direction. The truncation index in (3.72) is chosen to be 5. We examine six different values for α, namely $\alpha \in \{-0.01, -0.1, -0.5, -1, -10, -20\}$. We observe that the values of I^-_α are smaller for grid points inside the scattering object than outside, and that this number increases the farther away a grid point is from the scattering object, as we would expect from Theorem 3.20. Since we do not know an exact value for the constant C that appears in the condition $\alpha \geq C q_{\max}$ in Theorem 3.20 (a) we cannot determine whether all values chosen for α are admissible. Nevertheless, we notice that the lowest level set of the values of I^-_α approximates the cross-section better when α is chosen sufficiently small.

Next, we give a three-dimensional reconstruction in Figure 3.10 (middle). Figure 3.9 suggests choosing $\alpha = -20$, and inspecting the right picture in the bottom row we decide to plot the isosurface $I^-_{-20} = 2$. The position and the shape of the cuboid are nicely reconstructed.

To get an idea about the sensitivity of the reconstruction algorithm with respect to noise in the data, we redo our computation but add 0.1% complex-valued uniformly distributed additive error to the simulated far field data before starting the reconstruction procedure. The resulting

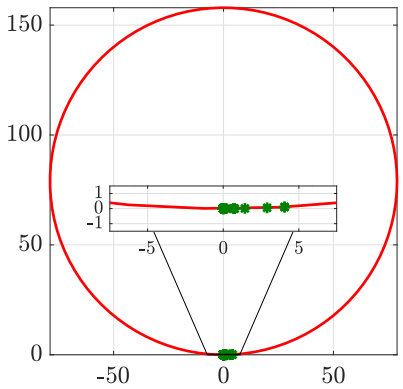

FIGURE 3.11. Eigenvalues of F_q (green) from Example 3.31 for $k = 1$ with $N = 5$.

reconstruction is shown in Figure 3.10 (right). In the reconstruction procedure, the noise is only accounted for via the threshold parameter δ in (3.84). In this example, we use $\delta = 0.001$ since the unitarity error is $\|\boldsymbol{S}_q^* \boldsymbol{S}_q - \boldsymbol{I}_Q\|_2 \approx 1.76 \cdot 10^{-4}$. The result gets worse, but it still contains useful information on the location and the shape of the scatterer. △

Now, we suppose the contrast function q to be strictly positive throughout the scatterer D. We summarize the findings from Theorem 3.21 implying that

(a) if $B \subseteq D$, then $\mathrm{Re}(F_q) - \alpha H_{B_{ij\ell}}^* H_{B_{ij\ell}}$ has only finitely many negative eigenvalues for all $\alpha \leq q_{\min}$, and

(b) if $B \not\subseteq D$, then $\mathrm{Re}(F_q) - \alpha H_{B_{ij\ell}}^* H_{B_{ij\ell}}$ has infinitely many negative eigenvalues for every $\alpha > 0$.

Proceeding similarly as before, we compute for each grid point $\boldsymbol{z}_{ij\ell} \in \triangle$ the eigenvalues $\lambda_1^{(ij\ell)}, \ldots, \lambda_Q^{(ij\ell)} \in \mathbb{R}$ of the self-adjoint matrices

$$\boldsymbol{A}_{B_{ij\ell}}^+ := -(\mathrm{Re}(\boldsymbol{F}_q) - \alpha \boldsymbol{T}_{B_{ij\ell}}) \in \mathbb{C}^{Q \times Q}, \qquad -J \leq i, j, \ell \leq J. \tag{3.85}$$

Then, we count for each test ball $B_{ij\ell}$ the number of positive eigenvalues of $\boldsymbol{A}_{B_{ij\ell}}^+$, and we define the *indicator function* $I_\alpha^+ : \triangle \to \mathbb{N}$,

$$I_\alpha^+(\boldsymbol{z}_{ij\ell}) := \#\{\lambda_n^{(ij\ell)} \mid \lambda_n^{(ij\ell)} > \delta,\ 1 \leq n \leq Q\}, \qquad -J \leq i, j, \ell \leq J. \tag{3.86}$$

Theorem 3.21 suggests that I_α^+ admits smaller values on sampling points $\boldsymbol{z}_{ij\ell} \in \triangle$ in the scattering object than on sampling points $\boldsymbol{z}_{ij\ell} \in \triangle$ outside of it.

Example 3.31. In this example, we examine a scattering object D that has the shape of a torus as sketched in Figure 3.13 (left). We consider a constant contrast function $q = 1/2$ (i.e., the relative electric permittivity is $\varepsilon_r = 2$), set the wave number $k = 1$ and use $N = 5$ for the truncation index in the vector spherical harmonics expansions (3.77) and (3.81). As in the previous example, the far field matrix $\boldsymbol{F}_q \in \mathbb{C}^{70 \times 70}$ is simulated by means of Bempp. We begin our considerations without noise and set the threshold $\delta = 10^{-14}$. In Figure 3.11, we present a plot of the eigenvalues of $\boldsymbol{F}_q$. On the one hand, it is obvious that the eigenvalues lie on a circle

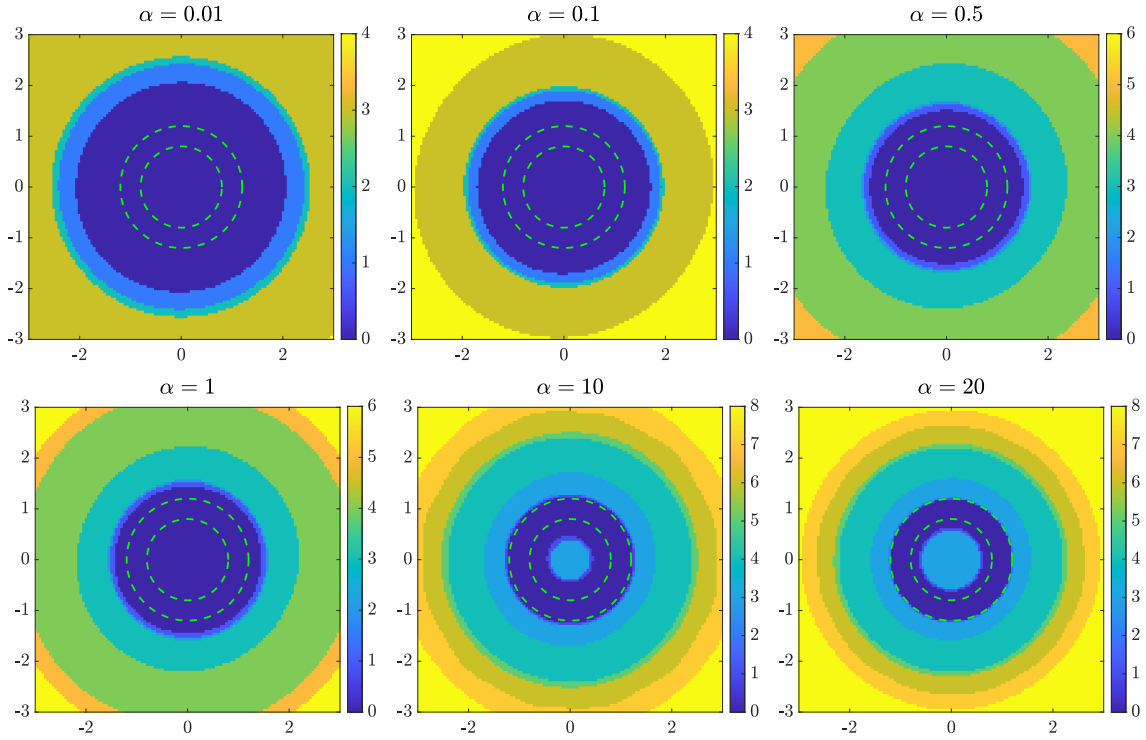

Figure 3.12. Visualization of the indicator function I_α^+ from (3.86) for different values $\alpha \in \{0.01, 0.1, 0.5, 1, 10, 20\}$ in the $\boldsymbol{x}_1, \boldsymbol{x}_2$-plane for $\boldsymbol{x}_3 = 0$ using simulated far field data without additional noise. The dashed lines show the exact boundaries of the cross-section of the scatterer from Example 3.31.

and converge to zero. On the other hand, we see that the eigenvalues converge to zero from the right side which corresponds to our findings in Corollary 3.14.

Figure 3.12 visualizes the indicator function I_α^+ from (3.86) as color-coded plots in the $\boldsymbol{x}_1, \boldsymbol{x}_2$-plane for $\boldsymbol{x}_3 = 0$. We again choose the step size $h = 0.05$ in the sampling grid $\triangle$ from (3.80) in the region of interest $[-3, 3]^3$, and we consider $\alpha \in \{0.01, 0.1, 0.5, 1, 10, 20\}$. As we would expect from Theorem 3.21, the values of I_α^+ are larger at sampling points that are sufficiently far away from the scatterer than at sampling points inside of it. The condition $\alpha \leq q_{\min}$ in Theorem 3.21 (a) is satisfied only for $\alpha \in \{0.01, 0.1, 0.5\}$. On the other hand, the hole inside the cross-section of the torus becomes visible in these reconstructions only when α is chosen sufficiently large.

Therefore, we nevertheless use $\alpha = 20$ for our three-dimensional reconstruction in Figure 3.13. Inspecting the right picture in the bottom row of Figure 3.12 suggests plotting the isosurface $I_{20}^+ = 2$, which is shown in Figure 3.12 (middle). The reconstruction approximates the position and the shape of the torus, in particular its hole in the middle, quite well. We note that it was observed in [GH18] for the corresponding scalar scattering problem governed by the Helmholtz equation that the quality of the reconstructions of this monotonicity-based scheme increases with increasing wave number also for larger values of α. However, in compliance to condition (3.78) we would have to enlarge the value of N for higher wave numbers. This leads to larger matrices and the computational effort increases.

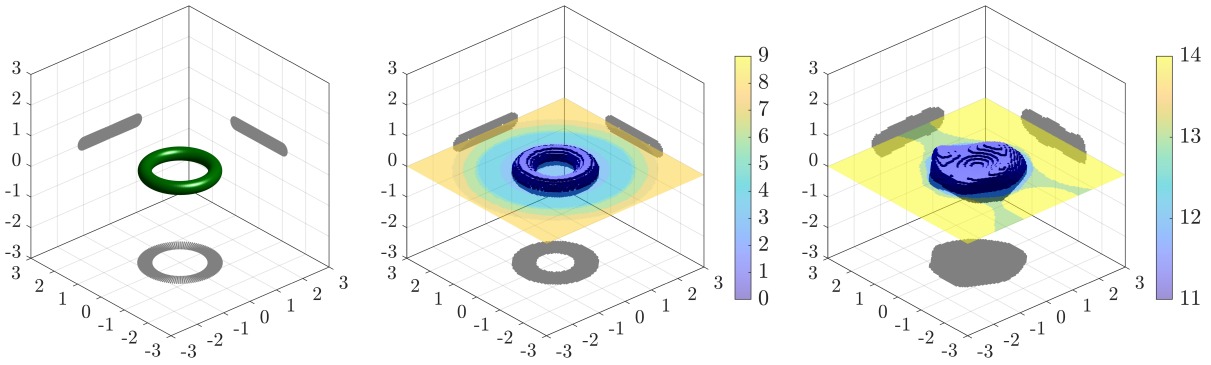

FIGURE 3.13. Visualization of the exact shape of the scattering object from Example 3.31 (left), Visualization of the isosurface $I_{20}^{+} = 2$ of the indicator function from (3.86) using simulated far field data without additional noise (center) and of the isosurface $I_{20}^{+} = 11$ using simulated far field data with 0.1% noise (right).

Finally, we repeat our computation with 0.1% complex-valued uniformly distributed additive error on the simulated far field data used for the reconstruction procedure. The resulting reconstruction is depicted in Figure 3.13 (right). Throughout the reconstruction procedure, we account for the noise via the threshold parameter $\delta = 0.001$ in (3.86). In this example, the magnitude of the non-unitarity of the scattering operator is $\|\boldsymbol{S}_q^* \boldsymbol{S}_q - \boldsymbol{I}_Q\|_2 \approx 1.84 \cdot 10^{-5}$. We observe that the result worsens, but it still gives an idea about the shape and position of the scatterer. Especially, we get an impression of where the hole of the torus is located. △

3.6.3. SEPARATING MIXED SCATTERERS

We discuss a numerical realization of the criteria established in Corollary 3.27. Therefore, we suppose that $D = D_1 \cup D_2$ is an indefinite scattering object with contrast function q such that $q_1 := q|_{D_1}$ is strictly negative on D_1 and $q_2 := q|_{D_2}$ is strictly positive on D_2. While the algorithm for sign-definite scattering objects in the previous subsection determines whether a sufficiently small probing domain B is contained inside the unknown scattering object D or not, the criteria from Corollary 3.27 describe whether a sufficiently large probing domain B contains the components D_1 or D_2 with strictly negative or strictly positive contrast functions, respectively, of the scattering object. We develop an algorithm to determine upper bounds $B_1, B_2 \subseteq \mathbb{R}^3$ such that $D_1 \subseteq B_1$ and $D_2 \subseteq B_2$. This is clearly less than full shape reconstruction but our numerical results below confirm that we can separate the two components of the scatterer with negative and positive scattering contrasts from far field data, at least when their supports are sufficiently far apart from each other.

We work on an equidistant sampling grid $\triangle$ as in (3.80). For each $\boldsymbol{z}_{ij\ell} \in \triangle$ we consider a probing operator $H_{B_{ij\ell}}^* H_{B_{ij\ell}}$ as in (3.55), where the probing domain $B_{ij\ell} = B_\rho(\boldsymbol{z}_{ij\ell})$ is a ball of radius ρ centered at $\boldsymbol{z}_{ij\ell}$. Here we assume that $\rho \geq \rho_0 > 0$, where $2\rho_0$ is an upper bound for the diameters of D_1 and D_2. We recapitulate the statements from Corollary 3.27 saying that

(a) if $D_1 \subseteq B$, then $\operatorname{Re}(F_q) - \alpha H_{B_{ij\ell}}^* H_{B_{ij\ell}}$ has only finitely many negative eigenvalues for all $\alpha \leq q_{1,\min}$, and

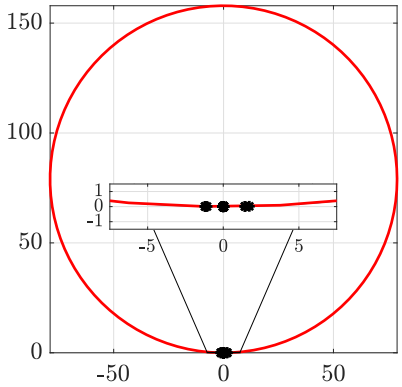

Figure 3.14. Eigenvalues of F_q (black) from Example 3.32 for $k = 1$ with $N = 5$.

(b) if $D_1 \not\subseteq B$, then $\mathrm{Re}(F_q) - \alpha H^*_{B_{ij\ell}} H_{B_{ij\ell}}$ has infinitely many negative eigenvalues for all $\alpha \in \mathbb{R}$, and

(c) if $D_2 \subseteq B$, then $\mathrm{Re}(F_q) - \alpha H^*_{B_{ij\ell}} H_{B_{ij\ell}}$ has only finitely many positive eigenvalues for all $\alpha \geq C q_{2,\max}$, and

(d) if $D_2 \not\subseteq B$, then $\mathrm{Re}(F_q) - \alpha H^*_{B_{ij\ell}} H_{B_{ij\ell}}$ has infinitely many positive eigenvalues for all $\alpha \in \mathbb{R}$.

This suggests computing for each grid point $\boldsymbol{z}_{ij\ell} \in \triangle$ the eigenvalues $\lambda_1^{(ij\ell)}, \ldots, \lambda_Q^{(ij\ell)} \in \mathbb{R}$ of the self-adjoint matrices $\boldsymbol{A}^-_{B_{ij\ell}}$ from (3.83) and $\boldsymbol{A}^+_{B_{ij\ell}}$ from (3.85). Moreover, assuming that the parameter α is chosen in compliance with the restrictions from (a) and (c), we count for each test ball $B_{ij\ell}$ the number of negative eigenvalues of $\boldsymbol{A}^{\mp}_{B_{ij\ell}}$, and we define for any $\boldsymbol{z} \in \triangle \cap B_{ij\ell}$,

$$\mathcal{I}^{\mp}_{\alpha,ij\ell}(\boldsymbol{z}) := \#\{\lambda_n^{(ij\ell)} \mid \lambda_n^{(ij\ell)} < -\delta\,,\ 1 \leq n \leq Q\}\,,$$

where $\delta > 0$ is a threshold parameter that depends on the quality of the data as in Subsection 3.6.2. Therewith, we define the *indicator function* $\mathcal{I}^{\mp}_{\alpha} : \triangle \to \mathbb{N}$,

$$\mathcal{I}^{\mp}_{\alpha}(\boldsymbol{z}) := \min\{\mathcal{I}^{\mp}_{\alpha,ij\ell}(\boldsymbol{z}) \mid -J \leq i,j,\ell \leq J\}\,. \tag{3.87}$$

Corollary 3.27 suggests that $\mathcal{I}^-_\alpha$ and $\mathcal{I}^+_\alpha$ are smaller on sampling points $\boldsymbol{z}_{ij\ell} \in \triangle$ that are close to D_1 and D_2 than on sampling points away from D_1 and D_2, respectively.

Example 3.32. We consider an indefinite scattering configuration with two scattering objects that are supported on cubes as shown in Figure 3.15 (left). The contrast function of the scatterer supported on the upper cube D_1 is $q_1 = -1$ (i.e., the relative electric permittivity is $\varepsilon_r = 1/2$), and the contrast function of the scatterer supported on the lower cube D_2 is $q_2 = 1/2$ (i.e., $\varepsilon_r = 2$). We use $k = 1$ for the wave number and $N = 5$ for the truncation index in the vector spherical harmonics expansions (3.77) and (3.81) (i.e., $Q = 70$ in (3.79), (3.82) and (2.82)). We simulate the far field matrix $\boldsymbol{F}_q \in \mathbb{C}^{Q\times Q}$ using the C++ boundary element library Bempp [SBA+15] and use $\delta = 10^{-14}$ for the threshold parameter. Figure 3.14 represents a plot of the eigenvalues of the matrix $\boldsymbol{F}_q$. We see that the eigenvalues lie on a circle and converge to zero. However, in contrast

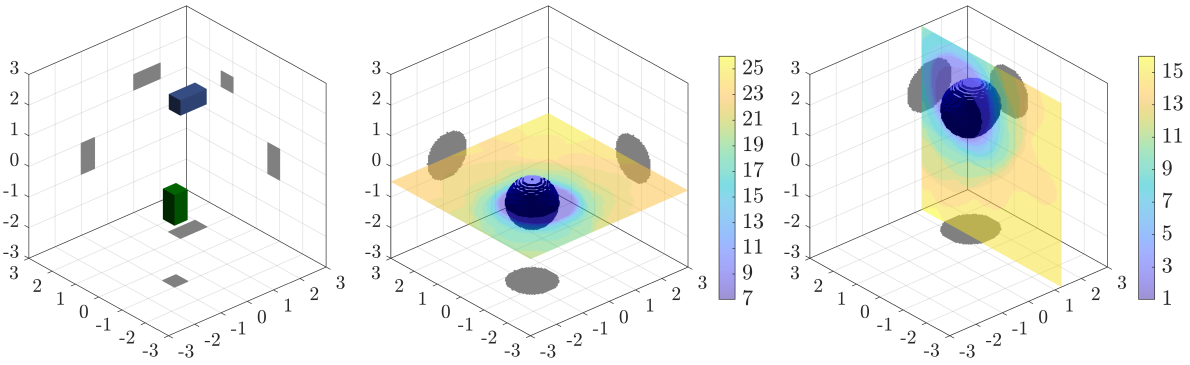

FIGURE 3.15. Visualization of the exact shape of the mixed scattering object from Example 3.32 (left) and of the isosurfaces $\mathcal{I}^{+}_{0.5} = 7$ (middle) and $\mathcal{I}^{-}_{-1} = 1$ (right).

to Figures 3.8 and 3.11 we cannot observe a side from which the eigenvalues seem to converge to zero. This illustrates that the matrix $\boldsymbol{F}_q$ is neither almost positive nor almost negative definite.

For the reconstructions we use the same sampling grid $\triangle$ as in the previous examples, i.e., (3.80) with step size $h = 0.05$ in the region of interest $[-3, 3]^3$. In Figure 3.15 (center and right) we show isosurfaces as well as cross-sections of color-coded plots of the indicator function $\mathcal{I}^{\mp}_{\alpha}$ from (3.87), where the radius of the test balls is $\rho = 0.75$. We use $\alpha = -1$ (right) to recover the approximate position and size of component D_1, where the contrast function q is strictly negative, and $\alpha = 0.5$ (center) to recover the approximate position and size of component D_2 where the contrast function q is strictly positive. We observe that the values of $\mathcal{I}^{-}_{-1}$ are smaller for grid points inside the component D_1 of the scattering object than outside. Similarly, the values of $\mathcal{I}^{+}_{0.5}$ are smaller for grid points inside the component D_2 of the scattering object than outside. These numbers increase the farther away a grid point is from the corresponding component of the scattering object, as we would expect from Corollary 3.27. The two isosurface plots $\mathcal{I}^{-}_{-1} = 1$ (right) and $\mathcal{I}^{+}_{0.5} = 7$ (center) in Figure 3.15 show that the components D_1 and D_2 of the indefinite scattering configuration can be nicely separated by the algorithm. $\triangle$

APPENDIX A

A Space of Continuous Piecewise Linear Functions

When establishing the existence of the simultaneously localized wave functions in Subsection 3.5.1 we employ a space of continuous piecewise linear functions supported in a relatively open part Γ of the considered boundary that vanish on $\partial\Gamma$. More precisely, this space finds use in the proofs of Lemmas 2.36 and 2.39. In the following, we construct this space and summarize some useful properties of it.

Lemma A.1. *Let $\Gamma \subseteq \partial\Omega$ be relatively open. Then, there exists an infinite-dimensional subspace X of $\widetilde{H}^{1/2}(\Gamma)$ such that*

$$X \cap H^{3/2}(\Gamma) \,=\, \{0\}\,.$$

In particular, zero is the only C^1-smooth function contained in X.

Proof. First, we notice that it suffices to consider functions on the $d-1$-dimensional ball $B'_r(0) \subseteq \mathbb{R}^{d-1}$ representing the domain of the local parameterization (2.4) of Γ.

Initially, we assume that $d = 2$. As a first step, we construct a continuous piecewise linear function on $B'_r(0) = (-r, r) \subseteq \mathbb{R}$ that vanishes on $\partial B'_r(0)$. Therefore, we choose an interval $[-a, a]$ that is strictly contained in $(-r, r)$ and define the hat function $h : (-r, r) \to \mathbb{R}$ by

$$h(t) \,=\, \begin{cases} 1 - \frac{1}{a}|t|\,, & |t| \leq a\,, \\ 0\,, & \text{otherwise}\,. \end{cases}$$

A plot of the function h is shown on the left-hand side of Figure A.1, where $r = 4.5$ and $a = 4$. Taking this function as a starting point, we introduce further hat functions by compressing and shifting h. For $n \in \mathbb{N}$, we divide the interval $[-a, a]$ into 2^n parts that have the length $2a/2^n$. The midpoint of each of these subintervals is given by

$$t_{n,j} \,:=\, \frac{2a(j+1)}{2^n} - a\,, \qquad j = 0, \ldots, 2^n - 1\,.$$

Then, we define 2^n hat functions $h_{n,j}$, $j = 0, \ldots, 2^n - 1$, such that each of these functions is a hat function supported on one of the intervals and takes the value one in the corresponding midpoint.

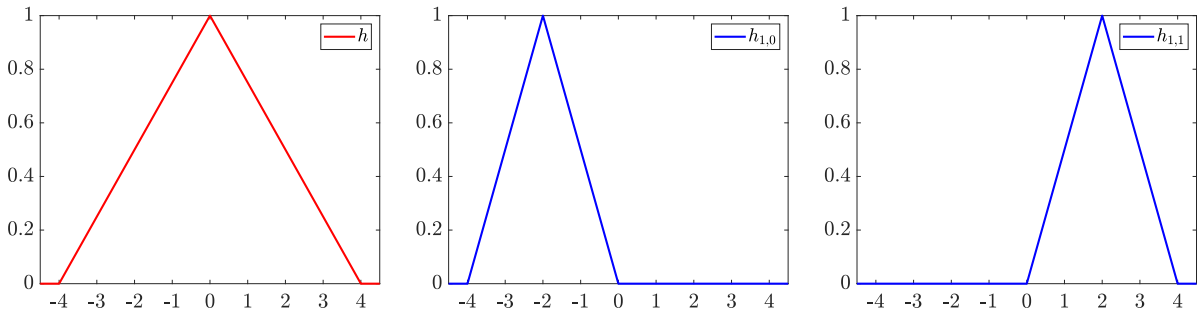

FIGURE A.1. Hat function h (left) and hat functions $h_{1,0}$, $h_{1,1}$ (middle, right) for $r = 4.5$ and $a = 4$.

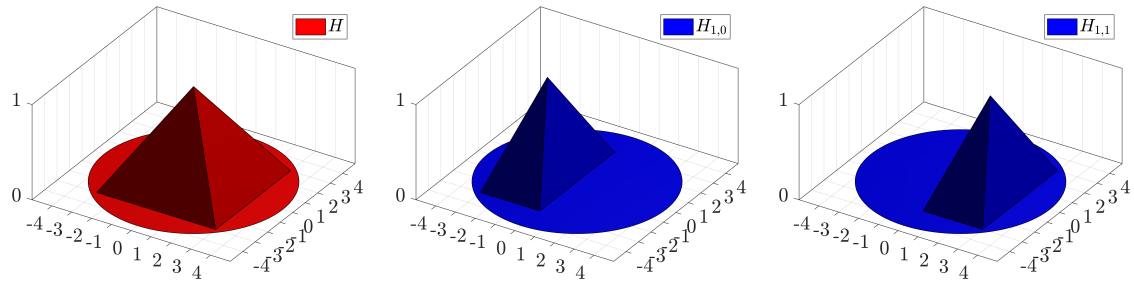

FIGURE A.2. Hat function H (left) and hat functions $H_{1,0}$, $H_{1,1}$ (middle, right) for $r = 4.5$ and $a = 3$.

Explicitly, they are given by

$$h_{n,j}(t) := h(2^n(t+a) - (2j+1)a)\,, \qquad j = 0, \dots, 2^n - 1\,.$$

For visualization, we show plots of the functions $h_{1,0}$ and $h_{1,1}$ in Figure A.1 (middle and right). We call these functions *basis functions* and denote the space spanned by them by

$$X_n := \operatorname{span}\{h_{n,j} \mid j = 0, \dots, 2^n - 1\}\,, \qquad n \in \mathbb{N}\,.$$

Next, we show that the basis functions contained in X_n are linearly independent. Let

$$\sum_{j=0}^{2^n-1} \alpha_j h_{n,j}(t) = 0\,, \qquad t \in (-r, r)\,. \tag{A.1}$$

Per definition, it is

$$h_{n,j}(t_{n,k}) = \delta_{j,k} := \begin{cases} 1\,, & j = k\,, \\ 0\,, & \text{otherwise}\,, \end{cases} \qquad j, k = 0, \dots, 2^n - 1\,.$$

Thus, inserting $t_{n,k}$, $k = 0, \dots, 2^n - 1$, in (A.1) yields $\alpha_j = 0$, $j = 0, \dots, 2^n - 1$. Eventually, we choose X to be the sum of the spaces X_n, $n \in \mathbb{N}$. Due to the linear independence of the basis functions in X_n, the space X is infinite dimensional.

Secondly, we consider $d = 3$ proceeding similarly. Let $S = [-a, a]^2$ be a square that is strictly contained in $B'_r(0) \subseteq \mathbb{R}^2$. Then, we define the hat function $H : B'_r(0) \to \mathbb{R}$ by

$$H(\boldsymbol{x}') := \begin{cases} 1 - \frac{1}{a}\|\boldsymbol{x}'\|_\infty\,, & \boldsymbol{x}' \in [-a, a]^2\,, \\ 0 & \text{otherwise}\,. \end{cases}$$

Figure A.2 (left) contains a plot of H for $r = 4.5$ and $a = 3$. As before, we use this function to create more families of hat functions. To this end, for each $n \in \mathbb{N}$, we vertically divide $[-a, a]^2$ into 2^n rectangles such that $\{t_{n,j}\} \times [-a, a]$, $j = 0, \dots, 2^n - 1$, is the vertical midline of the corresponding rectangle. By compressing and shifting H, we construct 2^n hat functions supported on $[t_{n,j} - a/2^n, t_{n,j} + a/2^n] \times [-a, a]$ with their tops in $(t_{n,j}, 0)^\top$. Following the 2-dimensional case, we denote the resulting functions by $H_{n,j}$ and call them basis functions. We exemplary show the functions $H_{1,0}$ and $H_{1,1}$ in Figure A.2 in the middle and on the right-hand side, respectively. We introduce the spaces

$$X_n := \operatorname{span}\{H_{n,j} \mid j = 0, \dots, 2^n - 1\}\,, \qquad n \in \mathbb{N}\,.$$

and define X to be the sum of all X_n, $n \in \mathbb{N}$. Analogous to our previous consideration, we find that the basis functions in X_n are linearly independent. For arbitrary x_2, it is $H_{n,j}(t_{n,k}) = \delta_{j,k}$, $j, k = 0, \dots, 2^n - 1$. Consequently, plugging $t_{n,k}$, $k = 0, \dots, 2^n - 1$, into the equation

$$\sum_{j=0}^{2^n-1} \alpha_j H_{n,j}(\boldsymbol{x}') = 0\,, \qquad \boldsymbol{x}' \in B'_r(0)\,,$$

shows that $\alpha_j = 0$, $j = 0, \dots, 2^n - 1$. Hence, X is infinite dimensional.

Finally, we investigate the regularity of functions belonging to X for $d = 2, 3$. Since the basis functions are continuous and piecewise linear, every function in X is also continuous and piecewise linear. This implies that they lie in $H^1(B'_r(0))$, and thus also in $H^{1/2}(B'_r(0))$, because their weak derivatives are piecewise constant. Accordingly, X is a subspace of $H^{1/2}(B'_r(0))$. The boundary condition on $\partial B'_r(0)$ ensures that zero is the only constant function in X. Therefore, the weak derivatives of nontrivial functions in X are non-constant piecewise constant functions. Since characteristic functions associated with nontrivial subsets of $\mathbb{R}^d$ are not in $H^{1/2}(\mathbb{R}^d)$ (see, e.g., [Sic21, Thm. 1]), these derivatives are not contained in $H^{1/2}(B'_r(0))$. Consequently, $X \cap H^{3/2}(B'_r(0)) = \{0\}$. Continuously differentiable functions possess weak derivatives and are therefore contained in $H^1(B'_r(0))$. Besides, $H^1(B'_r(0)) \subseteq H^{3/2}(B'_r(0))$ which guarantees that zero is the only C^1-smooth function in X. □

In Subsection 2.4.2, we investigate simultaneously localized vector wave functions and require an analogous result to Lemma A.1 in the proof of Lemma 3.25. More precisely, we extend the space X containing continuous piecewise linear functions to a space $\boldsymbol{X}$ of tangential continuous piecewise linear vector fields.

Lemma A.2. *Let $\Gamma \subseteq \partial\Omega$ be relatively open and smooth. Then, there exists an infinite-dimensional subspace $\boldsymbol{X}$ of $\widetilde{H}^{-1/2}(\mathrm{Div};\Gamma)$ such that*

$$\boldsymbol{X} \cap H_t^{3/2}(\Gamma,\mathbb{C}^3) \,=\, \{0\}\,.$$

Proof. As in the previous proof, without loss of generality, we restrict our considerations to the domain $B_r'(0) \subseteq \mathbb{R}^2$ of the local parameterization (2.4) of the boundary Γ. To construct continuous piecewise linear vector fields, we need to ensure that each of the components is continuous and piecewise linear. However, it does not suffice to assign arbitrary continuous piecewise linear functions to the single components because we additionally require tangential vector fields. Since Γ is C^1 smooth, by taking partial derivatives we can calculate the local tangent vectors $\boldsymbol{T}_1$ and $\boldsymbol{T}_2$ and obtain

$$\boldsymbol{T}_1(\boldsymbol{x}') \,=\, \frac{\partial}{\partial x_1}\begin{pmatrix} x_1 \\ x_2 \\ \zeta(x_1,x_2)\end{pmatrix} \,=\, \begin{pmatrix} 1 \\ 0 \\ \frac{\partial}{\partial x_1}\zeta(x_1,x_2)\end{pmatrix}, \qquad \boldsymbol{x}' \in B_r'(0)\,,$$

and

$$\boldsymbol{T}_2(\boldsymbol{x}') \,=\, \frac{\partial}{\partial x_2}\begin{pmatrix} x_1 \\ x_2 \\ \zeta(x_1,x_2)\end{pmatrix} \,=\, \begin{pmatrix} 0 \\ 1 \\ \frac{\partial}{\partial x_2}\zeta(x_1,x_2)\end{pmatrix}, \qquad \boldsymbol{x}' \in B_r'(0)\,.$$

Therewith, we define the tangential continuous piecewise linear vector fields $\boldsymbol{H}_{n,j} : B_r'(0) \to \mathbb{R}^3$ for $n \in \mathbb{N}$ by

$$\boldsymbol{H}_{n,j}(\boldsymbol{x}') \,:=\, H_{n,j}(\boldsymbol{x}')\boldsymbol{T}_1(\boldsymbol{x}') + H_{n,j}(\boldsymbol{x}')\boldsymbol{T}_2(\boldsymbol{x}')\,, \qquad j = 0,\ldots,2^n-1\,,$$

where $H_{n,j}$ are the hat functions constructed in the proof of Lemma A.1. Setting

$$\boldsymbol{X}_n \,:=\, \mathrm{span}\{\boldsymbol{H}_{n,j} \mid j = 0,\ldots,2^n-1\}\,, \qquad n \in \mathbb{N}\,,$$

and defining $\boldsymbol{X}$ to be the sum of $\boldsymbol{X}_n$, $n \in \mathbb{N}$, it follows from Lemma A.1 that $\boldsymbol{X} \subseteq H^{1/2}(B_r'(0),\mathbb{C}^3)$ and $\boldsymbol{X} \cap H^{3/2}(B_r'(0),\mathbb{C}^3) = \{0\}$. Due to the inclusion $H_t^{3/2}(B_r'(0),\mathbb{C}^3) \subseteq H^{3/2}(B_r'(0),\mathbb{C}^3)$, the latter implies that $\boldsymbol{X} \cap H_t^{3/2}(B_r'(0),\mathbb{C}^3) = \{0\}$. It remains to show that $\boldsymbol{X} \subseteq H^{-1/2}(\mathrm{Div};\partial B_r'(0))$. As a result of its construction, the space $\boldsymbol{X}$ only contains tangential vector fields, and therefore, it is $\boldsymbol{X} \subseteq H_t^{1/2}(B_r'(0),\mathbb{C}^3)$. On one side, we know that $H_t^{1/2}(B_r'(0),\mathbb{C}^3) \subseteq H_t^{-1/2}(B_r'(0),\mathbb{C}^3)$. On the other side, the surface divergence is a continuous operator from $H_t^{1/2}(B_r'(0),\mathbb{C}^3)$ to $H^{-1/2}(B_r'(0))$. This completes the proof. □

APPENDIX B

Vector and Differential Calculus

In this chapter, we list several vector and differential identities that we use throughout the work. Let $\boldsymbol{x}, \boldsymbol{y}, \boldsymbol{z} \in \mathbb{R}^3$. Then, it is

$$\begin{aligned} \boldsymbol{x} \times \boldsymbol{x} &= 0\,, \\ \boldsymbol{x} \times \boldsymbol{y} &= -\boldsymbol{y} \times \boldsymbol{x}\,, \\ (\boldsymbol{x} \times \boldsymbol{y}) \cdot \boldsymbol{z} &= (\boldsymbol{z} \times \boldsymbol{x}) \cdot \boldsymbol{y} = (\boldsymbol{y} \times \boldsymbol{z}) \cdot \boldsymbol{x}\,, \\ (\boldsymbol{x} \times \boldsymbol{y}) \times \boldsymbol{z} &= (\boldsymbol{z} \cdot \boldsymbol{x})\boldsymbol{y} - (\boldsymbol{z} \cdot \boldsymbol{y})\boldsymbol{x}\,. \end{aligned}$$

These identities are frequently used in Chapter 3 without indicating it.

Let $\Omega \subseteq \mathbb{R}^3$ be open and bounded. For any vector field $\boldsymbol{F} \in C^2(\Omega, \mathbb{C}^3)$, we have

$$\mathbf{curl}\,\mathbf{curl}\,\boldsymbol{F} = -\Delta \boldsymbol{F} + \nabla \operatorname{div} \boldsymbol{F} \tag{B.1}$$

and

$$\operatorname{div}\mathbf{curl}\,\boldsymbol{F} = 0\,. \tag{B.2}$$

With regard to the diagram (3.2), the latter identity also makes sense for $\boldsymbol{F} \in H(\mathbf{curl}; \Omega)$. At this point, we remind the reader that equalities involving L^2 functions are to be understood in the L^2 sense meaning $\|\operatorname{div}\mathbf{curl}\,\boldsymbol{F}\|_{L^2(\Omega)} = 0$.

If λ and $\boldsymbol{F}$ are differentiable, it holds

$$\mathbf{curl}(\lambda \boldsymbol{F}) = \nabla\lambda \times \boldsymbol{F} + \lambda\,\mathbf{curl}\,\boldsymbol{F}\,.$$

Moreover, it is possible to extend this product rule to less smooth vector fields. Let $\Omega \subseteq \mathbb{R}^3$ be open and bounded, and let $\boldsymbol{F} \in H(\mathbf{curl}; \Omega)$ and $\lambda \in C_0^\infty(\Omega)$. We define $\boldsymbol{G}$ as the extension of $\lambda\boldsymbol{F}$ by zero into $\mathbb{R}^3$, and we obtain

$$\mathbf{curl}\,\boldsymbol{G} = \begin{cases} \nabla\lambda \times \boldsymbol{F} + \lambda\,\mathbf{curl}\,\boldsymbol{F} & \text{in } \Omega\,, \\ 0 & \text{in } \mathbb{R}^3 \setminus \Omega \end{cases} \tag{B.3}$$

(see, e.g., [KH15, Lmm. 4.17]).

Now, let $\Omega \subseteq \mathbb{R}^3$ be open and Lipschitz bounded. Then, the exterior unit normal $\boldsymbol{\nu}$ exists almost everywhere and is in $L^\infty(\mathbb{R}^3)$. For any vector field, we have

$$\boldsymbol{F} \;=\; (\boldsymbol{F}\cdot\boldsymbol{\nu})\boldsymbol{\nu} + \big((\boldsymbol{\nu}\times\boldsymbol{F})\times\boldsymbol{\nu}\big) \qquad \text{on } \partial\Omega \tag{B.4}$$

in the L^∞-sense. If $\boldsymbol{F} \in C^1(\overline{\Omega},\mathbb{R}^3)$, we have

$$\boldsymbol{\nu}\cdot(\mathbf{curl}\,\boldsymbol{F})|_{\partial\Omega} \;=\; \mathrm{Curl}_{\partial\Omega}\big((\boldsymbol{\nu}\times\boldsymbol{F})\times\boldsymbol{\nu}\big)\,. \tag{B.5}$$

For $\boldsymbol{F} \in H(\mathbf{curl};\Omega)$, the right-hand side is well-defined in the sense of the trace operator π_t from (3.3) and we can extend this equality to $H(\mathbf{curl};\Omega)$-functions.

APPENDIX C

Spherical Harmonics

Solutions to Laplace's equation $\Delta u = 0$ are known as harmonics. A *spherical harmonic* of order n is the trace of a homogeneous harmonic polynomial of order n on the unit sphere S^{d-1}. First, we discuss spherical harmonics in $\mathbb{R}^2$ and investigate Bessel functions in Section C.1. We use these in Section 2.5 when presenting numerical examples in two dimensions for the inverse acoustic obstacle scattering problem. In Section C.2, we move on to three-dimensional space, and we give a brief summary of spherical Bessel functions and the associated spherical vector wave functions. These concepts are important when studying numerical examples in three dimensions for the inverse electromagnetic scattering problem in Section 3.6.

C.1. Bessel Functions

In this section, we restrict ourselves to the two-dimensional case and summarize the outline by Colton and Kress [CK19, Sec. 3.5]. In two dimensions, there exist exactly two linearly independent spherical harmonics of order n, $n = 1, 2, \ldots$, and one for $n = 0$. Writing $\boldsymbol{x} \in \mathbb{R}^2$ in polar coordinates $\boldsymbol{x} = r(\cos\varphi, \sin\varphi)^\top$, $r > 0$, $\varphi \in (-\pi, \pi]$, we employ an ansatz of separation of variables and use the expansion

$$\Delta = \frac{1}{r}\left[\frac{\partial}{\partial r}\left(r\frac{\partial}{\partial r}\right) + \frac{\partial}{\partial \varphi}\left(\frac{1}{r}\frac{\partial}{\partial \varphi}\right)\right] \tag{C.1}$$

of the Laplace operator in polar coordinates to find that the spherical harmonics of order n can be represented by $e^{\pm in\varphi}$ for $n \neq 0$ and by 1 for $n = 0$.

We are interested in solutions u to the Helmholtz equation $\Delta u + k^2 u = 0$ expressed in polar coordinates (r, ϕ). Separating the variables r and φ, and applying (C.1) yields that the solutions are of the form

$$u(\boldsymbol{x}) = f(kr)e^{\pm in\varphi}, \qquad \boldsymbol{x} = r(\cos\varphi, \sin\varphi)^\top, \quad r > 0, \, \varphi \in (-\pi, \pi].$$

The function f satisfies the *Bessel differential equation*

$$t^2 f''(t) + t f'(t) + (t^2 - n^2) f(t) \;=\; 0, \qquad n \in \mathbb{N}\,. \tag{C.2}$$

Two linearly independent solutions to this differential equation are given by the Bessel and the Neumann functions. The *Bessel function* of order n is denoted by J_n and analytic throughout $\mathbb{R}$. The *Neumann function* of order n is denoted by Y_n and analytic for positive arguments. Series expansions of these functions can, e.g., be found in [CK19, Equ. (3.97)–(3.98)]. The linear combinations

$$H_n^{(1)} \;:=\; J_n + \mathrm{i} Y_n \quad \text{ and } \quad H_n^{(2)} \;:=\; J_n - \mathrm{i} Y_n$$

are known as *Hankel functions* of the first and second kind of order n, respectively. We observe that these also are two linearly independent solutions to the Bessel differential equation (C.2).

We require several asymptotics for Bessel functions. On one hand, we are interested in their behavior for large arguments. In this case, the Hankel functions have the asymptotic behavior

$$H_n^{(1,2)}(t) \;=\; \sqrt{\frac{2}{\pi t}} e^{\pm \mathrm{i}(t - \frac{n\pi}{2} - \frac{\pi}{4})} \Big(1 + \mathcal{O}\Big(\frac{1}{t}\Big) \Big)\,, \qquad t \to \infty\,, \tag{C.3}$$

(see, e.g., [CK19, Equ. (3.105)]). On the other hand, we would like to know how Bessel functions behave when their order becomes arbitrarily large. The following asymptotic expansions hold for large orders $n \to \infty$ and fixed arguments $t \neq 0$. It is

$$J_n(t) \;\sim\; \frac{1}{\sqrt{2\pi n}} \Big(\frac{et}{2n} \Big)^n \tag{C.4}$$

and

$$Y_n(t) \;\sim\; -\mathrm{i} H_n^{(1)}(t) \;\sim\; -\sqrt{\frac{2}{\pi n}} \Big(\frac{et}{2n} \Big)^{-n} \tag{C.5}$$

(see, e.g., [OLBC10, 10.19.1–2]).

Next, we state an addition theorem that reads

$$H_0^{(1)}(k|\boldsymbol{x} - \boldsymbol{y}|) \;=\; H_0^{(1)}(k|\boldsymbol{x}|) J_0(k|\boldsymbol{y}|) + 2 \sum_{n=1}^{\infty} H_n^{(1)}(k|\boldsymbol{x}|) J_n(k|\boldsymbol{y}|) \cos(n\vartheta)$$

for all $\boldsymbol{x}, \boldsymbol{y} \in \mathbb{R}^2$, where $|\boldsymbol{x}| > |\boldsymbol{y}|$ and ϑ denotes the angle between $\boldsymbol{x}$ and $\boldsymbol{\theta}$ (see, e.g., [CK19, Equ. (3.111)]). The convergence is uniform on compact subsets of $|\boldsymbol{x}| > |\boldsymbol{y}|$. Taking the real part of this identity and using the relation $J_{-n}(t) = (-1)^n J_n(t)$ (see, e.g., [OLBC10, 10.4.1]), we arrive at

$$J_0(k|\boldsymbol{x} - \boldsymbol{y}|) \;=\; \sum_{n \in \mathbb{Z}} J_n(k|\boldsymbol{x}|) J_n(k|\boldsymbol{y}|) e^{\mathrm{i}n\vartheta} \tag{C.6}$$

for all $\boldsymbol{x}, \boldsymbol{y} \in \mathbb{R}^2$.

Furthermore, there holds the *Jacobi-Anger expansion*

$$e^{\mathrm{i}k\boldsymbol{x}\cdot\boldsymbol{\theta}} \;=\; J_0(k|\boldsymbol{x}|) + 2 \sum_{n=1}^{\infty} \mathrm{i}^n J_n(k|\boldsymbol{x}|) \cos(n\vartheta)\,, \qquad \boldsymbol{x} \in \mathbb{R}^2\,,$$

where $\boldsymbol{\theta}$ is a unit vector and ϑ again denotes the angle between $\boldsymbol{x}$ and $\boldsymbol{\theta}$ (see, e.g., [CK19, Equ. (3.112)]). The series converges uniformly on compact subsets of $\mathbb{R}^2$. We can rewrite the expression in the form

$$e^{\mathrm{i}k|\boldsymbol{x}|\cos\vartheta} = \sum_{n\in\mathbb{Z}} i^n J_n(k|\boldsymbol{x}|)e^{\mathrm{i}n\vartheta}\,, \qquad \boldsymbol{x}\in\mathbb{R}^2\,. \tag{C.7}$$

Finally, the following theorem allows us to expand radiating solutions to the Helmholtz equations in terms of so-called spherical wave functions.

Theorem C.1. *Every radiating solution $u \in C^2(\mathbb{R}^2 \setminus \overline{B_R(0)})$ to the Helmholtz equation possesses an expansion*

$$u(\boldsymbol{x}) = \sum_{n\in\mathbb{Z}} a_n H_n^{(1)}(kr)e^{-\mathrm{i}n\varphi}\,, \qquad r>R\,,\ \boldsymbol{x}=r(\cos\varphi,\sin\varphi)^\top\,,$$

where the coefficients $a_n \in \mathbb{C}$ are uniquely determined.

Proof. For a proof, we refer the reader to [CC14, p. 54]. □

C.2. Spherical Vector Wave Functions

From now on, we consider the space $\mathbb{R}^3$. The following short overview focuses on the aspects that are relevant for this work. For a detailed derivation of the presented concepts, we refer the reader, e.g., to [CK19, Sec. 2.3–2.4 and Sec. 6.5]. In three dimensions, there exist exactly $2n+1$ linearly independent spherical harmonics of order n, $n\in\mathbb{N}$ (see, e.g., [CK19, Thm. 2.7]). It can be shown that the functions Y_n^m, given by

$$Y_n^m(\widehat{\boldsymbol{x}}) := \sqrt{\frac{2n+1}{4\pi}\frac{(n-|m|)!}{(n+|m|)!}}P_n^{|m|}(\cos\theta)e^{\mathrm{i}m\varphi}\,,$$

for $m=-n,\dots,n$ and $n\in\mathbb{N}$, are spherical harmonics of order n and that they form a complete orthonormal system of $L^2(S^{d-1})$ (see, e.g., [CK19, Thm. 2.8]). Here, (θ,φ) are the spherical polar coordinates of $\widehat{\boldsymbol{x}}\in S^2$, and P_n^m, $n,m\in\mathbb{N}$, denotes the mth associated Legendre function of order n. Moreover, we define the *vector spherical harmonics* by

$$\boldsymbol{U}_n^m(\widehat{\boldsymbol{x}}) := \frac{1}{\sqrt{n(n+1)}}\mathbf{Grad}_{S^2}\,Y_n^m(\widehat{\boldsymbol{x}})\,, \qquad \boldsymbol{V}_n^m(\widehat{\boldsymbol{x}}) := \widehat{\boldsymbol{x}}\times\boldsymbol{U}_n^m(\widehat{\boldsymbol{x}})\,, \qquad \widehat{\boldsymbol{x}}\in S^2\,, \tag{C.8}$$

for $m=-n,\dots,n$, $n\in\mathbb{N}$. These form a complete orthonormal system in $L_t^2(S^2,\mathbb{C}^3)$ (see, e.g., [CK19, Thm. 6.25]).

Next, we introduce spherical Bessel and Neumann functions. These are linearly independent solutions to the *spherical Bessel differential equation*

$$t^2f''(t)+2tf'(t)+\big(t^2-n(n+1)\big)f(t) = 0\,, \qquad n\in\mathbb{N}\,. \tag{C.9}$$

This differential equation arises when seeking solutions to the Helmholtz equation $\Delta u + k^2u = 0$ that are of the form $u(\boldsymbol{x}) = f(k|\boldsymbol{x}|)u_n(\widehat{\boldsymbol{x}})$, where $\widehat{\boldsymbol{x}} = \boldsymbol{x}/|\boldsymbol{x}| \in S^2$ and u_n is a spherical harmonic

of order n. The *spherical Bessel function* of order n is denoted by j_n and analytic throughout $\mathbb{R}$. The *spherical Neumann function* of order n is denoted by y_n and analytic for positive arguments. For series representations of the functions, we refer to [CK19, Equ. (2.32)–(2.33)]. The *spherical Hankel functions* of the first and second kind of order n are given by

$$h_n^{(1)} := j_n + \mathrm{i}y_n \quad \text{and} \quad h_n^{(2)} := j_n - \mathrm{i}y_n$$

and also represent two linearly independent solutions to the spherical Bessel differential equation (C.9). The ordinary and the spherical Bessel functions are connected via

$$f_n(t) = \sqrt{\frac{\pi}{2t}} F_{n+1/2}(t), \qquad n \in \mathbb{N},$$

where $f_n \in \{j_n, y_n, h_n^{(1)}, h_n^{(2)}\}$ and $F_n \in \{J_n, Y_n, H_n^{(1)}, H_n^{(2)}\}$ are the corresponding Bessel functions (see, e.g., [OLBC10, 10.47.3–6]).

In this thesis, we use the asymptotic behavior of the spherical Hankel functions for large argument which reads

$$h_n^{(1,2)}(t) = \frac{1}{t} e^{\pm \mathrm{i}(t - \frac{n\pi}{2} - \frac{\pi}{4})} \Big(1 + \mathcal{O}\Big(\frac{1}{t}\Big)\Big), \qquad t \to \infty, \tag{C.10}$$

(see, e.g., [CK19, Equ. (2.42)]). Besides, we need to know what happens when the orders of the spherical Bessel and Hankel functions as well as of their derivatives tend to infinity. For fixed arguments $t \neq 0$, it holds

$$j_n(t) = \frac{t^n}{(2n+1)!!}\Big(1 + \mathcal{O}\Big(\frac{1}{n}\Big)\Big), \tag{C.11a}$$

$$j_n'(t) = n\frac{t^{n-1}}{(2n+1)!!}\Big(1 + \mathcal{O}\Big(\frac{1}{n}\Big)\Big), \tag{C.11b}$$

$$h_n^{(1)}(t) = \frac{(2n-1)!!}{\mathrm{i}t^{n+1}}\Big(1 + \mathcal{O}\Big(\frac{1}{n}\Big)\Big), \tag{C.11c}$$

$$(h_n^{(1)})'(t) = -(n+1)\frac{(2n-1)!!}{\mathrm{i}t^{n+2}}\Big(1 + \mathcal{O}\Big(\frac{1}{n}\Big)\Big) \tag{C.11d}$$

as $n \to \infty$, where $(2n+1)!! = 1 \cdot 3 \cdot 5 \cdots (2n+1)$ (see, e.g., [KH15, Thm. 2.31]).

Furthermore, we have the *Funk-Hecke formula*

$$\int_{S^2} e^{-\mathrm{i}kr\widehat{\boldsymbol{x}}\cdot\widehat{\boldsymbol{z}}} Y_n^m(\widehat{\boldsymbol{z}})\, \mathrm{d}s(\widehat{\boldsymbol{z}}) = \frac{4\pi}{\mathrm{i}^n} j_n(kr) Y_n^m(\widehat{\boldsymbol{x}}), \qquad \widehat{\boldsymbol{x}} \in S^2, r > 0,$$

for all $m = -n, \dots, n$ and $n \in \mathbb{N}$ (see, e.g., [CK19, p. 36]). In particular, setting $m = n = 0$ gives

$$\int_{S^2} e^{-\mathrm{i}kr\widehat{\boldsymbol{x}}\cdot\widehat{\boldsymbol{z}}}\, \mathrm{d}s(\widehat{\boldsymbol{z}}) = 4\pi j_0(kr), \qquad \widehat{\boldsymbol{x}} \in S^2, r > 0. \tag{C.12}$$

Now, we define the *spherical vector wave functions*

$$\boldsymbol{M}_n^m(\boldsymbol{x}) := -j_n(k|\boldsymbol{x}|)\boldsymbol{V}_n^m(\widehat{\boldsymbol{x}}), \qquad \boldsymbol{N}_n^m(\boldsymbol{x}) := -h_n^{(1)}(k|\boldsymbol{x}|)\boldsymbol{V}_n^m(\widehat{\boldsymbol{x}}), \qquad \boldsymbol{x} \in \mathbb{R}^3, \tag{C.13}$$

for $m = -n, \dots, n$, $n = 1, 2, \dots$. We note that the normalization factors used in (C.13) differ from what is used elsewhere in the literature (see, e.g., [CK19, Sec. 6.5]). The pair $(\boldsymbol{M}_n^m, \frac{1}{\mathrm{i}\omega\mu_0}\,\mathbf{curl}\,\boldsymbol{M}_n^m)$ is an entire solution to Maxwell's equations whereas the pair $(\boldsymbol{N}_n^m, \frac{1}{\mathrm{i}\omega\mu_0}\,\mathbf{curl}\,\boldsymbol{N}_n^m)$ is a radiating solution to the Maxwell's equations in $\mathbb{R}^3 \setminus \{0\}$ (see, e.g., [CK19, Thm. 6.26]). Using the asymptotic behavior (C.10) we find that the far field patterns of the vector wave functions $\boldsymbol{N}_n^m$ and $\mathbf{curl}\,\boldsymbol{N}_n^m$ are given by

$$(\boldsymbol{N}_n^m)^\infty(\widehat{\boldsymbol{x}}) \;=\; -\frac{1}{k}\frac{4\pi}{\mathrm{i}^{n+1}}\boldsymbol{V}_n^m(\widehat{\boldsymbol{x}})\,, \qquad (\mathbf{curl}\,\boldsymbol{N}_n^m)^\infty(\widehat{\boldsymbol{x}}) \;=\; \frac{4\pi}{\mathrm{i}^n}\boldsymbol{U}_n^m(\widehat{\boldsymbol{x}})\,, \qquad \widehat{\boldsymbol{x}} \in S^2\,, \tag{C.14}$$

for $m = -n, \dots, n$, $n = 1, 2, \dots$.

In Section 3.6, there appear the integrals

$$\int_{S^2} \boldsymbol{U}_n^m(\widehat{\boldsymbol{x}}) e^{\mathrm{i}k\widehat{\boldsymbol{x}}\cdot\boldsymbol{y}}\,\mathrm{d}s(\widehat{\boldsymbol{x}}) \quad \text{and} \quad \int_{S^2} \boldsymbol{V}_n^m(\widehat{\boldsymbol{x}}) e^{\mathrm{i}k\widehat{\boldsymbol{x}}\cdot\boldsymbol{y}}\,\mathrm{d}s(\widehat{\boldsymbol{x}})\,, \qquad \boldsymbol{y} \in \mathbb{R}^3\,.$$

We calculate them explicitly by using the following theorem.

Theorem C.2. *For every $\boldsymbol{p} \in \mathbb{C}^3$ it holds*

$$\begin{aligned}\frac{1}{k^2}\,\mathbf{curl}_{\boldsymbol{x}}\,\mathbf{curl}_{\boldsymbol{x}}(\Phi_k(\boldsymbol{y},\boldsymbol{x})\boldsymbol{p}) \;=\; \mathrm{i}k \sum_{n=1}^{\infty}\sum_{m=-n}^{m} \boldsymbol{N}_n^m(\boldsymbol{x})\overline{\boldsymbol{M}_n^m(\boldsymbol{y})}\cdot\boldsymbol{p} \\ + \frac{\mathrm{i}}{k}\sum_{n=1}^{\infty}\sum_{m=-n}^{m} \mathbf{curl}\,\boldsymbol{N}_n^m(\boldsymbol{x})\overline{\mathbf{curl}\,\boldsymbol{M}_n^m(\boldsymbol{y})}\cdot\boldsymbol{p}\,.\end{aligned}$$

For fixed $\boldsymbol{y}$, both series and its derivatives converge uniformly with respect to $\boldsymbol{x}$ on compact subsets of $|\boldsymbol{x}| > |\boldsymbol{y}|$.

Proof. This series expansion is derived in [CK19, Equ. (6.80)]. □

Let $\boldsymbol{p} \in L_t^2(S^2, \mathbb{C}^3)$. Then, we have

$$\frac{1}{k^2}\,\mathbf{curl}_{\boldsymbol{x}}\,\mathbf{curl}_{\boldsymbol{x}}(\Phi_k(\boldsymbol{y},\cdot)\boldsymbol{p})^\infty(\widehat{\boldsymbol{x}}) \;=\; e^{-\mathrm{i}k\widehat{\boldsymbol{x}}\cdot\boldsymbol{y}}(\widehat{\boldsymbol{x}}\times\boldsymbol{p}(\widehat{\boldsymbol{x}}))\times\widehat{\boldsymbol{x}} \;=\; \boldsymbol{p}(\widehat{\boldsymbol{x}})e^{-\mathrm{i}k\widehat{\boldsymbol{x}}\cdot\boldsymbol{y}}\,.$$

On the other hand, by applying Theorem C.2 and inserting the far field expansion (C.14) we obtain

$$\begin{aligned}\frac{1}{k^2}\,\mathbf{curl}_{\boldsymbol{x}}\,\mathbf{curl}_{\boldsymbol{x}}(\Phi_k(\boldsymbol{y},\cdot)\boldsymbol{p})^\infty(\widehat{\boldsymbol{x}}) \;=\; -\sum_{n=1}^{\infty}\sum_{m=-n}^{m} \frac{4\pi}{\mathrm{i}^n}\boldsymbol{V}_n^m(\widehat{\boldsymbol{x}})\overline{\boldsymbol{M}_n^m(\boldsymbol{y})}\cdot\boldsymbol{p}(\widehat{\boldsymbol{x}}) \\ + \sum_{n=1}^{\infty}\sum_{m=-n}^{m} \frac{1}{k}\frac{4\pi}{\mathrm{i}^{n-1}}\boldsymbol{U}_n^m(\widehat{\boldsymbol{x}})\overline{\mathbf{curl}\,\boldsymbol{M}_n^m(\boldsymbol{y})}\cdot\boldsymbol{p}(\widehat{\boldsymbol{x}})\,.\end{aligned}$$

We recall that $\{\boldsymbol{U}_n^m, \boldsymbol{V}_n^m\}$ is an orthonormal system and thus, we compute

$$\begin{aligned}\int_{S^2} \boldsymbol{U}_n^m(\widehat{\boldsymbol{x}}) e^{\mathrm{i}k\widehat{\boldsymbol{x}}\cdot\boldsymbol{y}}\,\mathrm{d}s(\widehat{\boldsymbol{x}}) \;&=\; \overline{\int_{S^2} \overline{\boldsymbol{U}_n^m(\widehat{\boldsymbol{x}})} e^{-\mathrm{i}k\widehat{\boldsymbol{x}}\cdot\boldsymbol{y}}\,\mathrm{d}s(\widehat{\boldsymbol{x}})} \\ &=\; \overline{\frac{1}{k}\frac{4\pi}{\mathrm{i}^{n-1}}\overline{\mathbf{curl}\,\boldsymbol{M}_n^m(\boldsymbol{y})}} \;=\; \frac{4\pi\mathrm{i}^{n-1}}{k}\,\mathbf{curl}\,\boldsymbol{M}_n^m(\boldsymbol{y})\end{aligned} \tag{C.15a}$$

and

$$\int_{S^2} \boldsymbol{V}_n^m(\widehat{\boldsymbol{x}}) e^{\mathrm{i}k\widehat{\boldsymbol{x}}\cdot\boldsymbol{y}} \,\mathrm{d}s(\widehat{\boldsymbol{x}}) = \overline{\int_{S^2} \overline{\boldsymbol{V}_n^m(\widehat{\boldsymbol{x}})} e^{-\mathrm{i}k\widehat{\boldsymbol{x}}\cdot\boldsymbol{y}} \,\mathrm{d}s(\widehat{\boldsymbol{x}})} = \overline{-\frac{4\pi}{\mathrm{i}^n}\overline{\boldsymbol{M}_n^m(\boldsymbol{y})}} = -4\pi\mathrm{i}^n \boldsymbol{M}_n^m(\boldsymbol{y}) \quad \text{(C.15b)}$$

for all $\boldsymbol{y} \in \mathbb{R}^3$.

Bibliography

[AG20] Annalena Albicker and Roland Griesmaier. Monotonicity in inverse obstacle scattering on unbounded domains. *Inverse Problems*, 36(8):085014, 2020.

[AG23] Annalena Albicker and Roland Griesmaier. Monotonicity in inverse scattering for Maxwell's equations. *Inverse Probl. Imaging*, 17(1):68–105, 2023.

[AH12] Kendall Atkinson and Weimin Han. *Spherical Harmonics and Approximations on the Unit Sphere: An Introduction*. Springer, Heidelberg, 2012.

[Arn18] Douglas N. Arnold. *Finite Element Exterior Calculus*. Society for Industrial and Applied Mathematics (SIAM), Philadelphia, 2018.

[BCTX12] John M. Ball, Yves Capdeboscq, and Basang Tsering-Xiao. On uniqueness for time harmonic anisotropic Maxwell's equations with piecewise regular coefficients. *Math. Models Methods Appl. Sci.*, 22(11):1250036, 2012.

[BHHM17] Andrea Barth, Bastian Harrach, Nuutti Hyvönen, and Lauri Mustonen. Detecting stochastic inclusions in electrical impedance tomography. *Inverse Problems*, 33(11):115012, 2017.

[BHKS18] Tommi Brander, Bastian Harrach, Manas Kar, and Mikko Salo. Monotonicity and enclosure methods for the p-Laplace equation. *SIAM J. Appl. Math.*, 78(2):742–758, 2018.

[CC14] Fioralba Cakoni and David Colton. *A Qualitative Approach to Inverse Scattering Theory*. Springer, New York, 2014.

[CCM01] Fioralba Cakoni, David Colton, and Peter Monk. The direct and inverse scattering problems for partially coated obstacles. *Inverse Problems*, 17(6):1997–2015, 2001.

[CCM11] Fioralba Cakoni, David Colton, and Peter Monk. *The Linear Sampling Method in Inverse Electromagnetic Scattering*. Society for Industrial and Applied Mathematics (SIAM), Philadelphia, 2011.

[CEFP+21] Antonio Corbo Esposito, Luisa Faella, Gianpaolo Piscitelli, Ravi Prakash, and Antonello Tamburrino. Monotonicity principle in tomography of nonlinear conducting materials. *Inverse Problems*, 37(4):045012, 2021.

[CK96] David Colton and Andreas Kirsch. A simple method for solving inverse scattering problems in the resonance region. *Inverse Problems*, 12(4):383–393, 1996.

[CK19] David Colton and Rainer Kress. *Inverse Acoustic and Electromagnetic Scattering Theory*. Springer, Cham, fourth edition, 2019.

[CM85] David Colton and Peter Monk. A novel method for solving the inverse scattering problem for time-harmonic acoustic waves in the resonance region. *SIAM J. Appl. Math.*, 45(6):1039–1053, 1985.

[CM86] David Colton and Peter Monk. A novel method for solving the inverse scattering problem for time-harmonic acoustic waves in the resonance region. II. *SIAM J. Appl. Math.*, 46(3):506–523, 1986.

[DFS20] Tomohiro Daimon, Takashi Furuya, and Ryuji Saiin. The monotonicity method for the inverse crack scattering problem. *Inverse Probl. Sci. Eng.*, 28(11):1570–1581, 2020.

[DS63] Nelson Dunford and Jacob T. Schwartz. *Linear Operators. Part II: Spectral Theory*. Interscience Publishers John Wiley & Sons, New York, London, 1963.

[EG92] Lawrence C. Evans and Ronald F. Gariepy. *Measure Theory and Fine Properties of Functions*. CRC Press, Boca Raton, 1992.

[Fur20] Takashi Furuya. The factorization and monotonicity method for the defect in an open periodic waveguide. *J. Inverse Ill-Posed Probl.*, 28(6):783–796, 2020.

[Gar18] Henrik Garde. Comparison of linear and non-linear monotonicity-based shape reconstruction using exact matrix characterizations. *Inverse Probl. Sci. Eng.*, 26(1):33–50, 2018.

[Geb08] Bastian Gebauer. Localized potentials in electrical impedance tomography. *Inverse Probl. Imaging*, 2(2):251–269, 2008.

[GH18] Roland Griesmaier and Bastian Harrach. Monotonicity in inverse medium scattering on unbounded domains. *SIAM J. Appl. Math.*, 78(5):2533–2557, 2018.

[GH21] Roland Griesmaier and Bastian Harrach. Erratum: Monotonicity in inverse medium scattering on unbounded domains. *SIAM J. Appl. Math.*, 81(3):1332–1337, 2021.

[GK04] Natalia I. Grinberg and Andreas Kirsch. The factorization method for obstacles with a priori separated sound-soft and sound-hard parts. *Math. Comput. Simulation*, 66(4-5):267–279, 2004.

[GKM22] Roland Griesmaier, Marvin Knöller, and Rainer Mandel. Inverse medium scattering for a nonlinear Helmholtz equation. *J. Math. Anal. Appl.*, 515(1):126356, 2022.

[Gri02] Natalia I. Grinberg. Obstacle visualization via the factorization method for the mixed boundary value problem. *Inverse Problems*, 18(6):1687–1704, 2002.

[Gri11] Pierre Grisvard. *Elliptic Problems in Nonsmooth Domains*. Society for Industrial and Applied Mathematics (SIAM), Philadelphia, 2011.

[GS17a] Henrik Garde and Stratos Staboulis. Convergence and regularization for monotonicity-based shape reconstruction in electrical impedance tomography. *Numer. Math.*, 135(4):1221–1251, 2017.

[GS17b] Roland Griesmaier and John Sylvester. Uncertainty principles for inverse source problems, far field splitting, and data completion. *SIAM J. Appl. Math.*, 77(1):154–180, 2017.

[GS18] Roland Griesmaier and John Sylvester. Uncertainty principles for inverse source problems for electromagnetic and elastic waves. *Inverse Problems*, 34(6):065003, 2018.

[GS19] Henrik Garde and Stratos Staboulis. The regularized monotonicity method: detecting irregular indefinite inclusions. *Inverse Probl. Imaging*, 13(1):93–116, 2019.

[GT01] David Gilbarg and Neil S. Trudinger. *Elliptic Partial Differential Equations of Second Order*. Springer, Berlin, 2001.

[GVL13] Gene H. Golub and Charles F. Van Loan. *Matrix Computations*. Johns Hopkins University Press, Baltimore, fourth edition, 2013.

[Het98] Frank Hettlich. The Landweber iteration applied to inverse conductive scattering problems. *Inverse Problems*, 14(4):931–947, 1998.

[HL19] Bastian Harrach and Yi-Hsuan Lin. Monotonicity-based inversion of the fractional Schrödinger equation I. Positive potentials. *SIAM J. Math. Anal.*, 51(4):3092–3111, 2019.

[HL20] Bastian Harrach and Yi-Hsuan Lin. Monotonicity-based inversion of the fractional Schödinger equation II. General potentials and stability. *SIAM J. Math. Anal.*, 52(1):402–436, 2020.

[HL23] Bastian Harrach and Yi-Hsuan Lin. Simultaneous recovery of piecewise analytic coefficients in a semilinear elliptic equation. *Nonlinear Anal.*, 228:113188, 2023.

[HLL18] Bastian Harrach, Yi-Hsuan Lin, and Hongyu Liu. On localizing and concentrating electromagnetic fields. *SIAM J. Appl. Math.*, 78(5):2558–2574, 2018.

[HM02] Houssem Haddar and Peter Monk. The linear sampling method for solving the electromagnetic inverse medium problem. *Inverse Problems*, 18(3):891–906, 2002.

[HM16] Bastian Harrach and Mach Nguyet Minh. Enhancing residual-based techniques with shape reconstruction features in electrical impedance tomography. *Inverse Problems*, 32(12):125002, 2016.

[HM18] Bastian Harrach and Mach Nguyet Minh. Monotonicity-based regularization for phantom experiment data in electrical impedance tomography. In *New Trends in Parameter Identification for Mathematical Models*. (Bernd Hofmann et al., editors), 107–120, Springer, New York, 2018.

[HPS19a] Bastian Harrach, Valter Pohjola, and Mikko Salo. Dimension bounds in monotonicity methods for the Helmholtz equation. *SIAM J. Math. Anal.*, 51(4):2995–3019, 2019.

[HPS19b] Bastian Harrach, Valter Pohjola, and Mikko Salo. Monotonicity and local uniqueness for the Helmholtz equation. *Anal. PDE*, 12(7):1741–1771, 2019.

[HU13] Bastian Harrach and Marcel Ullrich. Monotonicity-based shape reconstruction in electrical impedance tomography. *SIAM J. Math. Anal.*, 45(6):3382–3403, 2013.

[HU15] Bastian Harrach and Marcel Ullrich. Resolution guarantees in electrical impedance tomography. *IEEE Trans. Med. Imaging*, 34(7):1513–1521, 2015.

[Ike98a] Masaru Ikehata. Reconstruction of the shape of the inclusion by boundary measurements. *Commun. Partial Differ. Equ.*, 23:1459–1474, 1998.

[Ike98b] Masaru Ikehata. Size estimation of inclusion. *J. Inverse Ill-Posed Probl.*, 6(2):127–140, 1998.

[KG08] Andreas Kirsch and Natalia I. Grinberg. *The Factorization Method for Inverse Problems*. Oxford University Press, Oxford, 2008.

[KH15] Andreas Kirsch and Frank Hettlich. *The Mathematical Theory of Time-Harmonic Maxwell's Equations*. Springer, Cham, 2015.

[Kir93] Andreas Kirsch. The domain derivative and two applications in inverse scattering theory. *Inverse Problems*, 9(1):81–96, 1993.

[Kir98] Andreas Kirsch. Characterization of the shape of a scattering obstacle using the spectral data of the far field operator. *Inverse Problems*, 14(6):1489–1512, 1998.

[Kir04] Andreas Kirsch. The factorization method for Maxwell's equations. *Inverse Problems*, 20(6):S117–S134, 2004.

[KK87] Andreas Kirsch and Rainer Kress. A numerical method for an inverse scattering problem. In *Inverse Problems*. (Engl and Groetsch, editors), 279–290, Academic Press, Orlando, 1987.

[KR00] Andreas Kirsch and Stefan Ritter. A linear sampling method for inverse scattering from an open arc. *Inverse Problems*, 16(1):89–105, 2000.

[Kre95] Rainer Kress. On the numerical solution of a hypersingular integral equation in scattering theory. *J. Comput. Appl. Math.*, 61(3):345–360, 1995.

[Kre03] Rainer Kress. Newton's method for inverse obstacle scattering meets the method of least squares. *Inverse Problems*, 19(6):S91–S104, 2003.

[Kre14] Rainer Kress. *Linear Integral Equations*. Applied Mathematical Sciences. Springer, New York, 2014.

[KS03] Steven Kusiak and John Sylvester. The scattering support. *Comm. Pure Appl. Math.*, 56(11):1525–1548, 2003.

[KSS97] Hyeonbae Kang, Jin Keun Seo, and Dongwoo Sheen. The inverse conductivity problem with one measurement: stability and estimation of size. *SIAM J. Math. Anal.*, 28(6):1389–1405, 1997.

[Lax02] Peter D. Lax. *Functional Analysis*. Wiley, New York, 2002.

[McL00] William McLean. *Strongly Elliptic Systems and Boundary Integral Equations*. Cambridge University Press, Cambridge, 2000.

[Mon03] Peter Monk. *Finite Element Methods for Maxwell's Equations*. Oxford University Press, New York, 2003.

[Néd01] Jean-Claude Nédélec. *Acoustic and Electromagnetic Equations*. Springer, New York, 2001.

[NW12] Tu Nguyen and Jenn-Nan Wang. Quantitative uniqueness estimate for the Maxwell system with Lipschitz anisotropic media. *Proc. Amer. Math. Soc.*, 140(2):595–605, 2012.

[OLBC10] Frank W. J. Olver, Daniel W. Lozier, Ronald F. Boisvert, and Charles W. Clark, editors. *NIST Handbook of Mathematical Functions*. U.S. Department of Commerce, National Institute of Standards and Technology, Washington, DC; Cambridge University Press, Cambridge, 2010.

[Pot00] Roland Potthast. Stability estimates and reconstructions in inverse acoustic scattering using singular sources. *J. Comput. Appl. Math.*, 114(2):247–274, 2000.

[Pot06] Roland Potthast. A survey on sampling and probe methods for inverse problems. *Inverse Problems*, 22(2):R1–R47, 2006.

[Rog81] André Roger. Newton-Kantorovitch algorithm applied to an electromagnetic inverse problem. *IEEE Trans. Antennas Prop.*, 29(2):232–238, 1981.

[SBA+15] Wojciech Śmigaj, Timo Betcke, Simon Arridge, Joel Phillips, and Martin Schweiger. Solving boundary integral problems with BEM++. *ACM Trans. Math. Software*, 41(2):6, 2015.

[Sch09] Susanne Schmitt. The factorization method for EIT in the case of mixed inclusions. *Inverse Problems*, 25(6):065012, 2009.

[Sic21] Winfried Sickel. On the regularity of characteristic functions. In *Anomalies in Partial Differential Equations*. (Massimo Cicognani et al., editors), 395–441, Springer, Cham, 2021.

[SVUT17] Zhiyi Su, Salvatore Ventre, Lalita Udpa, and Antonello Tamburrino. Monotonicity based on imaging method for time-domain eddy current problems. *Inverse Problems*, 33(12):125007, 23, 2017.

[TPZ21] Antonello Tamburrino, Gianpaolo Piscitelli, and Zhengfang Zhou. The monotonicity principle for magnetic induction tomography. *Inverse Problems*, 37(9):095003, 2021.

[TR02] Antonello Tamburrino and Guglielmo Rubinacci. A new non-iterative inversion method for electrical resistance tomography. *Inverse Problems*, 18(6):1809–1829, 2002.

[TW09] Marius Tucsnak and George Weiss. *Observation and Control for Operator Semigroups*. Birkhäuser, Basel, 2009.

[Web81] Christian Weber. Regularity theorems for Maxwell's equations. *Math. Methods Appl. Sci.*, 3(4):523–536, 1981.

Notation

Basic notation

$\mathbb{N}$	natural numbers including zero	
$\mathbb{Z}$	integers	
$\mathbb{R}^d$	d-dimensional real Euclidean space	
$\mathbb{C}^d$	d-dimensional complex Euclidean space	
$\boldsymbol{x}$	point $\boldsymbol{x} = (x_1, \ldots, x_d)$ in $\mathbb{R}^d$	
$\boldsymbol{x}'$	point $\boldsymbol{x}' = (x_1, \ldots, x_{d-1})$ in $\mathbb{R}^{d-1}$	
$\boldsymbol{x} \cdot \boldsymbol{y}$	inner product of $\boldsymbol{x}, \boldsymbol{y} \in \mathbb{R}^d$	
$\boldsymbol{x} \times \boldsymbol{y}$	vector product of $\boldsymbol{x}, \boldsymbol{y} \in \mathbb{R}^d$	
$\lvert\boldsymbol{x}\rvert$	Euclidean norm of $\boldsymbol{x} \in \mathbb{R}^d$	
$\boldsymbol{\alpha}$	multi-index of order $\lvert\boldsymbol{\alpha}\rvert = \alpha_1 + \ldots + \alpha_d$	8
$\partial^{\boldsymbol{\alpha}} u$	(weak) partial derivative of the function u determined by $\boldsymbol{\alpha}$	8
Ω	open set	
$\partial\Omega$	boundary of Ω	
$\overline{\Omega}$	closure of Ω	
$\widetilde{\Omega} \subset\subset \Omega$	$\widetilde{\Omega}$ compactly contained in Ω	7
$B_R(\boldsymbol{x})$	ball of radius R in $\mathbb{R}^d$ centered in $\boldsymbol{x} \in \mathbb{R}^d$	7
$B'_R(\boldsymbol{x})$	ball of radius R in $\mathbb{R}^{d-1}$ centered in $\boldsymbol{x}' \in \mathbb{R}^{d-1}$	8
S^{d-1}	unit sphere in $\mathbb{R}^d$	7
$\widehat{\boldsymbol{x}}$	direction $\boldsymbol{x}/\lvert\boldsymbol{x}\rvert \in S^{d-1}$	
$\boldsymbol{\nu}$	exterior unit normal on $\partial\Omega$ or S^{d-1}	9
$\partial/\partial\boldsymbol{\nu}$	normal derivative on $\partial\Omega$ or S^{d-1}	10
D	scatterer, impenetrable	12
	scatterer, penetrable	77
D_1	Dirichlet scatterer	12
D_2	Neumann scatterer	12

c_0	speed of sound	12
p	pressure	12
ε_0	electric permittivity in free space	76
ε	electric permittivity	76
ε_r	relative electric permittivity	76
q	contrast function	77
μ_0	magnetic permeability in free space	76
μ	magnetic permeability	76
$\mathcal{E}$	electric field	76
$\mathcal{H}$	magnetic field	76
ω	angular frequency	12, 76
k	wave number	12, 77

FUNCTION SPACES

$C^0(\Omega)$	continuous functions on Ω	7
$C^j(\Omega)$	j times continuously differentiable functions on Ω, $j = 1, 2, \ldots$	7
$C_0^j(\Omega)$	C^j functions with compact support on Ω, $j \in \mathbb{N}$	7
$C^j(\overline{\Omega})$	functions in $C^j(\mathbb{R}^d)$ restricted to Ω, $j \in \mathbb{N}$	7
$C^\infty(\Omega)$	infinitely differentiable functions on Ω	7
$C^j(\partial\Omega)$	j times continuously differentiable functions on $\partial\Omega$, $j \in \mathbb{N}$	9
$C^{j,\alpha}(\Omega)$	Hölder space with exponent α on Ω, $0 < \alpha \leq 1$, $j \in \mathbb{N}$	7
$C^{j,\alpha}(\partial\Omega)$	Hölder space with exponent α on $\partial\Omega$, $0 < \alpha \leq 1$, $j \in \mathbb{N}$	9
$L^p(\Omega)$	Lebesgue space on Ω, $1 \leq p \leq \infty$	7
$\langle \cdot, \cdot \rangle = \langle \cdot, \cdot \rangle_{L^2(\Omega)}$	inner product in $L^2(\Omega)$	8
$L^p_{\mathrm{loc}}(\Omega)$	local Lebesgue space on Ω, $1 \leq p \leq \infty$	8
$L^p(\partial\Omega)$	Lebesgue space on $\partial\Omega$, $1 \leq p \leq \infty$	9
$\langle \cdot, \cdot \rangle_{L^2(\partial\Omega)}$	inner product in $L^2(\partial\Omega)$	9
$H^j(\Omega)$	Sobolev space on Ω, $j \in \mathbb{N}$	8
$H^j_{\mathrm{loc}}(\Omega)$	local Sobolev space on Ω, $j \in \mathbb{N}$	8
$H^s(\Omega)$	Sobolev space on Ω, $s \geq 0$	8
$H^1_\Delta(\Omega)$	functions in $H^1(\Omega)$ whose Laplacian is in $L^2(\Omega)$	10
$H^{1/2}(\partial\Omega)$	Sobolev space on the boundary $\partial\Omega$	9

$H^{-1/2}(\partial\Omega)$	dual space of $H^{1/2}(\partial\Omega)$	9
$\langle\cdot,\cdot\rangle_{\partial\Omega}$	duality pairing between $H^{-1/2}(\partial\Omega)$ and $H^{1/2}(\partial\Omega)$	9
$H^s(\partial\Omega)$	Sobolev space on $\partial\Omega$, $s>1$	9
$H^{1/2}(\Gamma)$	Sobolev space on $\Gamma\subseteq\partial\Omega$	10
$\widetilde{H}^{-1/2}(\Gamma)$	dual space of $H^{1/2}(\Gamma)$	10
$\widetilde{H}^{1/2}(\Gamma)$	Sobolev space on $\Gamma\subseteq\partial\Omega$	10
$H^{-1/2}(\Gamma)$	dual space of $\widetilde{H}^{1/2}(\Gamma)$	10
$L^2(\Omega,\mathbb{C}^3)$	Lebesgue space on Ω, vector-valued	73
$L^2(\partial\Omega,\mathbb{C}^3)$	Lebesgue space on $\partial\Omega$, vector-valued	73
$L^2_t(\partial\Omega,\mathbb{C}^3)$	tangential Lebesgue space on $\partial\Omega$, vector-valued	73
$L^2_t(S^2,\mathbb{C}^3)$	tangential Lebesgue space on S^2, vector-valued	73
$H(\mathbf{curl};\Omega)$	Sobolev space on Ω, vector-valued	73
$\langle\cdot,\cdot\rangle_{H(\mathbf{curl};\Omega)}$	inner product in $H(\mathbf{curl};\Omega)$	73
$H_{\mathrm{loc}}(\mathbf{curl};\Omega)$	local Sobolev space on Ω, vector-valued	73
$H(\mathbf{curl};\Omega)^*$	dual space of $H(\mathbf{curl};\Omega)$, vector-valued	74
$\langle\cdot,\cdot\rangle_*$	duality pairing between $H(\mathbf{curl};\Omega)^*$ and $H(\mathbf{curl};\Omega)$	74
$H_0(\mathbf{curl};\Omega)$	Sobolev space on Ω, vector-valued	75
$H(\mathrm{div};\Omega)$	Sobolev space on Ω, vector-valued	74
$H_{\mathrm{loc}}(\mathrm{div};\Omega)$	local Sobolev space on Ω, vector-valued	74
$H^{1/2}_t(\partial\Omega,\mathbb{C}^3)$	tangential Sobolev space on $\partial\Omega$, vector-valued	75
$H^{-1/2}_t(\partial\Omega,\mathbb{C}^3)$	dual space of $H^{1/2}_t(\partial\Omega,\mathbb{C}^3)$, vector-valued	76
$H^{3/2}_t(\partial\Omega,\mathbb{C}^3)$	tangential Sobolev space on $\partial\Omega$, vector-valued	76
$H^{-1/2}(\mathrm{Div};\partial\Omega)$	tangential Sobolev space on $\partial\Omega$, vector-valued	76
$H^{-1/2}(\mathrm{Curl};\partial\Omega)$	tangential Sobolev space on $\partial\Omega$, vector-valued	76
$\widetilde{H}^{-1/2}(\mathrm{Div};\Gamma)$	tangential Sobolev space on $\Gamma\subseteq\partial\Omega$, vector-valued	76
X	subspace of continuous piecewise linear functions	127
$\boldsymbol{X}$	subspace of tangential continuous piecewise linear vector fields	129

FUNCTIONS

$\operatorname{supp} u$	support of the function u	7
$\delta_{j,k}$	Kronecker delta	128
Φ_k	fundamental solution to the Helmholtz equation	13
SL_{D_1}	single layer potential	16
DL_{D_2}	double layer potential	16

Y_n^m	spherical harmonic of order n, $m = -n, \dots, n$, $n \in \mathbb{N}$	135
$\boldsymbol{U}_n^m, \boldsymbol{V}_n^m$	vector spherical harmonics of order n, $m = -n, \dots, n$, $n \in \mathbb{N}$	135
$\boldsymbol{M}_n^m, \boldsymbol{N}_n^m$	spherical vector wave functions, $m = -n, \dots, n$, $n = 1, 2, \dots$	136
J_n	Bessel function of order n, $n \in \mathbb{N}$	134
Y_n	Neumann function of order n, $n \in \mathbb{N}$	134
$H_n^{(1,2)}$	Hankel function of first, second kind of order n, $n \in \mathbb{N}$	134
j_n	spherical Bessel function of order n, $n \in \mathbb{N}$	136
y_n	spherical Neumann function of order n, $n \in \mathbb{N}$	136
$h_n^{(1,2)}$	spherical Hankel function of first, second kind of order n, $n \in \mathbb{N}$	136

OPERATORS

$\mathcal{R}(A)$	range of the operator A	10
$\mathcal{N}(A)$	null space of the operator A	10
A^*	adjoint operator of the operator A	10
$\mathrm{Re}(A)$	real part of the operator A	10
$\|A\|$	operator norm of the operator A	10
$\leq_r$, $\geq_r$	extension of the Loewner order	11
$\leq_{\mathrm{fin}}$, $\geq_{\mathrm{fin}}$	extension of the Loewner order	11
∇	(weak) gradient of a function	
Δ	(weak) Laplacian of a function	
div	(weak) divergence of a vector field	74
curl	(weak) rotation of a vector field	73
Grad	surface gradient	75
Div	surface divergence	75
Curl	surface vector curl	75
Curl	surface scalar curl	75
P_V	orthogonal projection onto V	27, 94
J	compact embedding operator	10
$\mathcal{J}$	compact embedding operator	87
γ	standard trace operator	9
γ_n	normal derivative trace operator	10
γ_t	tangential trace operator	74
π_t	projection on the tangent plane	74
r	rotation operator	75

$F_{D_1}^{\mathrm{dir}}$, $F_{D_2}^{\mathrm{neu}}$, F_D^{mix}	far field operators, acoustic	15
F_q	far field operator, magnetic	80
$\mathcal{S}_D^{\mathrm{mix}}$	scattering operator, acoustic	15
$\mathcal{S}_q$	scattering operator, magnetic	81
H_B	Herglotz operator, acoustic	23
	Herglotz operator, magnetic	98
$G_{D_1}^{\mathrm{dir}}$,$G_{D_2}^{\mathrm{neu}}$,G_D^{mix}	data-to-pattern operators	16, 37
R_Γ	restriction operator	24
R_{D_1}, R_{D_2}	restriction operators	42
$\widetilde{R}_{\Gamma_1}$, $\widetilde{R}_{\Gamma_2}$	restriction operators	43
S_{D_1}	single layer operator	17
$S_{D_1,\mathrm{i}}$	S_{D_1} for $k = \mathrm{i}$	17
$S_{D_1,\mathrm{i}}^{1/2}$	square root of $S_{D_1,\mathrm{i}}$	18
N_{D_2}	hypersingular operator	17
$N_{D_2,\mathrm{i}}$	N_{D_2} for $k = \mathrm{i}$	17
$\Lambda^{\mathrm{dir}\to\mathrm{neu}}$	Dirichlet-to-Neumann operator	24
$\Lambda^{\mathrm{neu}\to\mathrm{dir}}$	Neumann-to-Dirichlet operator	24
Λ	exterior Calderon operator	79

Index